University of South-Eastern Norway
Faculty of Technology, Natural Sciences and Maritime Studies

Doctoral dissertation no. 131
2022

Vasan Sivalingam

Syngas Fermentation and Microbial Electrosynthesis Process Integration to Advance Biogas Production

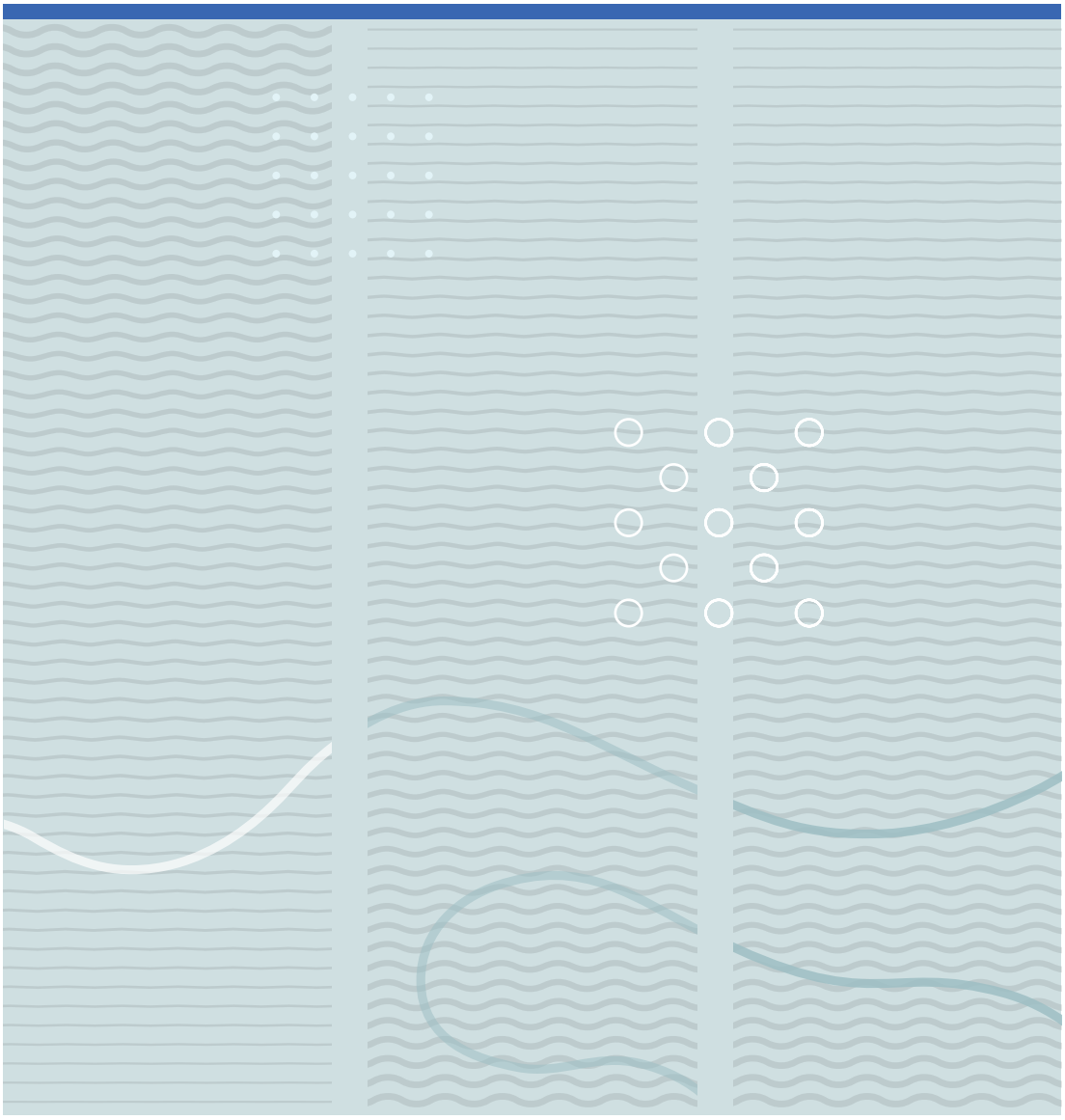

Vasan Sivalingam

Syngas Fermentation and Microbial Electrosynthesis Process Integration to Advance Biogas Production

A PhD dissertation in
Process, Energy and Automation Engineering

Faculty of Technology, Natural Sciences and Maritime Studies
University of South-Eastern Norway
Porsgrunn, 2022

Doctoral dissertations at the University of South-Eastern Norway no.131

ISSN: 2535-5244 (print)
ISSN: 2535-5252 (online)

ISBN: 978-82-7206-679-5 (print)
ISBN: 978-82-7206-680-1 (online)

Print: University of South-Eastern Norway

Dedication

To

My affectionate wife, Sharaniya

My kind-hearted parents, Sivalingam and Parimaladevi

Preface

This dissertation is submitted to the University of South-Eastern Norway (USN) to fulfil the partial requirements to obtain the degree of Philosophiae Doctor (PhD) in Process Energy and Automation Engineering. The work has been carried out under the supervision of Professor Carlos Dinamarca, late Professor Rune Bakke, and Researcher Dr Pai Lu. The Norwegian Ministry of Education and Research has funded this study.

The dissertation contains two parts. The first part reviews the research background, status, and perspective of syngas fermentation and microbial electrosynthesis technologies, research gaps, and strategies to fill these gaps. In addition, material and methods and a summary of scientific publications are presented. The report ends with conclusions and recommendations. The second part consists of all the articles on which this dissertation is based.

The reactors design, construction, operation, and chemical analyses were performed at USN-Porsgrunn Campus laboratories. The fermentation medium is collected from the local wastewater treatment plant (Knarrdalstrand, Porsgrunn, Norway). The microbial analyses were performed by Tone Haugen and Dr Alexander Wentzel, SINTEF Industry, Trondheim, Norway. The scanning electron microscopy was performed by Dr Pai Lu, USN, Campus Vestfold.

During this PhD study period, I have contributed to eleven articles. Six are core to this thesis work, including a level two article. I have been active on the “Environmental Biotechnology Research Group”, USN Porsgrunn and “Bioelectrochemical - as Energy and Environmental Measures USN-strategic research project” in collaboration with Campus Vestfold, contributing four additional articles. Moreover, I have been working on a commercial project, “Synolys” with WAI Environmental Solutions AS, Skoppum, Norway, and a research project “, Bio-oil decomposition”, collaboration with Scanship, Tønsberg, Norway.

Vasan Sivalingam, Porsgrunn: 28th of March 2022

Acknowledgements

"Who every good have killed, may yet destruction flee;
Who 'benefit' has killed, that man shall ne'er 'scape free" – Thirukkural, 109

I would like to express my profound gratitude to my main supervisor, Professor Carlos Dinamarca, for his guidance, commitment, and dedication to making my PhD journey to a conclusive end. Usually, PhD students get the opportunity to meet their supervisors, not frequently more than once a week. However, his door was always open for me, and I got the opportunity to clarify and discuss the research challenges instantly on a daily basis. I am deeply indebted to his support and kindness. I want to express my sincere appreciation to my co-supervisors, the late Professor Rune Bakke and Dr Pai Lu, for their support and motivation. I sincerely thank The Norwegian Ministry of Education and Research for the financial support (grant number: 2700095).

I am grateful to Professor Saba Mylvaganam, Professor Kim Esbensen, Associate professor Gamunu Samarakoon, Assistant Professor Dietmar Winkler, and Dr Anirudh Nelabhotla for their valuable suggestions during this study. Thanks to Tone Haugen and Dr Alexander Wentzel for their support on microbiome analysis. I express my sincere gratitude to Hildegunn Haugen, Kadja De Oliveira Borges, Chidapha Deeraksa, and Frank AArvak for their support during laboratory activities. I thank Øyvind Johansen, Odd Arne Ravnå and Fredrik Hansen for their support during the reactor building process. I thank Eshetu Janaka for helping me acquire inoculum from Knarrdalstrand WWTP. My sincere gratitude to Mariken Kjøhl-Røsand and Associate professor Per Morten Hansen for the administrative support throughout the program. I should thank Special librarian Dag-Even Martinsen Torsøe for his support in acquiring relevant reading materials. In addition, I am thankful to my fellow research mates and friends, Vibeke Karlsen, Vafa Ahmadi, Gudny Flatabø and Sandeep Gyawali, for their help. I highly appreciate my mother Parimaladevi, father Sivalingam, wife Sharaniya, sisters Vasuki and Vinopaa, uncles Kuna, Sri and Jeevan, who have provided enormous moral support in many ways to make this project successful. This would not be possible without them.

Abstract

Norway is implementing several CO_2 emissions control measures to become a low-emission society by 2050. As a part of this great vision, it strives to be the first nation to end the sales of fossil-fuelled vehicles by 2025. However, heavy transport still relies on fossil fuels that can be substantially replaced by liquified biogas. The demand-driven biogas market volume is more extensive than the current supply volume. The feedstock availability and lower methane yield are the potential bottlenecks that hinder the complete substitution of biomethane as a clean fuel. This PhD project studies syngas fermentation and microbial electrosynthesis (MES) as two sustainable technologies to advance methane yield.

Fermenting syngas into a biogas reactor is an arduous process. Inefficient gas-liquid (GL) mass transfer of H_2, the slow growth rate of the microorganisms that account for the fermentation, and lack of reducing equivalents are the foremost challenges. The original contribution of this PhD project to the knowledge is published as five open-access journal articles and a conference paper. Article 1 examines the effect of H_2 partial pressure on syngas fermentation to overcome the GL mass transfer limitation. Article 2 explores the possibility of using moving bed biofilm to overcome the kinetic growth limitation of the slow-growing microorganisms. Articles 3, 4, and 5 investigate the impact of MES integration as a source of reducing equivalents for syngas fermentation; herein, the lowest benchmark potential for acetate synthesis and GL mass transfer are scrutinised. In addition, preliminary modelling work was performed in Modelica as an interface between the power electronic side and the biochemical side of the MES reactor, presented in a conference (Article 6).

Digested sludge from Knarrdalstrand WWTP-AD, Porsgrunn, was pre-treated to enriched homoacetogens and utilised as the inoculum for all the experiments. In articles 1 to 4, the syngas was mimicked as H_2 in the headspace and CO_2 in the liquid medium as bicarbonate salt, while an industrially relevant syngas mixture (15 % CO, 15 % H_2, 20 % N_2 in 50 % CO_2) was used in article 5. Initially, the impact of 1 to 25 bar H_2 headspace

pressure on the homoacetogenic medium with 0.41 volatile and total solid ratio (VS: TS) was studied. The 15 bar was identified as the optimum headspace pressure. There 47.24 mmol of H_2 was consumed at an optimum rate of 6.22 mol h^{-1} L^{-1}, and 3.0 g L^{-1} of acetic acid was synthesised. In study two, moving bed biofilm was incorporated into a 15 bar H_2 pressurised reactor. The biofilm integrated batch depicted a 33 % improvement in the H_2 uptake rate (200 mmol L^{-1} d^{-1}) and 48 % in acetate synthesis rate (37.4 mmol L^{-1} d^{-1}). The stereo microscopic images affirmed the biofilm accumulation on the carriers at an average thickness of 160 µm.

In order to study the impact of MES on syngas fermentation (article 3), the experiment was performed in three phases. The fermentation was done with the suspended medium alone in the first phase. Then electrodes were integrated into the planktonic medium, referred to as a single-chamber MES reactor; therein, electrodes were not poised with any voltage in phase two (open circuit mode, OCM**),** while cathode was poised with negative potential in phase three (closed-circuit mode, CCM). In contrast to the planktonic fermentation, the biofilm assimilated on the electrodes in the OCM tripled the H_2 (1021 mmol) consumption. Also, the gas uptake rate (13.5 mmol L^{-1} d^{-1}) and acetate synthesis (57 mmol L^{-1}) improved by 125 % and 63 %. An optimum potential (– 0.8 V vs. SHE) for acetate synthesis was adapted from previous USN studies to perform phase three. The study hypothesised that potential could trigger the H_2 GL mass transfer and acetate synthesis. However, it failed because the applied potential (- 0.8 V) could have been deprived of its biotic nature; thus, the anodic potential exceeded the acetic acid oxidation potential, resulting in a rapid drop in concentration. Therefore article 4 attempted to determine the lowest benchmark potential for acetate synthesis and improved H_2 GL mass transfer.

Study 4 was performed in two phases, OCM and CCM. The CCM examined the impact of reducing power from – 25 to – 175 mV vs. Ag/AgCl (3.0 NaCl) on the acetic acid synthesis and H_2 GL mass transfer. Compared to the OCM, the -175 mV enhanced the acetate synthesis rate (0.225 mmol L^{-1} h^{-1}) by 26 % and was identified as the lowest benchmark potential, while there was no improvement in H_2 consumption. The direct electron

transfer from cathode to microorganism avoided the H_2 consumption from headspace. Article 5 is quite similar to article 4. However, the distinct advancement is that instead of pure H_2 in the headspace, industrial relevant syngas has been fermented to move the technology readiness level forward. The experiments were performed in both open and closed-circuit modes. During the CCM, the impact of reducing power from – 50 to – 400 mV vs. Ag/AgCl (3.0 NaCl) was examined on acetic acid synthesis, syngas utilisation and CO inhibition. The – 150 mV was figured out as the lowest benchmark potential for the optimum acetic acid synthesis rate (0.263 mmol L^{-1} h^{-1}), which is 15 times higher than the OCM rate. Sixty per cent of the CO from the headspace was consumed without any noticeable inhibition.

The overall PhD study concludes that elevated syngas pressure, MBB, and MES incorporation significantly enhanced acetate synthesis that can further be converted into methane into a biogas reactor, thus advancing biogas production.

Keywords: Syngas fermentation; CO_2 reduction; Wood-Ljungdahl; Microbial electrosynthesis (MES); Biogas production; Hydrogen; bioelectrochemistry

Sammendrag

Norge innfører flere tiltak for å redusere CO_2 utslipp og bli et lavutslippssamfunn innen 2050. Målet er å bli den første nasjonen til å stoppe nysalget av fossildrevne biler innen 2025. Elbiler utgjorde mer enn 50 % av nybilsalget i Norge de to siste årene. Tungtransportsektoren er fortsatt avhengig av fossilt drivstoff, men en vesentlig andel av dette kan erstattes med biogass. For å kunne benytte biogass som et rent drivstoff må metanutbyttet økes. I dette prosjektet undersøkes det om integrert syntesegassfermentering og mikrobiell elektrosyntese (MES) kan benyttes for å forbedre metanutbyttet. Det overordnede målet er å øke acetatsyntesen og dermed forbedre biogassproduksjonen.

Å fermentere syntesegass i en biogassreaktor er en krevende prosess. Hovedutfordringene er ineffektiv masseoverføring av H_2 fra gass- til væskefase, lav veksthastighet for mikroorganismene involvert i fermenteringsprosessen, og begrenset tilgang på reduserende ekvivalenter. PhD prosjektets nye bidrag til feltet er publisert i fem journaler med åpen tilgang og en konferanseartikkel. Artikkel 1 undersøker H_2 -deltrykkets påvirkning på syntesegassfermenteringen for å overkomme den begrensende masseoverføringen. Artikkel 2 utforsker muligheten for å benytte en moving bed biofilm (MBB) for å overkomme mikroorganismenes kinetiske vekstbegrensninger. I artikkel 3, 4 og 5 utforskes virkningen av å benytte MES som en kilde til reduserende ekvivalenter for fermentering av syntesegass. Dette inkluderer identifisering av det laveste benchmark potensialet for acetatsyntesen og masseoverføringen fra gass til væske. I tillegg ble modellering av en MES reaktor utført i Modelica og presentert på en konferanse (Artikkel 6). I dette innledende modelleringsarbeidet ble grensesnittet mellom den elektriske og biokjemiske siden av en MES reaktor modellert.

Utråtnet slam (digested sludge) fra Knarrdalstrand WWTP-AD, Porsgrunn, ble forbehandlet for å stimulere veksten av homoacetogene bakterier. Dette ble benyttet som fermenterinsgmedium i alle forsøkene. I artikkel 1 til 4 ble følgende benyttet for å simulere syntesegass: H_2 i headspace og CO_2 i form av bikarbonatsalt løst i væsken. I

artikkel 5 ble en syntesegassblanding (15 % CO, 15 % H_2, 20 % N_2 in 50 % CO_2) benyttet. Dette forholdet er representativt for industrielle prosesser. 15 bar ble identifisert som optimalt trykk i headspace, hvor 47,24 mmol H_2 ble forbrukt med en optimal hastighet på 6,22 mol h^{-1} L^{-1} og 3,0 g L^{-1} acetatsyre ble dannet. I den andre studien ble MBB benyttet for å motvirke mikroorganismenes kinetiske begrensninger. I batchreaktoren bidro biofilmen til en forbedring av H_2 opptakshastigheten med 33 % (200 mmol L^{-1} d^{-1}) og acetatsyntesehastigheten med 48 % (37,4 mmol L^{-1} d^{-1}). Stereomikroskopiske undersøkelser bekreftet dannelse av biofilm på biofilmbærerne med en gjennomsnittlig tykkelse på ~ 160 µm.

For å studere MES' påvirkning på fermenteringen av syntesegass ble fermenteringen utført i tre faser; 1) i suspended medium, 2) open circuit mode (OCM) og 3) closed circuit mode (CCM). Med biofilm på elektrodene i OCM ble H_2 forbruket tredoblet, gassopptakshastigheten økte med 125 % og acetatsyntesen med 63 % sammenlignet med suspended medium. I fase 3 ble et optimalisert potensiale på -0,8 V vs. SHE benyttet for å øke acetatsyntesen. Dette potensialet er tilpasset fra tidligere studier utført ved USN. Hypotesen var at både masseoverføringen av H_2 og acetatsyntesen vil forbedres ved -0,8 V, men det ble ikke observert i studien. Dette kan skyldes at potensialet er høyere enn den termodynamiske grensen hvor elektrodene mistet sine biotiske egenskaper og at potensialet er for høyt til å fremme acetatproduksjon. Målet i artikkel 4 var derfor å finne et benchmark potensiale hvor begge prosessene forbedres. -175 mV ble identifisert som det laveste benchmark potensialet. Acetatsyntesehastigheten økte med 26 %, men masseoverføringen av H_2 ble ikke forbedret fordi direkte elektronoverføring fra katoden til mikroorganismene hindret opptak av H_2 fra headspace. For å øke teknologiens modenhetsnivå, ble studien i artikkel 4 videreutviklet ved å benytte en syntesegass-sammensetning som er relevant for industrien (artikkel 5). En 15-ganger forbedring av acetatsyntesen ble oppnådd med -150 mV, og 60 % av karbonmonoksidet ble forbrukt uten å føre til toksisitet.

PhD-studien konkluderer med at et økt syntesegasstrykk, MBB og inkorporering av MES forbedrer acetatsyntesen betraktelig. Acetat kan videre omdannes til metan i en biogassreaktor og dermed forbedre biogassproduksjonen.

Nøkkelord: Syntesegassfermentering; CO_2 -reduksjon; Wood-Ljungdahl; Mikrobiell elektrosyntese (MES); Biogassproduksjon; Hydrogen; Bioelektrokjemi

விஞ்ஞான ஆய்வுச் சுருக்கம்

இந்த ஆய்வறிக்கையானது ஆற்றல், சுற்றுப்புறச்சூழல் மற்றும் தானியங்கிப் பொறியியல் துறையில் முனைவர் பட்டம் பெறும் ஒரு அங்கமாக வெளியீடு செய்யப்படுகின்றது. அண்மைக்காலங்களில் அதிகளவான காபனீரொட்சைட்டு உமிழ்வு பாரிய காலநிலை மாற்றத்தை உருவாக்கி அசாதாரணமான பொருளாதார, சமூக மற்றும் சுற்றுப்புற அசௌகரியங்களை ஏற்படுத்துகின்றது. இதனை கட்டுப்பாட்டிற்குள் கொண்டு வருவது எங்கள் ஒவ்வொருவருடையதும் கடமையாகும். இதன் பொருட்டு ஐ. நா சபை, காபனீரொக்சைட்டு உமிழ்வுக் குறைப்பை ஒரு நிலையான குறிக்கோளாகக் கொண்டு உலகநாடுகளை அதன் பால் நோக்கிப் பயணிக்க ஊக்கமளிக்கின்றது. அந்த வகையில் ஐ. நா உறுப்பு நாடுகளில் ஒன்றான நோர்வே, 2050ம் ஆண்டளவில் தன்னை குறைந்தளவு காபனீரொக்சைட்டு உமிழ்வை ஏற்படுத்தும் தேசமாக மாற்ற வேண்டும் என்ற உயரிய நோக்கோடு பயணித்துக்கொண்டிருக்கின்றது. என்னுடைய இந்த ஆய்வும், நோர்வேயினுடையதும், ஐ. நா வினுடையதும் காலநிலை குறிக்கோளிற்கு ஓர் வலிமை சேர்க்கும் அங்கமாகும்.

போக்குவரத்து துறையே கணிசமான அளவு காபனீரொக்சைட்டு உமிழ்விற்கு காரணம். ஆகவே கனிம எண்ணெயில் இயங்குகின்ற வாகனங்களை மின்சார வாகனங்களால் பிரதியீடு செய்வதன் மூலம் காபனீரொட்சைட்டின் உமிழ்வை கணிசமான அளவு குறைக்க முடியும். இதன் பொருட்டு கடந்த இரு ஆண்டுகளில் நோர்வேயில் விற்பனை செய்யப்பட்ட மகிழுந்துகளில் 50 % இற்கும் அதிகமானவை மின்சாரத்தில் இயங்குபவை. இதனடிப்படையில் 2025ம் ஆண்டளவில் அனைத்து கனிம எண்ணெய்ப் பயன்பாடுடைய வாகனங்களின் விற்பனையை முடிவிற்கு கொண்டுவரும் முதலாவது நாடாக உருவாக்குவதற்கு உத்தேசிக்கப்பட்டுள்ளது. இருப்பினும் கன ரக வாகனங்களை மின்சார வாகனங்களாக பிரதியீடு செய்வது சவால் மிகுந்தது. அவற்றில் மின்கலங்களின் உற்பத்தி, கொள்ளளவு மற்றும் மீள் சுழற்சி ஆகியவை பிரதானமானவை. ஆகவே கனிம எண்ணெய்க்குப் பதிலாக உணவு, விவசாய, கால்நடைக் கழிவுகளை மூலப்பொருட்களாகக் கொண்டு பெறப்படும் உயிர்வாயுவைப் பயன்படுத்துவதன். மூலம் கனரக வாகனங்களின் காபனீரொக்சைட்டு உமிழ்வைக் கட்டுப்படுத்த முடியும்.

இருப்பினும், இந்த மூலப்பொருட்களின் பற்றாக்குறை காரணமாக கனிம எண்ணெய்ப்பயன்பாட்டை கன ரக வாகனங்களில் முழுமையாக இல்லாதொழிக்க முடியாதுள்ளது. ஆகவே திண்மக் கழிவுகளை வெப்பச் சிதைவிற்குட்படுத்துவதன் மூலமோ, எரியூட்டுவதன் மூலமோ உருவாக்கப்படும் காபனீரொட்சைட்டு, காபனோரொட்சைட்டு, ஐதரசன் ஆகிய வாயுக்கலவையை மூலப்பொருட்களாக கொண்டு அவற்றை நொதித்தலுக்குட்படுத்தி அதன் மூலம் உயிர்வாயுவை உற்பத்தி செய்வதே இந்த ஆய்வின் பிரதான நோக்கம். வாயுக்களின் குறைந்த கரைதிறன், வளர்ச்சி வேகம் குறைந்த நொதித்தல் நுண்ணங்கிகள், வாயுக்களின் நச்சுத்தன்மை ஆகியன பிரதான சவால்களாக காணப்படுகின்றன.

இந்த மூன்று வருட தொடர் ஆராய்ச்சியில் இம் மூன்று சவால்களும் பல்வேறு கோணங்களில் பரிசோதனை மற்றும் ஆய்வு செய்யப்பட்டு ஆறு சர்வதேச ஆய்வுச்சஞ்சிகைகளில் பிரசுரிக்கப்பட்டுள்ளன. ஆய்வின் இறுதியில் 15 வளிமண்டல அமுக்கத்தில் நொதித்தலை மேற்கொள்வதன் மூலமும், உயிர்ப்படல ஒருங்கிணைப்பு வழியே நொதித்தல் நுண்ணங்கிகளின் அளவை அதிகரித்து மற்றும் நுண்ணுயிர் மின்பகுப்பு தொழில் முறை மூலமும் நொதித்தலை துரிதப்படுத்த முடியும் என உறுதி செய்யப்பட்டுள்ளது. மற்றும் வாயுக்கலவையில் உள்ள நச்சு வாயு மூலக்கூறான காபனோரொட்சைட்டினுடைய பாதிப்பையும் நுண்ணுயிர் மின் தொகுப்பு தொழிற்பாட்டினூடாக கணிசமான அளவு குறைக்க முடியும் எனவும் உறுதிசெய்யப்பட்டிருக்கின்றது.

சூழல் வெப்பமாதல் எனும் உலகளாவிய சவாலுக்கு இந்த ஆய்வுக்கட்டுரை நிச்சயம் வலிமை சேர்க்கும் என்பதில் ஐயமில்லை.

வாசன் சிவலிங்கம்.

நோர்வே, பங்குனி, 2022

List of core papers

Article 1

Sivalingam, V., Haugen, T., Wentzel, A., & Dinamarca, C. (2021). Effect of Elevated Hydrogen Partial Pressure on Mixed Culture Homoacetogenesis. *Chemical Engineering Science: X*, 100118. doi.org/10.1016/j.cesx.2021.100118

Article 2

Sivalingam, V., & Dinamarca, C. (2021). High Pressure Moving Bed Biofilm Reactor for Syngas Fermentation. *Chemical Engineering Transactions*, *86*, 1483–1488. doi.org/10.3303/CET2186248

Article 3

Sivalingam, V., Ahmadi, V., Babafemi, O., & Dinamarca, C. (2021). Integrating Syngas Fermentation into a Single-Cell Microbial Electrosynthesis (MES) Reactor. *Catalysts*, *11*(1), 40. doi.org/10.3390/catal11010040

Article 4

Sivalingam, V., Parhizkarabyaneh, P., Winkler, D., Lu, P., Haugen, T., Wentzel, A., & Dinamarca, C. (2022). Impact of Electrochemical Reducing Power on Homoacetogenesis. *Bioresource Technology*, 126512. doi.org/10.1016/j.biortech.2021.126512

Article 5

Sivalingam, V., Winkler D., Haugen, T., Wentzel, A., & Dinamarca, C. (2022). Syngas Fermentation and Microbial Electrosynthesis Integration as a Single Process Unit:

(Submitted on 23rd of March 2022 to Bioresource Technology journal)

Article 6

Samarakoon, G., Winkler, D., Sivalingam, V., Dinamarca, C., & Bakke, R. (2021). *Simple modelling approach using Modelica for microbial electrosynthesis. Proceedings of the 61st SIMS Conference on Simulation and Modelling SIMS 2020, September 22-24, Virtual, Finland,* 306–310. doi.org/10.3384/ecp20176306

List of other contributions

Article 7

Sivalingam, V., Dinamarca, C., Janka, E., Kukankov, S., Wang, S., & Bakke, R. (2020). Effect of Intermittent Aeration in a Hybrid Vertical Anaerobic Biofilm Reactor (HyVAB) for Reject Water Treatment. *Water*, *12*(4), 1151. doi.org/10.3390/w12041151

Article 8

Sivalingam, V., Dinamarca, C., Samarakoon, G., Winkler, D., & Bakke, R. (2020). Ammonium as a Carbon-Free Electron and Proton Source in Microbial Electrosynthesis Processes. *Sustainability*, *12*(8), 3081. doi.org/10.3390/su12083081

Article 9

Sivalingam, V., Samarakoon, G., Dinamarca, C. (2021). Moving Bed Biofilm Process in Activated Sludge Model 1 (ASM1) for Reject Water Treatment. Proceedings of the 62nd SIMS Conference on Simulation and Modelling SIMS 2021, September 21-23, Virtual, Finland.

Article 10

Tao, R., Sivalingam, V., Lin, L., Dinamarca, C., & Xin, G. (2022). *Enhancement of biogas production by integrating anaerobic digestion and pyrolysis. 30th* European Biomass *Conference & Exhibition 2022, May 9 – 22, France*: (Abstract accepted)

Article 11

Saroj, N., Samarakoon, G., Sivalingam, V., & Dinamarca, C. (2022). *Biofilm modelling for electrochemically mediated biogas upgrading:*

(Submitted on 11th of February 2022 to the *Proceedings of the 63rd SIMS Conference on Simulation and Modelling SIMS 2022, September 20-21, Norway)*

List of figures

Abbreviations

AC - Alternating Current

AD – Anaerobic Digestion

CCM – Closed Circuit Mode

CE - Columbic Efficiency

CH_4 - Methane

CO – Carbon monoxide

CO_2 – Carbon dioxide

COD – Chemical Oxygen Demand

CODH - Carbon Monoxide Dehydrogenase

CV – Cyclic Voltammetry

DC – Direct Current

DET - Direct Electron Transfer

EIS - Electrochemical Impedance Spectroscopy

EVs - Electric Vehicles

FT – Fischer Tropsch

H^+ - Hydrogen proton

H_2 – Hydrogen gas

HRT – Hydraulic Retention Time

ICE - Internal Combustion Engine

IDET - Indirect Electron Transfer

LSV – Linear Sweep Voltammetry

MBB – Moving Bed Biofilm

MBBR – Moving Bed Biofilm Reactor

MES – Microbial Electrosynthesis

N_2 – Nitrogen

NH_4^+ - Ammonium ion

O_2 – Oxygen gas

OCM – Open Circuit Mode

OH^- - Hydroxyl ion

Op-Amp - Operational Amplifier

p&e - Protons and Electrons

pH – Measure of hydrogen ion concentration

rpm – Revolutions per minute

sCOD – Soluble Chemical Oxygen Demand

SEM - Scanning Electron Microscopy

SHE – Standard Hydrogen Electrode

TS – Total Solids

UDC - Universal Dummy Cell

USN – University of South-Eastern Norway

VFAs – Volatile Fatty Acids

VS – Volatile Solids

WLP - Wood Ljungdahl pathway

WWTP – AD - Wastewater Treatment Plant Anaerobic Digester

WWTP – Wastewater Treatment Plant

° C – Degree Celsius

Ω – ohm

Table of contents

Part - I

1 Introduction – Literature review

Syngas fermentation and microbial electrosynthesis (MES) are studied here as two sustainable technologies for higher methane yields integrated as a single process unit. H_2 gas-liquid (GL) mass transfer limitation was addressed by elevating headspace pressure, and kinetic growth limitation was examined with high biomass density (MBBR) to increase syngas fermentation rate. Further, electrodes as biocatalysts were poised with different potentials to increase syngas consumption and acetic acid production, thus improving the overall syngas fermentation process.

The project objective follows general sustainable and clean fuel production guidelines by transforming CO_2 to methane using surplus electrical power.

1.1 Background

The current trend in CO_2 emissions has resulted in economic, social, and environmental imbalances (Allen et al., 2009; Friedlingstein et al., 2014; Gillett et al., 2013). Capturing and utilising CO_2 is one way of reducing its adverse effects while mitigating climate change. Climate action is one of the sustainable development goals (SDG) at the United Nations (UN) to confront these negative environmental consequences; SDG primarily focuses on carbon capture and utilisation (CCU) technology development. The 193 member countries of the UN espoused to work on the latest agenda (2030 Agenda) for the SDG. Reducing greenhouse gas emissions to keep the warming threshold below 2 °C compared to the pre-industrial period is the ultimate target of the climate action agenda (United Nations, Department of Economics and Social Affairs, n.d.).

Norway is among the 193 UN state members playing a vital role in implementing CO_2 emissions control measures that introduced a climate change act in 2017 to comply with the 2015 Paris agreement. The act aims to transform Norway into a low-emission society by 2050. The immediate action plan is to reduce greenhouse gas (GHG) emissions by at least 50 - 55 % by 2030 compared to the emission level measured in 1990, while achieving 90 - 95 % lower emission is the ultimate goal towards 2050 (LOVDATA, 2017).

Norway's transport sector accounts for 31 % of the national emissions. As 98 % of the country's electricity share comes from renewable energy sources (Norwegian Government, 2016), electrifying automobiles to reduce emissions is getting more attention. The government encourages people to move towards a sustainable transition in the mobility domain. Therefore, Norway holds the largest market share of the electric vehicle (EV) by phasing out the internal combustion engine (ICE) vehicles, mainly passenger cars. However, heavy transport still relies on fossil fuels.

Biogas is a clean biofuel produced from organic waste through anaerobic digestion (AD) that can significantly substitute the fossil-fuel demand in heavy vehicles. In June 2021, the Norwegian government declared that biogas should be treated equally to electricity and hydrogen (European Biogas Association (EBA), n.d.). In addition, the application process for financial support of the biogas vehicles is disentangled. Biogas-fuelled vehicles are considered zero-emission in all road tolls from January 2022 (EBA, n.d.). Even though governments encourage the use of biogas to phasedown the fossil fuel usage, the feedstock availability (Khan & Martin, 2016; Nevzorova & Kutcherov, 2019) for the biogas production and lower methane (CH_4) content appear as formidable hurdles (Angelidaki et al., 2018).

Usually, raw biogas consists of 50 – 70 % CH_4 and 30 – 50 % CO_2, emanating low calorific values, thereby demanding CO_2 removal or CH_4 concentration enhancement (Angelidaki et al., 2018). The CH_4 content needs to be upgraded above 97 % to consider biogas as biofuel (biomethane) (Angelidaki et al., 2019). The upgrading can be performed by removing CO_2 or converting it into CH_4.

Water and organic solvent scrubbing, cryogenic separation, membrane separation and pressure swing adsorption are the widely used CO_2 removal processes (Nguyen et al., 2021; Xie et al., 2020). However, those processes are energy-intensive, extortionate and cause indirect CO_2 emissions. Therefore, a bioelectrochemical technique called microbial electrosynthesis (MES, explained in section 1.3) is getting more attention as a sustainable strategy (Sonawane et al., 2021) for biogas upgradation, which converts CO_2 to CH_4. Since

98 % of the electricity acquired in Norway is from renewable sources, the MES that deploys renewable electricity becomes more promising in Norway towards sustainable biomethane production. Not only the CH_4 content but the MES integration can also accelerate hydrolysis, consequently enhancing CH_4 production yield (De Vrieze et al., 2018).

The critical function of the MES is to perform oxidation at the anode, which liberates both protons and electrons (p&e) to reduce CO_2 into CH_4 at the cathode. Water, ammonium, organics and sulphides are the common sources of p&e that undergo oxidation at the anode releases p&e. In addition, syngas is also considered as a promising gaseous substrate that can be utilised in the AD to enhance CH_4 quantity and content (Shah et al., 2017). Because it is a mixture of H_2, CO_2, and CO; therein, H_2 and CO act as electron sources/ reducing equivalents to convert CO_2 into valuable chemicals, while CO_2 and CO function as carbon sources.

Syngas is a product of waste valorisation processes such as pyrolysis, gasification, and combustion (Malico et al., 2019). Therefore, utilising it as a feedstock brings in dual benefits, thus enhancing CH_4 production as a green fuel and reducing the direct emission from waste valorisation processes, contributing to the overall climate action SDG.

Moreover, gasification of the digested sludge from AD becomes mandatory for existing biogas plants due to strict environmental restrictions for sludge disposal as fertilizer because the sludge is rich in microplastics and harmful chemicals which may get into foods (Nelabhotla et al., 2021). Therefore, utilising syngas and pyrolysis condensates derived from digestate gasification becomes vital for sustainable biogas production. Since H_2 availability is usually limited in the syngas mixture (Jack et al., 2019), it requires an auxiliary source of H_2 or other forms of reducing equivalents. Therefore, MES becomes attractive as a source of reducing equivalents in the form of either electrons or H_2 gas. The concept is graphically illustrated in Figure 1.1, where MES, AD and syngas fermentation are integrated.

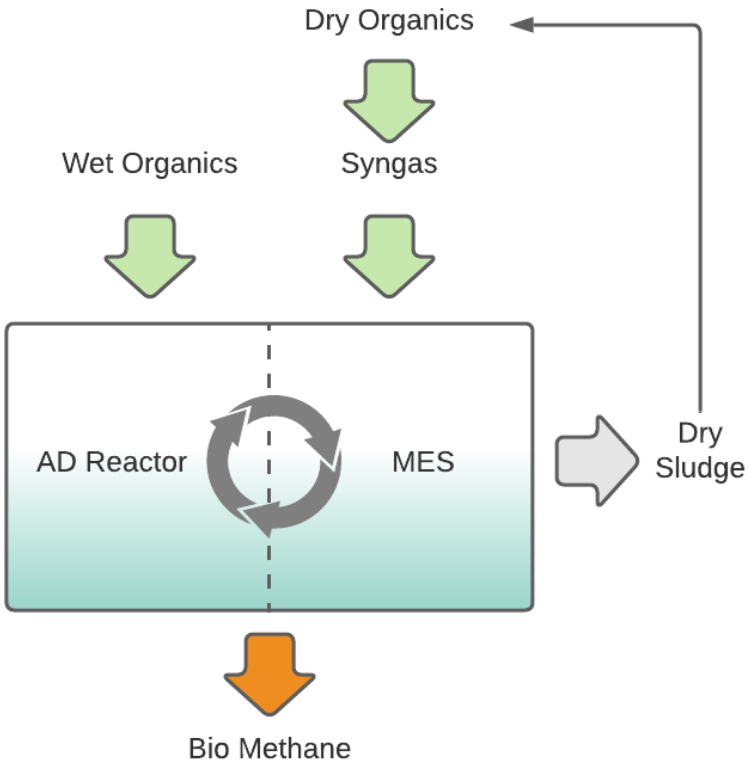

Figure 1.1: Integrated anaerobic digestion, syngas fermentation and MES.

Injecting syngas directly into the AD-reactor is not adequate to fulfil the bio CH_4 demand. The primary bottlenecks are inefficient gas-liquid (GL) mass transfer (Stoll et al., 2018; Van Hecke et al., 2019), slow growth rate of the autotrophic microorganisms which involved in the fermentation process (Grimalt-Alemany et al., 2018b; Regueira et al., 2018), lack of reducing power, propionic acid accumulation (Dinamarca, 2010) and CO toxicity (Ragsdale, 2004). These challenges have been well-known for decades and widely studied in different aspects (Drake, 2012; Phillips et al., 2017). The question is why there are no commercial biogas plants with an integrated syngas fermentation process. This research problem remains open and has received substantial interest. Moreover, applying the MES process to improve syngas fermentation remains unrevealed. Therefore, this thesis investigates various strategies to enhance syngas fermentation and the possibility of MES integration to overcome syngas fermentation challenges in the context of advancing the biogas production process.

1.2 Syngas fermentation

Syngas fermentation allows the transition of dried biomass and wastes into valuable chemicals without any advanced biomass pre-treatment. It is an alternative to the Fischer-Tropsch (FT) catalytic process that converts syngas into valuable, high-quality liquid fuels. Syngas fermentation is more gainful than FT because it requires no fixed CO: H_2 ratio and no need for higher temperature and inorganic catalysts (Liew et al., 2016).

The main product of syngas fermentation is acetate, which can be used as a precursor for biogas production, where it is converted into CH_4 and CO_2 through an acetoclastic heterotrophic pathway (Eq. 1.1). However, autotrophic microorganisms primarily perform the syngas fermentation (Debabov, 2021), referred to as homoacetogenesis (Eq. 1.2).

$$CH_3COOH \longrightarrow CH_4 + CO_2 \quad (1.1)$$

$$2CO_2 + 4H_2 \longrightarrow CH_3COOH + 2H_2O \quad (1.2)$$

H_2 is the prominent electron donor that produces the reducing equivalents through hydrogenase enzymes (Eq. 1.3) (Jack et al., 2019) to facilitate homoacetogenesis, while CO_2 is the carbon source. In addition, CO also provides reducing equivalents through carbon monoxide dehydrogenase enzymatic path (CODH) in biological water-gas shift reactions (Eq. 1.4) (Jack et al., 2019). The metabolic pathway of homoacetogenesis was discovered by Harland G. Wood and Lars G. Ljungdahl, therefore referred to as Wood Ljungdahl Pathway (WLP). Also, the WLP produces acetyl-CoA as the central intermediate, therefore named as an acetyl-CoA pathway.

$$H_2 \longrightarrow 2H^+ + 2e \quad (1.3)$$

$$CO + H_2O \longrightarrow CO_2 + 2H^+ + 2e \quad (1.4)$$

In the WLP, CO_2 is reduced to CO and formyl group; followed by several subsequent reduction stages, the formyl group is reduced to a methyl group. Eventually, the methyl group is merged with CO and co-enzymes to synthesize acetyl-CoA, converted to acetate. Since the WLP is extensively described in many articles (Bertsch & Müller, 2015; Drake,

2012; Wilkins & Atiyeh, 2011), a brief flow diagram is given in Figure 1.2, adapted from (Drake, 2012).

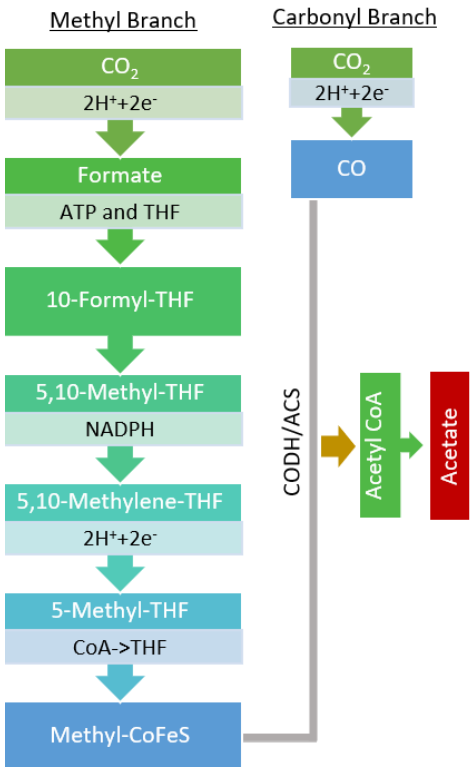

Figure 1.2: The WLP for acetate synthesis.

1.2.1 Importance of mixed culture syngas fermentation

Most syngas fermentation studies are performed on pure cultures to synthesise specific products (Demler & Weuster-Botz, 2011; Grimalt-Alemany et al., 2018a; Stoll et al., 2018). The pure microbial consortia require a sterile operation which is an energy-intense process; they are also less tolerant to variation in fermentation conditions, leading to a limited possibility for a scale-up. However, pure cultures have higher product selectivity than mixed cultures. The syngas fermentation as a carbon capture process into mixed culture anaerobic digestor provides an option to upgrade bio-methanation, where higher product selectivity is not the primary concern but the total VFAs synthesis. Therefore, in the present study, sludge from the local municipal wastewater treatment plant's anaerobic digester was used as the mixed culture fermentation medium. Such mixed cultures are locally available and efficiently utilised with less cost. This economic

perspective establishes more attention towards mixed culture fermentation in recent years, which will ease the scale-up process (Batlle-Vilanova et al., 2016), where captured carbon in the form of syngas is utilised to improve the biogas production. Different microbial strains in the mixed culture could offer efficient adaptation capacity, the possibility of co-fermentation with various substrates, and less sensitivity to syngas composition ratios (Drzyzga et al., 2015).

1.2.2 Gas transfer mechanisms

The low solubility of gaseous species in the syngas mixture is the main obstacle for an efficient fermentation. Lewis and Whitman explained the gas transfer phenomena across the gas-liquid interface for the first time (Lewis & Whiteman, 1924). Mass transfer from the gas phase to the liquid phase occurs through two different diffusion layers, thus stagnant gas and liquid films, where diffusion via liquid film is the key rate-limiting step. A brief graphical illustration of the two-film theory is illustrated in Figure 1.3.

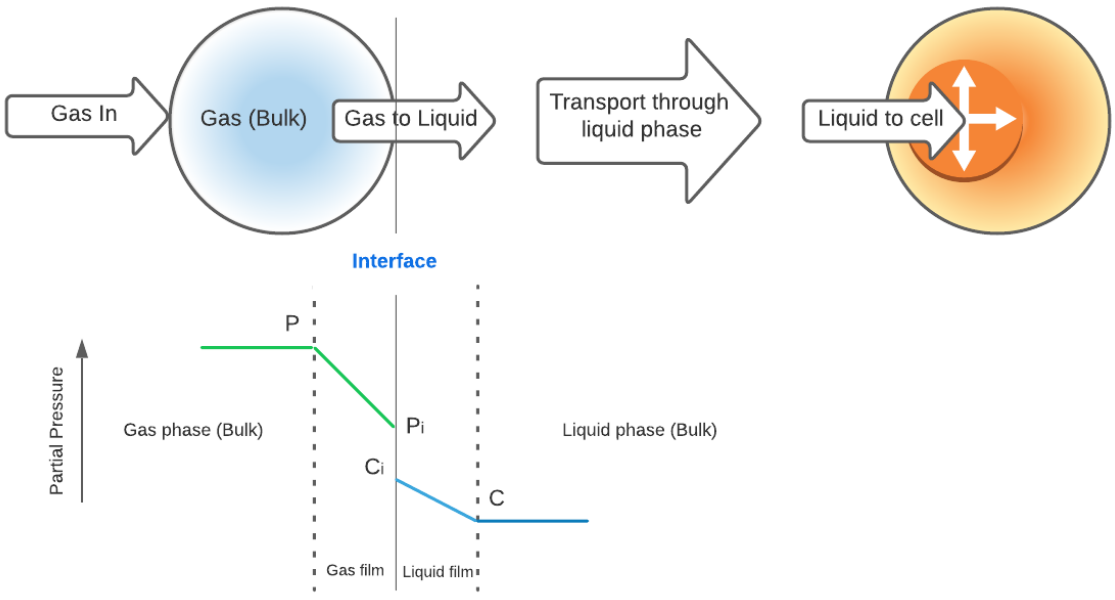

Figure 1.3: Simple sketch of two-film theory illustration.

After gas molecules are solubilised through the gas-liquid interface, they need to travel through many subsequent steps. i.e., diffuse from the liquid film to bulk liquid, bulk liquid

to the stagnant outer layer of the microbial cell, and diffuse through the membrane into the cell. Most of the cell membrane thickness varies between 6 to 9 nm. In a dense suspended culture, the cell concentration is usually around 1010 cell L^{-1} (Phillips et al., 2017), which provides an extremely high surface area for mass transfer. Eventually, the tiny membrane thickness and higher cell density make the diffusivity resistance negligible (Klasson et al., 1992; Phillips et al., 2017). Therefore, the dissolved gas is instantly consumed by the microorganisms.

The GL mass transfer limitation refers to the fact that the mass transfer rate is not adequate to cope with cell growth demand, resulting in inefficient fermentation. The quantity of the dissolved gas in the liquid medium is commensurate to that particular gas's partial pressure. The proportionality factor was contrived by William Henry, therefore named as Henry's law constant. The amount of gas transferred through the diffusion layer is directly proportional to the concentration difference between liquid film inter-face to bulk liquid (Stoll et al., 2018; Van Hecke et al., 2019). Since the H_2 has the lowest solubility from the syngas mixture (1.6 mg kg^{-1} water at 25 °C and 1 bar pressure), the solubility, pressure and temperature dependence are explained in the following working example.

1.2.2.1 H_2 solubility in water, pressure, and temperature dependence

According to Henry's law, elevating partial pressure of the H_2 can be an excellent approach to increase the solubility, and the dissolved concentration in the liquid medium (Phillips et al., 2017), explained in (Eq. 1.5). Subsequently, the H_2 molar transfer rate is presented in (Eq. 1.6), where only the physical GL mass transfer was considered (excluded the gas transport process in microbial cell).

$$C_{H_2} = y_{H_2} \frac{P_T}{H_{H_2}} \quad 1.5$$

$$-\frac{1}{V_L}\frac{dn_{H2}}{dt} = \frac{(k_L a)_{H_2}}{V_L}\left(C^*_{H_2} - C_{H_2}\right) \quad 1.6$$

Where C_{H_2} is the hydrogen concentration (mol L^{-1}) in the liquid medium. y_{H_2} is the hydrogen mole fraction in the gas phase. P_T is the total headspace pressure (atm) and H_{H_2} (atm mol^{-1} L) is Henry's law constant for H_2 gas. The hydrogen molar transfer rate is denoted as $\frac{dn_{H2}}{dt}$. V_L is the liquid volume. $\frac{(k_L a)_{H_2}}{V_L}$ V_L is the total liquid film mass transfer coefficient for hydrogen gas. The hydrogen gas concentration at the gas-liquid interface in equilibrium referred as $C^*_{H_2}$, while the concentration in the bulk liquid is denoted as C_{H_2}.

Increasing gas solubility by elevating partial pressure is always possible if it is considered as a physical process only. However, increasing dissolved H_2 tension and microorganisms' sensitivity to the partial pressure elevation (Abubackar et al., 2011) may adversely impact the microbial gas uptake rate.

As far as we know, no previous research has investigated over 10 bar H_2 (Van Hecke et al., 2019) partial pressure on mixed culture fermentation medium. Therefore, this thesis examines the impact of H_2 partial pressure up to 25 bar (Article 1).

Moreover, gas solubility also depends on temperature; it decreases with increasing temperature. However, H_2 solubility is less affected by temperature change than pressure; thus, solubility increases by 15 - 17 mg H_2/kg water by each bar increase in pressure (Figure 1.4). The Figure 1.4 depicts an approximate relationship between temperature (15 - 40 °C) and pressure (1- 40 bar) on H_2 gas solubility. These relationships are derived based on Van't Hoff and Henry's law equations, where temperature dependence on diffusion coefficients was not considered, partly compensating for the reduced solubility with increased temperature.

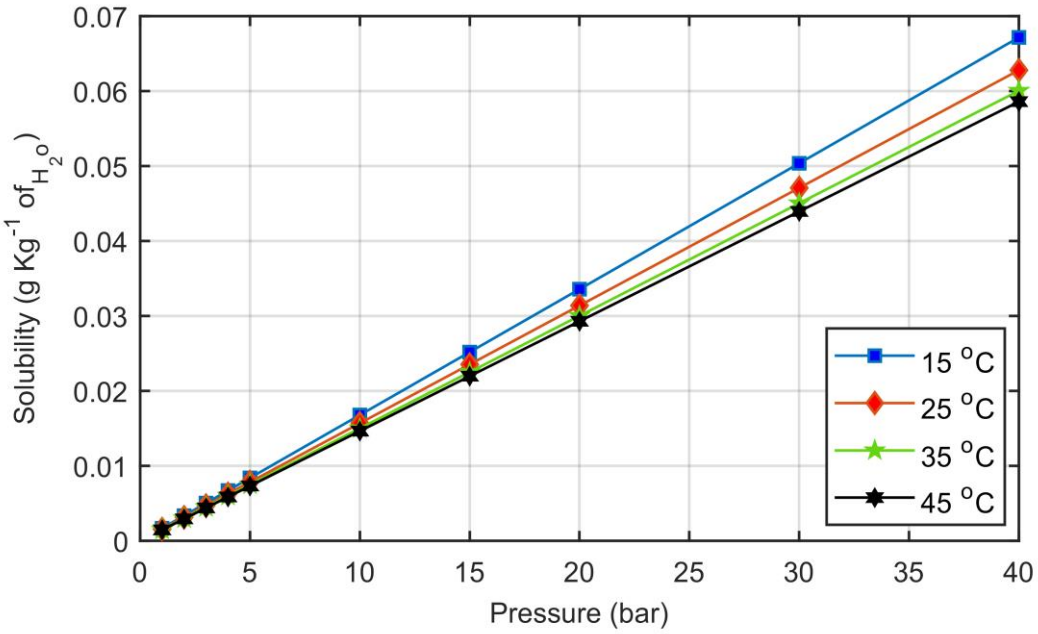

Figure 1.4: H_2 solubility in water, pressure, and temperature dependence.

1.2.3 Kinetic limitation in syngas fermentation

In addition to the GL mass transfer limitation, the kinetic-growth limitation is also a primary engineering bottleneck in syngas fermentation (Karekar et al., 2019; Regueira et al., 2018). The slow growth rate of homoacetogens kinetically limits the amount of available microorganisms in the fermentation medium to cope with dissolved gas.

Performing syngas fermentation into a biofilm reactor is one way of overcoming the kinetic-growth limitation by increasing the biomass abundance. Monolithic, hollow fibre membrane, rotating packed bed, and moving bed biofilm reactors (MBBR) are widely studied attached-growth biofilm mediated syngas fermentation reactors (Shen, 2013). MBBR is an excellent strategy that induces bacteria to grow inside the protective surface therein, densely assimilates to obtain higher cell density, thus compensating for the slow growth rate limitation. The bio carriers used in the MBBR are less dense than water, so it floats and gets agitated in the liquid medium, resulting in efficient GL mass transfer. In addition, the bio carriers can help to lower the hydraulic retention time (HRT), increase

the sludge retention time (SRT), and enhance the resistance to toxic substances (Tchobanoglous et al., 2014).

Robert Hickey patented the MBBR integrated syngas fermentation in 2009 (Hickey, 2009). That study was performed on monoculture *Clostridium ragsdalei* ATCC No. BAA-622 at 0.1 bar outlet pressure and 1 to 5 bar liquid pressure. However, MBBR integrated syngas fermentation is not widely implemented in the industries. Therefore this PhD project attempted to evaluate how a 15 bar elevated H_2 partial pressure, and MBBR can be integrated into a mixed culture medium to overcome GL mass transfer and kinetic limitations to accelerate the syngas fermentation process. The 15 bar is the optimum pressure for the particular fermentation medium collected from local WWTP-AD, adapted from article 1. The elevated H_2 pressure and mixed culture fermentation medium differentiate this research from Robert Hickey's patented study. As far as we know, this is the kind of first high-pressure syngas fermentation performed into a MBBR (Article 2).

It is well-proven that MBBR is an excellent habitant to form a biofilm consisting of slow-growing species (Gunes, 2021; Wang et al., 2019). Increasing the H_2 concentration by elevating the headspace pressure also increases the biomass concentration in the suspended broth. Therefore a working example explaining the relationship between H_2 partial pressure and biomass concentration in the suspended medium is presented in section 1.2.3.1.

1.2.3.1 Biomass estimation in different H_2 partial pressures

A stoichiometric equation, Eq. 1.7 (Sivalingam et al., 2022), which comprises biomass synthesis for homoacetogenic acetate production, is derived via the Rittmann & McCarty approach (Rittmann & McCarty, 2020). Ammonium is considered as the source of nitrogen, and the biomass composition is assumed to be $C_5H_7O_2N$. The homoacetogens are slow-growing microorganisms; thus, the maximal growth rate stays around 0.04 h^{-1} (Dinamarca, 2010). It is assumed that the rate is higher than the rate H_2 is being passed.

Therefore, dissolved H_2 as substrate does not limit the growth, then only increasing pressure enhances the consumption, resulting in improved biomass growth.

$$18.61\ CO_2 + 68.49\ H_2 + 15.62\ HCO_3^- + NH_4^+ \rightarrow 14.62\ CH_3COO^- + C_5H_7O_2N + 52.86\ H_2O \quad (1.7)$$

According to (Eq. 1.7), one mole of dissolved H_2 produces 0.015 mol of biomass (1.650 g). The reactor volume is assumed as 1 m^3, and the density of the fermentation medium is 1 g mL^{-1}. Based on these assumptions and the H_2 gas solubility presented in Figure 1.4, the amount of dissolved H_2 at 25 °C at a partial pressure range from 1 to 40 bar is quantified. Then the dissolved H_2 is corroborated to Eq. 1.7 to estimate the synthesised biomass. The results are presented in Figure 1.5 shows that biomass synthesis increased with pressure; the synergic effect of high pressure and biofilm carriers may clearly have an impact, improving syngas fermentation.

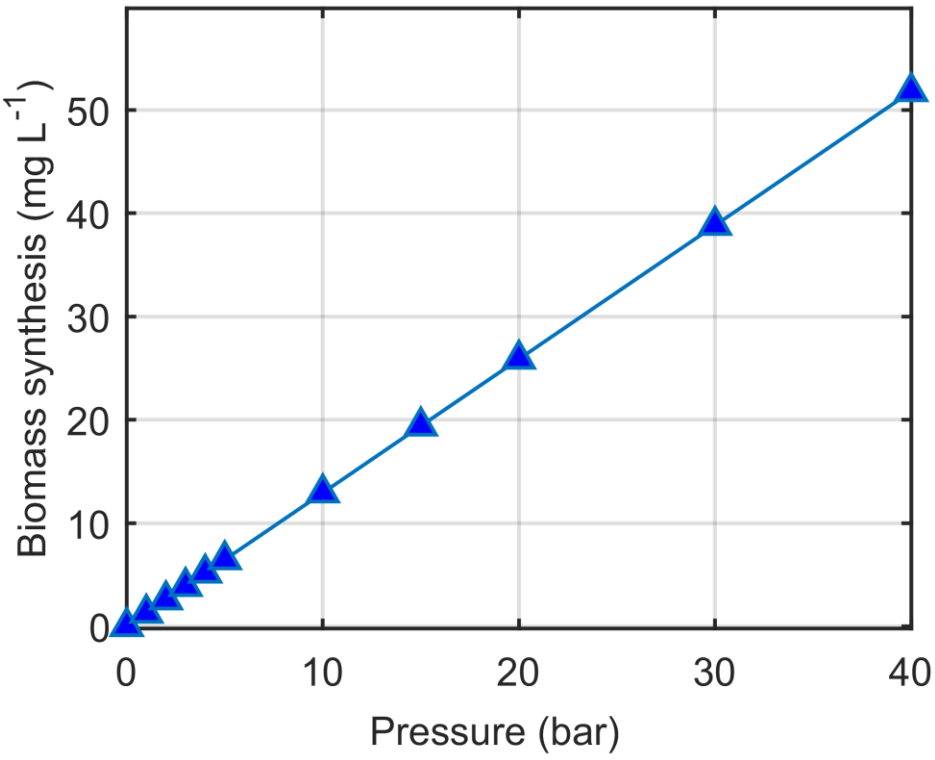

Figure 1.5: Biomass estimation in different H_2 partial pressures.

1.2.4 Impact of temperature on syngas fermentation

In syngas fermentation, temperature is a crucial factor that primarily affects both gas solubility and fermentation growth kinetics. Both factors show antagonistic behaviour; thus, a rise in temperature decreases the gas solubility while increasing the growth rate. Therefore, it needs to be optimized carefully. However, optimizing temperature is not in the scope of this study; instead, examining different process integrations is the major scope. All the experimental studies were performed at room temperature, and optimization is strongly recommended for future studies.

1.2.5 CO inhibition in syngas fermentation

The solubility of CO is about 60 times lower than CO_2, while the H_2 solubility is ca. 1050 times lower. Elevating headspace pressure to enhance the gas solubility strategy does not work on CO as it works on H_2 because higher CO concentration inhibits the syngas fermentation metabolic pathway (Sobieraj et al., 2022).

The carboxidotrophic species can oxidize CO for cell growth and energy conservation, resulting in acetate, butyrate, ethanol and butanol synthesis (Esquivel-Elizondo et al., 2017). The product type depends on the microbial communities present in the fermentation medium. Those products are synthesised via either direct CO utilisation (Eq. 1.8) or CO conversion into H_2 and CO_2 through water gas shift reaction (Eq. 1.4) (Esquivel-Elizondo et al., 2017). However, the tolerance limit to CO concentration is minimal (Phillips et al., 2017); therefore, elevating partial pressure alone is not always an attractive strategy to enhance the CO solubility and utilisation.

$$4CO + 2H_2O \longrightarrow CH_3COOH + 2CO_2 \qquad 1.8$$

CO consists of triple bonds (C≡O), forms low valent complexes with metal sites of the enzymes involved in WLP. Thus inhibits the metabolic process (Ragsdale, 2004). Moreover, CO fermentation has another hurdle in syngas fermentation. That one mole of CO conversion into acetate produces two moles of CO_2 (Eq. 1.8). The extra CO_2 liberation demands more reducing equivalents, generally H_2, from the syngas mixture. Since H_2 availability in the syngas mixture is limited, it requires additional reducing power.

MES integration plays an essential role in providing extra electrons/H_2 through anodic oxidation of water, ammonium, organics, and sulphides in the fermentation medium (Bian et al., 2020; Sivalingam et al., 2020).

MES has been widely studied to convert CO_2 to CH_4 and VFAs in biogas reactors (Aryal, 2017; Aryal et al., 2022; Nelabhotla & Dinamarca, 2018). However, there are no detailed studies about utilising MES to overcome the syngas fermentation bottlenecks. Therefore, this project aims to develop a fundamental framework for syngas fermentation and MES integration as a single process unit. The impact of MES integration on the acetic acid synthesis and H_2 gas uptake into a homoacetogenic medium is mainly investigated in article 3. Subsequently, articles 4 and 5 scrutinize the lowest benchmark potentials for the electrochemically mediated homoacetogenesis and CO rich syngas fermentation in the context of improving acetic acid synthesis.

1.3 Microbial electrosynthesis

Microbial electrosynthesis (MES) is a platform where renewable electricity is used to control the reduction potentials at the cathode. The particular potential favours electroactive microbial culture development as biofilm, which uses CO_2 and electrons from the cathode to synthesize reduced carbon compounds such as CH_4 and acetate (Aryal, 2017; Nelabhotla, 2020). This biocatalytic process requires significantly lower energy input to drive the electrochemical reactions, allowing H^+ and electrons to overcome the energy barriers and form H_2, CH_4, and other reduced chemicals. The required potential (~ 0.2 V) (Varanasi & Das, 2020) is far less than traditional electrolysis processes (> 1.2 V) (Rousseau et al., 2020), and the biocatalysts are self-replicating; thus, the MES system becomes as a sustainable solution. Moreover, MES does not release hazardous effluents to the environment, adding value to potential usage (Xiao et al., 2020). A schematic diagram of the MES process is presented in Figure 1.6, adapted from (Katuri et al., 2018) with permission from John Wiley and Sons, publisher.

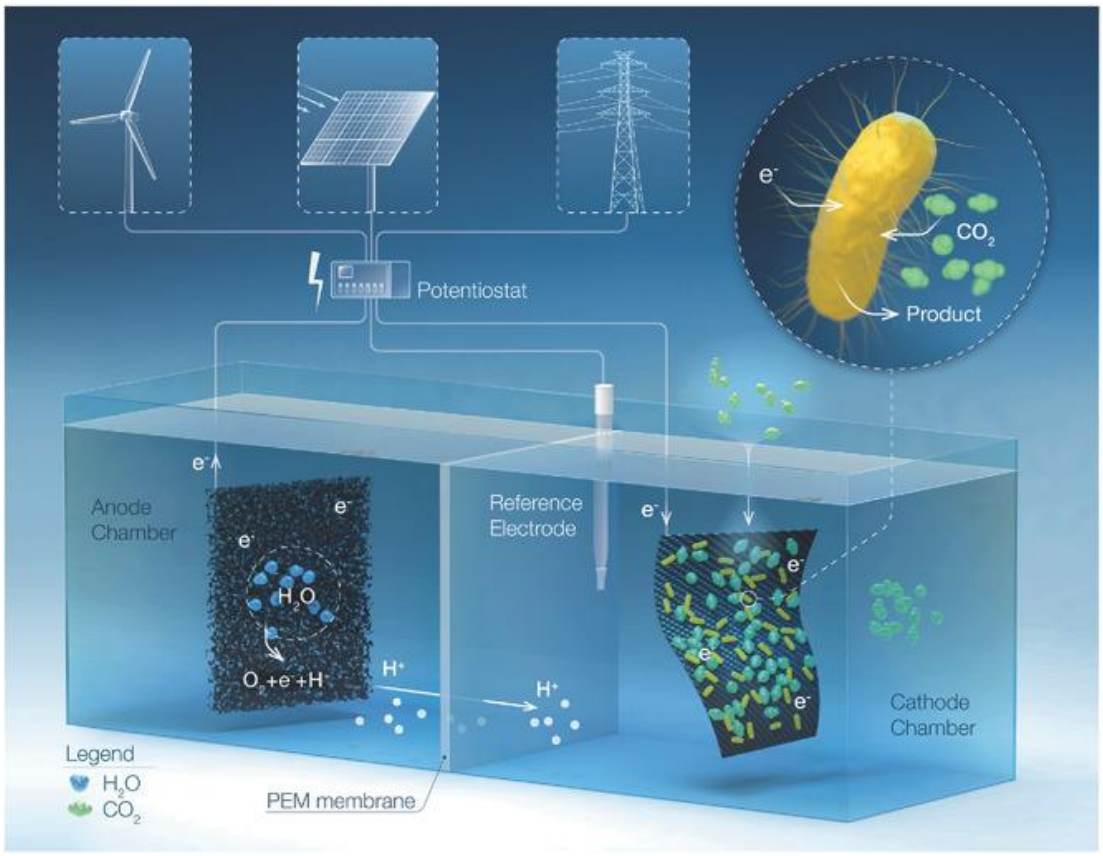

Figure 1.6: MES Schematic diagram (Katuri et al., 2018).

The MES technology is still under development, not beyond a few pilot-level plants worldwide. The primary reasons are the low production rate (Aryal, 2017) and large capital investments for scale-up. Therefore, numerous research is going on regarding production rate enhancement (Geppert et al., 2016; Nelabhotla & Dinamarca, 2018; Omidi et al., 2021). Besides, the MES potential is being investigated to solve many other environmental challenges, such as bioremediation, wastewater treatment and product recovery (Puig et al., 2021). This PhD study scrutinises how MES can help to overcome syngas fermentation limitations. Mainly, the impact of reducing power on acetate synthesis and GL mass transfer are investigated.

In the MES process, anodic oxidation of water (Eq. 1.9), organics (Eq. 1.10), ammonium (Eq. 1.11), and sulfides (Eqs. 1.12 and 1.13) are the common sources of protons and electrons (Bian et al., 2020; Katuri et al., 2019; Sivalingam et al., 2022). The electrons are pumped to the cathode by potentiostats. Protons migrate to the cathode through the

fermentation medium in a single-chamber reactor setup and through a proton permeable membrane in a dual-chamber setup (Wang et al., 2021). The electrons that arrive at the cathode follow two primary extracellular electron transfer mechanisms: direct and indirect.

$$4H_2O \rightarrow 2O_2 + 8H^+ + 8e^- \quad 1.9$$

$$C_nH_{2n+1} - COOH + 2nH_2O \rightarrow (n+1)CO_2 + (6n+2)H^+ + (6n+2)e^- \quad 1.10$$

$$2NH_4^+ \rightarrow N_2 + 8H^+ + 6e^- \quad 1.11$$

$$HS^- \rightarrow S^0_{(s)} + H^+ + 2e^- \quad 1.12$$

$$HS^- + 4H_2O \rightarrow SO_4^{2-} + 9H^+ + 8e^- \quad 1.13$$

Some companies are already in business improving methane yield through syngas fermentation and MES. For example, WAI Environmental Solutions As, Norway has a technology called Synolys, which focuses on double the biogas yield by incorporating pyrolysis products such as syngas and condensate into anaerobic digester (WAI Environmental Solutions, n.d.). Electrochaea GmbH, Germany, is another example that uses renewable electricity to produce hydrogen through water electrolysis and feed that to methanogenic archaea medium and CO_2 to synthesise pipeline grade methane (Electrochaea GmbH, n.d.).

1.3.1 Electron transfer mechanisms in MES

The direct electron transfer (DET) occurs through direct contact between the electrode surface and the electroactive microorganism's cytochrome c membrane proteins at the outer membrane. Besides, extracellular conductive connection pili/nanowires also accounts for the DET (Santoro et al., 2017). Equations 1.14 and 1.15 illustrate the way of CH_4 and acetate synthesis via DET. The indirect electron transfer (IDET) happens through mediators. The electrons available at the cathode reduce H^+ into H_2 (Eq. 1.16); subsequently, the molecular hydrogen reduces CO_2 into either CH_4 (Eq. 1.17) or acetate (Eq. 1.2). The equations 1.17 and 1.2 are identical to hydrogenotrophic methanogenesis and homoacetogenesis (Agler et al., 2011).

$$CO_2 + 8e^- + 8H^+ \rightarrow CH_4 + 2H_2O \quad 1.14$$

$$2CO_2 + 8e^- + 8H^+ \rightarrow CH_3COOH + 2H_2O \quad 1.15$$

$$4H^+ + 4e^- \rightarrow 2H_2 \quad 1.16$$

$$4H_2 + CO_2 \rightarrow CH_4 + 2H_2O \quad 1.17$$

1.3.2 A comparison - Single and dual chamber MES reactor

The MES is performed in two ways: single and dual chamber setups. Anode and cathode are placed into a single compartment at the single-chamber setup, while a proton permeable membrane separates the anodic and cathodic parts in the dual-chamber configuration.

Most MES studies have been performed in dual chamber (Zou et al., 2021) to ensure that the fermentation medium remains anaerobic because the water oxidation at the anode liberates O_2, adversely impacting the AD processes. In contrast, it has been proved that AD could withstand a significant amount of oxygen, and microaeration improves the reactor performance by a slight increase in the redox potential that in turn increases hydrolysis (Botheju & Bakke, 2011), resulting in higher methane yield. The AD effluent consists of reduced compounds that account for 40 – 60 % of total energy potential that can be retrieved through MES. Using a membrane in a dual-chamber setup brings in extra capital and operational costs. In addition, the process becomes inefficient due to enhancing resistance across the digestion medium (Tharak & Venkata Mohan, 2021).

The organics (VFAs) oxidation at the anode in a single-chamber configuration is a challenge because it diminishes the product yield and liberates CO_2 (Eq. 1.10) as a by-product, bringing down the net carbon capture efficiency. However, when syngas fermentation is performed into a single-chamber MES reactor, the organic oxidation at the anode become useful to some extent. Because syngas fermentation induces VFAs accumulation in the AD could negatively affect the AD process by decreasing pH (this depending on their concentration and alkalinity). Therefore, the anodic oxidation could

help to maintain certain VFAs concentrations in the reactor and control the product formation (Sivalingam et al., 2021a).

The dual-chamber configuration individually favours the anodic and cathodic culture enhancement. However, the membrane hinders the H^+ migration from anode to cathode, resulting in H^+ accumulation in the anodic chamber; consequently, pH gradient evolved (Koók et al., 2019), disfavouring microbial enrichment and increasing the charge transfer resistance in the electrolyte/ fermentation medium (Wang et al., 2021).

Reference

Abubackar, H. N., Veiga, M. C., & Kennes, C. (2011). Biological conversion of carbon monoxide: Rich syngas or waste gases to bioethanol. *Biofuels, Bioproducts and Biorefining*, *5*(1), 93–114.

Agler, M. T., Wrenn, B. A., Zinder, S. H., & Angenent, L. T. (2011). Waste to bioproduct conversion with undefined mixed cultures: The carboxylate platform. *Trends in Biotechnology*, *29*(2), 70–78.

Allen, M. R., Frame, D. J., Huntingford, C., Jones, C. D., Lowe, J. A., Meinshausen, M., & Meinshausen, N. (2009). Warming caused by cumulative carbon emissions towards the trillionth tonne. *Nature*, *458*(7242), 1163–1166.

Angelidaki, I., Treu, L., Tsapekos, P., Luo, G., Campanaro, S., Wenzel, H., & Kougias, P. G. (2018). Biogas upgrading and utilisation: Current status and perspectives. *Biotechnology Advances*, *36*(2), 452–466.

Angelidaki, I., Xie, L., Luo, G., Zhang, Y., Oechsner, H., Lemmer, A., Munoz, R., & Kougias, P. G. (2019). Chapter 33 - Biogas Upgrading: Current and Emerging Technologies. In A. Pandey, C. Larroche, C.-G. Dussap, E. Gnansounou, S. K. Khanal, & S. Ricke (Eds.), *Biofuels: Alternative Feedstocks and Conversion Processes for the Production of Liquid and Gaseous Biofuels (Second Edition)* (pp. 817–843). Academic Press.

Aryal, N. (2017). *Microbial electrosynthesis for acetate production from carbon dioxide: Innovative biocatalysts leading to enhanced performance*. [Doctoral dissertation, Technical University of Denmark]. Novo Nordisk Foundation Center for Biosustainability.

Aryal, N., Zhang, Y., Bajracharya, S., Pant, D., & Chen, X. (2022). Microbial electrochemical approaches of carbon dioxide utilisation for biogas upgrading. *Chemosphere*, *291*, 132843.

Batlle-Vilanova, P., Puig, S., Gonzalez-Olmos, R., Balaguer, M. D., & Colprim, J. (2016). Continuous acetate production through microbial electrosynthesis from CO2 with microbial mixed culture. *Journal of Chemical Technology & Biotechnology*, *91*(4), 921–927.

Bertsch, J., & Müller, V. (2015). Bioenergetic constraints for conversion of syngas to biofuels in acetogenic bacteria. *Biotechnology for Biofuels*, *8*(1), 210.

Bian, B., Bajracharya, S., Xu, J., Pant, D., & Saikaly, P. E. (2020). Microbial electrosynthesis from CO2: Challenges, opportunities, and perspectives in the context of circular bioeconomy. *Bioresource Technology*, 122863.

Botheju, D., & Bakke, R. (2011). Oxygen effects in anaerobic digestion-a review. *The Open Waste Management Journal, 4,* 1-19.

De Vrieze, J., Arends, J. B. A., Verbeeck, K., Gildemyn, S., & Rabaey, K. (2018). Interfacing anaerobic digestion with (bio)electrochemical systems: Potentials and challenges. *Water Research*, *146*, 244–255.

Debabov, V. G. (2021). Acetogens: Biochemistry, Bioenergetics, Genetics, and Biotechnological Potential. *Microbiology*, *90*(3), 273–297.

Demler, M., & Weuster-Botz, D. (2011). Reaction engineering analysis of hydrogenotrophic production of acetic acid by Acetobacterium woodii. *Biotechnology and Bioengineering*, *108*(2), 470–474.

Dinamarca, C. (2010). *Homoacetogenic H2 Consumption In Fermentative Hydrogen Production Processes*. [Doctoral dissertation, Norwegian University of Science and Technology].

Drake, H. L. (2012). *Acetogenesis*. Springer Science & Business Media.

Drzyzga, O., Revelles, O., Durante-Rodríguez, G., Díaz, E., García, J. L., & Prieto, A. (2015). New challenges for syngas fermentation: Towards production of biopolymers. *Journal of Chemical Technology and Biotechnology*, *90*(10), 1735–1751.

Electrochaea GmbH. (n.d.). *Power-to-Gas Energy Storage*. Retrieved March 11, 2022, from https://www.electrochaea.com/technology/

European Biogas Association. (n.d.). *Norway: Biogas equal to electricity and hydrogen in all policies*. Retrieved December 2, 2021, from https://www.europeanbiogas.eu/norway-biogas-equal-to-electricity-and-hydrogen-in-all-policies/

Friedlingstein, P., Andrew, R. M., Rogelj, J., Peters, G. P., Canadell, J. G., Knutti, R., Luderer, G., Raupach, M. R., Schaeffer, M., van Vuuren, D. P., & Le Quéré, C. (2014). Persistent growth of CO2 emissions and implications for reaching climate targets. *Nature Geoscience*, *7*(10), 709–715.

Geppert, F., Liu, D., van Eerten-Jansen, M., Weidner, E., Buisman, C., & ter Heijne, A. (2016). Bioelectrochemical Power-to-Gas: State of the Art and Future Perspectives. *Trends in Biotechnology*, *34*(11), 879–894.

Gillett, N. P., Arora, V. K., Matthews, D., & Allen, M. R. (2013). Constraining the Ratio of Global Warming to Cumulative CO2 Emissions Using CMIP5 Simulations. *Journal of Climate*, *26*(18), 6844–6858.

Grimalt-Alemany, A., Łężyk, M., Lange, L., Skiadas, I. V., & Gavala, H. N. (2018a). Enrichment of syngas-converting mixed microbial consortia for ethanol production and thermodynamics-based design of enrichment strategies. *Biotechnology for Biofuels*, *11*(1), 1–22.

Grimalt-Alemany, A., Skiadas, I. V., & Gavala, H. N. (2018b). Syngas biomethanation: State-of-the-art review and perspectives. *Biofuels, Bioproducts and Biorefining*, *12*(1), 139–158.

Gunes, B. (2021). A critical review on biofilm-based reactor systems for enhanced syngas fermentation processes. *Renewable and Sustainable Energy Reviews*, *143*, 110950.

He, Z., & Mansfeld, F. (2009). Exploring the use of electrochemical impedance spectroscopy (EIS) in microbial fuel cell studies. *Energy & Environmental Science*, *2*(2), 215–219.

Hickey, R. (2009). *Moving bed biofilm reactor (mbbr) system for conversion of syngas components to liquid products* (United States Patent No. US20090035848A1). https://patents.google.com/patent/US20090035848A1/en

Jack, J., Lo, J., Maness, P.-C., & Ren, Z. J. (2019). Directing Clostridium ljungdahlii fermentation products via hydrogen to carbon monoxide ratio in syngas. *Biomass and Bioenergy*, *124*, 95–101.

Karekar, S. C., Srinivas, K., & Ahring, B. K. (2019). Kinetic Study on Heterotrophic Growth of Acetobacterium woodii on Lignocellulosic Substrates for Acetic Acid Production. *Fermentation*, *5*(1), 17.

Katuri, K. P., Ali, M., & Saikaly, P. E. (2019). The role of microbial electrolysis cell in urban wastewater treatment: Integration options, challenges, and prospects. *Current Opinion in Biotechnology*, *57*, 101–110.

Katuri, K. P., Kalathil, S., Ragab, A., Bian, B., Alqahtani, M. F., Pant, D., & Saikaly, P. E. (2018). Dual-function electrocatalytic and macroporous hollow-fiber cathode for converting waste streams to valuable resources using microbial electrochemical systems. *Advanced Materials*, *30*(26), 1707072.

Khan, E. U., & Martin, A. R. (2016). Review of biogas digester technology in rural Bangladesh. *Renewable and Sustainable Energy Reviews*, *62*, 247–259.

Klasson, K. T., Ackerson, C. M. D., Clausen, E. C., & Gaddy, J. L. (1992). Biological conversion of synthesis gas into fuels. *International Journal of Hydrogen Energy*, *17*(4), 281–288.

Koók, L., Kaufer, B., Bakonyi, P., Rózsenberszki, T., Rivera, I., Buitrón, G., Bélafi-Bakó, K., & Nemestóthy, N. (2019). Supported ionic liquid membrane based on [bmim][PF6] can be a promising separator to replace Nafion in microbial fuel cells and improve energy recovery: A comparative process evaluation. *Journal of Membrane Science*, *570–571*, 215–225.

Lewis, W., K., & Whiteman, W., C. (1924). Principal of gas adsorption. *Industrial & Engineering Chemistry, 16, 1215-1221*

Liew, F., Martin, M. E., Tappel, R. C., Heijstra, B. D., Mihalcea, C., & Köpke, M. (2016). Gas Fermentation—A Flexible Platform for Commercial Scale Production of Low-Carbon-Fuels and Chemicals from Waste and Renewable Feedstocks. *Frontiers in Microbiology*, *7*.

LOVDATA. (2017). *Act relating to Norway's climate targets (Climate Change Act).* https://lovdata.no/dokument/NLE/lov/2017-06-16-60

Malico, I., Nepomuceno Pereira, R., Gonçalves, A. C., & Sousa, A. M. O. (2019). Current status and future perspectives for energy production from solid biomass in the European industry. *Renewable and Sustainable Energy Reviews*, *112*, 960–977.

Nelabhotla, A. B. T. (2020). *Electrochemical Unit Integration with Biogas Production Processes* (Publication No. 62). [Doctoral dissertation, University of South-Eastern Norway].

Nelabhotla, A. B. T., & Dinamarca, C. (2018). Electrochemically mediated CO2 reduction for bio-methane production: A review. *Reviews in Environmental Science and Bio/Technology*, *17*(3), 531–551.

Nelabhotla, A. B. T., Pant, D., & Dinamarca, C. (2021). Chapter 8—Power-to-gas for methanation. In N. Aryal, L. D. Mørck Ottosen, M. V. Wegener Kofoed, & D. Pant (Eds.), *Emerging Technologies and Biological Systems for Biogas Upgrading* (pp. 187–221). Academic Press.

Nevzorova, T., & Kutcherov, V. (2019). Barriers to the wider implementation of biogas as a source of energy: A state-of-the-art review. *Energy Strategy Reviews*, *26*, 100414.

Nguyen, L. N., Kumar, J., Vu, M. T., Mohammed, J. A. H., Pathak, N., Commault, A. S., Sutherland, D., Zdarta, J., Tyagi, V. K., & Nghiem, L. D. (2021). Biomethane production from anaerobic co-digestion at wastewater treatment plants: A critical review on development and innovations in biogas upgrading techniques. *Science of The Total Environment*, *765*, 142753.

Norwegian Government (2016, May 11). *Renewable energy production in Norway*. https://www.regjeringen.no/en/topics/energy/renewable-energy/renewable-energy-production-in-norway/id2343462/

Omidi, M., Mashkour, M., Biswas, J. K., Garlapati, V. K., Singh, L., Rahimnejad, M., & Pant, D. (2021). From Electricity to Products: Recent Updates on Microbial Electrosynthesis (MES). *Topics in Catalysis*.

Phillips, J. R., Huhnke, R. L., & Atiyeh, H. K. (2017). Syngas Fermentation: A Microbial Conversion Process of Gaseous Substrates to Various Products. *Fermentation*, *3*(2), 28.

Puig, S., Jourdin, L., & Kalathil, S. (2021). Editorial: Microbial Electrogenesis, Microbial Electrosynthesis, and Electro-bioremediation. *Frontiers in Microbiology*, *12*, 2636.

Ragsdale, S. W. (2004). Life with carbon monoxide. *Critical Reviews in Biochemistry and Molecular Biology*, *39*(3), 165–195.

Regueira, A., González-Cabaleiro, R., Ofiţeru, I. D., Rodríguez, J., & Lema, J. M. (2018). Electron bifurcation mechanism and homoacetogenesis explain products yields in mixed culture anaerobic fermentations. *Water Research*, *141*, 349–356.

Rittmann, B. E., & McCarty, P. L. (2020). *Environmental Biotechnology: Principles and Applications, Second Edition*. McGraw-Hill Education.

Rousseau, R., Etcheverry, L., Roubaud, E., Basséguy, R., Délia, M.-L., & Bergel, A. (2020). Microbial electrolysis cell (MEC): Strengths, weaknesses and research needs from electrochemical engineering standpoint. *Applied Energy*, *257*, 113938.

Santoro, C., Arbizzani, C., Erable, B., & Ieropoulos, I. (2017). Microbial fuel cells: From fundamentals to applications. A review. *Journal of Power Sources*, *356*, 225–244.

Shah, S., Bergland, W. H., & Bakke, R. (2017). *Methane from Syngas by Anaerobic Digestion*. Presented at the Proceedings of the 58th Conference on Simulation and Modelling (SIMS 58) Reykjavik, Iceland, September 25th – 27th, 2017.

Shen, Y. (2013). *Attached-growth bioreactors for syngas fermentation to biofuel.* [Doctoral dissertation, Iowa State University]. Digital Repository.

Sivalingam, V., Ahmadi, V., Babafemi, O., & Dinamarca, C. (2021). Integrating Syngas Fermentation into a Single-Cell Microbial Electrosynthesis (MES) Reactor. *Catalysts*, *11*(1), 40.

Sivalingam, V., Dinamarca, C., Samarakoon, G., Winkler, D., & Bakke, R. (2020). Ammonium as a Carbon-Free Electron and Proton Source in Microbial Electrosynthesis Processes. *Sustainability*, *12*(8), 3081.

Sivalingam, V., Parhizkarabyaneh, P., Winkler, D., Lu, P., Haugen, T., Wentzel, A., & Dinamarca, C. (2022). Impact of electrochemical reducing power on homoacetogenesis. *Bioresource Technology*, *345*, 126512.

Sobieraj, K. N., Stegenta-Dąbrowska, S., Luo, G., Koziel, J. A., & Białowiec, A. (2022). Carbon Monoxide Fate in the Environment as an Inspiration for Biorefinery Industry: A Review. *Frontiers in Environmental Science*, *10*, 3389.

Sonawane, J. M., Gupta, S., & Pant, D. (2021). Microbial electrosynthesis for bio-based production using renewable electricity. In *Electrochemistry* (pp. 130–177). Royal Society of Chemistry.

Stoll, I., Herbig, S., Zwick, M., Boukis, N., Sauer, J., Neumann, A., & Oswald, F. (2018). Fermentation of H2 and CO2 with Clostridium ljungdahlii at Elevated Process Pressure–First Experimental Results. *Chemical Engineering Transactions*, *64*, 151–156.

Tchobanoglous, G., Burton, F. L., Stensel, H. D., & Metcalf & Eddy (Boston). (2014). *Wastewater engineering: Treatment and resource recovery*. McGraw-Hill Higher Education.

Tharak, A., & Venkata Mohan, S. (2021). Electrotrophy of biocathodes regulates microbial-electro-catalyzation of CO2 to fatty acids in single chambered system. *Bioresource Technology*, *320*, 124272.

United Nations, Department of Economics and Social Affairs. (n.d). *The 17 Goals of Sustainable Development*. Retrieved December 2, 2021, from https://sdgs.un.org/goals

Van Hecke, W., Bockrath, R., & De Wever, H. (2019). Effects of moderately elevated pressure on gas fermentation processes. *Bioresource Technology*, *293*, 122129.

Varanasi, J. L., & Das, D. (2020). Maximizing biohydrogen production from water hyacinth by coupling dark fermentation and electrohydrogenesis. *International Journal of Hydrogen Energy*, *45*(8), 5227–5238.

WAI Environmental Solutions. (n.d.). *Synolys - Double biomethane yield in the most carbon negative way.* Retrieved December 20, 2021, from https://waies.no/solutions/

Wang, H., Du, H., Zeng, S., Pan, X., Cheng, H., Liu, L., & Luo, F. (2021). Explore the difference between the single-chamber and dual-chamber microbial electrosynthesis for biogas production performance. *Bioelectrochemistry*, *138*, 107726.

Wang, S., Parajuli, S., Sivalingam, V., & Bakke, R. (2019). Biofilm in Moving Bed Biofilm Process for Wastewater Treatment. *Bacterial Biofilms*.

Wilkins, M. R., & Atiyeh, H. K. (2011). Microbial production of ethanol from carbon monoxide. *Current Opinion in Biotechnology*, *22*(3), 326–330.

Xiao, S., Fu, Q., Xiong, K., Li, Z., Li, J., Zhang, L., Liao, Q., & Zhu, X. (2020). Parametric study of biocathodes in microbial electrosynthesis for CO2 reduction to CH4 with a direct electron transfer pathway. *Renewable Energy*, *162*, 438–446.

Xie, L., Xu, J., Zhang, Y., & He, Y. (2020). Chapter Seven—Biogas upgrading. In Y. Li & S. K. Khanal (Eds.), *Advances in Bioenergy* (Vol. 5, pp. 309–344). Elsevier.

Zou, R., Hasanzadeh, A., Khataee, A., Yang, X., Xu, M., Angelidaki, I., & Zhang, Y. (2021). Scaling-up of microbial electrosynthesis with multiple electrodes for in situ production of hydrogen peroxide. *IScience*, *24*(2), 102094.

2 Process Integration – Challenges and Perspectives

Injecting syngas directly to the anaerobic digester has several bottlenecks. Therefore, it is performed into a separate unit and connected to the main anaerobic digestor, thus increasing the methane yield. Utilising the MES unit to improve syngas fermentation is not much studied. However, the MES unit has been studied to upgrade the methane content in the biogas reactor. Annexing the MES unit into the AD recycle line or the reject water loop proved to be an efficient integration process (Nelabhotla, 2020). Therefore, this PhD work focuses on combining syngas fermentation into a MES unit that is already attached to the recycle loop of the AD reactor. The conceptual diagram is presented in Figure 2.1. In addition, the effect of elevated pressure on syngas fermentation and moving bed biofilm integration were studied. This chapter explains the challenges associated with direct syngas fermentation into a biogas reactor and the significance of integrating into MES.

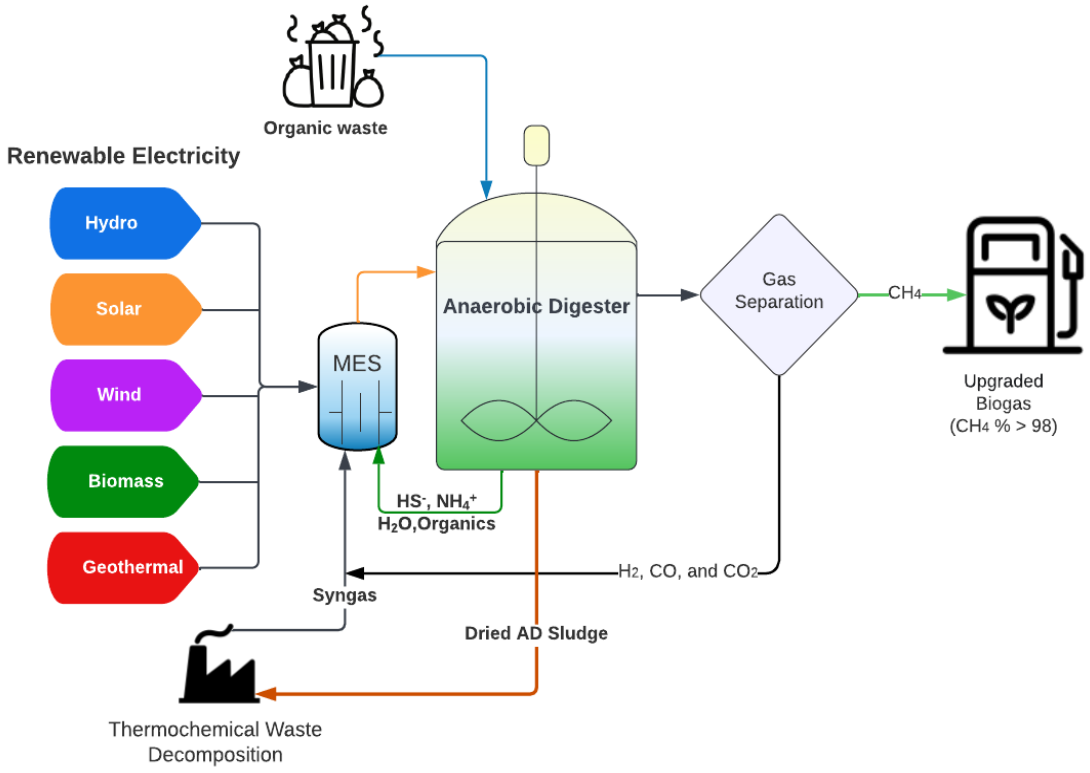

Figure 2.1: Conceptual illustration of process integration.

2.1 Challenges in direct syngas injection into AD

The hydrogenotrophic methanogens use H_2 from the syngas mixture to transform the endogenous CO_2 present in the biogas mixture into methane (Angelidaki et al., 2018). Also, the homoacetogens present in the digestate use H_2, CO, and CO_2 to perform homoacetogenesis through WLP. However, H_2 scarcity in the syngas mixture limits these processes. In addition, the low solubility of the gases becomes another challenge. Therefore, elevating syngas headspace pressure gets attention to enhance the fermentation process.

Suppose the dissolved hydrogen exceeds the hydrogenotrophic methanogenesis demand, which causes acetate accumulation. The acetate accumulation imbalances the pH and deteriorates the activity of acetoclastic methanogenesis, leading to a complete stop of biogas production (Agneessens et al., 2017; Batstone et al., 2002). Another issue is that higher dissolved H_2 concentration thermodynamically unfavoured the oxidation of VFAs, especially propionic acid, lowering the biogas production (Batstone et al., 2002; Dinamarca, 2010; Han et al., 2020). A syntrophic propionate oxidation dependence on H_2 dissociation is briefly described in Figure 2.2 in the context of the biogas production process (Dinamarca, 2010).

According to Dinamarca, 2010 the biogas production process is sensitive to a high propionic acid concentration. Propionate oxidation into acetate (acetogenesis) is thermodynamically not feasible (ΔG^o = +74 kJ or +5.9 kcal/mol H_2) at standard conditions (Eq. 2.1). However, coupling methanogenesis makes it thermodynamically feasible to synthesise 1 ATP energy. The H_2 partial pressure needs to be maintained at less than 10^{-4} bar to achieve this conversion. Overall, association of acetoclastic and hydrogenotrophic methanogenesis and homoacetogenesis are required to perform complete propionate oxidation. Therefore, integrating syngas fermentation alone into an AD becomes challenging.

$$\text{Propionate}^- + 3H_2O \rightarrow HCO_3^- + \text{Acetate}^- + H^+ + 3H_2 \qquad 2.1$$

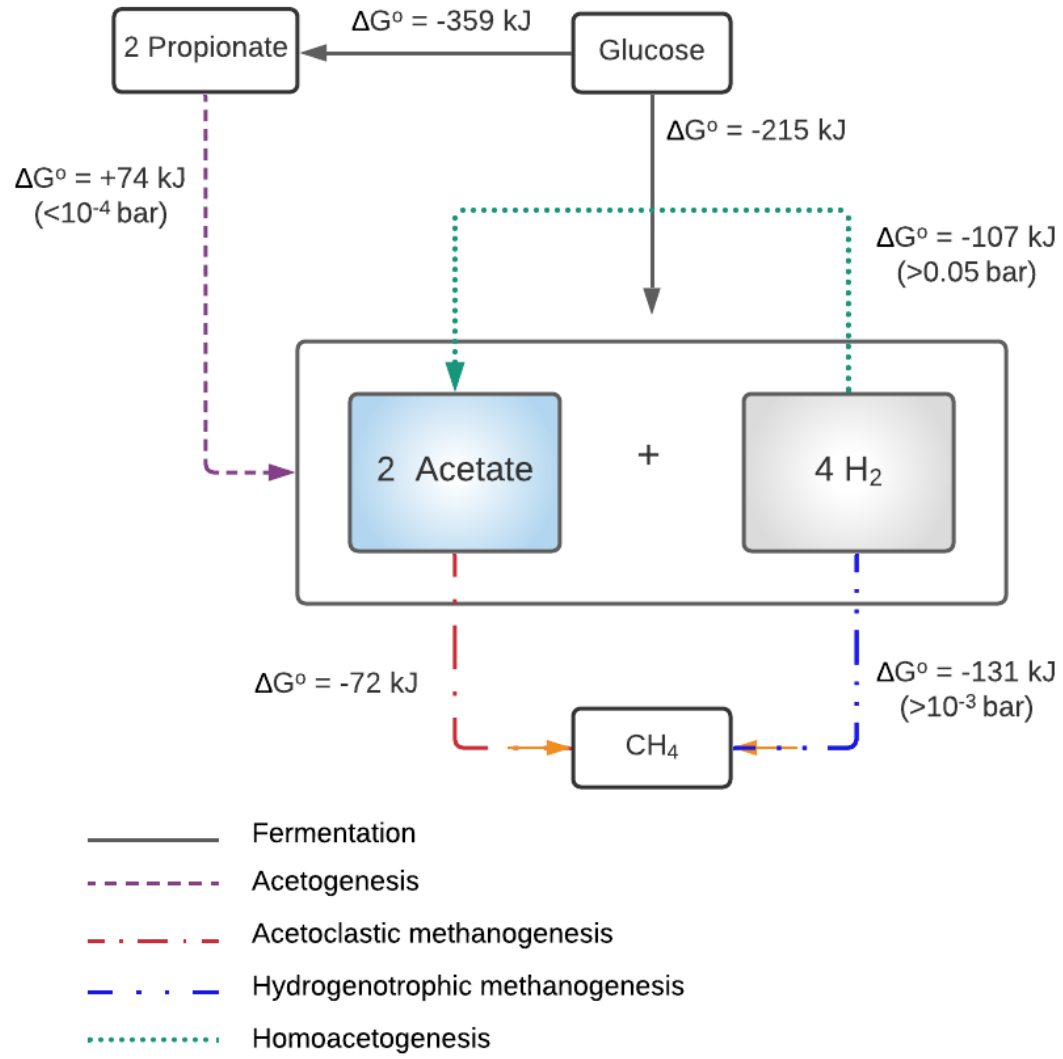

Figure 2.2: Sketch of trophic relationships in biogas process (Limiting H_2 partial pressure for reactions is given in parenthesis) (Dinamarca, 2010).

2.2 Significance of MES and syngas fermentation integration

Syngas fermentation requires a reducing environment to transform the CO_2 (therein carbon is at +4 oxidation state) molecule into a reduced chemical form. H_2 gas in the syngas mixture is the primary reducing equivalent. Though CO acts as both carbon and electron source, it releases CO_2 upon utilisation (Eqs. 1.4 and 1.8). The liberated CO_2 demands more reducing power (H_2). Usually, the syngas mixture from conventional pyrolysis and gasification consists of scanty amounts of H_2 (10 – 40 %) (Cameretti et al., 2020; El-Nagar & Ghanem, 2019; Shi et al., 2020), which is not adequate for complete

CO_2 reduction. Combining syngas fermentation into MES increases both carbon source and the amount of reducing equivalents. Since syngas mixture has limited H_2, MES seems to be a promising approach that gives additional reducing equivalents as electrons. This study examines how MES integration could provide extra p&e for complete carbon sequestration through syngas fermentation in the context of advancing biogas production.

The biofilm layers on the cathode could provide a sophisticated habitat for the microorganism against CO toxicity and other process imbalances. As explained in section 1.2.3, the microorganisms that perform syngas fermentation are slow growing; thereby, the cathodic biofilm could help overcome that kinetic growth limitation by increasing the biomass density on the cathode surface.

USN has already established a benchmark that biogas production rate (Nelabhotla et al., 2019) and the CH_4 content (Nelabhotla & Dinamarca 2019) can be upgraded up to 39 % and 90 % by integrating MES into an anaerobic digestor. Therefore, the optimum cathodic voltage (-0.8 V vs. SHE) is adapted from the benchmark in-house experiments (Nelabhotla, 2020). Based on that potential, a mimic syngas (H_2 in the headspace, CO_2 in the liquid as bicarbonate salt, CO excluded) fermentation is performed in a single-chamber MES reactor to evaluate how an applied reducing power can improve the acetate synthesis and H_2 GL mass transfer (Article 3).

The article 3 disclosed that during the OCM operation, biofilm growth on the cathode increased the H_2 uptake rate; however, the external electron supply by MES did not increase the gas uptake rate, instead producing H_2 by oxidizing acetic acid. This study concludes that the applied potential could be higher than the thermodynamic limit; thereby, the cathode could deprive of its biotic nature, and anode potential rose above the formal potential of the acetic acid oxidation, resulting in H_2 gas evolution. Therefore, the study was expanded with an advance experimental design. The cathodic voltage was increased from -25 mV to -175 mV vs. Ag/AgCl to establish the lower benchmark

potential that can improve acetate synthesis and keep the anodic voltage low enough (Article 4).

To move forward in technological readiness level (TRL), the study explained in article 4 was repeated with an industrially relevant syngas mixture (15 % H_2, 15 % CO, 20 % N_2 and 50 % CO_2). Though CO could inhibit the metabolic process, the cathodic biofilm is expected to protect against direct exposure to microorganisms. This study investigated the lowest benchmark potential for electrochemically mediated syngas fermentation; therein, acetate synthesis and GL mass transfer are mainly scrutinised (Article 5).

Syngas fermentation leads to VFAs accumulation that causes process instabilities or could completely stop the biogas production (Sivalingam et al., 2021a). The anodic oxidation during MES has an exceptional advantage in generating p&e for the acetate synthesis and controlling the VFAs concentrations.

Another essential benefit of integrating syngas fermentation and MES is that the H_2 shortage in the syngas mixture could be easily overcome through in situ H_2 generation. Therefore, it requires no separate H_2 production, storage, compression. Furthermore, MES can act as a biocatalyst that well functions at ambient temperature and pressure.

The MES anode oxidises the pollutants like ammonium and H_2S to produce p&e to reduce CO_2. Such p&e generation from waste compounds is an additional advantage. Since biocathode provides a specific potential during the MES, the microbes in the fermentation medium become more selective, leading to an efficient process.

The microorganisms that perform syngas fermentation are homoacetogens, autotrophic in nature and growing slowly. Therefore, enriching their biomass density in a biogas reactor is quite challenging since the heterotrophic methanogens grow relatively faster. However, integrating MES could provide the biocathode as a habitant to grow the microorganisms as biofilm that enhances biomass density. In addition, other attached growth biofilm strategies are also to be used to enhance the biomass density (Shen, 2013), particularly MBB is used in this study (Article 2).

Reference

Agneessens, L. M., Ottosen, L. D. M., Voigt, N. V., Nielsen, J. L., de Jonge, N., Fischer, C. H., & Kofoed, M. V. W. (2017). In-situ biogas upgrading with pulse H2 additions: The relevance of methanogen adaption and inorganic carbon level. *Bioresource Technology*, *233*, 256–263.

Angelidaki, I., Treu, L., Tsapekos, P., Luo, G., Campanaro, S., Wenzel, H., & Kougias, P. G. (2018). Biogas upgrading and utilisation: Current status and perspectives. *Biotechnology Advances*, *36*(2), 452–466.

Batstone, D. J., Keller, J., Angelidaki, I., Kalyuzhnyi, S. V., Pavlostathis, S. G., Rozzi, A., Sanders, W. T. M., Siegrist, H., & Vavilin, V. A. (2002). The IWA Anaerobic Digestion Model No 1 (ADM1). *Water Science and Technology*, *45*(10), 65–73.

Cameretti, M. C., Cappiello, A., De Robbio, R., & Tuccillo, R. (2020). Comparison between Hydrogen and Syngas Fuels in an Integrated Micro Gas Turbine/Solar Field with Storage. *Energies*, *13*(18), 4764.

Dinamarca, C. (2010). *Homoacetogenic H2 Consumption In Fermentative Hydrogen Production Processes*. [Doctoral dissertation, Norwegian University of Science and Technology].

El-Nagar, R. A., & Ghanem, A. A. (2019). Syngas Production, Properties, and Its Importance. In *Sustainable Alternative Syngas Fuel*. IntechOpen.

Han, Y., Green, H., & Tao, W. (2020). Reversibility of propionic acid inhibition to anaerobic digestion: Inhibition kinetics and microbial mechanism. *Chemosphere*, *255*, 126840.

Nelabhotla, A. B. T. (2020). *Electrochemical Unit Integration with Biogas Production Processes* (Publication No. 62). [Doctoral dissertation, University of South-Eastern Norway].

Nelabhotla, A. B. T., & Dinamarca, C. (2018). Electrochemically mediated CO2 reduction for bio-methane production: A review. *Reviews in Environmental Science and Bio/Technology*, *17*(3), 531–551.

Shi, K., Yan, J., Menéndez, J. A., Luo, X., Yang, G., Chen, Y., Lester, E., & Wu, T. (2020). Production of H2-Rich Syngas from Lignocellulosic Biomass Using Microwave-Assisted Pyrolysis Coupled With Activated Carbon Enabled Reforming. *Frontiers in Chemistry*, *8*, 3.

Sivalingam, V., Ahmadi, V., Babafemi, O., & Dinamarca, C. (2021a). Integrating Syngas Fermentation into a Single-Cell Microbial Electrosynthesis (MES) Reactor. *Catalysts*, *11*(1), 40.

3 Aim, Objective, and Approach

3.1 Aims

This study investigates how syngas fermentation and microbial electrosynthesis (MES) can be integrated to improve biogas production to comply with the national goal of transforming Norway into a low-emission society by 2050.

3.2 Objectives

The main objective is to achieve an efficient syngas fermentation to synthesize acetic acid, consequently improving biogas production. Based on this, the following objectives are defined.

1. Investigate the impact of H_2 partial pressure on syngas fermentation to overcome gas-liquid (GL) mass transfer limitation.

2. Study the feasibility of integrating moving bed biofilm into a high-pressure syngas fermentation to overcome the kinetic growth limitation.

3. Examine the impact of MES integration on syngas fermentation herein; lower benchmark potential for acetate synthesis, and GL mass transfer are mainly scrutinised.

3.3 Research strategy and organization

Direct addition of syngas into mixed culture anaerobic digestor should undergo several metabolic processes. Especially homoacetogenesis and methanogenesis are the predominant pathways. Therefore, this study started with investigating homoacetogenesis; therein impact of H_2 partial pressure, the contribution of the MBB, and the impact of MES on syngas fermentation are examined in this PhD study.

The research strategy is graphically presented in Figure 3.1. The homoacetogenic culture is enriched from biogas reactor digestate through several sequential treatment steps

(Section 4.1). Since H_2 from the syngas mixture has the lowest solubility, research begins with elevating headspace pressure to achieve efficient GL mass transfer. In this attempt, 1 – 25 bar H_2 pressure is examined and optimised therein; microbial sensitivity on H_2 partial pressure is mainly investigated (Objective 1).

Slow growth of homoacetogens is another hurdle that kinetically limits syngas fermentation. Therefore, MBBR is introduced to populate biomass density into a pressure reactor that operates at optimum H_2 partial pressure achieved from the previous study (Objective 2).

To fulfil objective 3, a homoacetogenic reactor is pressurized with H_2 together with inbuild electrodes to examine the impact of MES integration. The goal is to build a framework to study how the reducing potential imposed by MES could enhance the H_2 utilisation and product synthesis (Article 3 and 4). Eventually, an industrially relevant syngas mixture with CO is fermented into a MES integrated homoacetogenic medium to investigate the potential use of such process integration to improve biogas production (Article 5). In addition, the lowest benchmark potential for electrochemically mediated syngas fermentation, GL mass transfer and the impact on acetate synthesis are examined. The synthesised acetic acid can be converted into biogas through acetoclastic methanogenesis.

As far as we know, integrating MES into homoacetogenic syngas fermentation reactor to improve biogas production is not being studied elsewhere. Therefore, this PhD research becomes interesting and novel.

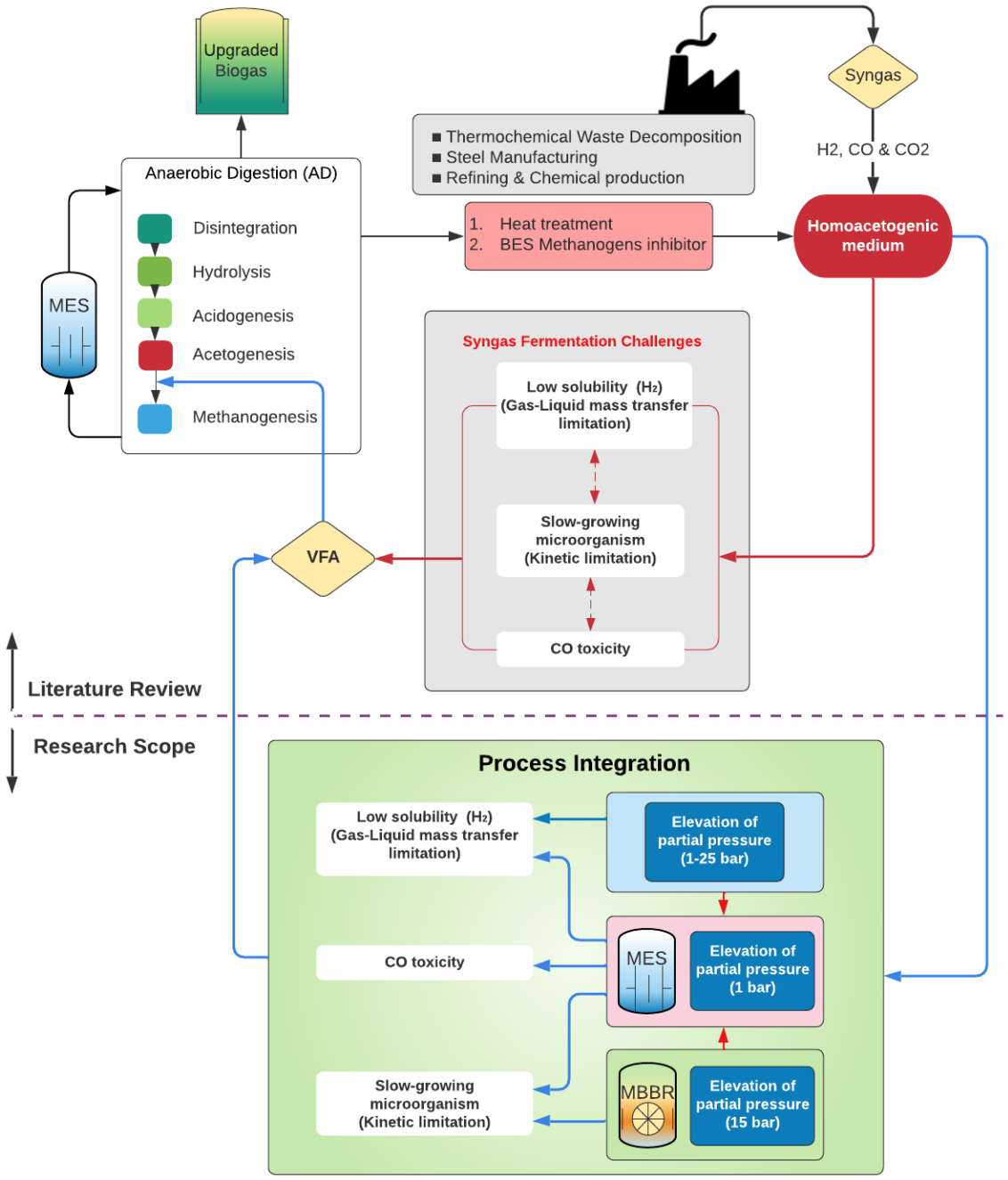

Figure 3.1: Research strategy.

4 Materials and Methods

Detailed material and methods are available in the attached articles; therefore, generally explained in this chapter. In addition, the reactor setups/schematic diagrams are presented.

4.1 Feed Preparation

Digested sludge from Knarrdalstrand WWTP, Porsgrunn Norway, was utilised as the fermentation medium for all the experiments performed in this study. The digestate sludge was pre-treated to enhance the homoacetogenic condition, facilitating syngas fermentation. It was sieved via 300 microns to remove coarse impurities. Then heat-treated at 105°C for 48 hours to eliminate methanogens and concentrate spore-forming acetogens. After that, it was cold down to room temperature, and a nutrient media was added, containing necessary vitamins, minerals, and salts for the biomass synthesis; the composition is adapted from (Dinamarca & Bakke, 2009).

4.2 Analysis

The ammonium, COD and total alkalinity were determined by Spectroquant® Pharo 300 UV/VIS photometer (Merck KGaA, Darmstadt, Germany). The spectroquant test methods for ammonium and COD are analogous to APHA 5220, 4500 (American Public Health Association (APHA), 1995) and the total alkalinity was quantified by following the manufacturer's defined procedure (Acid capacity cell test: 1.01758.0001). In addition, total and volatile solid contents were quantified according to the APHA Standard 2540 E (APHA, 1995).

A Clarius 500 PE gas chromatograph (Perkin Elmer, MA, USA) quantified the VFAs concentrations. The chromatograph was occupied with a scion-wax capillary column (25 m length, 0.25 mm diameter, and 0.2 µm film) and a flame ionization detector. H_2 was the carrier gas at a 45 mL min^{-1} flow rate. The detector temperature was 250 °C, and the

injector temperature was 270 °C. The initial oven temperate remains at 80 °C for 0.7 min, then increased to 200 °C at 25 °C min^{-1} rate, followed by 20 °C min^{-1} to achieve 240 °C.

A gas chromatograph (8610C, SRI Instruments, CA, USA) was used to quantify the gas composition. The chromatograph instrument contains 6' Haysep-D (MXT-1) and 6' Molecular Sieve (MS13X) column, a flame ionization detector (FID) and a thermal conductivity detector (TCD). Helium 5.0 was used as the carrier gas at 2.1 bar, at 20 mL min^{-1} flow rate. The oven temperature was maintained at 80°C for four minutes and ramped up to 120°C at 10 °C/min. The run time was 8 min. The TCD and FID operating temperature was 150°C.

4.3 Electrochemical methods

Electrochemical experiments were performed by Gamry 1010 E interfaces (Gamry Instruments, Philadelphia, PA, USA). Potentiostatic test was the primary experiment performed throughout the study, where certain negative potentials were poised at the cathode to promote reduction reactions. Moreover, cyclic voltammetry (CV), electrochemical impedance spectroscopy (EIS), linear sweep voltammetry (LSV) were performed to investigate the electrochemical behaviour of the fermentation medium as well as to study the electrodes' nature.

At the beginning of every experiment, the potentiostat and the cables were calibrated with 2000 ohm universal dummy cell 4 (UDC4). Only the DC side was calibrated since the AC calibration was performed at the factory. Ag/AgCl (3 M NaCl, Prosense, Netherland) was used as the reference electrode. The reference electrode viability was tested using a voltmeter, a solution of 3M NaCl and three similar reference electrodes. Thus the potential difference between the two electrodes assure to be ± 20 mV; otherwise, the filling solution was replaced by a new 3M NaCl solution, and the frit was replaced by CoralPor® MF-2064.

4.3.1 Potentiostatic test

An operational amplifier (Op-Amp) is the main electronic component of a potentiostat. The part of the output voltage is fed into via a feedback mechanism; thus, the potentiostat can control the working electrode potential at a certain level (Colburn et al., 2021; Bard & Faulkner, 2001). The applied potential needs to be constant during potentiostatic mode experiments. Therefore, a constant potential is applied as the cathode (working electrode) input signal with respect to the Ag/AgCl reference electrode. In this operation, the device measures both current and voltage simultaneously. The measured voltage is equal to the applied voltage.

In all the experiments, a negative potential was imposed on the working electrode (cathode); therefore, a positive potential emerged on the counter electrode (anode) because the charge at the working and the counter electrodes needs to be balanced. When current flow through the bioelectrochemical cell, iR drop occurs because of the changes in the fermentation medium and electrodes; consequently, the potential at the working sensor against the reference electrode also changes (V_feedback). That is fed back to the non-inverting input of the high gain Op-Amp in the potentiostat, which must equalise both the inverting and the non-inverting inputs; therefore, continue to adjust the counter electrode potential until it reaches a balance; thus, the anodic voltage varies. The anodic potential variation plays a vital role in the production of p&e for microbial electrosynthesis; therefore, it is logged with another potentiostat and corroborated to the relevant oxidation reactions.

4.3.2 Linear Sweep Voltammetry (LSV)

During the LSV test, voltage on a particular electrode is being changed at a specific scan rate (mV s^{-1}); therein, voltage and current were logged. This study performed LSV on the cathode before starting the MES operation. Simultaneously, the anodic potential was recorded and corroborated to the LSV results to determine the maximum reduction potential that could be given to the cathode without exceeding the anodic voltage above the water oxidation potential window. The voltammogram derived from LSV mainly

depends on the electron transfer rate in chemical reactions, scan rate and chemical reactivity of the electroactive species (University of Cambridge, 2013). The LSV was performed at the cathode in the voltage range of 0 to -1 V at 5 mV s^{-1} scan rate.

4.3.3 Cyclic Voltammetry (CV)

The CV is an extended version of LSV in which the same scan rate is employed, but the direction is swept at the end of LSV, creating a triangular profile. The voltage and current are the outputs. The current response to the voltage changes profile is called as the cyclic voltammogram. The general use of CV is to examine the reduction-oxidation processes and electron transfer mediated chemical reactions (Elgrishi et al., 2018). Moreover, the usage is widely extended in biofilm-related studies, especially to investigate redox catalytic current generation (Annie Modestra & Venkata Mohan, 2019). The study presented in articles 4 and 5, CV was performed on the plain cathode, cathode at the end of open and close circuit modes at the scan rate of 10 mV s^{-1} within the potential range of 0 to -1.0 V. Three cycles were performed, and the third one was selected as the best cyclic voltammogram to avoid the initial current transient effect. The results were analysed through Gamry Echem Analyst software.

4.3.4 Potentiostatic Electrochemical Impedance Spectroscopy (EIS)

The Potentiostatic EIS is an alternating current (AC) technique inputs a sine wave signal at a fixed voltage and different frequencies into a cell. The impedance spectroscopy examines the processes in the electrolyte and on the electrodes. This project mainly studies how the charge transfer and electrolyte resistances vary during MES integrated syngas fermentation. The output of EIS results phase and magnitude shifts in the current. The impedance measurement is similar to resistance but consists of a time-domain related to the applied frequency that quantifies how difficult it is to pass the applied AC through a circuit. The bioelectrochemical reactor or MES setup is analogous to the equivalent circuits. The EIS results are explained in different graphical forms, such as Bode and Nyquist plots (He & Mansfeld, 2009).

The EIS was performed on plain cathode and cathode at the end of open and closed circuit modes (articles 4 and 5). The frequency range was between 100 mHz to 2 MHz. Ten milli volt sinusoidal signal was used at 10 decay/points measurement rate. The results are presented as Nyquist plots where ohmic and charge transfer resistance are explicitly visible. In addition, Gamry Echem model editor 7.8.4 was used to fit the EIS data to an equivalent circuit model, where the impedance elements are individually quantified.

4.4 Equivalent Circuit Modelling

The EIS results are complex functions of several resistance elements. The major components are charge transfer, electrolyte resistances, and electrical double layer capacitance (Samarakoon et al., 2021). They can be identified by modelling an equivalent electric circuit, which studies the nature of electrodes and electrolyte medium. The EIS data were analysed by Gamry Echem Analyst software.

The EIS results were fitted with the representative equivalent circuit model (Figure 4.1) developed in the Gamry Model Editor 7.8.4 tool. The R_u and R_p denoted ohmic and charge transfer resistances. The ohmic resistance is the sum of the electrical resistance of the cathode and bulk electrolyte resistance (Heijne et al., 2018). The charge transfer resistance explains how difficult it is to move electrons in the system, lowered by the bacteria growth on the electrode as biocatalyst (Ha et al., 2010). The capacitance is represented as constant phase elements (Y_0) (Holm et al., 2021) because, during EIS experiments, the capacitors do not behave ideally. The Y_0_film represents the biofilm capacitance, while Y_0_dl explains the double-layer capacitance. The biofilm growth and adhesion account for the Y_0_film while the electrical double layer between the electrode and the adjacent fermentation medium cause Y_0_dl (Kim et al., 2011). The a_film and a_dl are the parameters that describe the frequency dependency's nature, depending on the medium.

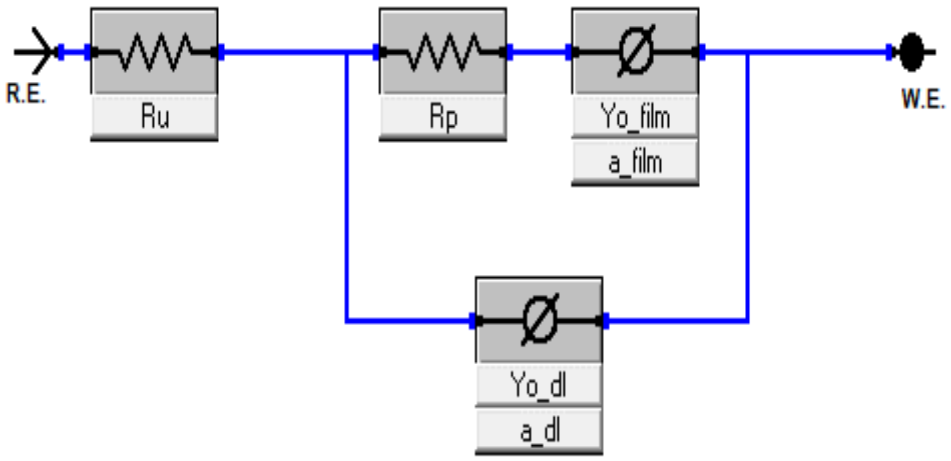

Figure 4.1: Equivalent circuit model.

4.5 Microbiome analysis

The 16S ribosomal RNA gene metagenomic studies were performed for the raw inoculum, heat-treated inoculum, fermentation medium and the biofilm extracted from electrodes under different operational conditions. All the microbiome analyses were performed by the Department of Biotechnology and Nanomedicine, SINTEF Industry, Trondheim, Norway. The detailed methodology is described in articles 1, 4 and 5; therefore, not repeated here.

4.6 Scanning Electron Microscopy

In the study presented in article 4, the electrode morphology and biofilm structural changes on the cathodic carbon felt prior to the experiment at the end of OCM and CCM were investigated by scanning electron microscopy (Hitachi S3500, Krefeld, Germany). Small pieces (~1x1 cm^2) of carbon felt were extracted from the cathode and gently washed with phosphate buffer saline (pH 7.2, gibco®, life technologies, UK). Then biofilm assimilated carbon felts were fixed with glutaraldehyde fixative (5 % v/v diluted with milli-Q water) and dried via gradient dehydration to preserve the biofilm and the electrode-microbe interaction (Xiao et al., 2020). The micrographs were obtained at 5 kV. The magnification area ranged from 500 to 10 µm. The biofilm fixation was performed at USN

Porsgrunn Campus. The drying and SEM analyses were performed by the Department of Microsystems, University of South-Eastern Norway, Campus Vestfold.

4.7 Experimental setups and methodology

Berghof pressure reactors (NR 1500 and BR 500, Eningen, Germany) were used to investigate the impact of H_2 partial pressure in syngas fermentation processes. The reactors are connected to the H_2 gas injection line. Digital manometers (LEO-3, Keller, Winterthur, Switzerland) and mechanical stirrers (BG 65X50, Dunkermotoren, Bonndorf, Germany) with speed controller (BRM1, Eningen, Germany) are attached to the reactor to log the pressure changes and to mix the fermentation medium. The complete setup is given in Figure 4.2

Article - 1

For the study investigating the impact of H_2 pressure on homoacetogenesis, a BR 500 reactor was used as the fermenter. The H_2 (H_2 laboratory 5.5, Linde Gas As, Oslo, Norway) was the only gaseous substrate, while CO_2 was provided as bicarbonate salt (mimicked syngas) to the liquid medium. To determine the optimum pressure, the manometric headspace pressures 1, 3, 5, 10, 15, 20 and 25 bar were tested as individual batch experiments. The medium was agitated at 200 rpm. The headspace pressure variation was logged in 10 min intervals. The H_2 uptake and acetate synthesis were mainly investigated (Article 1).

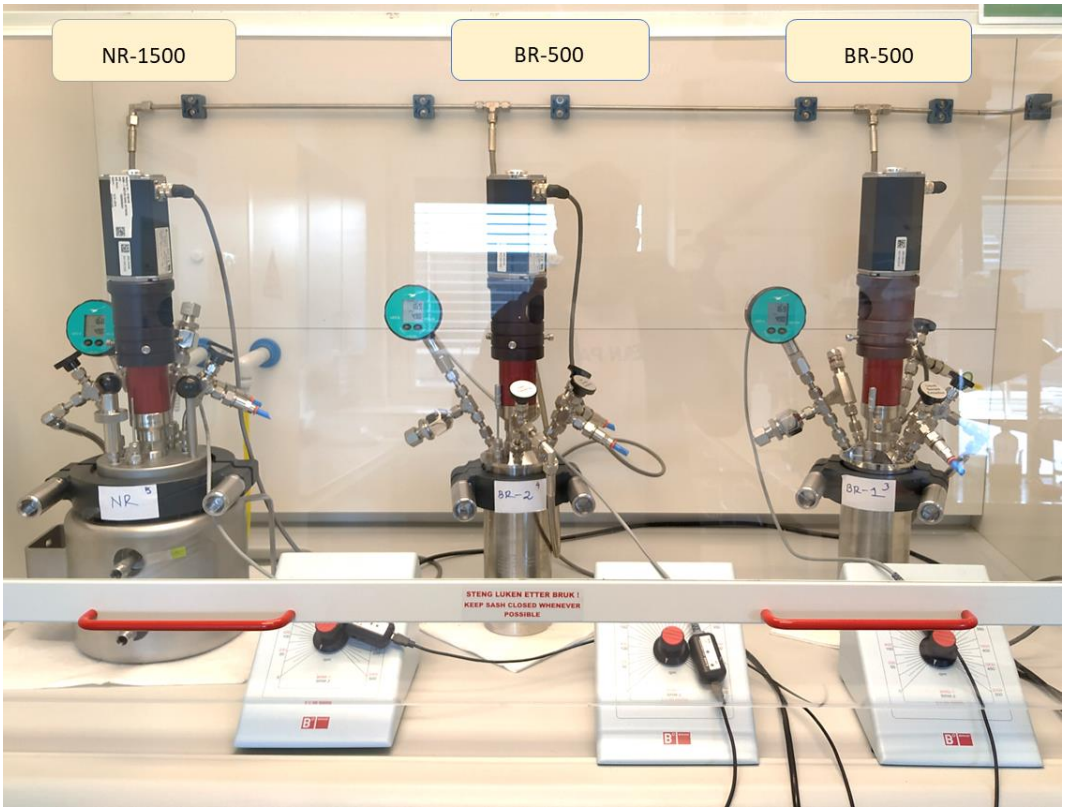

Figure 4.2: Pressure reactors arrangement.

Article - 2

To study the feasibility of integrating MBB into a high-pressure syngas fermentation, the NR-1500 Berghof pressure reactor was modified as a moving bed biofilm reactor (MBBR). BWT X type (Biowater Technology As, Tønsberg, Norway) moving bed biocarries (Dimensions: 14.5 x 14.5 x 8.2 mm and Protected surface: 650 m^2/m^3) were used as the biofilm media. The diagram of the experimental setup is given in Figure 4.3.

The fermentation medium is the same as used in article 1. The optimum H_2 pressure for this culture is 15 bar. The syngas was mimicked as H_2, and CO_2 therein H_2 was the only gaseous substrate while CO_2 was supplied as bicarbonate salt. The research was conducted in two phases as batch experiments. In phase one, the fermentation medium excluding MBB was pressurized with 15 bar H_2, while MBB carriers were incorporated in phase two. The H_2 consumption and acetate synthesis were mainly compared to examine the potential use of combining MBB into high-pressure syngas fermentation.

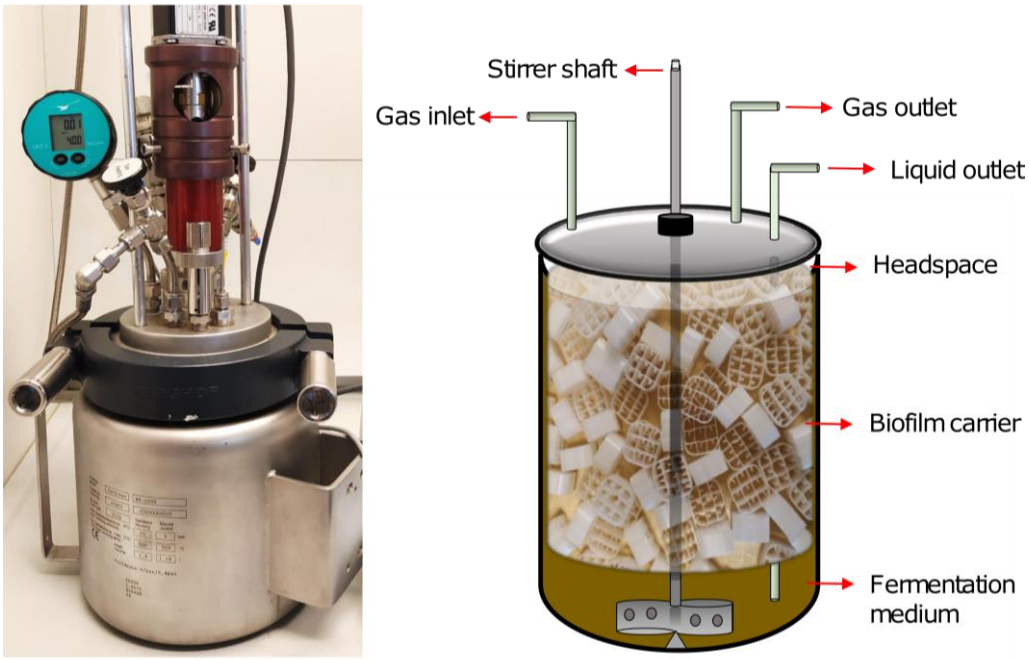

Figure 4.3: NR-1500 Pressure reactor and a sketch of MMB integration.

Article – 3

This study examines how the syngas fermentation hurdles can be overcome by integrating MES into the syngas fermenter. The experiments were performed in three phases. In phase one, H_2 fermentation was performed on a suspended medium into a 4.125 L borosilicate glass reactor (FG Mellum AS, Akershus, Norway) at 1 bar headspace pressure. Once the headspace pressure dropped, it was refed with H_2. This operation was continued till it reached minimal gas consumption. The change in headspace pressure was logged every ten minutes by a CPG 1500 digital pressure gauge (WIKA, Bavaria, Germany). Similar to articles 1 and 2, H_2 and CO_2 (in the form of bicarbonate) were used as the mimicked syngas. The phase one lasted 70 days to reach no or less change in headspace pressure (saturated gas consumption).

In phase 2, electrodes were integrated into the borosilicate glass reactor, referred to as a single-chamber MES reactor, and the reactor was re-seeded. Carbon felt (Alfa Aesar GmbH, Kandel, Germany), titanium metal sheet and Ag/AgCl (3.0 M NaCl, QVMF2052, ProSense, BB Oosterhout, Netherlands) electrodes were used as the cathode, anode and reference, respectively. The electrode configurations and the reactor setup are illustrated in Figure 4.4. Like phase one, the gas feeding operation was repeated in phase two, while no potential was applied on the electrodes (open circuit mode: OCM). Phase two took around 90 days to obtain a stable OCM potential and minimal gas consumption. After that cathode was poised with – 0.8 V in stage three (closed-circuit mode: CCM), and the headspace was pressurized similarly to stages one and two. The – 0.8 V was the optimum potential for acetic acid synthesis, adapted from previous USN studies (Nelabhotla, 2020). The stage three experiments aim to trigger the H_2 GL mass transfer and acetate synthesis through applying cathodic potential.

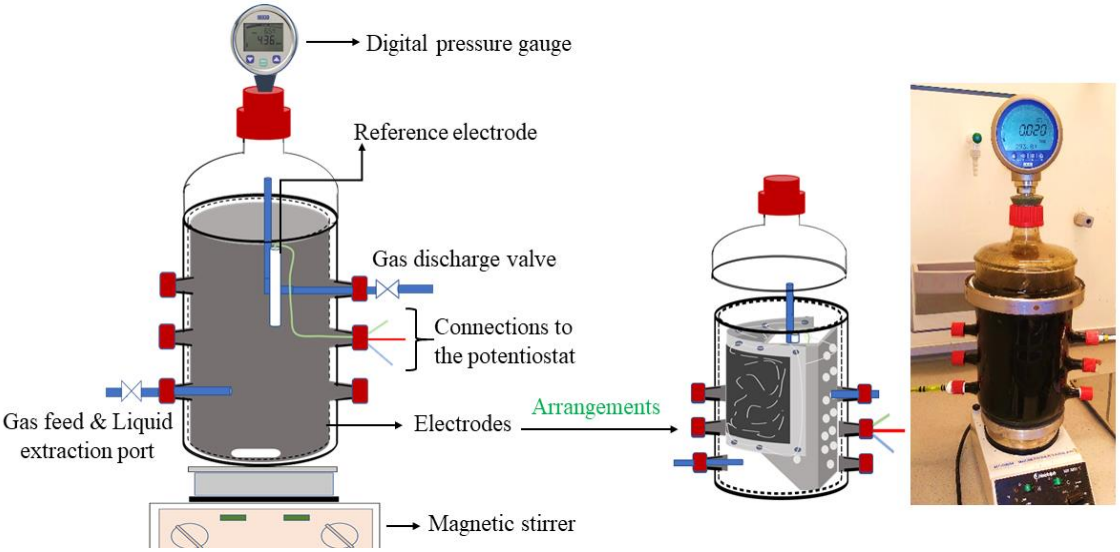

Figure 4.4: Single-Chamber MES integrated syngas fermentation reactor setup.

Article – 4

The stage three experiment failed because the applied -0.8 V potential could decrease the electrodes' biotic nature, resulting in acetic acid oxidation at the anode and H_2 production at the cathode. Therefore, based on the lesson learned from this study, an

advanced experimental study was performed to determine the lowest benchmark potential for efficient acetate synthesis and H_2 gas-liquid mass transfer. The article 3 experimental setup was reused with a modification in electrodes arrangement.

The anode consists of ten graphite rods, each 15.2 cm in length and 0.61 cm in diameter (ThermoFisher GmbH, Germany). Cathode is made of carbon felt (Alfa Aesar, Germany: 25 cm length, 12 cm width, and 24 punched holes with 0.4 cm radius). The electrodes are arranged in a specific way to enhance the liquid mixing and GL mass transfer (Figure 4.5). The complete electrode ensemblemet was integrated into the same borosilicate glass reactor. In addition, the headspace volume was extended by connecting a 0.64 L BR-500 pressure tank. The complete reactor sketch is presented in Figure 4.6.

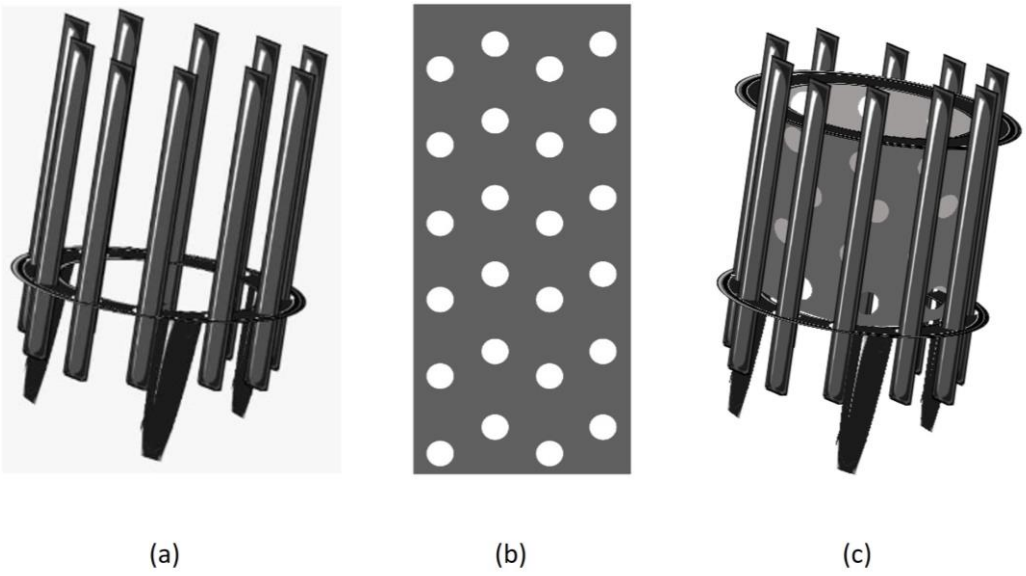

Figure 4.5: (a) Anode, (b) Cathode, and (c) Complete electrodes arrangement.

This study was performed in two phases, open and closed-circuit modes. The OCM operation is quite similar to the article 3 study's OCM, except continuous bicarbonate addition corresponds stoichiometrically to the headspace H_2 quantity. At the beginning of CCM, the cathode was poised with – 25 mV and the OCM operation was repeated until it achieved a stable H_2 consumption. After that, the potential was increased stepwise to – 75 mV, – 125 mV and – 175 mV, and the OCM operation was repeated.

Simultaneously, the anodic voltage was recorded throughout the CCM. Moreover, CV, EIS, SEM and microbiome analyses are performed to evaluate the biotic and electrochemical nature of the process. Once the H_2 consumption became minimal and the headspace pressure increased due to gas evolution, the experiment was stopped; therein, the lowest benchmark potential was figured out, and the impact of MES integration on acetate synthesis and H_2 consumption were investigated in contrast to the OCM.

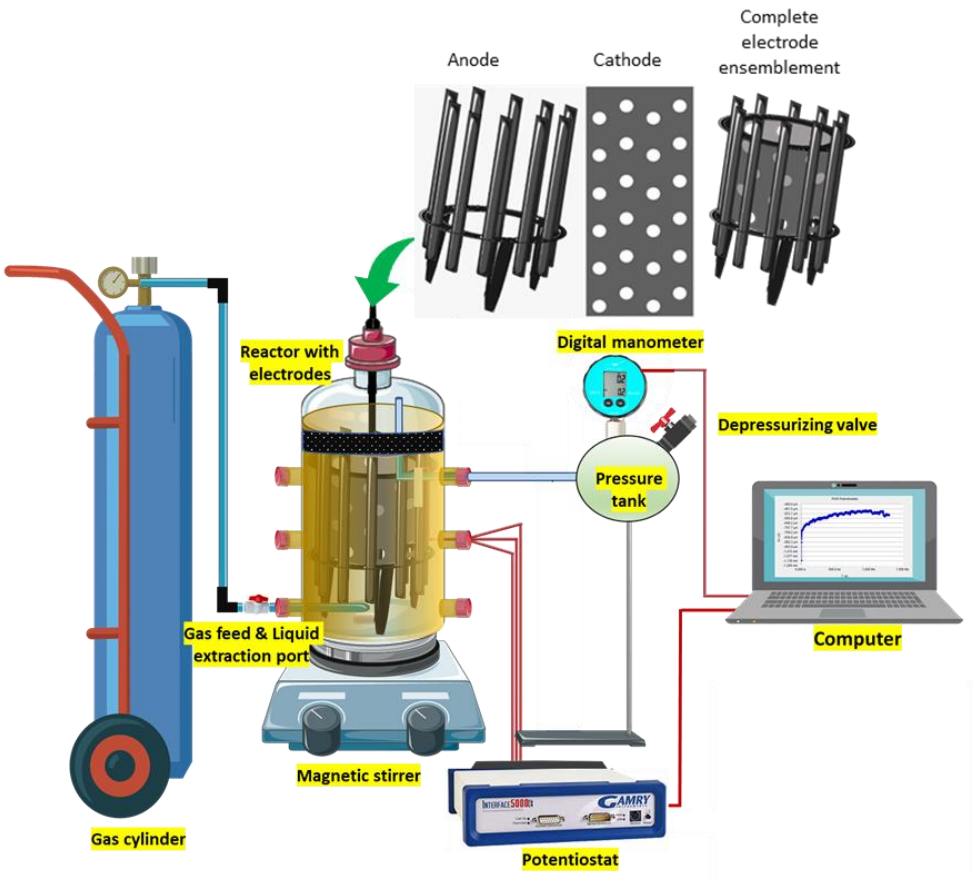

Figure 4.6 : Experimental setup used to study the impact of electrochemical reducing power on syngas fermentation.

Article – 5

The study forwards the achievement obtained from article 4. The distinct advancement is that industrially relevant syngas (15 % CO, 15 % H_2, 20 % N_2 and 50 % CO_2) was fermented instead of H_2. CO from the syngas mixture could inhibit the syngas

fermentation. However, MES integration is believed to protect against direct exposure through biofilms. Since the syngas contains CO_2, no bicarbonate salt was added to the liquid medium as the carbon source. Apart from that, all methodologies and operations were almost similar to article 4. The experiments were also performed in the same reactor setting with fresh medium and electrode materials.

The objective is to determine the lowest benchmark potential for electrochemically mediated industrially relevant syngas fermentation to move forward in technological readiness level. The OCM performed for 27 days; then, CCM started with – 50 mV and increased up to – 400 mV at a rate of - 50 mV per two weeks. Simultaneously, the anodic voltage was recorded. At – 400 mV CCM, the anodic potential exceeded 2.0 V, oxidizing the fermentation products, ammonium, and water, thus decreasing the fermentation product concentration. Therefore, at the end of – 400 mV CCM, the mode of operation was changed from batch to the fed-batch mode by replacing the fermentation medium with fresh inoculum, therein hypothesising that refreshing the fermentation medium could lower the anodic voltage to less than 2.0 V. That fed-batch experiments were carried out for 30 days. Overall, acetate synthesis and GL mass transfer are mainly scrutinised. EIS, CV and microbiome analyses were performed to support the research findings.

Article – 6

A simple mathematical modelling work was performed to contribute to the MES integration to the AD. This is a supplementary work to the main project goal. However, it contributes to the broad applicability of MES; therefore, concisely summarized in this section and the detailed results are available in article 6.

The accumulation of VFAs adversely impacts biogas production (Maurus et al., 2021). Therefore, it needs to be monitored, controlled, and optimised (Hill et al., 2020). The accumulation of VFAs increases the medium's conductivity, lowering ohmic resistance (Sivalingam et al., 2022). The articles 3, 4, and 5; suggest that integrated electrodes could

control the VFAs concentration therein; the impedance measures become essential and used as inputs for the model.

Fitting EIS experimental data to the equivalent circuit model and identifying the components through commercially available software (i.e., Gamry Model Editor) is an interesting task. However, such software is not suited to be an interface between the biochemical side and the power electronics side for the real-time process. Therefore, this modelling work developed a MES integrated potentiostat model (Figure 4.7) in Modelica 2017. The Modelica is an open-source modelling platform that can easily integrate the power and biochemical sides to perform real-time monitoring and control (Modelica Association, 2021)

The model examined the voltage level between anode and cathode, which needs to be below water oxidation potential while a constant potential is applied on the cathode. In this study, the biocathode impedance components were quantified by Gamry Model Editor and used as the input values. However, future modelling work focuses on developing a standalone equivalent circuit model editor in Modelica.

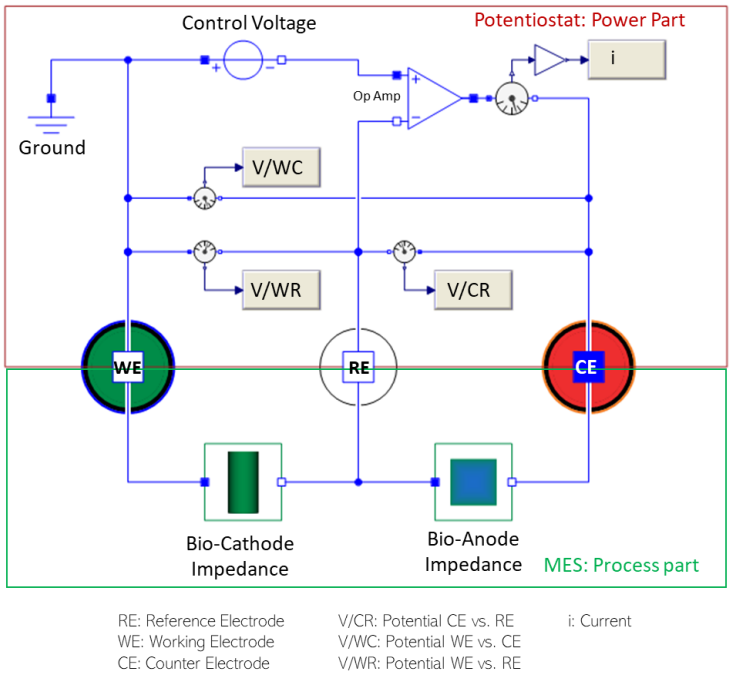

Figure 4.7: The potentiostat model.

Reference

American Public Health Association, American Water Works Association, Water Pollution Control Federation, & Water Environment Federation. (1995). *Standard methods for the examination of water and wastewater*. American Public Health Association.

Annie Modestra, J., & Venkata Mohan, S. (2019). Capacitive biocathodes driving electrotrophy towards enhanced CO2 reduction for microbial electrosynthesis of fatty acids. *Bioresource Technology*, *294*, 122181.

Bard, A. J., & Faulkner, L. R. (2001). *Electrochemical Methods: Fundamentals and Applications, Second Edition*. Wiley.

Colburn, A.W., Levey, K.J., O'Hare, D., & Macpherson,J.V. (2021). Lifting the Lid on the Potentiostat: A Beginner's Guide to Understanding Electrochemical Circuitry and Practical Operation. *Physical Chemistry Chemical Physics 23*(14), 8100–8117.

Dinamarca, C., & Bakke, R. (2009). Apparent hydrogen consumption in acid reactors: Observations and implications. *Water Science and Technology*, *59*(7), 1441–1447.

Elgrishi, N., Rountree, K. J., McCarthy, B. D., Rountree, E. S., Eisenhart, T. T., & Dempsey, J. L. (2018). A Practical Beginner's Guide to Cyclic Voltammetry. *Journal of Chemical Education*, *95*(2), 197–206.

Ha, P. T., Moon, H., Kim, B. H., Ng, H. Y., & Chang, I. S. (2010). Determination of charge transfer resistance and capacitance of microbial fuel cell through a transient response analysis of cell voltage. *Biosensors and Bioelectronics*, *25*(7), 1629–1634.

He, Z., & Mansfeld, F. (2009). Exploring the use of electrochemical impedance spectroscopy (EIS) in microbial fuel cell studies. *Energy & Environmental Science*, *2*(2), 215–219.

Heijne, A. ter, Liu, D., Sulonen, M., Sleutels, T., & Fabregat-Santiago, F. (2018). Quantification of bio-anode capacitance in bioelectrochemical systems using Electrochemical Impedance Spectroscopy. *Journal of Power Sources*, *400*, 533–538.

Hill, A., Tait, S., Baillie, C., Virdis, B., & McCabe, B. (2020). Microbial electrochemical sensors for volatile fatty acid measurement in high strength wastewaters: A review. *Biosensors and Bioelectronics*, *165*, 112409.

Holm, S., Holm, T., & Martinsen, Ø. G. (2021). Simple circuit equivalents for the constant phase element. *PLOS ONE*, *16*(3), e0248786.

Kim, T., Kang, J., Lee, J.-H., & Yoon, J. (2011). Influence of attached bacteria and biofilm on double-layer capacitance during biofilm monitoring by electrochemical impedance spectroscopy. *Water Research*, *45*(15), 4615–4622.

Maurus, K., Kremmeter, N., Ahmed, S., & Kazda, M. (2021). High-resolution monitoring of VFA dynamics reveals process failure and exponential decrease of biogas production. *Biomass Conversion and Biorefinery*.

Modelica Association. (2021, February). *Modelica Language Documents.* https://modelica.org/documents

Nelabhotla, A. B. T. (2020). *Electrochemical Unit Integration with Biogas Production Processes* (Publication No. 62). [Doctoral dissertation, University of South-Eastern Norway].

Samarakoon, G., Winkler, D., Sivalingam, V., Dinamarca, C., & Bakke, R. (2021). *Simple modelling approach using Modelica for microbial electrosynthesis*. Presented at the Proceedings of the 61st SIMS Conference, Virtual Finland, September 22-24, 2020.

Sivalingam, V., Parhizkarabyaneh, P., Winkler, D., Lu, P., Haugen, T., Wentzel, A., & Dinamarca, C. (2022). Impact of electrochemical reducing power on homoacetogenesis. *Bioresource Technology*, *345*, 126512.

University of Cambridge. (2013, November 14). *Linear Sweep and Cyclic Voltametry: The Principles*. https://www.ceb.cam.ac.uk/research/groups/rg-eme/Edu/linear-sweep-and-cyclic-voltametry-the-principles

Xiao, S., Fu, Q., Xiong, K., Li, Z., Li, J., Zhang, L., Liao, Q., & Zhu, X. (2020). Parametric study of biocathodes in microbial electrosynthesis for CO2 reduction to CH4 with a direct electron transfer pathway. *Renewable Energy*, *162*, 438–446.

5 Summary Results

This section summarises the research work performed throughout the PhD study. The key findings are concisely described and corroborated back to the aim of this project. In addition, some of the supplementary results are appended to support.

5.1 Article 1: Effect of Elevated Hydrogen Partial Pressure on Mixed Culture Homoacetogenesis

The effect of H_2 partial pressure from 1 to 25 bar on mixed culture fermentation was examined. Elevating gas partial pressure increases the solubility, following Henry's law. However, it was hypothesised that microorganisms could be sensitive to the H_2 pressure and dissolved H_2 tension, substantially limiting the rate of H_2 consumption. The pressure from 1 to 15 bar depicted a clear upward trend in gas consumption, acetic acid production (Figure 5.1) and gas uptake rate (Figure 5.2); the further increase affects negatively. Therefore 15 bar headspace pressure was found to be the optimum for the particular fermentation medium (volatile and total solid (VS:TS) ratio, 0.41) was used in this study (Knardalstrand WWTP-AD, Porsgrunn); therein, 47.24 mmol of H_2 was consumed within 120 h, and 3.0 g L^{-1} of acetic acid was synthesised. The optimum gas uptake rate was 6.22 mol h^{-1} L^{-1}.

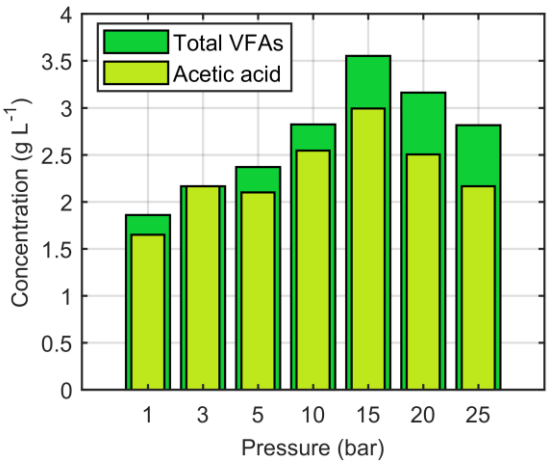

Figure 5.1: Acetic acid synthesis at different headspace pressures.

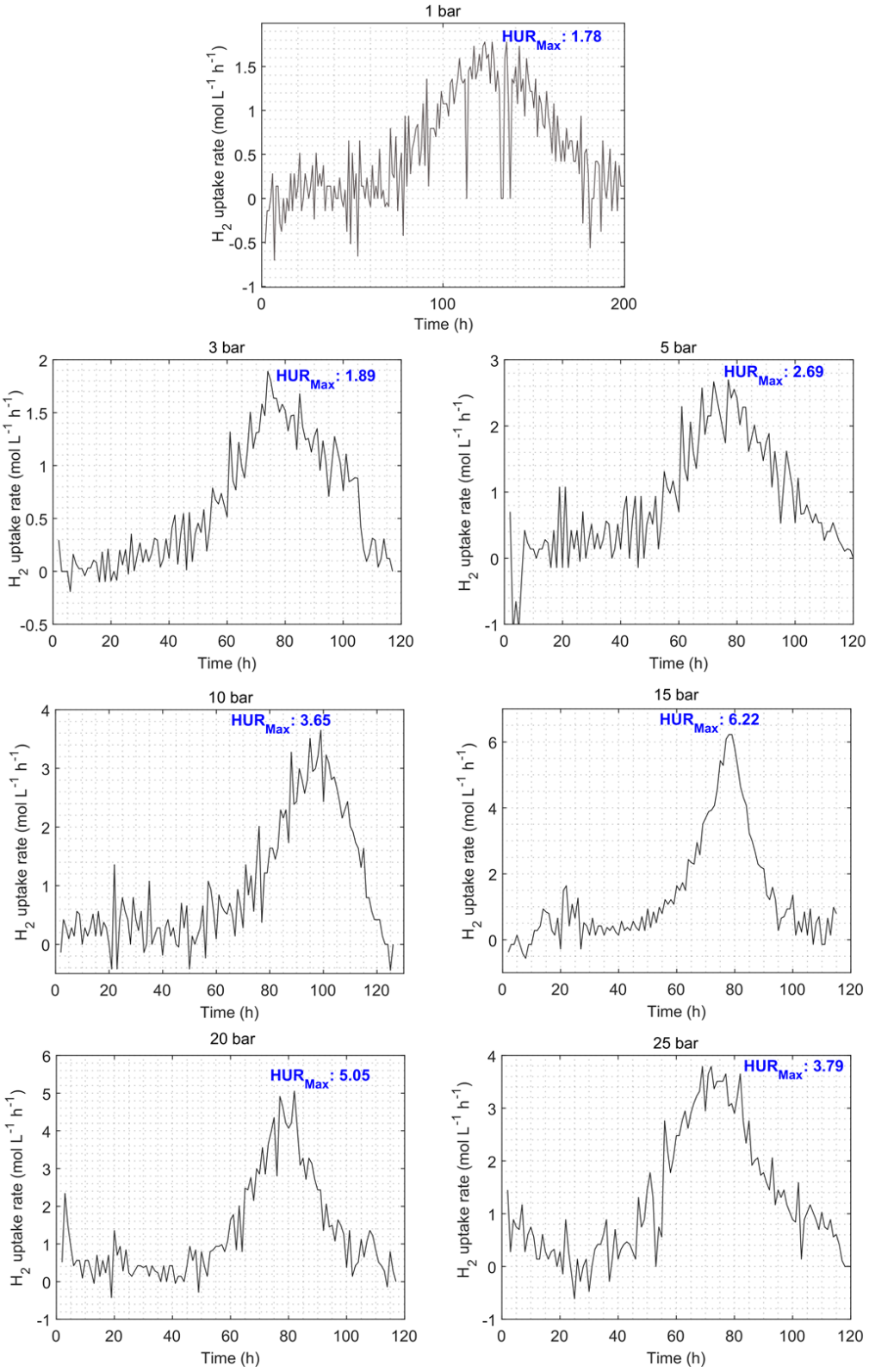

Figure 5.2: H_2 gas uptake rate, the maximum rate is denoted as HUR_{Max}.

5.2 Article 2: High-Pressure Moving Bed Biofilm Reactor for Syngas Fermentation

Homoacetogens are slow-growing microorganisms that catalyse the acetate synthesis from syngas. The slow growth rate kinetically limits the microorganism availability (cell density) in the fermentation broth, not to cope with the amount of dissolved gas. Integrating moving bed biofilm (MBB) into a syngas fermentation process significantly improved the GL mass transfer and product synthesis, patented by Robert Hickey (Hickey, 2009). That study was carried out on monoculture *Clostridium ragsdalei* at 1 to 5 bar liquid pressure. However, the study has not reached a full-scale level. Therefore, a part of this PhD project investigated the possibility of applying elevated H_2 partial pressure into a MBB integrated mixed culture syngas fermenter.

The research was conducted in two phases at batch mode. In phase one, inoculum excluding MBB was pressurized at 15 bar H_2 (abbreviated as PSFR: Pressure Syngas Fermentation Reactor), while MBB carriers were integrated in phase two (abbreviated as B-PSFR: Biofilm Pressure Syngas Fermentation Reactor). The change in headspace pressure and the accumulative gas consumption of those two phases are presented in Figure 5.3.

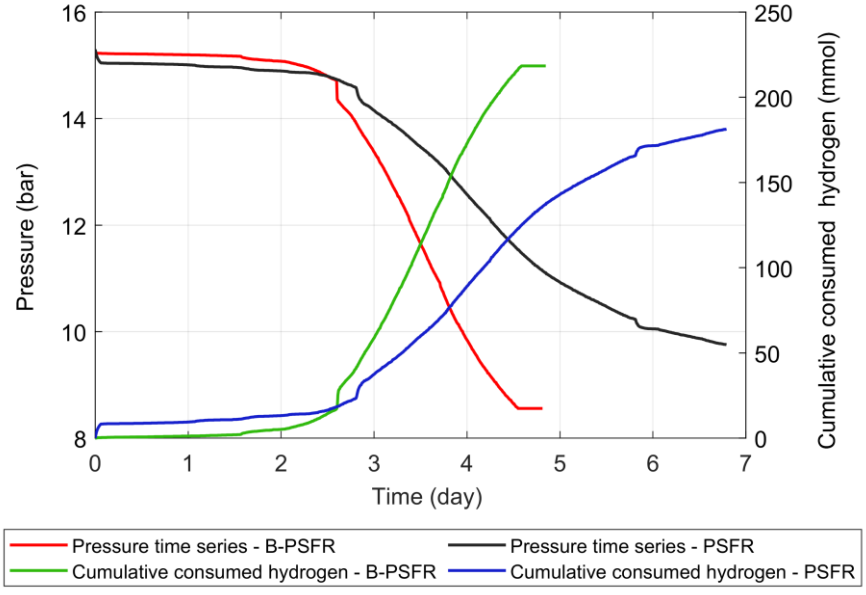

Figure 5.3: Pressure time series and accumulative H_2 consumption profiles.

The batch with biofilm reached the saturated gas consumption within 4.5 days, while the batch without biofilm took seven days. The MBB integration improved the gas consumption (218 mmol) by 20 % and the uptake rate (200 mmol L^{-1} d^{-1}) by 33 %. In addition, acetic acid production (2.7 g L^{-1}) and the rate (37.4 mmol L^{-1} d^{-1}) were also remarkably enhanced by 40 and 48 per cent (Figure 5.4). The biofilm assimilation on the carriers was confirmed via a stereo microscopic analysis. The average biofilm thickness was ~ 160 µm. Eventually, the study concluded that applying elevated H_2 partial pressure into MBB integrated reactor enhanced the cell density. Therefore, it improved the kinetic growth limitation resulting in efficient fermentation.

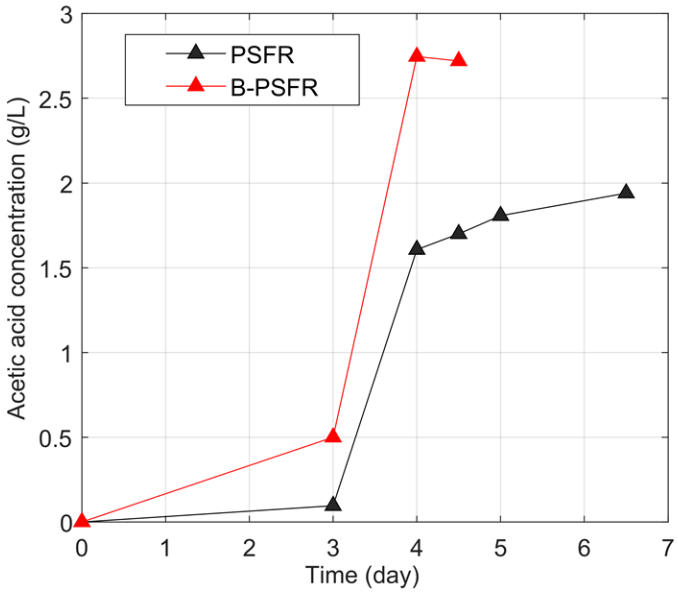

Figure 5.4: Acetic acid concentration profiles.

5.3 Article 3: Integrating Syngas Fermentation into a Single-Cell Microbial Electrosynthesis (MES) Reactor

This study examines the impact of MES integration into syngas (especially H_2 as the gas substrate) fermentation on GL mass transfer and product synthesis. The experiments were performed in three phases. In the first phase, H_2 fermentation was performed on a suspended medium. Afterwards, the reactor was reseeded with fresh medium and incorporated with electrodes, called as single-cell MES reactor. The phase one operation

was repeated while no external potential was applied on the electrodes, named phase two, OCM. After attaining a stable open circuit potential, cathode was poised with - 0.8 V as the third phase to trigger the gas consumption and acetate synthesis. The - 0.8 V was the optimum for acetic acid synthesis, adapted from previous USN studies.

In contrast to phase one, the biofilm assimilated on the electrodes in phase two enhanced the H_2 gas consumption (1021 mmol) by three times and gas uptake rate (13.5 mmol L^{-1} d^{-1}) by 2.3 times and acetate synthesis (57 mmol L^{-1}) by 1.6 times. This is comparable with the study performed on MBBR; herein, the biofilm grows on the electrodes instead of plastic carriers, thus elucidating the effect of high cell concentration, overcoming the kinetic growth limitation.

However, in stage three, gas production was observed instead of consumption. The headspace pressure was maintained at one bar by releasing excess gas production for ten more days. During those ten days of CCM operation, the acetic acid concentration fell by 80 % (Figure 5.5); consequently, H_2 and CO_2 evolved to the headspace. In addition, a trace amount of methane production was also observed.

Eventually, the study concludes that the applied potential (- 0.8 V) could be higher than the thermodynamic limit; thereby, the electrodes could deprive the biotic nature. Simultaneously the anode potential rose above the formal potential of the acetic acid oxidation, liberating extra p&e resulting in evolution of CO_2 from anode and H_2 from the cathode. Unfortunately, the anodic potential was not recorded in this study. Though the ultimate goal of stage three failed, the overall study confirmed that biofilm assimilated on electrodes improved the gas uptake and product synthesis.

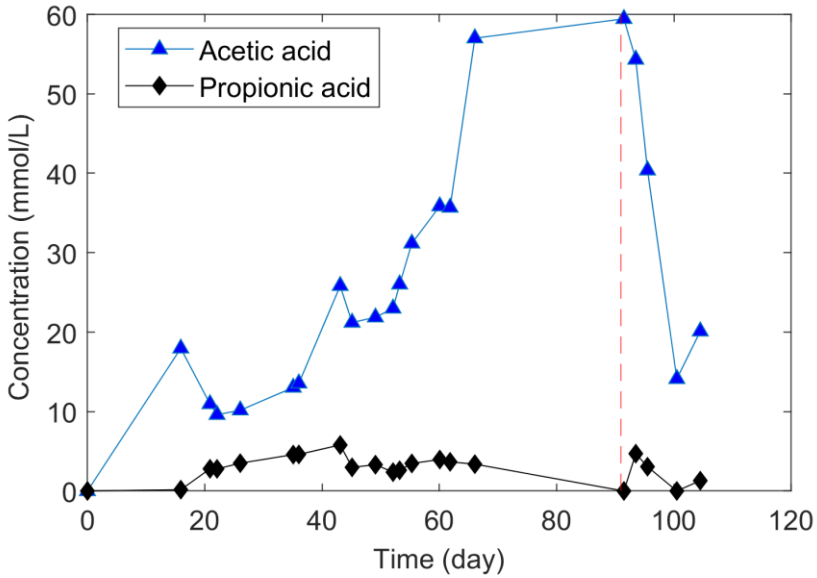

Figure 5.5: Fermentation product concentration during phase 2 and 3.

5.4 Article 4: Impact of Electrochemical Reducing Power on Homoacetogenesis

Based on the lesson learnt from article 3, this research is expanded with fine-tuned experimental design. The – 0.8 V failed to improve the H_2 GL mass transfer and acetic acid synthesis. Therefore, the lowest benchmark potential for efficient H_2 GL mass transfer and acetate synthesis are scrutinised.

The experimental setup used in article 3 was reused with modifications in electrode arrangement and the headspace volume. The experiments were conducted in two phases (OCM and CCM). The OCM was quite similar to the study performed for article 3 at OCM, while significant changes in CCM. The CCM started with – 25 mV at the cathode, and the OCM operation was repeated until it achieved a stable H_2 consumption; then, the potential was stepwise increased to – 75 mV, – 125 mV and – 175 mV, and the OCM operation was repeated. Not like article 3, most importantly, the anodic voltage was recorded throughout the CCM to examine the anodic oxidation reactions that are the sources of p&e. This is one of the key novelties of article 4.

At OCM, 172 mmol of acetic acid was synthesised and continued to increase up to 428 mmol towards the end of CCM. A stable acetic acid production rate, 0.178 mmol L^{-1} h^{-1} was achieved in OCM, then dropped to 0.05 mmol L^{-1} h^{-1} during – 25 to – 125 mV CCM. However, after a week of operation at – 175 mV, the rate ramped up to 0.225 mmol L^{-1} h^{-1} (Figure 5.6, top). The sudden improvement in acetic acid production rate complies with the current generation; it rapidly increased from 0.5 mA to 55.0 mA, the anodic voltage also exceeded 2.0 V (Figure 5.6, bottom) towards the end of the experiment.

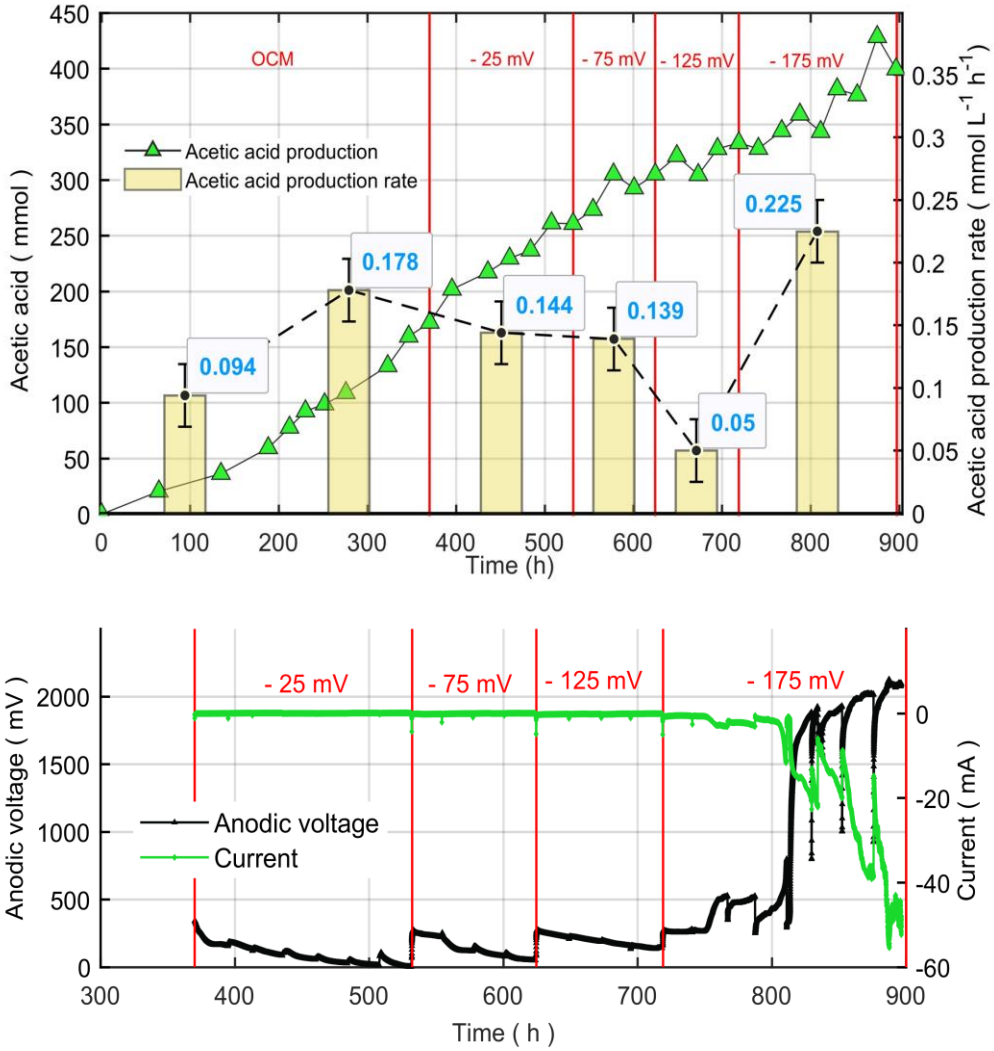

Figure 5.6: Top - Accumulated acetic acid production and the rate profiles, Bottom - Current and anodic voltage trends during CCM operation.

During OCM, the H_2 consumption reached a stable rate at 0.8 mmol L^{-1} h^{-1}, then dropped to 0.7 mmol L^{-1} h^{-1} once the CCM started. When the anodic voltage reached 2.0 V, the rate immediately fell to a negative value, gas production was observed. The change in headspace H_2 pressure and the gas consumption rate are presented in Figure 5.7.

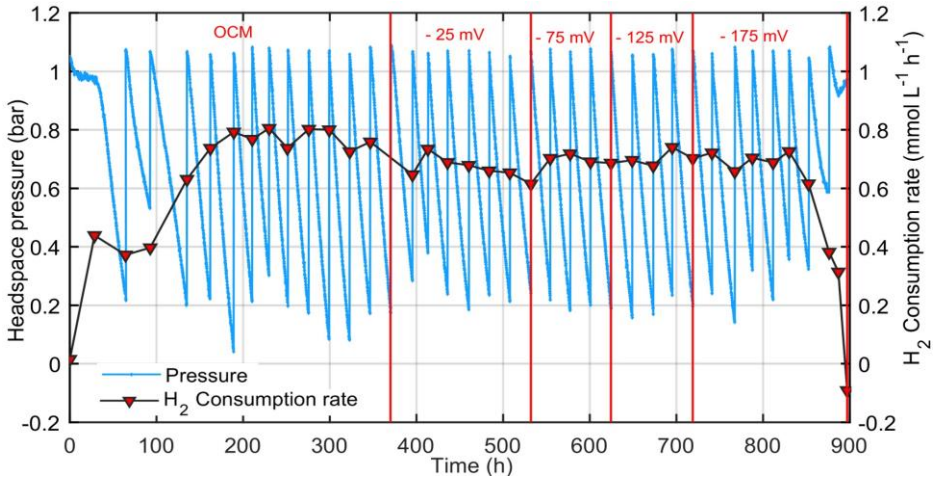

Figure 5.7: H_2 headspace pressure and consumption rate profiles.

The study concluded that – 175 mV reducing power applied on the cathode improved the acetic acid synthesis at 75 % of columbic efficiency. The – 175 mV was the lowest benchmark potential among relevant studies. The applied redox potential did not increase the H_2 consumption because the direct electron transfer from cathode to microorganisms diminishes that H_2 requirement from the headspace.

At – 175 mV, the gas composition analysis revealed O_2, CO_2, and N_2 evolution. This is due to the anodic oxidation of water, organics, and ammonium. A clear descent in ammonium concentration from 620 to 570 mg L^{-1} complies with N_2 production. Therefore, it indicates that water, organics, and ammonium are the carbon-free p&e sources that substantially improved acetic acid synthesis at MES integrated syngas fermentation.

The CV results showed a significant rise in catalytic current generation from the plain electrode (– 0.22 A) to towards the end of CCM (– 0.86 A). The SEM images and microbial analysis confirmed that the cathode is populated with a dense biofilm that complies with higher current production. Moreover, a notable reduction in charge transfer and ohmic

resistances also adds value to the argument that cathode is assimilated with biofilm that catalyses electrochemically mediated acetic acid synthesis.

5.5 Article 5: Impact of Electrochemical Reducing Power on Syngas Fermentation

This study advances the lessons learnt from article 4. A significant difference is that industrially suitable syngas (15% CO, 15% H2, 20% N_2, and 50% CO_2) was fermented instead of H_2. All methodologies were quite similar to article 4, and the experiments were performed with the same reactor settings with fresh inoculum and electrodes. OCM lasted for 27 days. Then the CCM was started at -50 mV and increased to -400 mV at a rate of 50 mV every two weeks. The purpose is to determine the lowest benchmark potential for electrochemically mediated industrially relevant syngas fermentation to move forward in technological readiness level; therein, acetate synthesis and GL mass transfer are mainly studied.

At the OCM, acetic acid synthesis stabilised around 36 mmol at an average rate of 0.017 mmol L^{-1} h^{-1}. During – 150 mV CCM, the acetate synthesis ramped up to 262 mmol at a rate of 0.263 mmol L^{-1} h^{-1}, CE was around 49 %. At that point, the anodic voltage reached 2.0 V; therefore, electrodes were deprived of the biotic nature, resulting in a remarkable reduction in acetate synthesis. A clear drop in current from 30 mA to 1 mA and anodic voltage from 2.0 V to 0.5 V complied with lower product synthesis. However, the microorganisms adapted and recovered from – 350 mV to – 400 mV; therein, the current surged up to 60 mA, and anodic voltage reached 2.0 V again. The higher anodic voltage oxidised the acetic acid, lowered the product synthesis. In addition, ammonium and water also get oxidised, confirmed by the evolution of CO_2, N_2, and O_2 in the headspace. Figure 5.8 shows the acetic acid, current generation, and anodic voltage profiles at one glance.

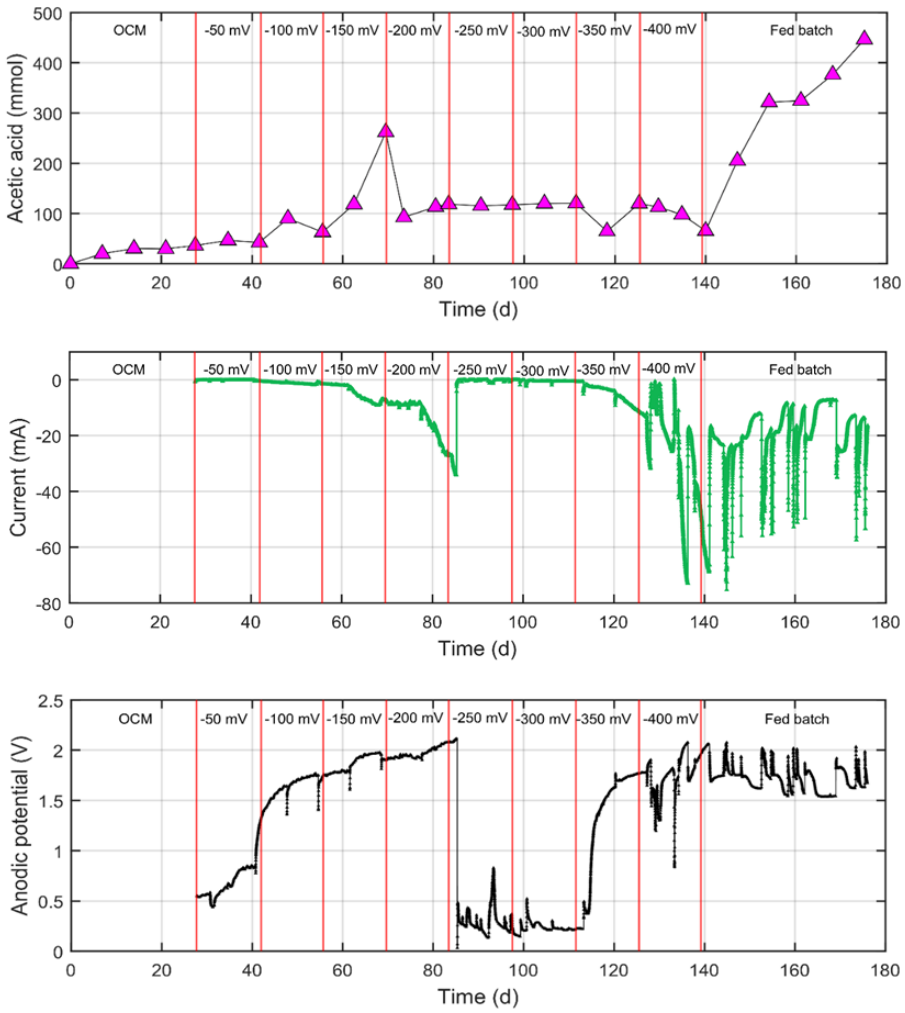

Figure 5.8: Top - Accumulated acetic acid, Middle - Current, and Bottom - Anodic potential profiles.

Approximately 50 % of the CO was consumed during OCM when 62 % was in – 250 mV CCM. Around 37 % of the CO_2 was consumed throughout the experiment. However, the CO and CO_2 consumption profiles do not well comply with acetic acid production. Because of stochastic changes in CO_2 production due to organic oxidation and CO production through catalytic reduction of CO_2.

The study concludes that industrially relevant syngas can be bio electrochemically fermented. – 150 mV was identified as the lowest benchmark potential for the particular fermentation medium (Knardalstrand WWTP, Porsgrunn) and specific syngas composition. In addition, results from fed-batch experiments depicted a clear upward

trend in acetate synthesis and affirmed that replacing the fermentation medium could maintain the anodic voltage lower than 2.0 V. Therefore, detailed fed-batch mode experiments are suggested for future studies. Similar to article 4, CV shows a clear catalytic current improvement from – 0.18 A to – 0.97 A, towards the end of CCM. Moreover, charge transfer resistance also decreased from 1.067 ohm to 0.569 ohm. These observations proved the assimilation of active biofilm on the cathode.

5.6 Article 6: Simple Modelling Approach Using Modelica for Microbial Electrosynthesis

This study aims to create a simple model as an interface between the power electronic side and the biochemical side of the MES reactor. Open-source modelling tool Modelica was used as the platform. The impedance values are the essential inputs for the model that are quantified through EIS analysis. The model examines the variation in the resistances in the MES integrated AD due to the biofilm growth. In addition, the required voltage to keep the potential difference across the cathodic biofilm within optimal conditions was investigated.

The simulation results depicted that keeping a particular voltage level between anode and cathode is possible without exceeding a specific set value (V_biofilm = - 0.42 V) at the cathode. At the same time, the anodic voltage also stayed well below to prevent anodic oxidation. The EIS experiment estimated that catholyte resistance was 60 ohm. The cathode was poised at -0.42 V at potentiostatic mode. At the start, 13 µA cathodic current was measured that continued to increase up to 150 µA during 21 days of operation. Simultaneously the biofilm resistance was also dropped from 32 kΩ to 3 kΩ.

The modelling work concludes that it is possible to keep the desired potential across the cathodic biofilm while the voltage between anode and cathode remains in the acceptable range without accounting for the anodic oxidation. In addition, the model becomes useful to extrapolate the experimental results for better understating of the MES system.

5.7 Additional results

5.7.1 Source of electrons and protons

Electrons and protons are generated from the anode to perform MES on the cathode. Most studies revealed that water oxidation is the primary source of p&e. In addition, organics, ammonium, and sulphides oxidation also can generate p&e upon oxidation. Among them, ammonium and sulphides are carbon free-electron sources. The studies performed in articles 3, 4, and 5 confirmed that electrochemically mediated acetate synthesis was performed by p&e generated at anode mainly through water, ammonium oxidation Eqs. 1.9 – 1.11. This has also been previously demonstrated at USN laboratories (Nelabhotla, 2020).

5.7.2 Microbiome analysis

At the end of the 15 bar H_2 headspace pressure experiment (article 1), the fermentation medium was dominated (65 %) by *Pseudomonadaceae* and *Clostridiaceae,* which comprise species of spore-forming anaerobes that accounts for VFA and biogas production (Buettner et al., 2019).

The study presented in article 4, the raw inoculum consists of a higher diversity of bacterial families; some of them were non-spore-forming, obliterated upon sludge heat treatment. Planococcaceae dominated the treated inoculum. The OCM planktonic medium was rich in 45 % *Clostridiaceae,* and 25 % *Veillonellaceae*, which are families consisting of spor-forming obligate anaerobic homoacetogenic bacteria. Once the operation mode shifted to CCM, *Clostridiaceae* presence increased to 53 %, while *Veillonellaceae* declined to 3 % in the suspended medium. However, the electrodes depicted a higher abundance of Veillonellaceae, suggesting that they are likely growing as biofilms and, therefore, not dominant in the liquid medium.

Reference

Buettner, C., von Bergen, M., Jehmlich, N., & Noll, M. (2019). Pseudomonas spp. Are key players in agricultural biogas substrate degradation. *Scientific Reports*, *9*(1), 12871.

Hickey, R. (2009). *Moving bed biofilm reactor (mbbr) system for conversion of syngas components to liquid products* (United States Patent No. US20090035848A1). https://patents.google.com/patent/US20090035848A1/en

Nelabhotla, A. B. T. (2020). *Electrochemical Unit Integration with Biogas Production Processes* (Publication No. 62). [Doctoral dissertation, University of South-Eastern Norway].

6 Conclusions

Syngas fermentation and MES can advance biogas production by allowing higher yields, substantially replacing fossil fuels. However, GL mass transfer, kinetic growth limitations, and lack of reducing equivalents hinder the process integration. Therefore, this PhD project examined the impact of H_2 partial pressure on syngas fermentation to overcome the GL mass transfer limitation, therein, figured out the optimum pressure. Then MBB was integrated into that optimum pressure condition, where the kinetic limitation was studied. The impact of MES integration on syngas fermentation implicit in biogas production is investigated. The compendium of the overall research findings is presented in the summarizing conclusion section, while the supplementary findings are under externalizing conclusion.

6.1 Summarizing conclusion

6.1.1 Impact of H_2 partial pressure

In theory, enhancing the H_2 GL mass transfer by elevating the headspace pressure is true if it is only a physical process. However, syngas fermentation is professed due to the microbial gas uptake limitation. Increasing H_2 headspace pressure from 1 to 15 bar improved the gas uptake rate (6.22 mmol L^{-1} h^{-1}) by 250 % and acetic acid concentration (49.96 mmol L^{-1}) by 81 %; after that, it declined. The microbial consortium at the 15-bar experiment depicted a significant reduction in complexity, dominated by *Pseudomonadaceae* and *Clostridiaceae.* Eventually, the study concluded that 15 bar was the optimum H_2 pressure for that particular fermentation medium from Knardalstrand WWTP-AD.

6.1.2 Effect of moving bed biofilm into high-pressure syngas fermentation

The biocarries acted as a habitat for the slow-growing microorganisms (biofilm thickness: 157±20 µm); thus, minimal the kinetic growth limitation. In contrast to the pressurized (15 bar) fermentation on planktonic medium, the MBB integration aggrandized the gas

uptake rate (8.333 mmol L^{-1} h^{-1}) by 33 % and the acetate synthesis rate (1.558 mmol L^{-1} h^{-1}) by 48 %. Therefore, it is concluded that MBB can be combined with elevated pressure syngas fermentation reactors to overcome, at least partially, both the GL and kinetic growth limitations, thus accelerating the syngas fermentation process.

6.1.3 MES integration into syngas fermentation

Compared to the suspended culture fermentation, MES integration at open circuit mode promoted 125 % more H_2 gas uptake rate (0.563 mmol L^{-1} h^{-1}) and improved acetate synthesis (57 mmol L^{-1}) by 63 %. Because the MES unit consists of carbon felt and titanium as electrodes that provided a surface area for the biofilm growth, thus kinetic limitation became minimal. This is analogue to the MBBR, where plastic biocarriers were the medium that facilitated the attached growth.

However, the hypothesis of increasing H_2 gas uptake rate and acetate synthesis through – 0.8 V cathodic potential failed at CCM. This is due to either the electrodes could deprive of the biotic nature, or the anodic potential could have exceeded the formal potential of the acetic acid oxidation, resulting in H_2 gas evolution. Therefore, finding the lowest benchmark potential became vital; a separate study scrutinised it.

The benchmark study set - 175 mV as the lowest benchmark cathodic potential therein anodic voltage reached 2.0 V. In contrast to the OCM performed in this study, the – 175 mV reducing power improved the acetate synthesis rate (0.225 mmol L^{-1} h^{-1}) by 26 %. However, there was no improvement in the headspace H_2 consumption because the direct electron transfer from cathode to microorganisms lowered the H_2 demand from the headspace.

An industrially relevant syngas gas (15 % CO, 15 % H_2, 20 % N_2 in 50 % CO_2) was fermented into a MES integrated reactor to move forward in the technology readiness level. The feasibility of such process integration was examined within the range of – 50 to – 400 mV to determine the lowest benchmark. The study concluded that – 150 mV, as the lowest possible potential, enhanced the acetate synthesis rate (0.263 mmol L^{-1} h^{-1})

by 15-fold compared to the OCM. The CO did not show any remarkable inhibition; 60 % of it was consumed. Anodic potential over 2.0 V lowered the acetate synthesis; however, superseding the fermentation medium with fresh Inoculum through fed-batch mode appears to be a promising strategy to lower the anodic potential.

The results collectively proved that elevated syngas pressure, MBB, and MES incorporation improved the acetate synthesis, which further converted into methane, thus advancing the biogas production.

6.2 Externalizing conclusion

- Electrode incorporation into a syngas fermenter improves acetate synthesis volumetric rate.
- Oxidizing VFAs at the anode via controlling the potential is possible, therefore could be a valuable tool for process monitoring and control.
- Ammonium, water and organics are the sources of electrons and protons.
- The bacteria colonisation on the electrodes to form biofilm lowers the ohmic and charge transfer resistances and increases the current generation.
- Modelica is an attractive interface to combine the power electronics and biochemical sides.
- The simple modelling approach presented in article six could potentially be helpful to extrapolate the experimental part of MES integration into biogas.

Research at USN has shown that CO_2 can be converted to CH_4 at the cathode while oxidizing water, ammonium, and sulphide as the source of p&e. This dissertation opens the possibility for a future single unit biogas system where energy contained in sulphides, ammonium, and synthesis gas will be part of one single unit MES integrated AD reactor, solving all of the most important processes issues in biogas plants.

7 Recommendations

This PhD project performed all the experiments on a homoacetogenic medium, where methanogens were suppressed. Therefore, it is recommended to investigate the effect of methanogens rich inoculum on syngas fermentation and MES to comply with industrially relevant biogas process integration.

Syngas fermentation and MES processes are complex and multivariable (i.e., pH, temperature, type of fermentation medium, reactor design, electrode material etc.); therefore, a detailed chemometric study is suggested for disentangling these complexities.

Temperature is a critical factor affecting gas solubility and growth kinetics in syngas fermentation. Both factors behave appositively; thus, an increase in temperature decreases the gas solubility while increasing the growth rate to a certain extent. Therefore, it needs to be optimised. All the experiments in this study were performed at room temperature; therefore, optimization is strongly recommended for future studies.

Understanding the different electron transfer mechanisms could open up new avenues in the MES fields therefore considered as a vital element for future studies.

The simple Modelica model should be advanced with a standalone equivalent circuit model editor to be able to use as a complete process control platform.

The study presented in article 5 revealed the CO evolution at some point of the experiment. CO synthesize from CO_2 is usually metal catalyst mediated and requires higher redox potentials (E^0= - 0.53 V); therefore, less likely possible in this reactor setup. However, the biofilm accumulated on the electrodes could function as the biocatalyst, thus lowering the required potential. To confirm is observation, a detailed future study is recommended.

Article 5 introduced the fed-batch operation as a strategy to lower the anodic potential. Since it was a preliminary finding, a detailed study is suggested to explore its unlimited

usage. In addition, during this PhD project, most of the experiments were performed on batch and fed-batch modes. Therefore, continuous flow experiments are suggested for future studies.

The microbiome analysis performed in this study was mainly based on the family level. A genus-level detail future study is recommended to determine the electroactive nature and microbial dependence of syngas fermentation.

Only a specific inoculum from Knarrdalstrand WWTP-AD, Porsgrunn, Norway, was utilised as the fermentation medium. Future research could examine different inoculum types, especially from the local commercial biogas plants.

Most of the MES studies performed in this project is based on carbon electrodes. Therefore, a detailed future study is recommended to examine different electrode materials and the affinity of the biofilm. Especially, study about stainless steel as electrodes is essential to move forward in the scaling-up process.

The elevated pressure impact, integration of MBBR and MES are examined individually during this PhD program; however, combining these three strategies as a single process unit would be an interesting future work.

Part – II

Article 1

Effect of Elevated Hydrogen Partial Pressure on Mixed Culture Homoacetogenesis

Vasan Sivalingam[1], Tone Haugen[2], Alexander Wentzel[2], and Carlos Dinamarca[1]

[1]Department of Process, Energy and Environmental Technology, University of South-Eastern Norway, Porsgrunn, Norway
[2]Department of Biotechnology and Nanomedicine, SINTEF Industry, Trondheim, Norway

Published in Chemical Engineering Science – X, 2021 (Level 2) Journal.
DOI: 10.1016/j.cesx.2021.100118

Chemical Engineering Science: X 12 (2021) 100118

Contents lists available at ScienceDirect

Chemical Engineering Science: X

journal homepage: www.elsevier.com/locate/cesx

Effect of Elevated Hydrogen Partial Pressure on Mixed Culture Homoacetogenesis

Vasan Sivalingam [a], Tone Haugen [b], Alexander Wentzel [b], Carlos Dinamarca [a,*]

[a] Department of Process, Energy and Environmental Technology, University of South-Eastern Norway, Porsgrunn, Norway
[b] Department of Biotechnology and Nanomedicine, SINTEF Industry, Trondheim, Norway

ARTICLE INFO

Article history:
Received 27 February 2021
Received in revised form 22 September 2021
Accepted 31 October 2021

Keywords:
Syngas fermentation
CO_2 utilization
Wood-Ljungdahl
High-pressure
Hydrogen
Mixed culture

ABSTRACT

This study aimed to systematically investigate the effect of elevated hydrogen partial pressure on mixed culture homoacetogenesis in the range of 1–25 bar. Seven batch experiments were performed at different initial headspace pressures, i.e., 1, 3, 5, 10, 15, 20, and 25 bar. The 15 bar batch showed the highest gas uptake rate (6.22 mol $h^{-1}L^{-1}$) and volatile fatty acids synthesis (3.55 g L^{-1}) by a final microbial consortium that was found to be largely reduced in complexity compared to the original inoculum culture and dominated by members of the *Pseudomonadaceae* and *Clostridiaceae*. Product distribution shifted from acetate to C_3-C_5 acids at a pressure above 15 bar. 15 bar was found to be the optimum elevated pressure for the used mixed culture fermentation medium and biodiversity used in this study, and pressure above 15 bar inhibited the microbial consortia and resulted in lowered gas uptake rate and product synthesis.

1. Introduction

Syngas is a key product of biomass pyrolysis and gasification processes, contains carbon monoxide (CO), hydrogen (H_2) and carbon dioxide (CO_2) (Grimalt-Alemany et al., 2018). It can be converted to biofuels through bacteria-mediated acidogenesis, solventogenesis, and methanogenesis or thermochemical processes like Fischer-Tropsch (Daniell et al., 2012). Acetate is the most common metabolic intermediate, further converted to biogas in an anaerobic digestor (Anukam et al., 2019; Geppert et al., 2016). Biogas production from syngas is a sustainable approach in the field of clean biofuel production (Torri et al., 2020). Utilizing syngas to produce biofuels brings sustainable value addition (Daniell et al., 2012) and reduces the alternative cost of carbon capture and storage.

Homoacetogens are a group of acetogenic bacteria that have the capability to ferment syngas into acids and alcohols (Mohammadi et al., 2011). Fischer et al. (1932) first reported that the homoacetogens with capabilities to use CO_2 and H_2 as carbon and energy sources, respectively, to produce acetate (Drake, 2012), Equation (1). However, Wood and Ljungdahl presented the detail reduction pathway in the late 1980 s. They identified the acetyl-CoA as an essential intermediate (Diekert & Wohlfarth, 1994). Therefore, referred to as Wood Ljungdahl Pathway and the acetyl-CoA pathways. Moreover, the theory behind the WLP is briefly presented in section 1.1 to ensure the good flow of understanding.

$$4H_2 + 2CO_2 \rightarrow CH_3COOH + 2H_2O \ \Delta G^0 = -74.3 \text{ kJ/mol} \quad (1)$$

The formation of metabolic intermediates is essentially influenced by the concentration of chemical compounds in the liquid phase, primarily on mass transfer at the gas–liquid interface (Cuff et al., 2020; Mulat et al., 2017; Phillips et al., 2017; Yasin et al., 2019). The solubility of CO and H_2 are 60 and 1056 times less than CO_2 (Phillips et al., 2017), respectively. Temperature and partial pressure of the gaseous species are the main parameters that influence the gas solubility in a liquid medium (Pereira et al., 2013; Phillips et al., 2017). Temperature and pressure impact syngas fermentation have been studied for many years (Conrad & Wetter, 1990; Kundiyana et al., 2011; Shen et al., 2020; Stoll et al., 2019; Van Hecke et al., 2019). However, H_2 in the syngas mixture needs more attention because of its lower solubility. The H_2 utilization rate by bacteria depends on H_2 partial pressure, fermentation product concentrations such as Volatile fatty acids (VFAs) available in the medium, and the mass transfer rates (Dinamarca et al., 2011).

According to Henry's law, a rise in partial pressure of H_2 in the headspace increases the gas solubility, referred in Equation (2).

* Corresponding author at: University of South-Eastern Norway, Kjønes ring 56, 3918 Porsgrunn, Norway.
E-mail addresses: vasan.sivalingam@usn.no (V. Sivalingam), carlos.dinamarca@usn.no (C. Dinamarca).

https://doi.org/10.1016/j.cesx.2021.100118
2590-1400/

Where C_{H_2} is the H_2 concentration (mol L^{-1}) in the liquid medium, y_{H2} is the H_2 mole fraction (at gas phase), P_T is the total headspace pressure (atm) and H_{H2} (atm mol^{-1} L) is Henry's law constant of the H_2 gas (Kantzow & Weuster-Botz, 2016; Phillips et al., 2017).

$$C_{H_2} = y_{H2}\frac{P_T}{H_{H2}} \quad (2)$$

However, microorganisms also could be sensitive to partial pressure (Abubackar et al., 2011) and the dissolved gas tension. Their pressure tolerability could decide the upper limit of partial pressure that can be applied, depending on the type of microorganisms (Van Hecke et al., 2019).

Even though it is substantiated that rising partial pressure increases the gas–liquid mass transfer, to the best of our knowledge, there is not enough research in this field conducted over 10 bar H_2 headspace pressure on mixed culture homoacetogenesis process (Stoll et al., 2018; Van Hecke et al., 2019). This is because of the higher cost of operation and process safety concerns; however, it has become economically viable in recent years due to the technological advancement. Therefore, this study is a first attempt to evaluate the impact of highly elevated H_2 partial pressure up to 25 bar on a sludge-based mixed culture homoacetogenic medium.

1.1. The Wood-Ljungdahl pathway

The Wood-Ljungdahl (WLP) pathway has been extensively studied over several decades because it is an attractive and sustainable way of fixing CO_2 to mitigate global warming and produce valuable chemicals such as acetate and ethanol (Fernández-Naveira et al., 2017; Hu et al., 2011; Saady, 2013; Stoll et al., 2018). The carbon in the CO_2 molecule is at the highest possible oxidation state (+4). H_2 gas acts as the reducing equivalent/electron donor and donates electrons to this CO_2 fixation process, which results in acetate as the primary product. Since many pieces of literature explain the WLP in detail, a brief flow diagram is present in Fig. 1 with relevant sequenced chemical reactions (Bertsch & Müller, 2015; Hu et al., 2011; Liew et al., 2016; Saady, 2013; Schuchmann & Müller, 2014; Wilkins & Atiyeh, 2011). In brief, acetate production via the WLP pathway consists of two branches of reactions, i.e., methyl branch and carbonyl branch. The methyl branch consists of several reductive steps to reduce CO_2 to the methyl group ($-CH_3$), while the carbonyl branch is a shorter reduction branch where CO_2 is reduced into CO/carbonyl group (C═O) by two units of reducing equivalent. Methyl, carbonyl groups and coenzyme merge to form acetyl-CoA, which is further converted into acetate. The H_2 gas oxidation produces reducing equivalents, facilitated by electron bifurcating hydrogenase enzyme (Bertsch & Müller, 2015).

2. Material and methods

In this section, culture enrichment, experimental and analytical methodology, and microbiome analysis procedures are explained in detail.

2.1. Homoacetogenic culture enrichment

The anaerobe seed sludge was collected from a biogas digester at Knarrdalstrand wastewater treatment plant, Porsgrunn, Norway. The sludge went through several pretreatment steps to obtain the desired fermentation quality. First, a 600 μm sieve was used to eliminate coarse impurities such as plastic and woody debris. It was then incubated for seven days at 35 °C for further thickening and depleted the remaining degradable organic matters. The thickened sludge was heat-treated at 105 °C for 48 h to obliterate

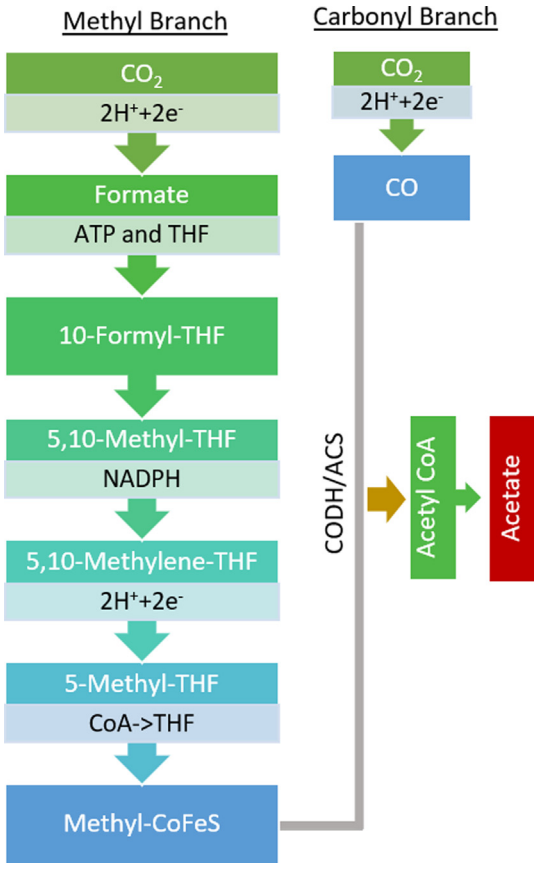

Fig. 1. *The WLP for acetate synthesis;* (). *adapted from* Drake, 2012

methanogens (Sivalingam et al., 2021). While the methanogens are obliterated, homoacetogens remain in the sludge in the form of spores. Following the heat treatment process, the sludge was left to cool down to room temperature and was used as an inoculum. The treated inoculum density in terms of volatile and total solids ratio (VS/TS) was 0.41. A salt solution (10 mL/L inoculum), a vitamin solution (1 mL/ L inoculum), and a mineral solution (1 mL/ L inoculum) were added to the inoculum to make a nutrient base for microbial growth. The nutrient base medium was prepared according to a similar study performed earlier (Dinamarca & Bakke, 2009; Sivalingam & Dinamarca, 2021). The content of the nutrient base is listed in table 1.

2.2. Fermentation reactor and experimental methodology

A stainless steel 640 mL pressure vessel (BR-500, Berghof, Eningen, Germany) was used as the fermentation reactor. The reactor

Table 1
Content of nutrient base media used to support the growth of homoacetogenic culture.

Vitamin solution (g/L)	Mineral solution (g/L)	Salt solution (g/L)
Biotin: 0.02	$MnSO_4{\cdot}H_2O$: 0.04	NH_4Cl: 100
Folic acid: 0.02	$FeSO_4{\cdot}7H_2O$: 2.7	NaCl: 10
Pyridoxine hydrochloride: 0.1	$CuSO_4{\cdot}5H_2O$: 0.055	$MgCl_2{\cdot}6H_2O$: 10
Riboflavin: 0.05	$NiCl_2{\cdot}6H_2O$: 0.1	$CaCl_2{\cdot}2H_2O$: 5
Thiamine: 0.05	$ZnSO_4{\cdot}7H_2O$: 0.088	
Nicotinic acid: 0.05	$CoCl_2{\cdot}6H_2O$: 0.05	
Pantothenic acid: 0.05	H_3BO_3: 0.05	
Vitamin B12: 0.001		
p-aminobenzoic acid: 0.05		
Thioctic acid: 0.05		

comprises a digital manometer (LEO-3, Keller, Winterthur, Switzerland) connected to the computer via RS485 interface to log the pressure every 10 min. The Control Center Series-30 from the Keller software package was used as the automatic pressure logging platform. A mechanical stirrer (BG 65X50, Dunkermotoren, Bonndorf, Germany) continuously mixed the fermentation medium at 200 rpm.

The experimental plan is to run seven batch experiments, where only the initial H_2 partial pressure was changed from 1 to 25 bar. First the pressure vessel was filled with 300 mL treated inoculum with added nutrient base and sodium bicarbonate, which leaves 340 mL headspace. Nitrogen gas was purged for 5 min to push out the air from the inoculum and the headspace; subsequently, the residual nitrogen was flushed out with pure H_2 gas for 2 min to ensure the anaerobic environment. Then the reactor was pressurized to desired values according to the experimental plan, thus 1, 3, 5, 10, 15, 20, and 25 bar manometric pressure, respectively in independent batch experiments, using the H_2 gas (H_2 gas Laboratory 5.5 = $\geq$ 99.9995 %, Linde Gas AS, Oslo, Norway).

All experiments were performed at ambient temperature, 25 °C. Since the study aims to evaluate the impact of the H_2 partial pressure, 3.4 g/L sodium bicarbonate ($NaHCO_3$) was added to the inoculum as the dissolved inorganic carbon source (Gardner et al., 2013; Sivalingam & Dinamarca, 2021). Though the inoculum contains intrinsic inorganic carbon originated from bacterial biomass decay, $NaHCO_3$ was added to corroborate appropriate culturing conditions. The initial pH of the inoculum was 8.5, which was neither adjusted nor controlled throughout the experiments. Such higher pH ensures that added bicarbonate will remain in the liquid medium at equilibrium with carbonate ion without escaping to the headspace as carbon dioxide gas (Tchobanoglous et al., 2014).

During each experiment, H_2 in the headspace diffuses into the bulk-liquid. As the inoculum consumes it, the headspace pressure decreases over time. The experiments were completed when H_2 consumption rate becomes significantly low, indicating depletion of the carbon source, HCO_3^-. The 1 bar batch was re-pressurized two times to reach no further change in pressure, while the other batches reached this state with one time pressurizing. Because the research aim is to perform repeated batch process only replenishing the initial H_2 partial pressure between batch experiments.

Various analyses were performed on the liquid medium are described in section 2.3. Experimental conditions were identical for all seven batch cultivations, except the initial H_2 headspace pressure.

2.3. Analytical methodology

Volatile fatty acids (VFAs), pH, total solids (TS), ammonium and volatile solids (VS) were analyzed at the beginning and the end of each batch experiments. The pH was measured by a Beckman 390 pH-meter (Beckman Instruments, Indiana, USA). The fermentation products/VFAs were quantified by gas chromatography (PerkinElmer, Clarus 500, Massachusetts, USA) equipped with a capillary column (length 25 m × 0.25 mm diameter × film 0.2 µm) and Flame Ionization Detector (FID) having H_2 as the carrier gas (45 mL/min). The injector and detector temperatures were 270 °C and 250 °C, respectively. The initial oven temperature was set at 80 °C and kept constant for 0.7 min, then let it rise by 25 °C/min until it reached 200 °C. Subsequently, a 20 °C/min ramp-up rate was assigned to achieve 240 °C. A Spectroquant® Pharo 300 UV/VIS photometer (Merck KGaA, Darmstadt, Germany) was used to quantify the ammonium concentration according to the standard method (2500 A) of the America Public Health Association (APHA, 1995). Volatile solids were determined according to US standard 2540 E (APHA, 1995).

2.4. Microbiome analysis by 16s rRNA gene metabarcoding

Total metagenomic DNA was extracted from the pellet of various amounts of the samples using the Quick DNA-Fecal/ Soil Microbe DNA Miniprep Kit (Zymo Research) according to the manufacturer's protocol. Sequencing amplicon libraries were generated by PCR following the "16S Metagenomic Sequencing Library Preparation, Preparing 16S Ribosomal RNA Gene Amplicons for the Illumina MiSeq System" protocol (Illumina part number 15044223 rev. B). Internal parts of the 16S ribosomal RNA (rRNA) gene, covering variable regions V3 and V4, were PCR-amplified with the KAPA HiFi HotStart ReadyMix (KAPA Biosystems) and the primers 5′-TCGTCGGCAGCGTCAGATGTGTATAAGAGACAGCCTACGGGNGGC WGCAG-3′ and 5′-GTCTCGTGGGCTCGGAGATGTGTATAAGAGACAG GACTACHVGGGTATCTAATCC-3′ and purified with the Agencourt AMPure XP kit (Beckman Coulter). The Nextera XT Index Kit was used to add sequencing adapters and multiplexing indices by PCR, and the products were purified by Agencourt AMPure XP followed by quantification on a Qubit v2 using the Qubit dsDNA BR Assay Kit (Thermo Fisher Scientific). Pooled DNA libraries were sequenced on an Illumina MiSeq sequencer using the MiSeq Reagent Kit v3 in the 2x·300 bp paired-end mode. After sequencing, raw sequencing reads were demultiplexed, filtered, combined, and taxonomically classified by the Metagenomics Workflow within MiSeq Reporter v. 2.5.1 (Illumina), generating abundance tables and biodiversity indices like Phylogenetic diversity and Shannon index, which were further processed in Microsoft Excel.

3. Results and discussion

3.1. H_2 gas consumption and product formation

Fig. 2 presents 7 time series plots for different start pressures, i.e., 1, 3, 5, 10, 15, 20, and 25 bar. Only the 1 bar batch's pressure reached close to zero during incubation and was then repeatedly re-pressurized to 1 bar until the gas consumption stopped. For 16.7 h, pressure remained approximately unchanged for the 1, 3, and 5 bar experiments, while higher pressure batches showed an immediate reduction in headspace pressure. The impact of elevated pressure could be the reason for such instant pressure reduction; according to equation (2), the increase pressure-gradient, consequently, increase the H_2 molar transfer rate that results in the headspace pressure reduction. However, equation (2) does not explain the impact of the constant pressure observed at the beginning of every batch, almost the first 10 h. It could be the lag phase of the microbial community. The one bar experiment took around 13 days to reach the saturated gas consumption level, while other batches took only 4 – 5 days. In order to evaluate the amount of total consumed H_2, cumulative consumed H_2 graphs are presented in Fig. 3.

The one bar batch cultivation showed a cumulative H_2 consumption of 39 mmol after 300 h. The other batch cultivations all reached maximum cumulative H_2 consumption much earlier by 120 h. Up to 15 bar, the total amount of dissolved H_2 gas consumed increased with the partial pressure applied, thus 21.1 mmol in 3 bar, 32.18 mmol in 5 bar, 36.56 mmol in 10 bar and 47.24 mmol in 15 bar batches. The consumed H_2 in the 15 bar batch was approximately five times higher than the 1 bar batch cultivation. The 20 and 25 bar batches consumed respectively 43.27 and 47.75 mmol H_2, which do not comply with the observed trend in pressure versus consumed H_2 from 1 bar to 15 bar batches. This result indicates that the partial pressure improves gas solubility and uptake rate until 15 bar, while further increase apparently affects the uptake rate negatively.

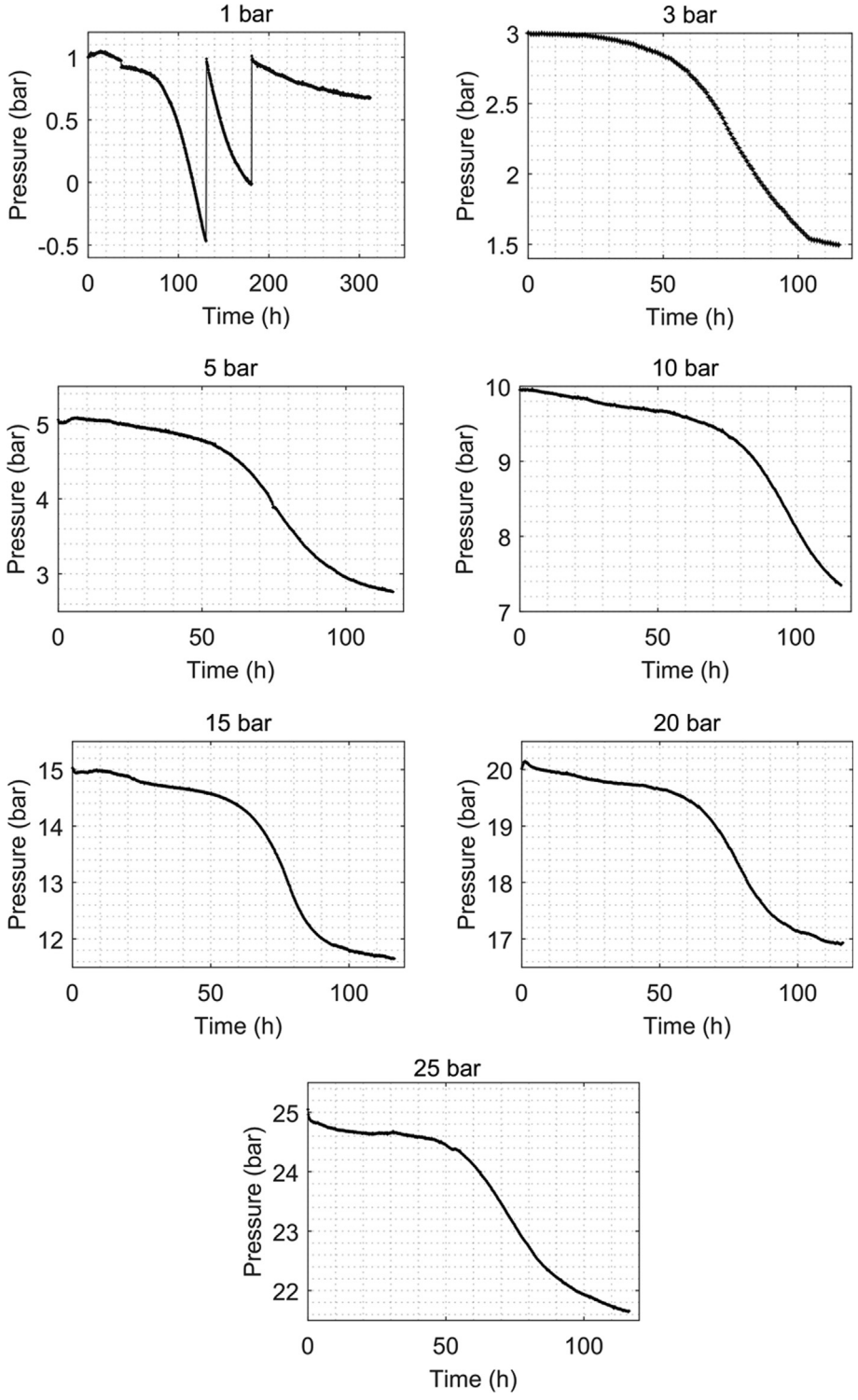

Fig. 2. Headspace pressure time series.

However, the changes in pressure gradients (gas uptake rate) are not clearly seen in Fig. 3; therefore, the gas uptake rates are presented separately in Fig. 4. Increasing gas solubility by elevating partial pressure is always possible if it is considered as the physical process only. However, the increasing dissolved H_2 tension may negatively impact the microbial gas uptake rate.

The characteristics and state of the microbial inoculum could represent a key limiting factor, as the assemblage may be sensitive to factors such as pressure, pH, temperature, and other physio-chemical parameters. However, in this systematic experimental approach, only the H_2 partial pressure was the parameter changed throughout all the batches indicates the pressure as the critical parameter for H_2 gas consumption. This is in line with previous studies that earlier showed that acetogens are very diverse and primarily respond to inoculum (Van Hecke et al., 2019). Increasing pressure on microorganisms produce changes cell structures and

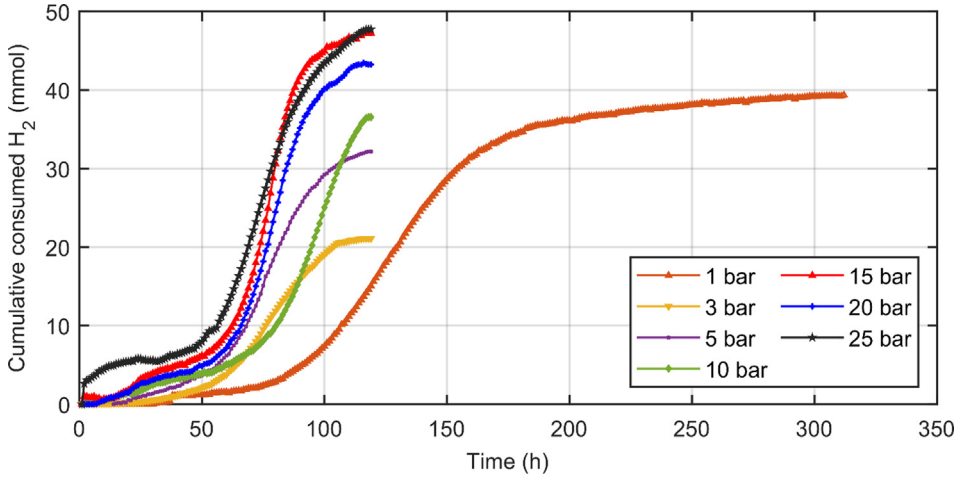

Fig. 3. *Cumulative consumed* H_2 *gas profiles.*

cell functions, sometimes cause for inhibition or cell death (Mota et al., 2013); however not many detail studies have been available particularly about how acetogens behave in different pressures.

The one bar batch reached the maximum gas uptake rate (1.78 mol $h^{-1}L^{-1}$) after 125 h, while the other batches reached their maxima after 70 – 80 h, except for the 10 bar batch that took around 100 h. The 15 bar experiment achieved the highest uptake rate (6.22 mol $h^{-1}L^{-1}$) among all seven batches. Overall, from 1 bar to 15 bar batches, we can see a clear upward trend in maximum uptake rate, consistent with pressure increment. However, the 20 and 25 bar batches showed contradictory behavior. At 20 bar batch, the maximum uptake rate dropped slightly to 5.05 mol h^{-1}-L^{-1} and decreased nearly half of the 15 bar test's uptake rate at 25 bar test (3.79 mol $h^{-1}L^{-1}$). This remarkable reduction in the gas uptake rate explains that pressure above 15 bar inhibits the gas uptake rate, which could be due to microorganisms are inhibited by high dissolved gas tension. As shown in Fig. 2, the pressure time series for 20 and 25 bar batches indicate that the final pressure of the batches at the end of experiments was above 15 bar, i.e., 17 and 21.5 bar, respectively. This is a clear evidence that our inoculum is sensitive to pressures higher than 15 bar.

3.2. Fermentation product synthesis

The acetic acid and total VFAs concentrations with relevant pressures for all seven batches are presented in Fig. 5. The total VFAs concentration grew along with pressure from 1 bar to 15 bar, followed a gradual downward trajectory at 20 and 25 bar tests. The total VFAs consisted of 90 % acetic acid. From 1 to 15 bar, the balance 10 % was contributed by propionic acid, except 3 bar batch, for which only acetic acid could be detected as the fermentation product. Among the seven batches, the highest concentration of the acetic acid (3 g/L) was observed in the 15 bar batch, for which also the highest concentration of total VFAs (3.55 g/L) was detected. This fermentation product analysis confirms that 15 bar is the optimum pressure for this particular mixed culture fermentation, yielding both the highest gas uptake rate and the highest VFA product yield, primarily limited by the added inorganic carbon (bicarbonate salt) in the fermentation medium. The depletion of bicarbonate was ensured stoichiometrically (Equation (1)), which shows that the consumed H_2 and produced acetic acid are more than the available bicarbonate stoichiometric ratio.

In addition to acetic and propionic acid synthesis, the 20 and 25 bar batches showed in addition small amounts of isobutyric and isovaleric acid production. However, all these medium-chain VFAs contributed less than 5 % of the total VFAs production. Ethanol production was observed only for the 25 bar batch and in very small amounts (less than 1 %). All these VFAs concentration are presented in FigureS1 under supplementary section. Although the concentrations of medium-chain VFAs are significantly lower than the short-chain VFAs, this result indicates that elevated headspace pressure can change microorganisms' metabolism, resulting in a different fermentation product spectrum. A similar study performed by Oswald et al. (2018), noticed that increasing partial pressure of H_2 and CO_2 on *Clostridium ljungdahlii* shifted the primary fermentation product acetate to formate (Oswald et al., 2018). However, in this study, acetate shift from formate was not observed; this could be due to different fermentation mediums. Oswald et al., used the pure *Clostridium ljungdahlii* culture, while mixed culture is used in this study which is dominated by *Pseudomonadaceae* and *Clostridiaceae.*

3.3. Physiochemical analysis

pH was measured at the beginning and the end of each experiment, tabulated in Table 2. Overall, an increment in pH from 8.5 to 9.1 – 9.6 was observed. Even though all seven batches produced significant amounts of VFAs, none of them showed a pH reduction. The possible reasons for such a rise in pH are discussed in general.

According to inorganic carbon species equilibrium and pH dependence (Dodds & Dodds, 2002), pH above 8.5 ensures that there is no CO_2 exchange between the headspace and the fermentation medium in our reactors, but the bicarbonate and carbonate species will be in equilibrium (Eq. (3)).

$$HCO_3^- \leftrightarrow CO_3^{2-} + H^+ \quad (3)$$

During the fermentation, process bicarbonate is consumed by the homoacetogens at the expense of H_2 (Equation (4)) (Angelidaki et al., 2011) gas which causes a subsequent leftward shift in equation (3). Such bicarbonate consumption causes a reduction in protons, resulting in an increase in pH.

$$4H_2 + 2HCO_3^- + H^+ \rightarrow CH_3COO^- + 4H_2O \quad (4)$$

Sodium ions (Na^+) are freely available in the fermentation medium due to $NaHCO_3$ added at the beginning of each experiment. The produced acetic acid (pKa = 4.7) will be in the carboxylate ion form (de-protonated) due to the high pH of the fermentation medium (>8.5). Half of the acid will be de-protonated at the pH of pKa, and more will be de-protonated while the pH increases above 4.7 (Trček et al., 2015). Therefore, the de-protonated acetic

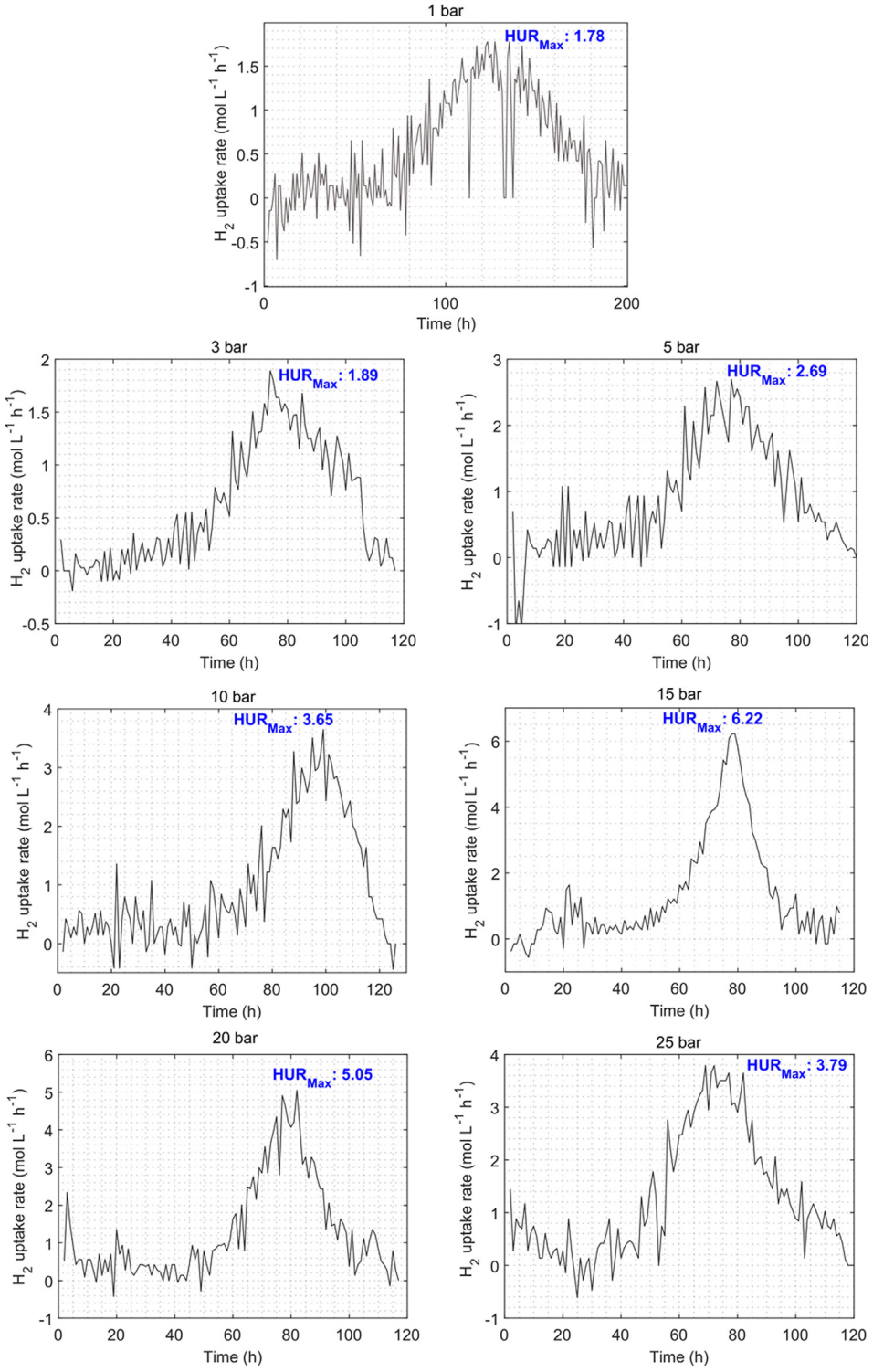

Fig. 4. *H_2 gas uptake rate time series. (Maximum H_2 gas uptake rate (HUR_{Max})* is denoted in blue. (For interpretation of the references to colour in this figure legend, the reader is referred to the web version of this article.)

acid (CH_3COOH^-) and the free sodium ion could form sodium acetate (CH_3COONa). Sodium acetate is a conjugated base, which could trap protons (H^+) from the water and leaves hydroxyl ion (OH^-). The increment in the OH^- concentration could be one possible cause of the pH rise.

Ammonia (NH_3) is usually produced during the anaerobic digestion process due to the breakdown of proteins molecules (Yenigün & Demirel, 2013), which consequently increases the pH by capturing protons from water molecules and leaves hydroxyl ions in the liquid medium. A slight increment in ammonium concentration was observed in our experiments. The ammonium concentration of the inoculum at the start of the experiments was 573 ± 20 mg/L and increased slightly up to 609 ± 22 mg/L towards the end of experiments (Table 2). This shows that protein breakdown and utilization of the amino acids as carbon source could be another possible reason for the observed pH increment.

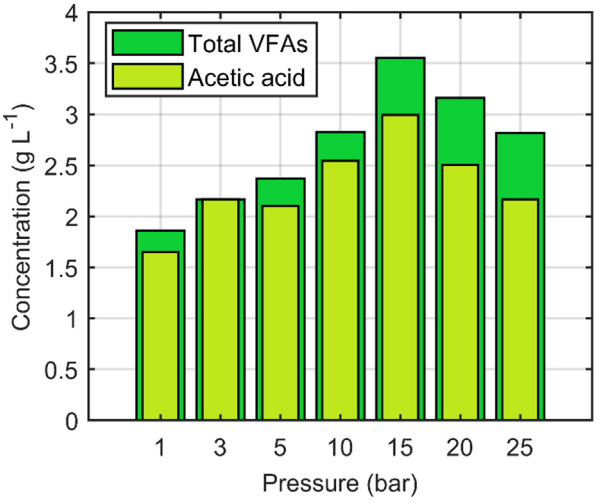

Fig. 5. Acetic acid and total VFAs concentration variations in all seven batches.

However, more control experiments are needed to figure out the individual contributions of above discussed processes.

The volatile solids (VS) and total solids (TS) ratio (VS/TS) was quantified (Table 2) at the beginning and at the end of each batch to evaluate the biomass growth. The fresh fermentation medium's VS/TS was 0.41 and remained approximately in the same range (±0.03) for the pressure batches from 3 to 15 bar. The one bar batch showed a slightly higher ratio than other because this batch was operated for the longest time (13 days). The batches with 20 and 25 bar showed a remarkable VS/TS ratio reduction, respectively 0.37 and 0.34. This observation adds value to our arguments that microorganisms are inhibited (less biomass synthesis) by elevated pressure above 15 bar. The less biomass synthesis coincides with lower product formation at relevant batches (Fig. 5).

Moreover, the overall stoichiometric equation includes energy and synthesis for acetate synthesis from CO_2 and H_2 is derived (Equation (5)) based on approach presented in (Rittmann and McCarty, 2020), therein stoichiometrically possible ammonium consumption and biomass synthesis were evaluated.

Table 2
Initial and final values of pH, ammonium concentration of the liquid medium, and VS/TS ratio at all seven batches.

Parameters	Raw medium	Pressure (bar)						
		1	3	5	10	15	20	25
pH	8.5 ± 0.5	9.1	9.3	9.2	9.4	9.3	9.7	9.6
VS/TS	0.41 ± 0.004	0.46	0.44	0.43	0.41	0.41	0.37	0.34
NH_4^+ (mg/L)	573 ± 20	600	610	610	601	618	572	654

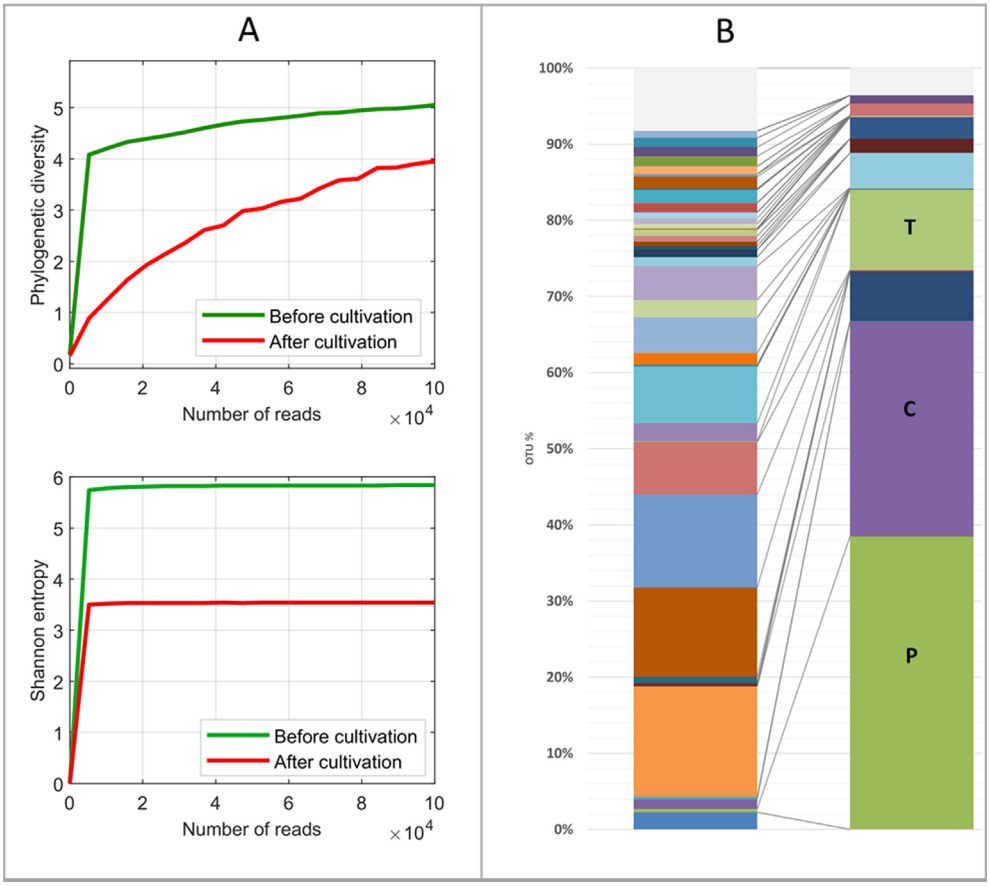

Fig. 6. Changes in the microbial assemblage upon gas fermentation at 15 bar. A: Changes in Phylogenetic diversity and Shannon entropy. B: Changes in community composition at Family level towards a few families known to comprise acetogenic anaerobic taxa that are well-known for the observed metabolic conversions and products. P, Pseudomonadaceae, C, Clostridiaceae, T, Tissierellaceae. For details on Families covered, see Supplementary Figure S2.

$$0.1359CO_2 + 0.5H_2 + 0.114HCO_3^- + 0.0073NH_4^+ \rightarrow 0.1067CH_3COO^- + 0.0073C_5H_7O_2N + 0.3859H_2O \quad (5)$$

Since the ammonium ion is the nitrogen source for the biomass synthesis, the concentration should drop in the fermentation medium, but contradictorily the concentration increased, which elucidates that hydrolysis processes of the remaining organics could be the reason. However, the calculated biomass growth associated with homoacetogenesis is thirty times magnitude lower than the measured VS concentration; therefore, the changes in VS/TS could be a stochastic variation and challenging to correlate with the hydrolysis process. Future studies could investigate the association with hydrolysis, VS and ammonium release in detail.

3.4. Microbiome analysis

In order to assess the changes in microbial community structure and complexity, we performed 16S rRNA gene amplicon sequencing of the original raw sludge sample (before the pretreatment) used as inoculum for all seven batch cultivations at different pressures and the final microbial assemblage of the best performing batch culture at 15 bar. Fig. 6 clearly shows both the reduction of community complexity by means of a reduced phylogenetic diversity and Shannon entropy (Fig. 6A) and the overall change in community composition at family level (Fig. 6B). While the inoculum featured a multitude of families with significant shares in the overall microbial assemblage, the final consortium was with approx. 65 % dominated by *Pseudomonadaceae* and *Clostridiaceae*, while members of the *Tissierellaceae, Porphyromonadaceae*, *Erysipelotrichaceae*, *Peptostreptococcaceae*, *Eubacteriaceae*, and *Ruminococcaceae* held distinguishable shares within the remaining 35 % (Fig. 6B). Species within the two dominating families, *Pseudomonadaceae* and *Clostridiaceae,* were annotated as unknown genera of *Pseudomonadaceae*-2 and or unknown species of *Natronincola-Anaerovirgula*, respectively. Both families and predicted genera/species comprise known, spore-forming anaerobes that play central roles in biogas production and the formation of VFAs (Buettner et al., 2019). In particular, among the Clostridiaceae, many species are capable of fixating carbon dioxide in the presence of H_2 as the energy source using the WLP and performing acetogenesis.

4. Conclusions

To our knowledge, this study represents the first attempt to systematically assess the effect of highly elevated H_2 headspace pressure on mixed culture homoacetogenesis, demonstrating a remarkable impact on gas uptake rate and VFAs synthesis. The gas uptake rate and the amount of synthesized fermentation products increased with increasing headspace pressure from 1 to 15 bar by 250 %, while higher pressures of 20 and 25 bar had the opposite effect. At 15 bar, an optimum H_2 gas uptake rate of 6.22 mol $h^{-1}L^{-1}$ and the highest concentration of VFAs (3.55 g/L) were determined. Though the consumed amount of H_2 was directly proportional to the elevation in pressure, the reduction in gas uptake rate and product synthesis at pressures higher than 15 bar suggests that the microorganisms were inhibited by elevated pressure (>15 bar). The fermentation medium turned out more alkaline throughout the experiments (pH > 9.3). Higher buffer capacity and higher fermentation medium pH let the bicarbonate to behave as an acid. Therefore, the consumption of bicarbonate increased the pH.

The primary fermentation product was acetate (90 %) in all batches. However, for pressures above 15 bar, the presence of C_3-C_5 acids were enhanced but the acetic acid is still the major product. In addition to C_3-C_5 acids, limited ethanol production was observed at 25 bar. Microbial consortium analysis revealed a significant reduction in the microbial assemblage's complexity obtained through cultivation at 15 bar, with members of the *Pseudomonadaceae* and *Clostridiaceae*, families well-known to include many anaerobic acetogens, representing the majority of OTUs determined by 16S rRNA gene metabarcoding. These observations also provide evidence that elevation in H_2 headspace pressure impacts fermentation metabolic pathways. The results show that 15 bar is the optimum headspace pressure for the used mixed culture fermentation inoculum (Knardalstrand municipal wastewater treatment plant's anaerobic sludge) to accomplish the highest gas uptake rate and enhanced VFAs production. Future research will examine the impact of pH and provide a more detailed analysis of the microbial community's metabolic potential to elucidate these initial findings further.

Funding

The Norwegian Ministry of Education and Research funded this research through the PhD program in Process, Energy, and Automation Engineering at the University of South-Eastern Norway, grant number 2700095. Parts of this work were performed in the frame of Research Council of Norway supported IPN project DECARBONIZE, grant number 296286.

CRediT authorship contribution statement

Vasan Sivalingam: Conceptualization, Methodology, Formal analysis, Investigation, Validation, Writing – original draft, Writing – review & editing. **Tone Haugen:** . **Alexander Wentzel:** Investigation, Writing – review & editing. **Carlos Dinamarca:** Conceptualization, Methodology, Investigation, Validation, Writing – review & editing, Supervision, Project administration, Funding acquisition.

Declaration of Competing Interest

The authors declare that they have no known competing financial interests or personal relationships that could have appeared to influence the work reported in this paper.

Acknowledgements

The authors want to thank the Norwegian Ministry of Education and Research for this project's financial support.

Appendix A. Supplementary data

Supplementary data to this article can be found online at https://doi.org/10.1016/j.cesx.2021.100118.

References

Abubackar, H.N., Veiga, M.C., Kennes, C., 2011. Biological conversion of carbon monoxide: Rich syngas or waste gases to bioethanol. Biofuels, Bioprod. Biorefin. 5 (1), 93–114. https://doi.org/10.1002/bbb.256.

Angelidaki, I., Karakashev, D., Batstone, D.J., Plugge, C.M., Stams, A.J.M., 2011. Chapter sixteen—Biomethanation and Its Potential. In: Rosenzweig, A.C., Ragsdale, S.W. (Eds.), Methods in Methane Metabolism, Part A, Vol. 494. Academic Press, pp. 327–351. https://doi.org/10.1016/B978-0-12-385112-3.00016-0.

Anukam, A., Mohammadi, A., Naqvi, M., Granström, K., 2019. A Review of the Chemistry of Anaerobic Digestion: Methods of Accelerating and Optimizing Process Efficiency. Processes 7 (8), 504. https://doi.org/10.3390/pr7080504.

APHA (1995). *Standard methods for the examination of water and wastewater*. American Public Health Association, American Water Works Association and Water Environment Federation. Editors: Eaton, A.; Clesceri L., Greenberg.

Bertsch, J., Müller, V., 2015. Bioenergetic constraints for conversion of syngas to biofuels in acetogenic bacteria. Biotechnol. Biofuels 8 (1), 210. https://doi.org/10.1186/s13068-015-0393-x.

Mohammadi, M., Najafpour, G.D., Younesi, H., Lahijani, P., Uzir, M.H., Mohamed, A. R., 2011. Bioconversion of synthesis gas to second generation biofuels: A review. Renew. Sustain. Energy Rev. 15 (9), 4255–4273. https://doi.org/10.1016/j.rser.2011.07.124.

Geppert, F., Liu, D., van Eerten-Jansen, M., Weidner, E., Buisman, C., ter Heijne, A., 2016. Bioelectrochemical Power-to-Gas: State of the Art and Future Perspectives. Trends Biotechnol. 34 (11), 879–894. https://doi.org/10.1016/j.tibtech.2016.08.010.

Buettner, C., von Bergen, M., Jehmlich, N., Noll, M., 2019. Pseudomonas spp. Are key players in agricultural biogas substrate degradation. Sci. Rep. 9 (1), 12871. https://doi.org/10.1038/s41598-019-49313-8.

Conrad, R., Wetter, B., 1990. Influence of temperature on energetics of hydrogen metabolism in homoacetogenic, methanogenic, and other anaerobic bacteria. Arch. Microbiol. 155 (1), 94–98. https://doi.org/10.1007/BF00291281.

Cuff, G., Nelting, K., Trautmann, N., Mohammad-pajooh, E., 2020. Production and upgrading of biogas through controlled hydrogen injection for renewable energy storage. Bioresource Technology Reports 9, 100373. https://doi.org/10.1016/j.biteb.2019.100373.

Daniell, J., Köpke, M., Simpson, S., 2012. Commercial Biomass Syngas Fermentation. *Energies* 5 (12), 5372–5417. https://doi.org/10.3390/en5125372.

Diekert, G., Wohlfarth, G., 1994. Metabolism of homoacetogens. Antonie Van Leeuwenhoek 66 (1-3), 209–221.

Dinamarca, C., Bakke, R., 2009. Apparent hydrogen consumption in acid reactors: Observations and implications. Water Sci. Technol.: J. Int. Assoc. Water Pollut. Res. 59 (7), 1441–1447. https://doi.org/10.2166/wst.2009.135.

Dinamarca, C., Ganan, M., Liu, J., & Bakke, R., 2011. H2 consumption by anaerobic non-methanogenic mixed cultures. Water Sci. Technol. : A J. Int. Assoc. Water Pollut. Res. https://doi.org/10.2166/wst.2011.214.

Dodds, W.K., Dodds, P.W.K., 2002. Freshwater Ecology: Concepts and Environmental Applications. Elsevier Sci. Technol. http://ebookcentralproquest.com/lib/ucsn-ebooks/detail.action?docID=294137.

Drake, H.L., 2012. Acetogenesis. Springer Science & Business Media.

Fernández-Naveira, Á., Veiga, M.C., Kennes, C., 2017. H-B-E (hexanol-butanol-ethanol) fermentation for the production of higher alcohols from syngas/waste gas. J. Chem. Technol. Biotechnol. 92 (4), 712–731. https://doi.org/10.1002/jctb.2017.92.issue-410.1002/jctb.5194.

Gardner, R.D., Lohman, E., Gerlach, R., Cooksey, K.E., Peyton, B.M., 2013. Comparison of CO2 and bicarbonate as inorganic carbon sources for triacylglycerol and starch accumulation in Chlamydomonas reinhardtii. Biotechnol. Bioeng. 110 (1), 87–96. https://doi.org/10.1002/bit.24592.

Grimalt-Alemany, A., Łężyk, M., Lange, L., Skiadas, I.V., Gavala, H.N., 2018. Enrichment of syngas-converting mixed microbial consortia for ethanol production and thermodynamics-based design of enrichment strategies. Biotechnol. Biofuels 11 (1), Scopus. https://doi.org/10.1186/s13068-018-1189-6.

Hu, P., Bowen, S.H., Lewis, R.S., 2011. A thermodynamic analysis of electron production during syngas fermentation. Bioresour. Technol. 102 (17), 8071–8076. https://doi.org/10.1016/j.biortech.2011.05.080.

Kantzow, C., Weuster-Botz, D., 2016. Effects of hydrogen partial pressure on autotrophic growth and product formation of Acetobacterium woodii. Bioprocess Biosyst. Eng. 39 (8), 1325–1330. https://doi.org/10.1007/s00449-016-1600-2.

Kundiyana, D.K., Wilkins, M.R., Maddipati, P., Huhnke, R.L., 2011. Effect of temperature, pH and buffer presence on ethanol production from synthesis gas by "Clostridium ragsdalei". Bioresour. Technol. 102 (10), 5794–5799. https://doi.org/10.1016/j.biortech.2011.02.032.

Liew, F., Martin, M.E., Tappel, R.C., Heijstra, B.D., Mihalcea, C., Köpke, M., 2016. Gas Fermentation—A Flexible Platform for Commercial Scale Production of Low-Carbon-Fuels and Chemicals from Waste and Renewable Feedstocks. Front. Microbiol. 7. https://doi.org/10.3389/fmicb.2016.00694.

Mota, M.J., Lopes, R.P., Delgadillo, I., Saraiva, J.A., 2013. Microorganisms under high pressure—Adaptation, growth and biotechnological potential. Biotechnol. Adv. 31 (8), 1426–1434. https://doi.org/10.1016/j.biotechadv.2013.06.007.

Mulat, D.G., Mosbæk, F., Ward, A.J., Polag, D., Greule, M., Keppler, F., Nielsen, J.L., Feilberg, A., 2017. Exogenous addition of H2 for an in situ biogas upgrading through biological reduction of carbon dioxide into methane. Waste Manage. 68, 146–156. https://doi.org/10.1016/j.wasman.2017.05.054.

Oswald, F., Stoll, I.K., Zwick, M., Herbig, S., Sauer, J., Boukis, N., Neumann, A., 2018. Formic Acid Formation by Clostridium ljungdahlii at Elevated Pressures of Carbon Dioxide and Hydrogen. Front. Bioeng. Biotechnol. 6, 6. https://doi.org/10.3389/fbioe.2018.00006.

Pereira, F. M. R., Alves, M., & Sousa, D. (2013). *Effect of pH and pressure on syngas fermentation by anaerobic mixed cultures*. 1–4.

Phillips, J.R., Huhnke, R.L., Atiyeh, H.K., 2017. Syngas Fermentation: A Microbial Conversion Process of Gaseous Substrates to Various Products. Fermentation 3 (2), 28. https://doi.org/10.3390/fermentation3020028.

Rittmann, B.E., McCarty, P.L., 2020. Environmental Biotechnology: Principles and Applications. Second Edition, McGraw-Hill Education.

Saady, N.M.C., 2013. Homoacetogenesis during hydrogen production by mixed cultures dark fermentation: Unresolved challenge. Int. J. Hydrogen Energy 38 (30), 13172–13191. https://doi.org/10.1016/j.ijhydene.2013.07.122.

Schuchmann, K., Müller, V., 2014. Autotrophy at the thermodynamic limit of life: A model for energy conservation in acetogenic bacteria. Nat. Rev. Microbiol. 12 (12), 809–821.

Shen, S., Wang, G., Zhang, M., Tang, Y., Gu, Y., Jiang, W., Wang, Y., Zhuang, Y., 2020. Effect of temperature and surfactant on biomass growth and higher-alcohol production during syngas fermentation by Clostridium carboxidivorans P7. Bioresources and Bioprocessing 7 (1), 56. https://doi.org/10.1186/s40643-020-00344-4.

Sivalingam, V., Ahmadi, V., Babafemi, O., Dinamarca, C., 2021. Integrating Syngas Fermentation into a Single-Cell Microbial Electrosynthesis (MES) Reactor. Catalysts 11 (1), 40. https://doi.org/10.3390/catal11010040.

Sivalingam, V., Dinamarca, C., 2021. High Pressure Moving Bed Biofilm Reactor for Syngas Fermentation. Chem. Eng. Trans. 86, 1483–1488. https://doi.org/10.3303/CET2186248.

Stoll, I.K., Boukis, N., Sauer, J., 2019. Syngas Fermentation at Elevated Pressure—Experimental Results. In: European Biomass Conference and Exhibition Proceedings. https://doi.org/10.5071/27thEUBCE2019-3CV.3.4.

Stoll, I., Herbig, S., Zwick, M., Boukis, N., Sauer, J., Neumann, A., Oswald, F., 2018. Fermentation of H_2 and CO_2 with Clostridium ljungdahlii at Elevated Process Pressure – First Experimental Results. Chem. Eng. Trans. 64, 151–156. https://doi.org/10.3303/CET1864026.

Tchobanoglous, G., Burton, F.L., Stensel, H.D., 2014. & Metcalf & Eddy (Boston). Wastewater engineering, Treatment and resource recovery. McGraw-Hill Higher Education.

Torri, C., Pambieri, G., Gualandi, C., Piraccini, M., Rombolà, A.G., Fabbri, D., 2020. Evaluation of the potential performance of hyphenated pyrolysis-anaerobic digestion (Py-AD) process for carbon negative fuels from woody biomass. Renew. Energy 148, 1190–1199. https://doi.org/10.1016/j.renene.2019.10.025.

Trček, J., Mira, N.P., Jarboe, L.R., 2015. Adaptation and tolerance of bacteria against acetic acid. Appl. Microbiol. Biotechnol. 99 (15), 6215–6229. https://doi.org/10.1007/s00253-015-6762-3.

Van Hecke, W., Bockrath, R., De Wever, H., 2019. Effects of moderately elevated pressure on gas fermentation processes. Bioresour. Technol. 293, 122129. https://doi.org/10.1016/j.biortech.2019.122129.

Wilkins, M.R., Atiyeh, H.K., 2011. Microbial production of ethanol from carbon monoxide. Curr. Opin. Biotechnol. 22 (3), 326–330. https://doi.org/10.1016/j.copbio.2011.03.005.

Yasin, M., Cha, M., Chang, I.S., Atiyeh, H.K., Munasinghe, P., Khanal, S.K., 2019. In: Biofuels: Alternative Feedstocks and Conversion Processes for the Production of Liquid and Gaseous Biofuels. Elsevier, pp. 301–327. https://doi.org/10.1016/B978-0-12-816856-1.00013-0.

Yenigün, O., Demirel, B., 2013. Ammonia inhibition in anaerobic digestion: A review. Process Biochem. 48 (5), 901–911. https://doi.org/10.1016/j.procbio.2013.04.012.

Article 1: E - Supplementary Material

Effect of Elevated Hydrogen Partial Pressure on Mixed Culture Homoacetogenesis

Vasan Sivalingam[1], Tone Haugen[2], Alexander Wentzel[2], and Carlos Dinamarca[1]

[1]Department of Process, Energy and Environmental Technology, University of South-Eastern Norway, Porsgrunn, Norway
[2]Department of Biotechnology and Nanomedicine, SINTEF Industry, Trondheim, Norway

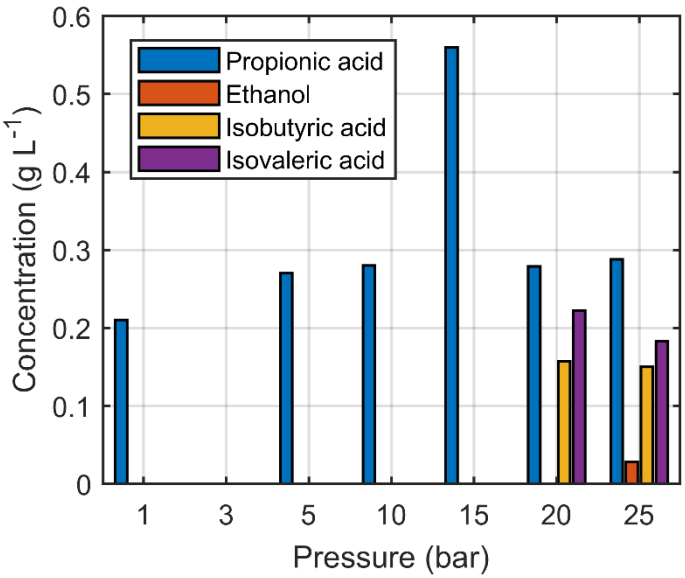

Figure S1. This is the supplementary figure for Figure 5, where all the detected VFAs except acetic acid concentration is presented with corresponding H_2 partial pressure.

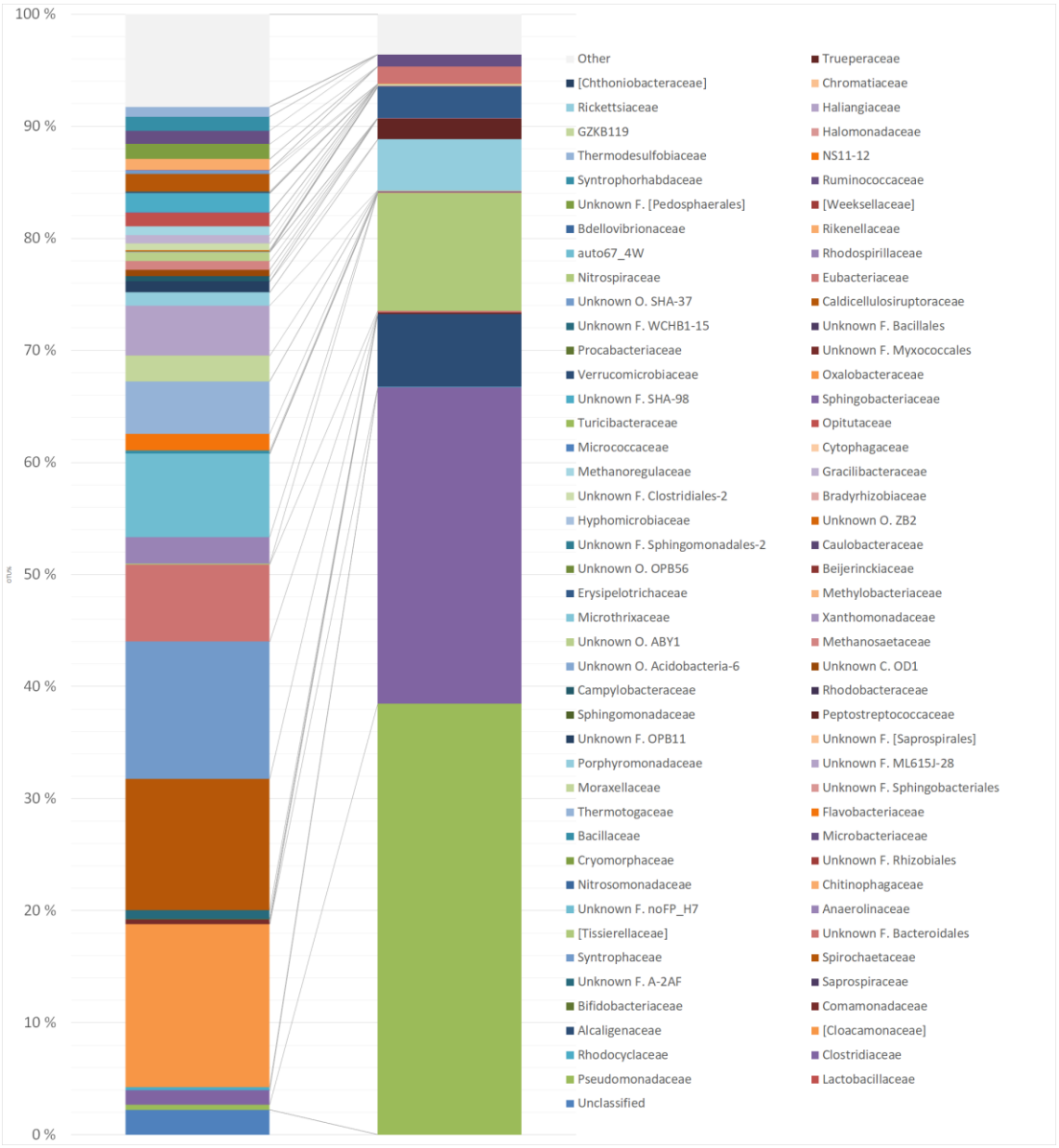

Figure S2. Detailed representation of Figure 6. Left bar, inoculum microbiome; right bar, microbiome at the end of the 15-bar cultivation. 16S rRNA gene amplicon-based biodiversity at Family level.

Article 2

High Pressure Moving Bed Biofilm Reactor for Syngas Fermentation

Vasan Sivalingam, and Carlos Dinamarca

Department of Process, Energy and Environmental Technology, University of South-Eastern Norway (USN), Porsgrunn, Norway

Published in Chemical Engineering Transactions, 2021 (Level 1) Journal.
DOI: 10.3303/CET2186248

CHEMICAL ENGINEERING TRANSACTIONS
VOL. 86, 2021
A publication of AIDIC
The Italian Association of Chemical Engineering
Online at www.cetjournal.it
Guest Editors: Sauro Pierucci, Jiří Jaromír Klemeš

ISBN 978-88-95608-84-6; **ISSN** 2283-9216
DOI: 10.3303/CET2186248

High Pressure Moving Bed Biofilm Reactor for Syngas Fermentation

Vasan Sivalingam, Carlos Dinamarca*

Department of Process, Energy and Environmental Technology, University of South-Eastern Norway (USN), Porsgrunn, Norway
carlos.dinamarca@usn.no

Two well-studied strategies to enhance syngas fermentation are elevated headspace pressure, increasing gas-liquid (GL) mass transfer, and moving bed biofilms (MBB) to overcome kinetic growth limitation. A combination of these two methods has not received much attention. This study evaluates the integration of these two strategies in one single reactor. The hydrogen (H_2) GL mass transfer is the primary bottleneck in syngas fermentation due to the lowest solubility among syngas components. The syngas composition is mimicked here as a mixture of H_2 gas and sodium bicarbonate ($NaHCO_3$) salt. Initially, fermentation is performed at 15 bar H_2 headspace pressure in the suspended culture, then the experiment is repeated with MBB integration, and the performance is critically evaluated. The study with integrated biofilm shows a 33 % improvement in H_2 gas uptake rate (200 mmol/L·day) and 48 % enhancement in acetate synthesis rate (37.4 mmol/L· day). This study concludes that MBB could successfully be integrated into an elevated pressure syngas fermenter, enhancing the fermentation process efficiency.

1. Introduction

Increasing energy demand and climate change are the foremost current world challenges. Even though the world is actively engaging in the clean energy transition, 80 % of the total global energy demand has been base on fossils fuel for the last three decades (World Energy Outlook Analysis, 2020). Growth in energy production increases carbon dioxide (CO_2) emission and causes a significant impact on climate change. Moreover, waste disposal practices (landfills, open burning, incineration, gasification, pyrolysis) and industrial processes as cement and metals production are the substantial sources of greenhouse gasses. Carbon dioxide is the component that indeed needs to be either captured or utilised to stop climate change. Several capture and separation technologies are available; however, those technologies call for expensive and energy-intensive steps. Therefore we need climate-friendly solutions to capture and utilise CO_2 in more sustainable ways.

Homoacetogenesis is one of such sustainable approach. It is a biochemical process performed by autotrophic bacteria, which reduces CO_2 into acetate (Kanchanasuta et al., 2016) through an intermediate enzymatic pathway called acetyl-CoA (Eq 1). It is also called the Wood-Ljungdahl pathway to honour Harland G. Wood and Lars G. Ljungdahl, the scientists who introduced this process in 1986 (Drake, 2012). The CO_2 reduction process requires electrons as an energy source. H_2 and carbon monoxide (CO) can serve as electron donors. Moreover, CO can contribute as a carbon source also. This is where the syngas plays a pivotal role in the acetyl-CoA path because syngas is a mixture of CO, H_2 and CO_2, that can be directly used as the substrate for the homoacetogenic fermentation process. Gasification and pyrolysis are the primary sources of syngas. Emitted CO_2 from power plants and other process-related industries can also be used as substrate with alternative electron sources, such as H_2 produced from water electrolysis by utilising renewable electricity.

$$4H_2 + 2CO_2 \rightarrow CH_3COOH + 2H_2O \quad \Delta G^0 = -74.3\ \mathrm{kJ/mol} \tag{1}$$

Paper Received: 30 October 2020; Revised: 24 January 2021; Accepted: 21 April 2021
Please cite this article as: Sivalingam V., Dinamarca C., 2021, High Pressure Moving Bed Biofilm Reactor for Syngas Fermentation, Chemical Engineering Transactions, 86, 1483-1488 DOI:10.3303/CET2186248

Though homoacetogenesis was discovered several decades ago, industrial level applications are still under maturation. Gas-Liquid (GL) mass transfer and kinetic-growth limitation are the primary engineering bottlenecks that have slow down the scale-up process. Especially, the lowest solubility of H_2 demands more energy-intensive strategies. The mass transfer rate is insufficient to cope with cell growth demand, resulting in low biomass growth and product synthesis, leading to an inefficient carbon reduction. The autotrophic homoacetogens specific growth rate is relatively low (Karekar et al., 2019; Regueira et al., 2018), results in poor cell density, which is referred to as a kinetic-growth limitation, which leads to inefficient product synthesis. Increasing H_2 gas headspace pressure is a well-known (Stoll et al., 2018; Van Hecke et al., 2019) lower-cost strategy than using energy-intensive agitators to counteract GL mass transfer limitation.

At the same time, increasing the cell density with biofim substrates can overcome kinetic-growth limitations. Hollow fibre membrane biofilm, monolithic biofilm, rotating packed bed biofilm and moving bed biofilm (MBB) reactors are a few examples of attached-growth biofilm syngas fermentation reactors (Shen, 2013). MBB reactors are a salient strategy that can surpass both GL mass transfer and kinetic growth limitations. Biocarriers' surface area facilitates biofilm growth, which helps to attain higher cell density (Wang et al., 2019), and movement in biocarriers induce an efficient GL mass transfer. Moreover, the MBB integration within the syngas fermentation reactor has many other process advantages, such as lower hydraulic retention time, higher sludge retention time, higher resistance to the toxic substances that come along with the syngas mixture.

The moving bed biofilm concept is a Norwegian invention, patented by Kaldnes Miljøteknologi in 1991 (Ødegaard, 2019). Initially, it was designed for nitrogen removal in wastewater treatment. However, over time MBB has been used in various applications such as organic substances removal, phosphorous removal and recovery (Rudi et al., 2019) and reject water treatment (Sivalingam et al., 2020). As a result of continuous advancement, Robert Hickey integrated the MBB reactor into a fermentation reactor to convert syngas components to liquid products, patented in 2009 (Hickey, 2009). Hickey used a pure culture of *Clostridium ragsdalei* ATCC No. BAA-622 as the fermentation medium and operated at 0.1 bar outlet pressure while the liquid pressure was between 1 to 5 bar.

Using pure cultures in a syngas fermentation medium gives efficient product specificity but maintaining a sterilised environment, to keep only the specific culture, add an extra cost, which becomes a significant challenge when upscaling. Therefore, using mixed cultures is getting more attention where the product specificity is not the primary concern, instead of carbon fixation. In this research, anaerobic sludge from the local municipal wastewater treatment plant is used as the mixed culture fermentation, easily available with relatively no cost.

Even though elevating headspace pressure and the use of MBB carriers in syngas fermentation has been individually investigated to enhance performance. A combination of these technologies has rarely been studied. As far as the authors know, this is the first time an investigation integrates elevated H_2 pressure (15 bar) into a MBB reactor mixed culture fermentation process.

This study consists two-phase batch experiments. Phase 1 deals with H_2 fermentation at an elevated pressure of 15 bar. In phase two, the pressure reactor is modified as a moving bed biofilm syngas fermentation reactor. The phases 1 and 2 are named as pressure syngas fermentation reactor (PSFR) and biofilm pressure syngas fermentation reactor (B-PSFR) . The results are compared and evaluated in terms of hydrogen consumption rate and product formation.

2. Material and methods

2.1 Fermentation medium preparation and bio carrier adaptation

Sludge from the biogas digester at Knarrdalstrand wastewater treatment plant, Porsgrunn, Norway, was used as mixed culture. The sludge underwent several pretreatment steps to obtain a homoacetogenic rich culture. Firstly, the coarse impurities such as plastics and woody debris were removed by sieving at 600 microns. The sludge was then incubated for seven days at 35 °C for further thickening and to get rid of remaining easily degradable organic matters. The thickened sludge was heat-treated at 105 °C for 48 hours to eliminate methanogens and to enrich spores forming acetogens. Subsequently, the heat-treated sludge was cooled down to ambient temperature. Finally, salt (10 mL/L), vitamin (1mL/ L), and mineral (1mL/ L) solutions were mixed with the inoculum to provide nutritional supplements for microbial growth. The nutrient base media composition was adapted from a similar study (Sivalingam et al., 2021), shown in Table 1.

Table 1: Nutrient base media compositions

Vitamin solution (g/L)	Mineral solution (g/L)	Salt solution (g/L)
Biotin: 0.02	$MnSO_4 \cdot H_2O$: 0.04	NH_4Cl: 100
Folic acid: 0.02	$FeSO_4 \cdot 7H_2O$: 2.7	NaCl: 10
Pyridoxine hydrochloride: 0.1	$CuSO_4 \cdot 5H_2O$: 0.055	$MgCl_2 \cdot 6H_2O$: 10
Riboflavin: 0.05	$NiCl_2 \cdot 6H_2O$: 0.1	$CaCl_2 \cdot 2H_2O$: 5
Thiamine: 0.05	$ZnSO_4 \cdot 7H_2O$: 0.088	
Nicotinic acid: 0.05	$CoCl_2 \cdot 6H_2O$: 0.05	
Pantothenic acid: 0.05	H_3BO_3: 0.05	
Vitamin B12: 0.001		
p-aminobenzoic acid: 0.05		
Thioctic acid: 0.05		

6.8 g/L sodium bicarbonate ($NaHCO_3$) was added to the inoculum as the carbon source. Once the fermentation medium is placed into the reactor, 10 mL of homoacetogens riched sludge was added as seed to trigger the startup process. The pH was neither adjusted nor controlled throughout the experiments. The characteristics of the treated inoculum are presented in Table 2.

BWT X type biocarriers (Dimensions 14,5 x 14,5 x 8,2 mm and Protected surface: 650 m^2/m^3) from Biowater Technology As, Tønsberg, Norway was used as the biofilm media. Homoacetogens have a low growth rate; therefore, the biocarriers (# 70, 200 mL bulk volume) were adapted for two weeks into a homoacetogens rich medium. The adaptation could help microorganisms establish a necessary foundation on carrier surfaces, consequently shortening the experimental period.

Table 2: Characteristics of the treated inoculum.

Parameters	pH	TS* (g/L)	VS‡ (g/L)	TCOD# (g/L)	NH_4-H (g/L)	Alkalinity (g/L as $CaCO_3$)
Values	8.5	14.3	7.5	9.4	0.8	1.97

* Total solids, ǂ Volatile solids, # Total Chemical Oxygen Demand

2.2 Experimental setup and procedure

This research was performed in two phases. In phase 1 (PSFR), a 1.8 L stainless steel stirred-tank pressure reactor (NR-1500, Berghof, Eningen, Germany) was used as a fermenter (Figure 1, Left). The reactor was equipped with a digital manometer (LEO-3, Keller, Winterthur, Switzerland) and connected to a computer via a RS485 interface. The Control Center Series-30 (Keller, Winterthur, Switzerland) software package recorded the headspace pressure changes. The reactor lid has a fixed mounted mechanical stirrer (BG 65X50, Dunkermotoren, Bonndorf, Germany) which run continuously at 200 rpm. All the experiments were performed at 25°C. At the start of phase 1, the reactor was filled with 1 L treated inoculum with supplements. The fermentation medium was purged with N_2 gas for 5 min, followed by H_2 gas for 2 min, to ensure anaerobic conditions. The headspace was then pressurised to 15 bar (Laboratory H_2 gas 5.5 = ≥ 99.9995 %, Linde Gas AS, Oslo, Norway). The headspace pressure 15 bar was determined from the authors' laboratory study. There, different H_2 headspace pressure varies from 1 to 25 bar were tested and figured out 15 bar is the optimum (Results are not presented here) for this particular mixed culture fermentation medium. The phases one and two experiments were continued until a static pressure was observed (approximately a week).

In phase 2 (B-PSFR), the pressure reactor used in phase 1 was modified as a moving bed biofilm syngas fermenter (Figure 1, Right). The adapted MBB carrier was incorporated into the fresh treated suspended fermentation medium. The working volume was maintained at 1 L same as phase 1. Successively, all other steps performed in phase 1 were repeated. The biocarriers were observed with a Nikon Stereo Microscope SMZ745T, and the Infinity Analyze software measured biofilm thickness.

2.3 Analytical methods

pH, TS, VS, ammonium, alkalinity and TCOD were performed based on the standard method of the America Public Health Association (APHA, 1995). Volatile fatty acids (VFAs) were analysed by gas chromatography (PerkinElmer, Clarus 500, Massachusetts, USA), the instrument was equipped with a capillary column (SCION Instruments, Livingston, Scotland; length 25 m x diameter 0.25 mm x film 0.2 µm) and Flame Ionization Detector. The carrier gas was H_2 at a flow rate of 45 mL/min. The injector and detector temperatures were 270 °C and 250 °C, respectively. The initial oven temperature was constant at 80 °C for 0.7 minutes and then increased to 200 °C by 25 °C/min followed by 20 °C/min ramp-up rate until reach 240 °C.

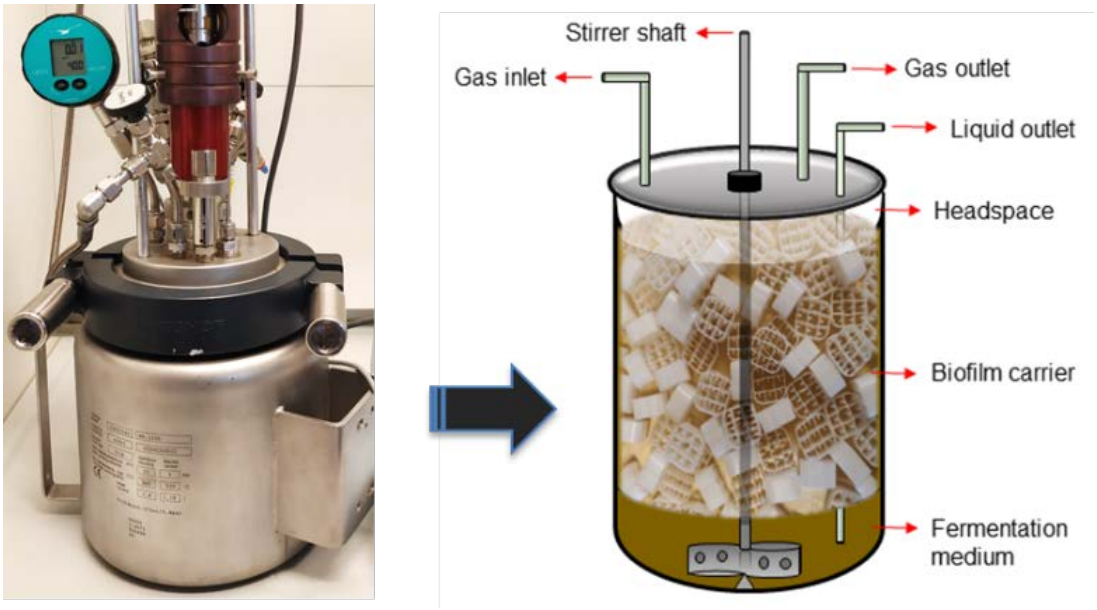

Figure 1: Left: Pressure reactor (PSFR), Right: Sketch of pressure reactor with MBB (B-PSFR).

3. Results and discussion

Figure 2a describes the pressure time series and cumulative H_2 consumption profiles for both PSFR and B-PSFR. The PSFR took seven days to reach the static headspace pressure, while B-SFR took only 4.5 days. However, the lag phase duration is the same, 2.5 days. The B-PSFR depicted the highest gas uptake rate (200 mmol/L·day) and sizeable cumulative gas consumption (218 mmol), respectively, 33 % and 20 % higher than PSFR. This is a clear evidence that MBB integration significantly improved the GL mass transfer and minimised the kinetic limitation. The gas uptake rate of PSFR is 150 mmol/L·day. This is a considerably large number compared to other experiments performed at lower headspace pressure (Stoll et al., 2018). According to Henry's law, the enhancement in headspace pressure increased the GL mass transfer, resulting a rise in gas solubilisation and utilisation.

Figure 2b shows the acetic acid concentration change in both PSFR and B-PSFR. Acetic acid was the only detected VFA as the fermentation product. The increment in acetic acid concurs with cumulative H_2 consumption profiles. There was a rapid rise in concentration from day 3 to 4, after that flattened out. The B-PSFR showed a predominant acetic acid synthesis (2.7 g/L); it is 40 % higher than PSFR (without biofilm). Not only the concentration but the acetic acid production rate (48 %) was also remarkably higher in B-PSFR (37.4 mmol/L· day). The notable acceleration in acetic acid production rate affirms that biofilm integration as a promising strategy for making the H_2 fermentation process more efficient.

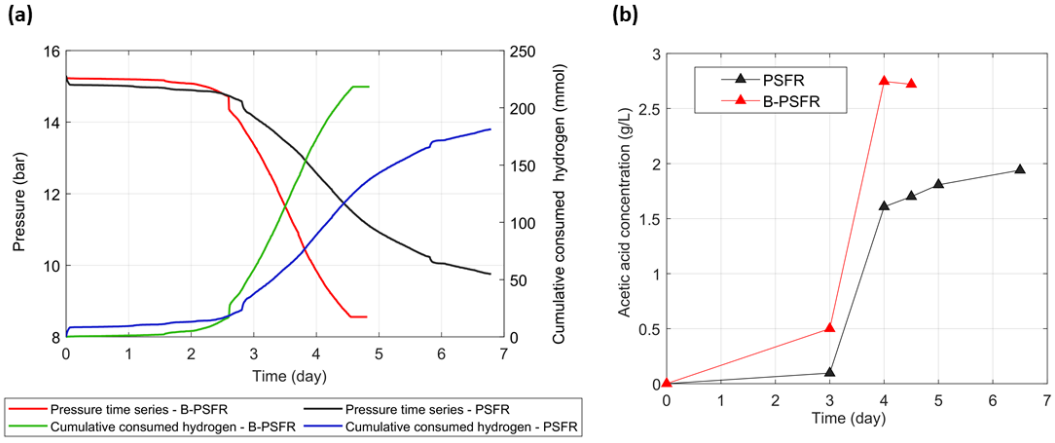

Figure 2: a - Pressure time series, and cumulative H_2 consumption profiles, b – Acetic acid profiles.

The H_2 utilisation and carbon capture efficiencies (HUE and CCE) are critical factors that determine the efficiency of a syngas fermentation process, calculated according to Eq (2) and (3) based on the stoichiometric Eq (1), tabulated in Table 3. The efficiency calculations proved that the MBB integration enhanced the HUE and CCE by 12 % and 32 %, respectively. The B-PSFR resulted in 112 % CCE. The percentage above a hundred is due to the carbon present in the fermentation medium as alkalinity. The treated inoculum contains inherent alkalinity, about 1.97 g/L as $CaCO_3$ (Table 2). The CCE calculation is based on added $NaHCO_3$ as the only carbon source.

$$\mathrm{HUE} = \frac{\mathrm{H_2\ equivalent\ to\ the\ produced\ acetic\ acid}}{\mathrm{Total\ consumed\ H_2}} \quad (2)$$

$$\mathrm{CCE} = \frac{\mathrm{CO_2\ \ equivalent\ to\ the\ produced\ acetic\ acid}}{\mathrm{Available\ CO_2}} \quad (3)$$

Table 3: The H_2 utilisation and carbon capture efficiencies.

Phases	HUE (%)	CCE (%)
Phase 1 - PSFR	71	80
Phase 2 – B-PSFR	83	112

The stereo microscopic images of the biocarriers are presented in Figure 3. The biofilm thickness was measured in different locations of the carriers; the average biofilm thickness was about 157 ± 20 µm. It was observed that the carriers' protected/inner surface area was populated with attached biofilm growth. The significant assemblage of biofilm and enhancement in the fermentation process at B-PSFR affirm that enhanced cell density reduced the kinetic growth limitation, heightening the fermentation efficiency.

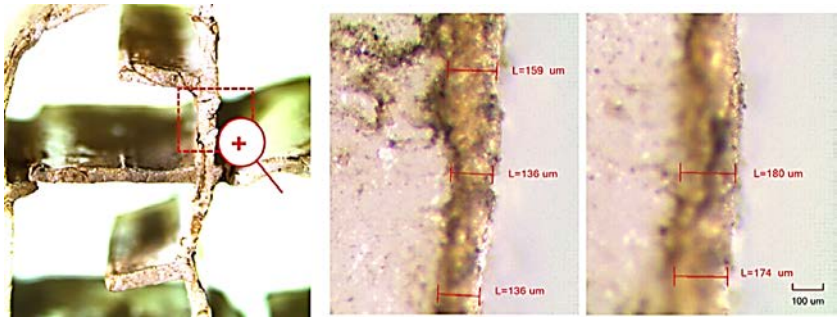

Figure 3: Stereo micrograph of the biocarrier and magnified version of attached growth on the carrier surface.

4. Conclusions

A high-pressure syngas fermentation reactor combined with MBB carriers demonstrated an enhancement in H_2-gas uptake (33 %), acetic acid synthesis rate (48 %) and carbon fixation efficiency (>20 %) compared to high-pressure suspended culture alone. The significant assemblage of biofilm on carriers enhanced the fermentation process at B-PSFR. The improved cell density of biofilms reduced the kinetic growth limitation compared to suspended cultures. This novel study demonstrated that combining both approaches accelerates the syngas fermentation process.

Acknowledgements

Authors want to acknowledge the Norwegian Ministry of Education and Research for funding this research project throughout the Ph.D. program in Process, Energy and Automation Engineering at USN, grant number 2700095.

References

Drake, H. L., 2012, Acetogenesis: Chapman and Hall, New York, USA.

Hickey, R., 2009. Moving bed biofilm reactor (MBBR) system for conversion of syngas components to liquid <patents.google.com/patent/US20090035848A1/en> accessed 21.08.2020.

Kanchanasuta, S., Haosagul, S., Pisutpaisal, N., 2016. Metabolic Flux Analysis of Hydrogen Production from Rice Starch by Anaerobic Sludge under Varying Organic Loading. Chemical Engineering Transactions, 49, 409–414. doi.org/10.3303/CET1649069

Karekar, S. C., Srinivas, K., Ahring, B. K., 2019. Kinetic Study on Heterotrophic Growth of Acetobacterium woodii on Lignocellulosic Substrates for Acetic Acid Production. Fermentation, 5(1), 17. doi.org/10.3390/fermentation5010017

Regueira, A., González-Cabaleiro, R., Ofiţeru, I. D., Rodríguez, J., Lema, J. M., 2018. Electron bifurcation mechanism and homoacetogenesis explain products yields in mixed culture anaerobic fermentations. Water Research, 141, 349–356. doi.org/10.1016/j.watres.2018.05.013

Rudi, K., Goa, I. A., Saltnes, T., Sørensen, G., Angell, I. L., Eikås, S., 2019. Microbial ecological processes in MBBR biofilms for biological phosphorus removal from wastewater. Water Science and Technology, 79(8), 1467–1473. doi.org/10.2166/wst.2019.149

Shen, Y., 2013. Attached-growth bioreactors for syngas fermentation to biofuel, PhD Thesis, Iowa State University, Ames, USA. doi.org/10.31274/etd-180810-712

Sivalingam, V., Ahmadi, V., Babafemi, O., Dinamarca, C., 2021. Integrating Syngas Fermentation into a Single-Cell Microbial Electrosynthesis (MES) Reactor. Catalysts, 11(1), 40. doi.org/10.3390/catal11010040

Sivalingam, V., Dinamarca, C., Janka, E., Kukankov, S., Wang, S., Bakke, R., 2020. Effect of Intermittent Aeration in a Hybrid Vertical Anaerobic Biofilm Reactor (HyVAB) for Reject Water Treatment. Water, 12(4), 1151. doi.org/10.3390/w12041151

Stoll, I., Herbig, S., Zwick, M., Boukis, N., Sauer, J., Neumann, A., Oswald, F., 2018. Fermentation of H_2 and CO_2 with Clostridium ljungdahlii at Elevated Process Pressure–First Experimental Results. Chemical Engineering Transactions, 64, 151–156.

Van Hecke, W., Bockrath, R., De Wever, H., 2019. Effects of moderately elevated pressure on gas fermentation processes. Bioresource Technology, 293, 122129. doi.org/10.1016/j.biortech.2019.122129

Wang, S., Parajuli, S., Sivalingam, V., Bakke, R., 2019. Bacterial Biofilms: Biofilm in Moving Bed Biofilm Process for Wastewater Treatment, IntechOpen, London, UK. doi.org/10.5772/intechopen.88520

World Energy Outlook 2020 – Analysis, International Energy Agency <www.iea.org/reports/world-energy-outlook-2020> accessed 21.11.2020

Ødegaard, H., 2019. Advances in Wastewater Treatment: MBBR and IFAS systems, IWA Publishing, London, UK. doi.org/10.2166/9781780409719_0101

Article 3

Integrating Syngas Fermentation into a Single-Cell Microbial Electrosynthesis (MES) Reactor

Vasan Sivalingam, Vafa Ahmadi, Omodara Babafemi and Carlos Dinamarca

Department of Process, Energy and Environmental Technology, University of South-Eastern Norway (USN), Porsgrunn, Norway

Published in catalysts, 2020 (Level 1) Journal.
DOI: 10.3390/catal11010040

catalysts

MDPI

Article

Integrating Syngas Fermentation into a Single-Cell Microbial Electrosynthesis (MES) Reactor

Vasan Sivalingam, Vafa Ahmadi, Omodara Babafemi and Carlos Dinamarca *

Department of Process, Energy and Environmental Technology, University of South-Eastern Norway, 3918 Porsgrunn, Norway; vasan.sivalingam@usn.no (V.S.); vvaaffaaahmadi@gmail.com (V.A.); omodarafemi@yahoo.com (O.B.)

* Correspondence: carlos.dinamarca@usn.no

Abstract: This study presents a series of experiments to test the integration of syngas fermentation into a single-cell microbial electrosynthesis (MES) process. Minimal gas–liquid mass transfer is the primary bottleneck in such gas-fermentation processes. Therefore, we hypothesized that MES integration could trigger the thermodynamic barrier, resulting in higher gas–liquid mass transfer and product-formation rates. The study was performed in three different phases as batch experiments. The first phase dealt with mixed-culture fermentation at 1 bar H_2 headspace pressure. During the second phase, surface electrodes were integrated into the fermentation medium, and investigations were performed in open-circuit mode. In the third phase, the electrodes were poised with a voltage, and the second phase was extended in closed-circuit mode. Phase 2 demonstrated three times the gas consumption (1021 mmol) and 63% more production of acetic acid (60 mmol/L) than Phase 1. However, Phase 3 failed; at –0.8 V, acetic acid was oxidized to yield hydrogen gas in the headspace.

Keywords: hydrogen; syngas; homoacetogenesis; pressure reactor; microbial electrosynthesis

Citation: Sivalingam, V.; Ahmadi, V.; Babafemi, O.; Dinamarca, C. Integrating Syngas Fermentation into a Single-Cell Microbial Electrosynthesis (MES) Reactor. *Catalysts* **2021**, *11*, 40. https://doi.org/10.3390/catal11010040

Received: 30 November 2020
Accepted: 28 December 2020
Published: 31 December 2020

1. Introduction

Pyrolysis and gasification technologies are attractive organic waste decomposition strategies that result in a gaseous product known as syngas, which is a mixture of carbon monoxide (CO), carbon dioxide (CO_2), and hydrogen (H_2). Due to its energy content, syngas is considered as an energy vector for heat- and power-generation processes [1]. CO_2, the final product of such processes, has no energy value, and requires a further capturing process. A typical CO_2 capturing process involves either a chemical or mass transfer. Such methods are energy-intensive and expensive. Homoacetogens are microorganisms that perform CO_2 fixation at room temperature and pressure using hydrogen gas as the energy source. Therefore, syngas fermentation in a homoacetogenic culture has been considered as one of the most sustainable methods of CO_2 fixing.

The CO present in the syngas mixture can serve as both the carbon and energy source for fermentation, while CO_2 and H_2 serve only as the carbon and energy sources, respectively. Acetate is the primary end-product of homoacetogenesis (Equation (1)). Acetate synthesis from CO_2 and H_2 flows through the acetyl-CoA pathway, an intermediate reductive pathway also known as the Wood–Ljungdahl (WLJ) pathway [2]. The primary challenge in this fermentation process is the gas–liquid mass transfer, especially for hydrogen gas, which has lower solubility. Increasing the gas headspace pressure is one approach to improve the gas solubility and, consequently resulting in the gas–liquid mass transfer and product formation [3].

$$4H_2 + 2CO_2 \rightarrow CH_3COOH + 2H_2O\ \Delta G^0 = -74.3\ kJ/mol \quad (1)$$

Microbial electrosynthesis (MES) is an evolving bioprocess that transforms electrical energy into chemical energy. It uses CO_2 as the substrate to synthesis-reduced forms of

carbon compounds, such as methane, acetate, and other short- and medium-chain acids and alcohols [4,5]. Renewable energy is used to keep the desired potential at the cathode [6,7]. The mild potential induces nonspontaneous reactions to overcome the thermodynamic barrier [8] and reduces the activation energy. Microorganisms present at the cathode are specific to the applied potential, and consequently synthesize particular products. For example, methane synthesis from CO_2 occurs at −0.65 V, while acetate formation requires a more negative potential [9]. Reducing CO_2 into valuable organic chemicals is receiving more attention than transforming it into methane [10–12] due to challenges in handling gaseous products and the demand for the synthesized organic chemicals.

This research investigated the impact of the partial pressure of hydrogen gas on the gas consumption rate increment as a baseline. The process was extended by introducing MES to increase the gas consumption rate even further. The experiment was performed in three successive phases: (1) A mixed-culture homoacetogenic reactor was pressurized with hydrogen gas, and the gas uptake rate and fermentation products were investigated; (2) Phase 1 was repeated with surface-electrodes installed in the reactor, which was operated in open-circuit mode (OCM); and (3) Phase 2 was continued in closed-circuit mode (CCM).

Having only H_2 gas in the headspace simplified the experiments; therefore, the syngas was mimicked as a mixture of CO_2 and H_2. Only pure H_2 was supplied in the headspace at approximately one bar elevated pressure, while CO_2 was provided indirectly as sodium bicarbonate salt in the liquid medium [5,13]. During the two-month operation period, hydrogen gas consumption ceased. After that, the MES process was integrated within the elevated pressure in the syngas fermentation reactor, with the intention to enhance the gas uptake and product formation rate.

Elevating the partial pressure of a gas increases its solubility and consumption rate. Many studies of MES integration with fermentation to enhance gas uptake and product synthesis have been performed. However, most studies were carried out in two-chamber MES reactors [5,11,14], which mainly focus on CO_2 use and the formation of methane and acetic acid. A two-chamber reactor arrangement is mostly preferred for MES because the oxygen gas evolution at the anode could poison the anaerobic environments by oxidizing the redox species. No known studies have examined a single-cell MES to enhance H_2 gas consumption rate in a mixed-culture homoacetogenic syngas fermentation process. However, Nelabhotla and Dinamarca have performed several MES experiments with a single-cell MES reactor setup, and found a significantly higher product-synthesis efficiency without oxygen gas evolution [15–17]. These studies also sought to decrease the CO_2 content in the biogas.

2. Results and Discussion

2.1. Experimental Results

The pressure time series and cumulative hydrogen-consumption profiles found in Phases 1 and 2 are shown in Figures 1 and 2, respectively. The hydrogen pressure drop was significantly improved by the presence of biofilm in Phase 2. Phase 1, which was conducted without biofilm, had a shorter lag phase, but also a slower and limited H_2 consumption rate, which flattened at the 10th injection (Figure 1a) when the accumulated hydrogen uptake reached 342 mmol (Figure 2). In comparison, the reactor run with electrodes had a longer lag phase, with a higher H_2 consumption rate that resulted in a total hydrogen accumulation of 1021 mmol H_2 (Figure 2). The key results from Phases 1 and 2 are shown in Table 1.

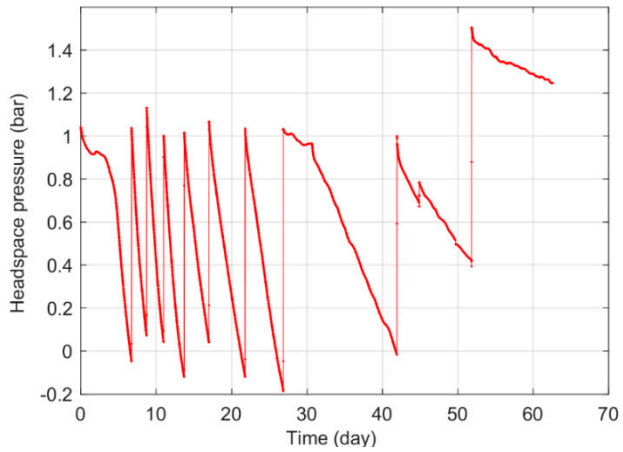

(**a**)

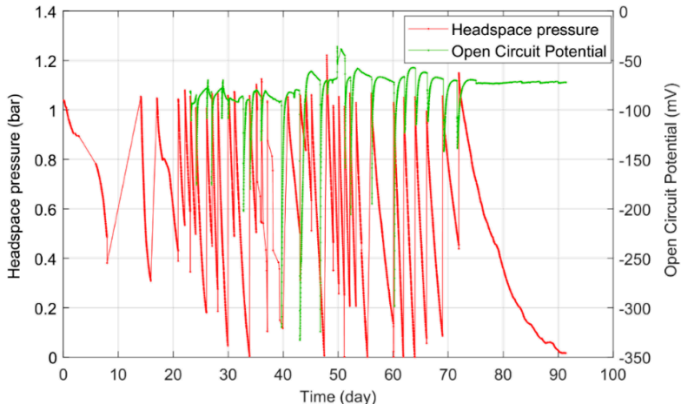

(**b**)

Figure 1. (**a**) The Phase 1 headspace pressure time series; (**b**) the Phase 2 headspace pressure time series and OCM at the cathode vs. the reference electrode (Ag/AgCl, 3 M NaCl).

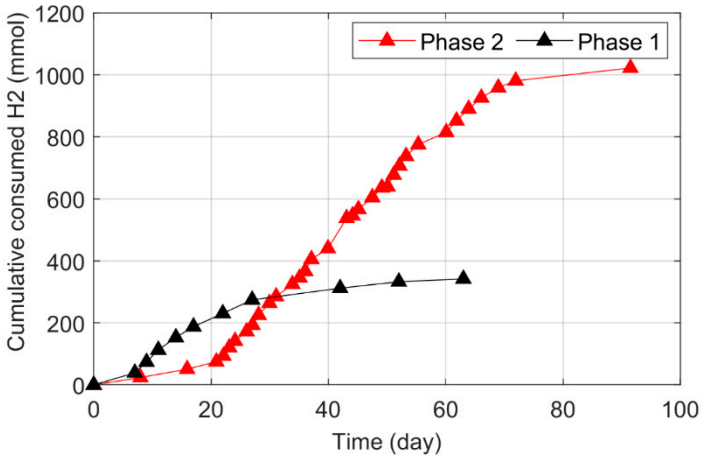

Figure 2. The cumulative hydrogen-consumption profiles for Phases 1 and 2.

Table 1. The comparison of essential results for Phases 1 and 2.

Measures	Phase 1	Phase 2
Highest achieved gas uptake rate (mmol/L·day)	6	13.5
Time to reach the highest gas uptake rate (day)	11	43
Total consumed H_2 (mmol)	342	1021
Time to reach the saturated gas consumption level (day)	60	90
Highest acetic acid concentration (mmol/L)	35	57
Acetic acid content in total VFAs (%)	80	85

The total amount of consumed H_2 gas and the gas uptake rate during Phase 2 was 3 and 2.3 times higher than during Phase 1, respectively, and there was 63% more acetic acid production during Phase 2 (Figure 3b). Phase 2 required 90 days to reach the saturation level, while Phase 1 required only 60 days. The relative abundance of active biofilm on the electrodes caused more H_2 gas dissociation and enhanced the acetic acid synthesis. In both phases, acetic acid was the primary product of the total VFAs matrix.

The open-circuit potential in Phase 2 is presented together with the headspace pressure change in Figure 1b. During the first two weeks of the experiment, the gas consumption rate was significantly lower. The rate then began to increase, and reached 13.5 mmol/L·day on day 43, then subsequently slowed to zero by the end of day 90. During the first 60 days, the OCP fluctuated widely between –350 and –80 mV, and then reached a stable range of around −70 mV on day 75. This could be a notable indication of a steady biofilm on the cathode.

When a saturation in gas consumption and a stable OCP were reached, the reactor was pressurized with H_2 to 1 bar, and the cathode was poised with −0.8 V. We expected to observe a higher gas consumption during Phase 3; however, the reactor behaved in the opposite manner, and an increase in headspace pressure was observed due to significant acetate oxidation. The headspace was depressurized when it rose above 1 bar to avoid reactor rupture, and the gas was collected to perform a composition analysis. Even though the reactor produced gas instead of uptaking it, we decided to continue with Phase 3, and quantified the product formation and gas composition for a short time. We think that sharing these negative results could be a good starting point for the development of a process integration.

Phase 3 was prolonged for 10 more days. Figure 3a shows the gas-composition variation and the generated current. At the beginning of Phase 3, H_2 was the only gas product (100%). After five days of operation, a trace amount (3%) of CO_2 started to evolve, followed by methane (CH_4) evolution (6%) on day 7. The H_2 gas occupied more than 90% of the headspace. It is difficult to conclude whether the produced hydrogen had an abiotic or biotic origin; this will require several more experiments at different potentials to establish the shares of hydrogen production. However, the decrease in acetic acid concentration (Figure 3b) in CCM partially confirmed that hydrogen could be produced abiotically at the cathode. The decline in acetic acid concentration implied that acetic acid could be the source of the protons and electrons for the produced gases.

There was no oxygen gas measured in the gas mixture. This absence confirmed that single-cell MES could be integrated with the fermentation process without any countereffect due to oxygen evolution at the anode, which may oxidize redox fermentation intermediates, reducing efficiency. If the oxygen evolution is considerably large, it could result in aerobic conditions in MES, which cause severe damage to the anaerobic fermentation process. At the start of CCM, the generated current was −200 mA, which was gradually raised, reaching a peak at –600 mA (current density = 8.57 A/m^2) when methane was formed. After that, it fell to –400 mA and remained stable.

Figure 3b shows the generation of VFAs throughout Phases 2 and 3. Though acetic acid and propionic acid were the primary fermentation products, at the end of Phase 2, 85% of the total VFAs was acetic acid. The added amount of bicarbonate limited the

concentration of VFAs. Once the CCM started, a reduction in acetic acid was observed, which corresponded to the rise in H_2 evolution.

Even though the inoculum underwent heat treatment, methane production confirmed that methanogens could not be completely eliminated by heat treatment. However, during the first 96 days of operation, the reactor did not exhibit any methane evolution. Once the electrodes were poised with voltage only, methane evolution was observed. It appeared that the electroactive methanogens were activated during Phase 3 due to the applied potential.

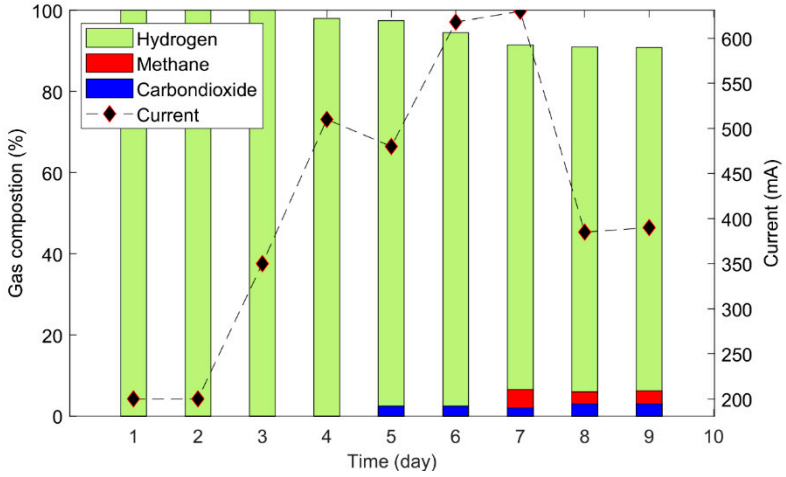

(**a**)

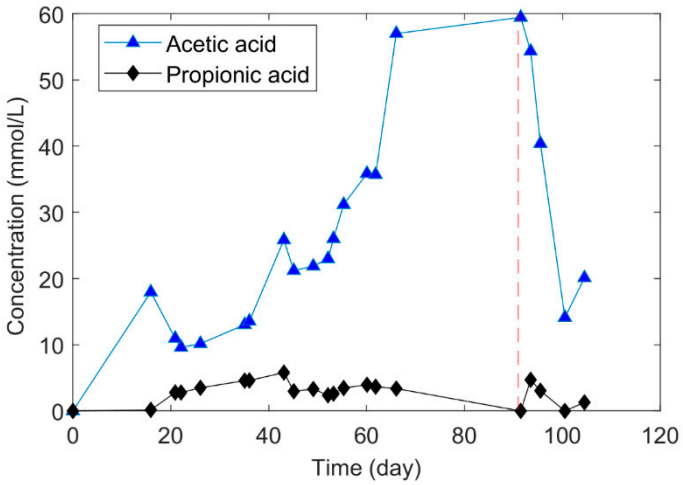

(**b**)

Figure 3. (**a**) The gas composition and the current variation during Phase 3. (**b**) The fermentation-product formation throughout Phases 2 and 3 (separated by a red vertical line).

2.2. Why Is Bioelectrochemical-Mediated Syngas Fermentation Essential?

The availability of organic waste will not be sufficient to meet the future demand for biomethane. It is expected that heavy transport, both land-based and maritime, will expand and diversify the use of this commodity, especially in Nordic countries. To meet this demand, it is necessary to increase production. The sources of organic waste for methane are limited, but CO_2 from industrial exhaust is readily available, while equivalent electrons from water, sulfides, and ammonium are also available.

Additional methane can be co-generated during the bioelectrochemical reduction of CO_2 and the fermentation of energy gases in one single reactor. Syngas can be converted

directly to methane through hydrogenotrophic methanogenesis, or indirectly using acetate as an intermediate. To meet energy demands while safeguarding the environment with near-circular economy, we think that future biogas plants will use anaerobic digestion (AD), syngas fermentation, and bioelectrochemical systems (BES) in an integrated manner (Figure 4).

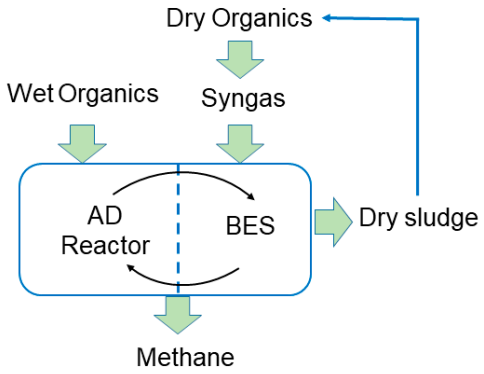

Figure 4. Integrated anaerobic digestion, syngas fermentation, and BES.

In an integrated AD-BES process as described by Nelabhotla and Dinamarca [10], an electric potential will drive electrons from water, organics, sulfides [18], and ammonium [7] to the cathode, where CO_2 will be reduced to methane. We propose that methane can be produced from syngas using the same process. However, H_2, CO, and CO_2 may take different metabolic routes depending on the applied potential. Our experiment showed that in a BES system with a titanium-anode and carbon-felt cathode poised at a −0.8 V potential, hydrogen was produced due to acetate oxidation, while the main goal was to achieve a higher rate of hydrogen consumption. This is because syngas cannot be injected directly to AD due to the higher partial pressure of hydrogen, which inhibited the propionate degradation that halts biogas production. We set a goal of a combining AD-BES with syngas fermentation. In that combined system, hydrogen gas is converted directly to either methane or acetic acid while avoiding acetic acid oxidation, as was observed in our study.

Although Phases 1 and 2 of our experiment demonstrated a promising value addition to the syngas fermentation process, we recognize that Phase 3 was a preliminary attempt to integrate a single-cell MES into a syngas fermentation to improve the gas consumption and product-formation rates. A detailed study of optimized voltage (which would facilitate an increase in the H_2 gas-uptake rate and would not oxidize the acetic acid) is necessary for proper process implications. Microbial analysis was vital at every phase to better understand the biochemical process involved. However, this attempt at a successful process integration suggested that the voltage optimization and microbial consortia analysis are essential elements in future research. Mathematical models for the reactor and the processes are also important in verifying the experimental results, and could constitute the objective of future studies.

3. Materials and Methods

3.1. Inoculum Preparation

Anaerobic digested sludge from the local wastewater treatment plant (Knarrdalstrand, Porsgrunn, Norway) was used to seed the reactor. The inoculum went through several treatment steps. First, it was sieved via 600 microns and incubated at 35 °C for a week to eliminate readily biodegradable organics. The inoculum was then heat-treated at 105 °C for 48 h to eliminate methanogens, while spore-forming acetogens were retained. The fermentation medium was facilitated with a nutrient solution composed of a mixture of salts (10 mL/L), trace elements (10 mL/L), and vitamins (10 mL/L). The nutrient solution's composition was adapted from a similar study performed by Dinamarca and Bakke [19] (Table 2).

Table 2. The content of the nutrient base media used to support the growth of the homoacetogenic culture.

Vitamin Solution (g/L)	Mineral Solution (g/L)	Salt Solution (g/L)
Biotin: 0.02	$MnSO_4 \cdot H_2O$: 0.04	NH_4Cl: 100
Folic acid: 0.02	$FeSO_4 \cdot 7H_2O$: 2.7	NaCl: 10
Pyridoxine hydrochloride: 0.1	$CuSO_4 \cdot 5H_2O$: 0.055	$MgCl_2 \cdot 6H_2O$: 10
Riboflavin: 0.05	$NiCl_2 \cdot 6H_2O$: 0.1	$CaCl_2 \cdot 2H_2O$: 5
Thiamine: 0.05	$ZnSO_4 \cdot 7H_2O$: 0.088	-
Nicotinic acid: 0.05	$CoCl_2 \cdot 6H_2O$: 0.05	-
Pantothenic acid: 0.05	H_3BO_3: 0.05	-
Vitamin B_{12}: 0.001	-	-
p-aminobenzoic acid: 0.05	-	-
Thioctic acid: 0.05	-	-

3.2. Phase 1

Phase 1 of the experiment was performed in a 4.125 L borosilicate glass reactor (FG Mellum AS, Akershus, Norway). It was modified as a lab-scale bioelectrochemical syngas fermentation reactor with a maximum pressure tolerance of 3 bar. The reactor was filled with 3.25 L of treated inoculum with incorporated nutrient solution and 3.4 g $NaHCO_3$/L (CO_2). A Heidolph MR 3001 magnetic stirrer (Heidolph Instruments, Schwabach, Germany) was used to provide proper agitation at 1000 rpm. The inoculum was purged with N_2 gas for 5 min to strip off the oxygen, followed by a flushing with pure hydrogen gas (laboratory 5.5 = $\geq$ 99.9995%, Linde Gas AS, Oslo, Norway). The headspace pressure was then elevated to approximately 1 bar with H_2, and the changes were logged using a CPG 1500 digital pressure gauge (WIKA, Bavaria, Germany) at 10 min intervals. Once the headspace pressure reached approximately zero, the reactor was repressurized to 1 bar and continued until no change in the pressure reading was observed. This experiment lasted 60 days.

3.3. Electrode Design and Experimental Setup

The anode and cathode were designed based on the reactor's volume to achieve the optimum surface area. Carbon felt (3.18 mm thickness, 99.0% $\approx$ 2.4 g/10 $\times$ 10 cm) from Alfa Aesar (GmbH, Kandel, Germany) was used as the cathode. The cathode was framed with a titanium sheet (1 cm) to keep it stable inside the reactor, and wrapped with titanium wire to enhance the electrical contact. A titanium metal sheet was used as the anode. It was modified to a particular shape to fit into the reactor and achieve more efficient agitation of the fermentation medium (Figure 5). The designs of the anode and cathode and an upper cross-sectional view of the reactor is presented in Figure 1. The surface area of anode and cathode were approximately 700 cm^2. An Ag/AgCl electrode (3 M NaCl, QVMF2052, ProSense, BB Oosterhout, The Netherlands) was used as the reference electrode. A Gamry 1010B Potentiostat-Galvanostat-ZRA (Gamry Instruments, Philadelphia, PA, USA) was used to perform electrochemical measurements.

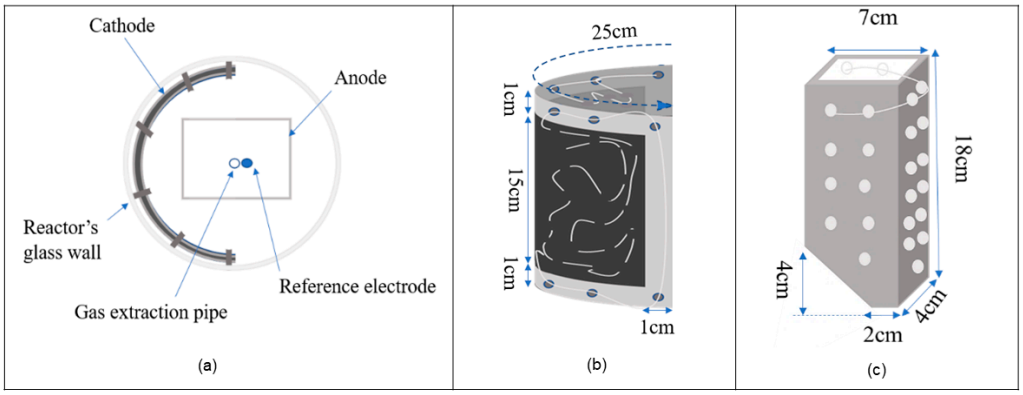

Figure 5. An upper cross-section of the reactor with electrode arrangements and electrode design with dimensions. (**a**) The upper cross-section, (**b**) the cathode, and (**c**) the anode.

3.4. Phase 2: Open-Circuit Mode

The electrodes were installed into the same glass reactor used in Phase 1 (Figure 6), and the Phase 1 procedure with fresh inoculum was repeated until it reached the stable headspace pressure. During this phase, the electrodes were not poised with voltage, and the experiments were performed in OCM. During this phase, it took 90 days to for the gas consumption or saturated gas consumption to cease.

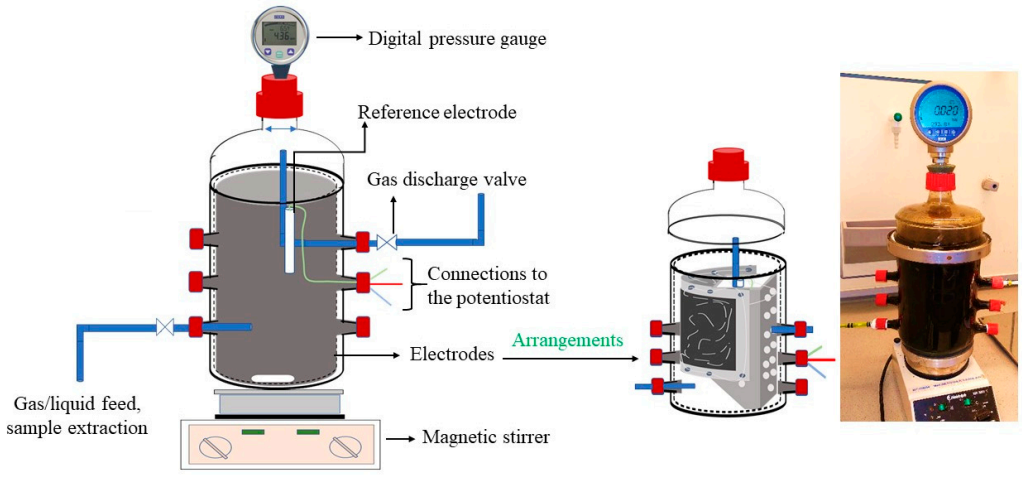

Figure 6. A sketch of the designed reactor (**left**), the anode and cathode arrangements within the reactor (**center**), and the complete reactor setup (**right**).

3.5. Phase 3: Closed-Circuit Mode

Once the saturated gas-consumption level was reached in Phase 2, it was prolonged in CCM. During CCM, the cathode was poised with −0.8 V vs. SHE by using a Gamry 1010B Potentiostat-Galvanostat-ZRA (Gamry Instruments, Philadelphia, PA, USA). This particular potential value was selected in accordance with similar studies performed by Nelabhotla et al. [16], during which they observed significant acetic acid production within the potential range of −0.8 to −0.9 V vs. SHE in a single-cell MES reactor.

We intended to pressurize the reactor with hydrogen gas during Phase 1 when the cathode was poised with −0.8 V. However, the reactor produced some gases (H_2, CH_4, and CO_2) when the cathode was poised with voltage, so the hydrogen feeding was stopped. Since the glass rector had limited pressure tolerance, the gas that accumulated in the headspace was released when it approached 1 bar of pressure, and gas composition analyses were performed, along with measurements of volatile fatty acids (VFAs).

3.6. Analytical Measurements

The concentration of VFAs was measured using a Clarius 500 PE auto-system gas chromatograph integrated with a built-in autosampler (Perkin Elmer, Waltham, MA, USA). The instrument was equipped with a capillary column (scion-wax temperature 20–250 °C) and a flame ionization detector (FID). The dimensions of the column were 25 m length, 0.25 mm diameter, and 0.2 µm film. The carrier gas was H_2 at a rate of 45 mL/min. The injector and detector temperatures were 270 and 250 °C, respectively. The initial oven temperature was set at 80 °C and maintained for 0.7 min, then was increased at a rate of 25 °C/min to 200 °C, followed by 20 °C increments until attaining an operating temperature of 240 °C.

The gas-composition analyses were performed using an 8610C gas chromatograph (SRI Instruments, Torrance, CA, USA) equipped with 6′ Haysep-D (MXT-1) and 6′ Molecular Sieve (MS13X) columns. The oven was operated at a constant 80 °C, with helium as the carrier gas at 2.1 bar pressure and a 20 mL/min flow rate. The thermal conductivity detector (TCD) was operated at 150 °C with helium and airflow rates of 25 and 250 mL/min, respectively.

4. Conclusions

The biofilm that formed on the electrodes facilitated an H_2 gas dissociation three times higher than the reactor without electrode surface, resulting in 63% more acetic acid production. Our hypothesis that an increase in gas consumption would be realized by negatively poising −0.8 V at the cathode failed; instead, gas production was observed, with 90% of the gas in the form of hydrogen. The reduction in acetic acid concentration and the evolution of gaseous products occurred simultaneously, which suggested that hydrogen and CO_2 products can be produced from acetic acid. As the findings of our study provided a good starting point toward integrating a successful syngas fermentation process into a single-cell MES. The interface of MES and syngas fermentation could be used to control product formation. Short-chain organic products can be obtained at a high rate due to the presence of densely packed biomass on the electrodes, and overproduced compounds can be oxidized as hydrogen gas to maintain target product concentration in the liquid medium.

Author Contributions: Conceptualization, C.D.; methodology, V.S. and C.D.; software, V.S., C.D., V.A., and O.B.; validation, V.S. and C.D.; formal analysis, V.S., C.D., V.A., and O.B.; investigation, V.S. and C.D.; resources, C.D.; data curation, V.S. and V.A.; writing—original draft preparation, V.S.; writing—review and editing, V.S. and C.D.; visualization, V.S.; supervision, C.D.; project administration, C.D.; funding acquisition, C.D. All authors have read and agreed to the published version of the manuscript.

Funding: This research was funded by the Norwegian Ministry of Education and Research through the Ph.D. program in Process, Energy and Automation Engineering at the University of South-Eastern Norway, grant number 2700095. The University of South-Eastern Norway funded the APC.

Acknowledgments: The authors wish to thank the Norwegian Ministry of Education and Research for funding.

Conflicts of Interest: The authors declare no conflict of interest.

References

1. Solarte-Toro, J.C.; Chacón-Pérez, Y.; Cardona-Alzate, C.A. Evaluation of biogas and syngas as energy vectors for heat and power generation using lignocellulosic biomass as raw material. *Electron. J. Biotechnol.* **2018**, *33*, 52–62. [CrossRef]
2. Phillips, J.R.; Huhnke, R.L.; Atiyeh, H.K. Syngas fermentation: A microbial conversion process of gaseous substrates to various products. *Fermentation* **2017**, *3*, 28. [CrossRef]
3. Stoll, I.; Herbig, S.; Zwick, M.; Boukis, N.; Sauer, J.; Neumann, A.; Oswald, F. Fermentation of H_2 and CO_2 with clostridium ljungdahlii at elevated process pressure—First experimental results. *Chem. Eng. Trans.* **2018**, *64*, 151–156.
4. Ganigué, R.; Puig, S.; Batlle-Vilanova, P.; Balaguer, M.D.; Colprim, J. Microbial electrosynthesis of butyrate from carbon dioxide. *Chem. Commun.* **2015**, *51*, 3235–3238. [CrossRef]

5. Mohanakrishna, G.; Abu Reesh, I.M.; Vanbroekhoven, K.; Pant, D. Microbial electrosynthesis feasibility evaluation at high bicarbonate concentrations with enriched homoacetogenic biocathode. *Sci. Total Environ.* **2020**, *715*, 137003. [CrossRef] [PubMed]
6. Rago, L.; Pant, D.; Schievano, A. Chapter 14—Electro-Fermentation—Microbial Electrochemistry as New Frontier in Biomass Refineries and Industrial Fermentations. In *Advanced Bioprocessing for Alternative Fuels, Biobased Chemicals, and Bioproducts*; Hosseini, M., Ed.; Woodhead Publishing: Cambridge, UK, 2019; pp. 265–287, ISBN 978-0-12-817941-3.
7. Sivalingam, V.; Dinamarca, C.; Samarakoon, G.; Winkler, D.; Bakke, R. Ammonium as a carbon-free electron and proton source in microbial electrosynthesis processes. *Sustainability* **2020**, *12*, 3081. [CrossRef]
8. Jiang, Y.; Jianxiong Zeng, R. Expanding the product spectrum of value added chemicals in microbial electrosynthesis through integrated process design—A review. *Bioresour. Technol.* **2018**, *269*, 503–512. [CrossRef] [PubMed]
9. Nelabhotla, A.B.T.; Dinamarca, C. Bioelectrochemical CO_2 reduction to methane: MES integration in biogas production processes. *Appl. Sci.* **2019**, *9*, 1056. [CrossRef]
10. Nevin, K.P.; Hensley, S.A.; Franks, A.E.; Summers, Z.M.; Ou, J.; Woodard, T.L.; Snoeyenbos-West, O.L.; Lovley, D.R. Electrosynthesis of organic compounds from carbon dioxide is catalyzed by a diversity of acetogenic microorganisms. *Appl. Environ. Microbiol.* **2011**, *77*, 2882–2886. [CrossRef] [PubMed]
11. Jiang, Y.; Su, M.; Zhang, Y.; Zhan, G.; Tao, Y.; Li, D. Bioelectrochemical systems for simultaneously production of methane and acetate from carbon dioxide at relatively high rate. *Int. J. Hydrogen Energy* **2013**, *38*, 3497–3502. [CrossRef]
12. Lehtinen, T.; Efimova, E.; Tremblay, P.-L.; Santala, S.; Zhang, T.; Santala, V. Production of long chain alkyl esters from carbon dioxide and electricity by a two-stage bacterial process. *Bioresour. Technol.* **2017**, *243*, 30–36. [CrossRef] [PubMed]
13. del Pilar Anzola Rojas, M.; Zaiat, M.; Gonzalez, E.R.; De Wever, H.; Pant, D. Effect of the electric supply interruption on a microbial electrosynthesis system converting inorganic carbon into acetate. *Bioresour. Technol.* **2018**, *266*, 203–210. [CrossRef] [PubMed]
14. Batlle-Vilanova, P.; Puig, S.; Gonzalez-Olmos, R.; Balaguer, M.D.; Colprim, J. Continuous acetate production through microbial electrosynthesis from CO_2 with microbial mixed culture. *J. Chem. Technol. Biotechnol.* **2016**, *91*, 921–927. [CrossRef]
15. Nelabhotla, A.B.T.; Khoshbakhtian, M.; Chopra, N.; Dinamarca, C. Effect of hydraulic retention time on MES operation for biomethane production. *Front. Energy Res.* **2020**, *8*. [CrossRef]
16. Nelabhotla, A.B.T.; Bakke, R.; Dinamarca, C. Performance analysis of biocathode in bioelectrochemical CO2 reduction. *Catalysts* **2019**, *9*, 683. [CrossRef]
17. Nelabhotla, A.B.T. Electrochemical Unit Integration with Biogas Production Processes. Ph.D. Thesis, University of South-Eastern Norway, Porsgrunn, Norway, 2020.
18. Bian, B.; Bajracharya, S.; Xu, J.; Pant, D.; Saikaly, P.E. Microbial electrosynthesis from CO_2: Challenges, opportunities and perspectives in the context of circular bioeconomy. *Bioresour. Technol.* **2020**, 122863. [CrossRef] [PubMed]
19. Dinamarca, C.; Bakke, R. Apparent hydrogen consumption in acid reactors: Observations and implications. *Water Sci. Technol. J. Int. Assoc. Water Pollut. Res.* **2009**, *59*, 1441–1447. [CrossRef] [PubMed]

Article 4

Impact of Electrochemical Reducing Power on Homoacetogenesis

Vasan Sivalingam[1], Pouria Parhizkarabyaneh[1], Dietmar Winkler[2], Pai Lu[3], Tone Haugen[4], Alexander Wentzel[4], Carlos Dinamarca[1]

[1] Department of Process, Energy and Environmental Technology, University of South-Eastern Norway, Norway
[2] Department of Electrical Engineering, Information Technology and Cybernetics, University of South-Eastern Norway, Norway
[3] Department of Microsystems, University of South-Eastern Norway, Norway
[4] Department of Biotechnology and Nanomedicine, SINTEF Industry, Trondheim, Norway

Published in Bioresource Technology, 2022 (Level 1) Journal.
DOI: 10.1016/j.biortech.2021.126512

Bioresource Technology 345 (2022) 126512

Contents lists available at ScienceDirect

Bioresource Technology

journal homepage: www.elsevier.com/locate/biortech

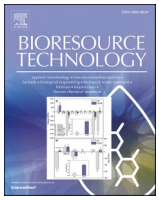

Impact of electrochemical reducing power on homoacetogenesis

Vasan Sivalingam [a], Pouria Parhizkarabyaneh [a], Dietmar Winkler [b], Pai Lu [c], Tone Haugen [d], Alexander Wentzel [d], Carlos Dinamarca [a,*]

[a] Department of Process, Energy and Environmental Technology, University of South-Eastern Norway, Norway
[b] Department of Electrical Engineering, Information Technology and Cybernetics, University of South-Eastern Norway, Norway
[c] Department of Microsystems, University of South-Eastern Norway, Norway
[d] Department of Biotechnology and Nanomedicine, SINTEF Industry, Trondheim, Norway

HIGHLIGHTS

- Homoacetogenesis performed in a single-chamber microbial electrosynthesis reactor.
- Providing −175 mV reducing power increased the acetic acid synthesis.
- −175 mV sets a new benchmark for the lowest reducing power for acetate synthesis.
- Ancillary reducing power does not increase the H_2 gas–liquid mass transfer.

ARTICLE INFO

Keywords:
Syngas fermentation
CO_2 reduction
Microbial electrosynthesis
Homoacetogenesis
Hydrogen

ABSTRACT

Homoacetogenesis was performed in a microbial electrosynthesis single-chamber reactor at open and closed circuits modes. The aim is to investigate how an applied reducing power affects acetic acid synthesis and H_2 gas–liquid mass transfer. At a cathode voltage of −175 mV vs. Ag/AgCl (3.0 NaCl), the acetic acid synthesis rate ramped up to 0.225 mmol $L^{-1}h^{-1}$ due to additional electrons and protons liberation from carbon-free sources such as water and ammonium via anodic oxidation. The study sets a new lowest benchmark that acetic acid can be bioelectrochemical synthesized at − 175 mV. The applied reducing power did not increase the H_2 gas–liquid mass transfer because the direct electron transfer from cathode to microorganisms reduced the demand for H_2 in the fermentation medium. Microbial analysis shows a high presence of *Veillonellaceae* spore-forming clostridia, which are identified as homoacetogens.

1. Introduction

The rise in atmospheric CO_2 concentration, consequently global warming, is one of the critical challenges for modern society (Chatterjee et al., 2021). Population growth and industrialization consume more resources and leave behind a surfeit of wastes (Avtar et al., 2019). In order to comply with the United Nations sustainable development goals, the waste feedstocks need to be treated, and the carbon should be captured and utilized in eco-friendly ways (Olabi et al., 2022).

Thermochemical conversion processes, such as pyrolysis, gasification, and combustion, are valorization strategies to transfer waste feedstock into energy-rich gases (Stąsiek and Szkodo, 2020; Malico et al., 2019). The syngas, a mixture of carbon monoxide (CO), hydrogen (H_2) and carbon dioxide (CO_2), is a major product of such valorization processes (Figueras et al., 2021; Kwon et al., 2019; Shen et al., 2017), which demand further carbon capture and sequestration steps to mitigate the global warming caused by CO_2 and CO. In recent years, several efforts have been made to biocatalytic carbon capture and transform C_1 gases into valuable fuels and value-added chemicals (Annie Modestra et al., 2020; ElMekawy et al., 2016). The biocatalytic process is performed by living microorganisms such as bacteria and archaea through enzymes or electrocatalytic activities (Espina et al., 2021; Schievano et al., 2019). Syngas fermentation and microbial electrosynthesis (MES) are getting more attention due to their sustainability (Köpke and Simpson, 2020; Shi et al., 2021). The syngas fermentation is carried out mainly through an autotrophic metabolism (homoacetogenesis). H_2 is used as the reducing equivalent to convert CO_2 into acetic acid during this bioconversion process, Eq. (1).

* Corresponding author at: University of South-Eastern Norway, Kjølnes ring 56, 3918 Porsgrunn, Norway.
E-mail address: carlos.dinamarca@usn.no (C. Dinamarca).

https://doi.org/10.1016/j.biortech.2021.126512
Received 30 October 2021; Received in revised form 1 December 2021; Accepted 3 December 2021
Available online 7 December 2021

Firstly, CO_2 is reduced to CO and formic acid or formyl group; due to several subsequent reduction steps, the formyl groups are reduced to a methyl group. Eventually, the methyl group is combined with CO and co-enzymes to synthesize acetyl-CoA, which is further converted to acetate. Since the acetyl-CoA is the primary intermediate, the process is referred to as the acetyl-CoA reductive pathway and Wood Ljungdahl Pathway (WLP) in order to credit the scientists Harland G. Wood and Lars G. Ljungdahl, who have discovered this metabolic pathway (Drake, 2012). The WLP has been extensively presented in many publications, therefore not repeated here, and suggested (Drake, 2012) for interested readers. Gas-liquid mass transfer is the primary bottleneck for the WLP due to the low solubility of H_2 (Sivalingam et al., 2021b).

Most recently, a bioelectrochemical technique called microbial electrosynthesis (MES) is getting more attention as a sustainable strategy to furnish reducing power for biological CO_2 fixation (Schievano et al., 2019). The reducing power is produced from renewable power sources, used to maintain specific potentials at the cathode where electrons are used by the microorganisms that exist on the cathodic biofilm to synthesize value-added products from CO_2. A plethora of studies have evidenced that ancillary reducing power provided in the MES improves the metabolic pathway of CO_2 conversion to either methane (CH_4), volatile fatty acids (VFAs) or alcohols (Li et al., 2012; Lim et al., 2020; Lu et al., 2014; Nelabhotla and Dinamarca, 2018; Izadi et al., 2021). The reducing power directly transfers electrons from the biocathode to microorganisms (Direct extracellular electron transfer, DET) to reduce CO_2; also, the electrons reduce protons into H_2. Subsequently, the H_2 is utilized by microorganisms to reduce the CO_2 (Indirect extracellular electron transfer, IDET) (Choi and Sang, 2016; Enzmann et al., 2018; Pant et al., 2016). Most recent MES studies involve in biogas upgradation (CO_2 to CH_4) and electrochemically mediated acetate synthesis mainly evaluate CO_2 sequestration processes and electron transfer mechanisms (Das et al., 2020; Nelabhotla et al., 2021; Nelabhotla and Dinamarca, 2018).

$$2CO_2 + 4H_2 \rightarrow CH_3COOH + 2H_2O \quad (1)$$

This study hypothesizes that integrating MES unit into a homoacetogenic reactor can provide additional reducing power for the homoacetogenesis process, leading to an enhanced acetic acid synthesis and efficient H_2 gas–liquid mass transfer. In this regard, Sivalingam et al., performed a series of homoacetogenic experimental studies in a single-chamber MES reactor (Sivalingam et al., 2021a; Yerga, 2021). In that study, the biocathode was poised at −0.800 V vs. SHE. The experimental study revealed neither improved gas consumption nor acetate synthesis; instead, acetate oxidation was observed. This finding suggests that the applied potential might be beyond the thermodynamic limit; thus, the cathode had lost its biotic function, as anode potential exceeded the formal oxidation potential of the acetic acid (Sivalingam et al., 2021a).

The acetic acid oxidation at the anode is a particular challenge for studies performed in single-chamber reactors. Because, while the cathode reduction potential is lowered, the anode's oxidation potential increases, resulting in acetic acid oxidation, decreasing product synthesis and releasing CO_2, which negatively impacts net carbon capture efficiency.

In this study, the lesson learned from Sivalingam et al. (Sivalingam et al., 2021a) is extended with an advanced experimental design. Fine tuning the cathode voltage to achieve an efficient acetate synthesis and H_2 gas–liquid mass transfer were the primary objectives of this research.

Moreover, homoacetogenic fermentation and bioelectrodes' biotic nature was evaluated by microbiome analysis and scanning electron microscopy (SEM). At the end of the study, acetic acid production performance and coulombic efficiency were determined. Cyclic voltammetry (CV) and electrochemical impedance spectroscopy (EIS) analysis were also performed to explore the reactor's electrochemical nature. As far as the authors know, there is not much research conducted in this context. Therefore, believe that this detailed study will be a cornerstone in the electro-microbial and fermentation related fields.

2. Material and methods

2.1. Inoculum preparation/culture enrichment

Digested sludge from a local biogas reactor (Knarrdalstrand, Porsgrunn Norway) was collected as inoculum. It was sieved via 300 μm to remove coarse impurities and heat-treated at 105 °C for 48 h to deplete methanogens and as well as to concentrate spore-forming acetogens. At the final stage of culture-enrichment, pH was adjusted to neutral, a nutrient media was added, containing necessary vitamins, minerals and salts for the biomass synthesis; the composition is adapted from (Sivalingam and Dinamarca, 2021). The treated inoculum consists of 22.2 g L^{-1} total solids (TS), 3.8 g L^{-1} volatile solids (VS), 3.9 g L^{-1} soluble chemical oxygen demand (sCOD) and 0.93 g L^{-1} ammonium.

2.2. Electrode, reactor designs and system configuration

Carbon felt (Alfa Aesar, Germany) and graphite rods (ThermoFisher GmbH, Germany) were used as cathode and anode. An Ag/AgCl electrode (3.0 M NaCl, Prosense, Netherland) was the reference electrode. The carbon felt (25.0 cm length; 12.0 cm width) was punched with 24, 0.4 cm radius holes and folded as a hollow cylinder to enhance the liquid flow. Ten graphite rods (15.2 cm length; 0.6 cm diameter) were placed around the carbon felt with 1.0 cm equidistance. The reference electrode was placed near (0.5 cm) the cathode to reduce ohmic losses.

The designed electrodes were placed into a 4.125 L borosilicate glass reactor (Single-Chamber MES). 3.250 L volume was utilized as the liquid part. The balance volume (0.875 L) was expanded by adding a pressure tank with a volume of 0.640 L (BR-1500, Berghof, Eningen, Germany). The total headspace volume became 1.515 L, attached to a digital manometer (LEO-3, Keller, Winterthur, Switzerland), and the headspace gauge pressure was logged in 10 min intervals. Two potentiostats (1010E Interface, Gamry Instruments, Pennsylvania, USA) were used for the electrochemical analysis.

2.3. Operation

The study was performed in two phases, thus open circuit mode (OCM) and closed-circuit mode (CCM). In both phases, the single-chamber MES was operated in batch mode. The reactor was inoculated with treated inoculum. Though the inoculum underwent heat treatment, 5 mM 2-bromoethanesulfonic acid was added to ensure the methanogens suppression. The experiment was performed at room temperature, and the fermentation media was agitated at 1000 rpm by a magnetic stirrer (Heidolph Instruments, Schwabach, Germany).

In phase 1, the headspace was pressurized by H_2 (Laboratory H_2 5.5 = 99.9995 %, Linde Gas AS, Oslo, Norway) to 1 bar. Based on stoichiometry equation (1), the required amount of carbon dioxide was added as sodium bicarbonate ($NaHCO_3$). Mimicking CO_2 gas as a bicarbonate salt creates a liquid medium saturated with carbon, thus the microorganisms can efficiently utilize. In addition, it reduces the costs associated with feeding, separating, and storing pure CO_2 gas (Gutiérrez-Sánchez et al., 2021). The digital manometer recorded the change in headspace pressure. Once the pressure drops close to zero bar, the reactor is repressurized to ~ 1 bar. Also, bicarbonate was added based on stoichiometric demand. This cyclic operation was continued until observing a stable H_2 consumption rate. The electrodes were not polarised at this phase one, therefore referred to as open circuit mode (OCM). During every cycle, samples were collected, and reactor performance was assessed by analysing pH, VFAs, sCOD and ammonium concentration changes in the suspended fermentation broth.

In phase 2, the cathode was poised by a range of negative voltages, referred to as closed-circuit mode (CCM). All the potential referred hereafter is with respect to Ag/AgCl (3.0 M NaCl) reference electrode.

Initially, the cathode was poised at −25 mV at potentiostatic mode. The cyclic operation described in the OCM was repeated until observing a steady H_2 consumption rate. Then the reducing power was step by step increased to −75 mV, −125 mV, and −175 mV, and the OCM cyclic operation was also repeated. When the cathode was poised with voltages, the anode voltage was also kept recorded. Once the gas consumption slowed down, headspace gas composition was measured. At the start of every CCM operation, medium pH was adjusted and maintained near-neutral to favour microbial activity (Tharak and Venkata Mohan, 2021)

2.4. Analytical methodology

The sCOD and ammonium analyses were performed in Spectroquant cell and, the concentrations were determined by Spectroquant® Pharo 300 UV/VIS photometer (Merck KGaA, Darmstadt, Germany). The spectroquant COD and ammonium test methods are analogous to APHA 5220 and 4500 (American Public Health Association (APHA), 1995). The concentration of VFAs was measured by Clarius 500 PE gas chromatograph (Perkin Elmer, MA, USA). The instrument was occupied with a scion-wax capillary column (25.00 m length, 0.25 mm diameter, and 0.20 μm film) and a flame ionization detector. H_2 was used as the carrier gas at a 45 mL min^{-1} flow rate. The detector temperature was 250 °C, and the injector temperature was 270 °C. The initial oven temperate remains at 80 °C for 0.7 min, then increased to 200 °C at 25 °C min^{-1} ramps followed by 20 °C min^{-1} to attain 240 °C.

A 8610C gas chromatograph (SRI Instruments, CA, USA) was used to quantify the gas composition. The chromatograph instrument contains 6′ Haysep-D (MXT-1) and 6′ Molecular Sieve (MS13X) columns and a thermal conductivity detector. The oven temperature was maintained at 80 °C. Helium was the carrier gas used at 2.1 bar at 20 mL min^{-1} flow rate.

2.5. Electrochemical experiments

Two Gamry 1010 E interfaces were used for the electrochemical experiments. Potentiostatic test was the primary technique carried out through the CCM, where the negative potential range from −25 mV to −175 mV was applied on the cathode with respect to the Ag/AgCl (3.0 M NaCl) reference electrode. Moreover, CV at a scan rate of 10 mV s^{-1} and EIS were performed for the plain electrodes, at the end of OCM and at the end of CCM. The CV on the fresh electrode was performed in a potential window of 0 V to −1.0 V, while the OCM and CCM were performed on potential windows of 0.2 V to −1.0 V and 0 V to −0.6 V, respectively. The EIS was carried out at 10.0 mV sinusoidal signal perturbation at a frequency range of 2.0 MHz to 0.2 Hz at 10 decay/points measurement rate. Subsequently, Gamry Echem Analyst software was used for electrochemical data analysis, and an in build graphical model editor, version 7.8.4 was used to create an equivalent circuit model for the EIS results to investigate the possible circuit elements, especially the ohmic (R_{ohm}) and charge transfer resistances (R_{ct}). Linear sweep voltammetry (LSV) was performed between 0.0 and −1.0 V at the scan rate of 5.0 mV s^{-1} on the cathode at the end of OCM. Simultaneously the anode potential vs. reference electrode was recorded by another potentiostat (Gamry, 1010 E) to determine the maximum reducing power that can be applied at the cathode, thereby which cannot induce higher overpotential at the anode. The relevant voltammetry and anodic potential profiles can be found on the E-supplementary data of this paper's online version.

2.6. Microbiome analysis

Microbiome analysis was performed for the raw inoculum, heat-treated inoculum, fermentation medium at the end of OCM and CCM. In addition, biofilm from the electrodes was extracted, and microbial assemblage was investigated at the end of CCM. According to the manufacturer's protocol, samples were centrifuged, and DNA was extracted from the pellet using Quick DNA-Fecal/ Soil Microbe DNA Miniprep Kit (Zymo Research). Sequencing amplicon libraries were generated by PCR following the "16S Metagenomic Sequencing Library Preparation, Preparing 16S Ribosomal RNA Gene Amplicons for the Illumina MiSeq System" protocol (Illumina part number 15,044,223 rev. B). Internal parts of the 16S ribosomal RNA (rRNA) gene, covering variable regions V3 and V4, were PCR-amplified with KAPA HiFi HotStart ReadyMix (KAPA Biosystems) and the primers 5′-TCGTCGGCAGCGTCAGATGTGTATAAGAGA-CAGCCTACGGGNGGCWGCAG-3′ and 5′-GTCTCGTGGGCTCGGA-GATGTGTATAAGAGACAGGACTACHVGGGTATCTAATCC-3′ and purified with the Agencourt AMPure XP kit (Beckman Coulter). The Nextera XT Index Kit was used to add sequencing adapters and multiplexing indices by PCR, and the products were once more purified by Agencourt AMPure XP followed by quantification on a Qubit v2 using the Qubit dsDNA BR Assay Kit (Thermo Fisher Scientific). Pooled DNA libraries were sequenced on a MiSeq sequencer (Illumina) using the MiSeq Reagent Kit v3 in the 2·300 bp paired-end mode. After sequencing, raw sequencing reads were demultiplexed, filtered, combined, and taxonomically classified by the Metagenomics Workflow within MiSeq Reporter v. 2.5.1 (Illumina), generating abundance tables, which were further processed in Microsoft Excel.

2.7. SEM analysis

The SEM analysis was performed on plain carbon felt cathode and cathode at the end of the OCM and CCM. A piece of the carbon felt cathode was extracted from the reactor at the end of OCM and CCM. The impurities were removed by washing with phosphate buffer. Scanning electron microscopy (Hitachi S3500, Krefeld, Germany) was used to characterize the morphology of different electrodes. To preserve the original morphology of the cultured biofilm and the electrode-microbe interphases, the electrodes with up-loaded microbes were first fixed in glutaraldehyde fixative and dried via gradient dehydration, according to Xiao et al. (Xiao et al., 2020).

2.8. Performance analysis

In the OCM, acetic acid is produced only via the typical WLP (homoacetogenesis). However, at the CCM, acetic acid is synthesized by both usual Wood Ljungdahl and bioelectrochemical pathways due to the additional reducing power applied to the cathode. The reducing power impact on homoacetogenesis efficiency was denoted as η which is the ratio between produced acetic acid at the CCM and the estimated acetic acid production in CCM by homoacetogenic pathway. The homoacetogenically produced acetic acid in CCM was estimated based on the optimum acetic acid production rate achieved in the OCM. The η above hundred indicates the amount of acetic acid produced due to the impact of reducing power applied on the cathode.

The electrochemically assisted acetic acid synthesis efficiency is quantified by Columbic Efficiency (CE), as shown in equation (2): where F is the Faraday constant, 96 485C/mol e. The mole of surplus acetic acid production in CCM is denoted as n_{AA}. The $\int_{t_i}^{t_f} I(t)dt$ represents the total charge transferred from anode to cathode, calculated by integrating measured current over time (Nelabhotla and Dinamarca, 2019). A constant value eight in equation (2) represents that eight electrons/reducing equivalence are necessary to produce one mole of acetic acid from CO_2, as explained in equation (3) (Tharak and Venkata Mohan, 2021).

$$CE(\%) = \frac{8 \times F \times n_{AA}}{\int_{t_i}^{t_f} I(t)dt} * 100 \quad (2)$$

$$2CO_2 + 8e^- + 8H^+ \rightarrow CH_3COOH + 2H_2O \quad (3)$$

3. Results and discussion

3.1. Acetic acid synthesis

The acetic acid is the only fermentation product detected both in the OCM and CCM samples. Fig. 1 depicts the cumulative acetic acid synthesis and production rates with corresponding reducing power applied on the cathode. The acetic acid concentration profile was partitioned into six intervals (0–188 h, 188–370 h, 370–532 h, 532–625 h, 625–719 h and 719–830 h), and segmented regression analyses were performed. Based on the regression models, the acetic acid production rates were determined and presented as bars in Fig. 1.

At the OCM operation, the synthesized acetic acid increased from 0 to 172 mmol and, the production rate stabilized at 0.178 mmol $L^{-1}h^{-1}$. Once the CCM operation started, the acetic acid synthesis surged forward continuously and reached 428 mmol at the end of CCM. However, when the reactor operation shifted to CCM, the production rate decreased to the lowest rate of 0.05 mmol $L^{-1}h^{-1}$ at −125 mV operation. During these CCM periods, the induced anodic potential reached up to 300 mV (Fig. 2), sufficient to oxidize a portion of the acetic acid at the anode (Ray and Ghangrekar, 2017), consequently lowering the production rate. However, the CO_2 released to the headspace was not observed (Equation (4)). Higher H_2 headspace pressure and the alkali pH of the medium could have forced the CO_2 to remain in the liquid fermentation medium. Another reason for the fall in acetic acid production rate is that the applied reducing power −125 mV is insufficient (Ray and Ghangrekar, 2017) to facilitate electron transfer from the electrode to microorganisms for acetate synthesis.

During the −175 mV operation period, the acetic acid rate ramped up to 0.225 mmol $L^{-1}h^{-1}$. This is 26 % higher than the OCM rate. The current profile also showed a dramatic increment, from 0.5 mA to ~ 55.0 mA, corresponding to the rise of the sudden acetic acid production rate. This is because, when the cathode was poised at −175 mV, the anodic potential exceeded 2.0 V (Fig. 2). The oxidation potential above 2.0 V is sufficient to oxidize substances like water, ammonium, and acetic acid (Bian et al., 2020). The acetic acid synthesis at the cathode counteracted the loss of acetic acid due to anodic oxidation and did not impact the production rate. However, the water and ammonium oxidation deliver significantly better acetic acid production because carbon-free electron sources do not release CO_2 upon oxidation (Sivalingam et al., 2020). More substance oxidation transfers extra electrons from anode to cathode, consequently, increase the current.

The −175 mV is much lower than the theoretical reduction potential for acetate synthesis (-0.485 V vs. Ag/AgCl) (Arends et al., 2017).

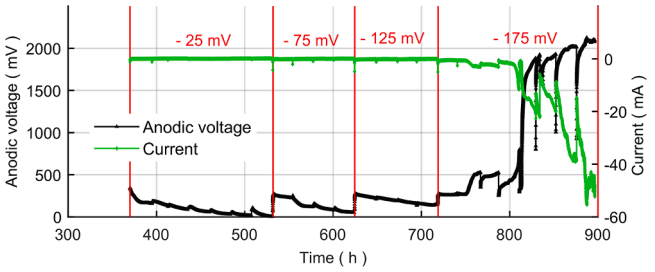

Fig. 2. Current and the anodic voltage trends in the CCM.

Therefore, insufficient to promote indirect electron transfer from cathode to microorganisms (Izadi et al., 2020). However, it is in the voltage range adequate to facilitate the direct electron transfer at the cathode (Choi and Sang, 2016; Hartshorne et al., 2007), resulting in an enhanced acetic acid production rate.

These observations validated the first research hypothesis that additional reducing power imposed on the cathode in the homoacetogenic reactor improved the acetic acid synthesis rate. The other part of the hypothesis regarding the impact of reducing power on H_2 gas–liquid mass transfer is discussed in section 3.2.

3.2. Hydrogen gas consumption

Fig. 3 shows the H_2 headspace pressure profiles for the OCM and CCM experiments. The H_2 consumption rate was calculated for every cycle and plotted together with respective headspace pressure profiles. In the OCM operation, the H_2 consumption rate gradually reached 0.8 mmol $L^{-1}h^{-1}$ by 200 h. The experiment was prolonged by 170 h (370 h) to ensure a stable consumption rate. However, when the cathode was poised with voltage (CCM), the H_2 gas consumption decreased to 0.7 mmol $L^{-1}h^{-1}$. It remained approximately stable from – 25 mV to the first 110 h of the – 175 mV operation cycle. This is because the microorganisms present in the cathodic biofilm directly consumed the electrons instead of H_2 gas, consequently decreasing the H_2 consumption from the headspace; thereby consumption rate dropped. Moreover, some part of the bicarbonate consumption for the cell synthesis of electroactive microorganisms exists on the cathodic biofilm, reducing the amount of available carbon source for the acetate synthesis. Therefore, less hydrogen is converted to acetate (Equation (1)), resulting in a lower consumption rate.

The SEM images confirm the presence of biofilm on the cathode, which are given in the E-supplementary data of this online version of the

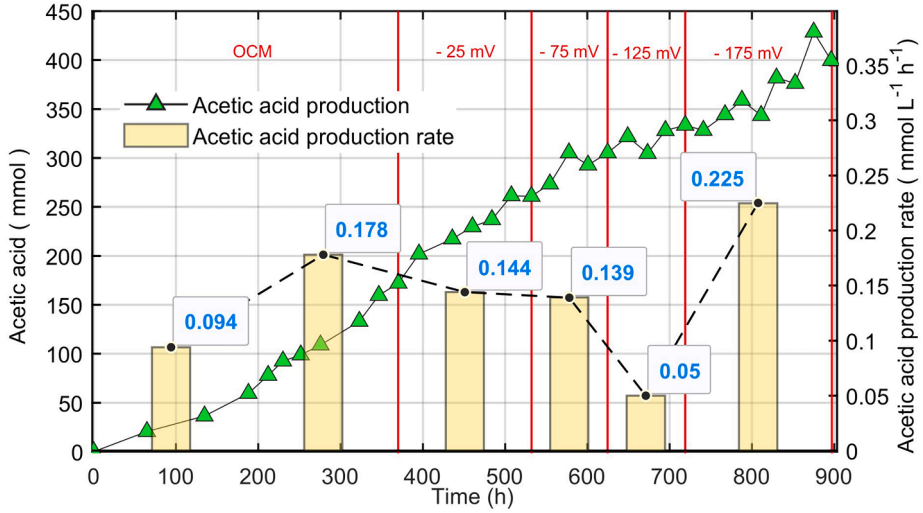

Fig. 1. Accumulated acetic acid production profile and the production rates in OCM and CCM operations.

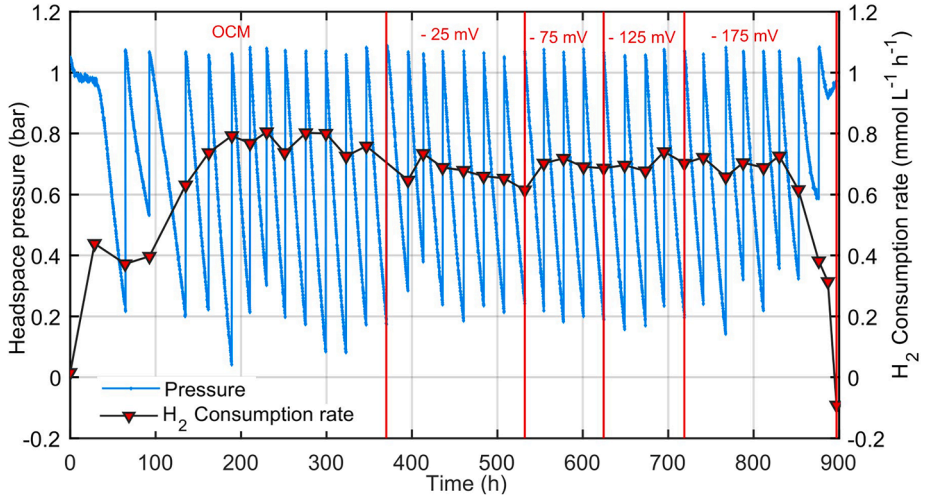

Fig. 3. Headspace pressure and the H_2 consumption rate profiles for OCM and CCM experiments.

paper. In contrast to the plain cathode and the cathode at the end of OCM, it can be seen that the biofilm remarkably assimilated between the carbon felt fibre surface at the end of the CCM. Although cathode at OCM does not display a significant biofilm growth, a few bacterial cells were noticed compared to the plain cathode. This observation is consistent with what has been found in a similar study performed by Izadi et al. (Izadi et al., 2020).

At the beginning of the −175 mV period, the gas consumption rate remained the same for 110 h; after that, the rate dropped drastically towards the end of the experiment because of the headspace pressure increment. The cathodic H_2 evolution is not possible at such a lower voltage, −175 mV. Many researchers also have reported that biohydrogen evolution needs reducing voltage greater than −200 mV (Arends et al., 2017; Baek et al., 2021; Wang et al., 2019). The gas composition analyses revealed that the headspace was occupied with O_2, N_2 and CO_2 in addition to the fed H_2. Therefore, it is summarized that substantial release of O_2, N_2 and CO_2 due to the anodic oxidation of water, ammonium, and acetic acid, is the reason for the headspace pressure increment, which resulted in a negative gas consumption rate (Fig. 3).

3.3. Gas composition analysis

There was neither rise in headspace pressure nor gas evolution observed during the first 800 h operation. However, the headspace pressure rose after 800 h, where the cathode was experiencing −175 mV reduction potential. The composition analysis performed at 825 h revealed that headspace was occupied by 3 % O_2 and 2.8 % CO_2 in addition to the fed H_2. After a day follow-up (856 h), the O_2 percentage increased to 6.5 %, while the CO_2 reached 5 %. At 896 h, remarkable gas evolution was observed (Fig. 3), resulting in a pressure increment. The pressure increment complies with anodic voltage (greater than 2.0 V) rise, as well as remarkably noticed a higher current (~ 55 mA) generation (Fig. 2). The gas composition at 896 h depicted 1 % O_2, 4.5 % CO_2, and 4 % N_2 evolution. Oxidation of water, acetic acid, and ammonium at the anode (2.0 V) is the reason for such gases evaluation, respectively O_2, CO_2 and N_2. The corresponding oxidation reactions are given in equations (4), (5) and (6); therein, acetic acid is denoted by a general formula of organic acids C_nH_{2n+1} −COOH.

Even though the cathode reduction potential was carefully lowered step by step to avoid higher overpotential occurrence at the anode, the anode potential reached above 2.0 V, resulting in oxidation of water, acetic acid, and ammonium. These oxidation reactions substantially liberate protons and electrons. The organics/acetic acid oxidation decreases acetic acid concentration and releases CO_2, therefore not contributing to the acetic acid production rate enhancement. However, ammonium and water oxidation liberate carbon-free electrons and protons (Liang et al., 2021; Sivalingam et al., 2020), facilitating a higher acetic acid production rate.

$$C_nH_{2n+1} - COOH + 2nH_2O \rightarrow (n+1)CO_2 + (6n+2)H^+ + (6n+2)e^- \quad (4)$$

$$4H_2O \rightarrow 2O_2 + 8H^+ + 8e^- \quad (5)$$

$$2NH_4^+ \rightarrow N_2 + 8H^+ + 6e^- \quad (6)$$

3.4. Chemical analysis

Soluble organic concentration was measured in terms of sCOD, which increased from 4 to 10 g COD L^{-1} throughout the experiment and followed the same trend of acetic acid profile.

The pH and the ammonium profiles are presented in Fig. 4. Since acetic acid is synthesized as the only fermentation product, a pH profile expected a reciprocal relationship. However, the pH of the fermentation medium gradually increased from 7 to 9 during the OCM operation. The utilization of dissolved CO_2 decreases the availability of proton in the medium, which is the primary reason for such a pH rise. Bicarbonate consumption at the expense of H_2 and the formation of sodium acetate (a conjugated base) also could be another reason (Sivalingam et al., 2021b). A slight increment in the ammonium concentration from 660 to 700 mg L^{-1} was noted. Ammonia could be released during the anaerobic fermentation processes due to protein breakdowns (Yenigün and Demirel, 2013). The released ammonia captures the H^+ from water to form ammonium ions and leaves behind OH^-, consequently enhancing the pH (Tchobanoglous et al., 2014).

The pH increment was observed in both open and closed-circuit modes operations. However, it was adjusted back to near neutral to favour microbial activity at the start of every CCM cycle. The OH^- ion is a by-product of MES and is unavoidable in the CCM. Therefore, a basification of electrolyte occurs in the CCM, which increases the pH. Another reason could be that the OH^- deprotonates the bicarbonate and forms carbonate, thereby increasing pH. The pH rise due to the carbonation effect cannot be eliminated in MES reactors, especially in the batch mode of operation (Hernandez-Aldave and Andreoli, 2020). However, it can be minimized by operating the reactor in continuous mode. Also, a flow cell reactor setup diminishes this effect by circulating and refreshing the electrolyte (Weekes et al., 2018). On the other hand, higher pH may lower the overpotential of CO_2 fixation (Dinh et al., 2018), and the highly alkaline environment reduces the electrical resistance in the reactor (Hernandez-Aldave and Andreoli, 2020).

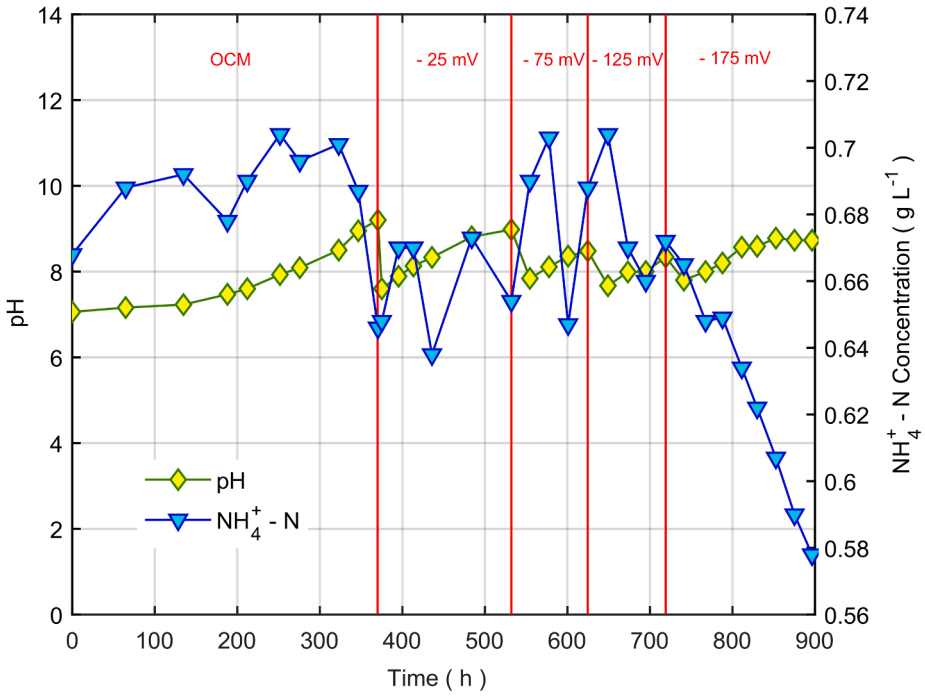

Fig. 4. pH and the ammonium concentration profile.

However, investigating these concepts in more detail is beyond the scope of this article.

The ammonium concentration depicted an upward trend in the OCM while fluctuating around 620 ± 20 mg L^{-1} at the CCM operation from – 25 to – 125 mV and plummeted to 570 mg L^{-1} during the – 175 mV operation due to the oxidation transpired at the anode. The remarkable drop in the ammonium concentration corresponds with nitrogen gas evolution and the higher acetic acid synthesis discussed, where ammonium acted as a carbon-free proton and electron source (Sivalingam et al., 2020).

3.5. Electrochemical studies

In this section, the bio-electrochemical behaviour of the reactor and the cathodic biofilm are investigated to support the research hypothesis. CV and EIS analyses were performed on the plain cathode at the beginning of the experiment and at the end of OCM and CCM experiments.

Redox catalytic current generation capacity of the biocatalyst was mainly studied by the CV (Annie Modestra and Venkata Mohan, 2019). The cathodic catalytic current of the plain cathode was − 0.22 A, which substantially improved to −0.54 A and −0.86 A, respectively, in OCM and CCM. The detailed voltammetry graphs are available in the E-supplementary data of this article (online version). The significant amount of current enhancement at CCM affirms that the cathode has been enriched with electroactive biofilm due to the supplied reduction potential, resulting in efficient electrochemically mediated acetic acid synthesis. Modestra et al., mentioned that the redox catalytic current could also facilitate the substrate uptake for biomass growth and cellular maintenance (Annie Modestra et al., 2020). In addition, Tharak et al., (Tharak and Venkata Mohan, 2021) also stated that higher redox current match up with enhanced VFAs production rates and the electrotrophy of the biocathode with increased substrate reducing capabilities. The higher acetic acid production rate (0.225 mmol $L^{-1}h^{-1}$), remarkable catalytic current generation during – 175 mV CCM (Fig. 2), and abundant biofilm growth on the cathode in this research comply well with the studies of (Annie Modestra et al., 2020) and (Tharak and Venkata Mohan, 2021).

Fig. 5 shows the Nyquist plots for the plain electrode, electrodes at the end of OCM and CCM experiments. Also, the equivalent circuit model used to fit the experimental data is presented in Fig. 5. Electrolyte or fermentation medium resistance is denoted as Ru (ohmic resistance). Rp and Y_o represent the charge transfer resistance and constant phase elements, respectively. The equivalent circuit fitted well with the experimental data (Goodness of fit is in the order of 10^{-4}).

At the beginning of the experiment (plain electrode), the Ru was 990 mΩ and tended to decrease to 549 mΩ towards the end of the CCM,

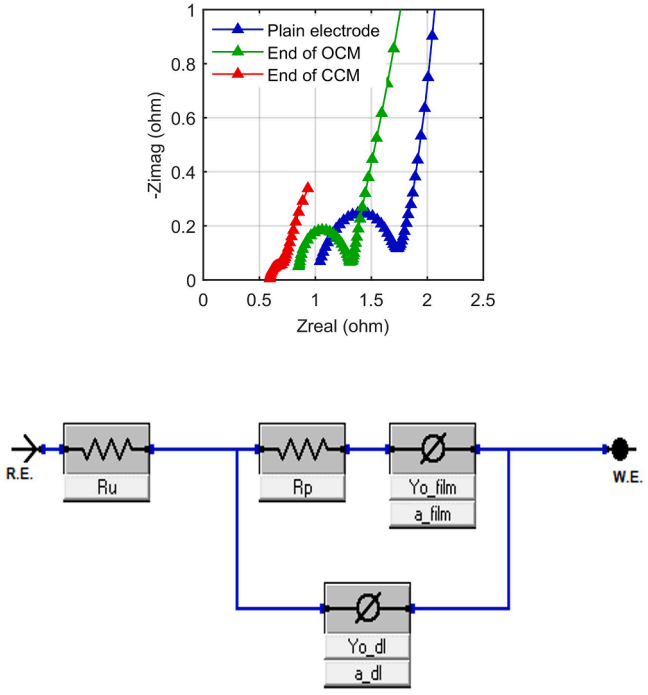

Fig. 5. Top: Nyquist plots for the plain electrode, electrode at the end of OCM and CCM EIS experiments; bottom: Equivalent circuit model.

which is 45 % lower. Addition of bicarbonate salt as the carbon source and the accumulation of fermentation products such as acetic acid in the electrolyte are the most significant reasons for increasing the medium's conductivity, resulting in lower ohmic resistance. At the beginning of the experiment, the charge transfer resistance (Rp) was 830 mΩ and decreased to 709 mΩ towards the end of the experiment. The constant phase element at lower frequency also dropped by half of the initial value of the biofilm. These results clearly indicate that electroactive biofilm assimilated on the cathode while it is poised with reducing power. Moreover, the culture transition into stationary phase also could be the reason for such decrement in charge transfer resistance (Martin et al., 2018). The CV, SEM and microbiome analyses also validate these observations that cathode is occupied with *Clostridiaceae* and *Veillonellaceae* rich biofilm, which lowers the resistance, consequently, favours electron transfer to synthesize acetic acid at a higher rate. However, a detailed metabolic study is required to investigate the electron transfer mechanism and the impact of reducing power on the electrode and the culture media, in the context of CO_2 conversion into value-added chemicals.

3.6. Microbial analysis

To assess the changes in microbial community structure and complexity (Fig. 6), the authors performed 16S rRNA gene amplicon sequencing on the original inoculum before (sample 0) and after (sample 1) heat-treatment. In addition, samples were taken from the different parts of the reactor at different operational modes, also considered for the microbial analysis. Thereby samples 2 and 3 were taken from the suspended medium at the end of OCM and CCM, respectively. Samples 4 and 5 were from the cathode and the anode at the end of CCM.

Sample 0, taken before heat-treatment, shows high diversity of bacterial families, some of which are non-spore formers, which explain their absence in the heat-treated samples. Sample 1 shows an overwhelming dominance of *Planococcaceae*, a family consisting of Gram-variable, spore-forming or non-spore-forming, motile or non-motile species. Sample 2 shows the presence of *Clostridiaceae* and *Veillonellaceae,* which are families known to contain both spor forms and obligate anaerobic homoacetogenic bacteria. *Clostridiaceae* are present in the heat-treated sample but in a minor fraction and, therefore, are not visible in Fig. 6. Among the *Clostridiaceae,* many species are capable of fixating carbon dioxide in the presence of hydrogen as the energy source using the Wood Ljungdahl pathway and performing acetogenesis.

Samples 3, 4 and 5 show a high presence of *Clostridiaceae* and *Veillonellaceae.* Among them, sample 3 from the end of CCM shows the highest presence of *Clostridiaceae* (53 %). Sample 4, from the carbon felt cathode shows a higher presence of *Veillonellaceae,* which may suggest that a large portion of this family adheres to the carbon felt surface and prefers growing in biofilms, explaining a lower abundance in the suspended medium. This is also the case with sample 5, where the anode also shows a higher presence of *Veillonellaceae*.

3.7. Performance analysis

The acetic acid production efficiency was 63 % at the −25 mV CCM operation, continuing to fall up to 44 % towards the end of −125 mV due to the anodic oxidation. Besides, the applied reducing power range between −25 to −125 mV was insufficient for a notable microbial acetate synthesis. However, during the −175 mV period, the production efficiency up swung to 105 %. The 5 % more than a hundred per cent represents the electrochemically assisted acetic acid production; based on that, calculated CE was 75 %. The calculation details are available in the E-Supplementary document (online version).

4. Conclusion

Hypothesis one is confirmed. Reducing power applied on the cathode enhances homoacetogenesis by increasing the acetic acid synthesis rate. Moreover, this study sets a new benchmark that acetic acid can be bioelectrochemical synthesized at − 175 mV, the lowest value among the other articles published in similar aspects. However, the outperformed experimental results revealed that no improvements in the H_2 gas consumption rate due to applied reducing power, because the direct electron transfer from cathode to microorganisms reduces the demand for H_2 in the fermentation medium.

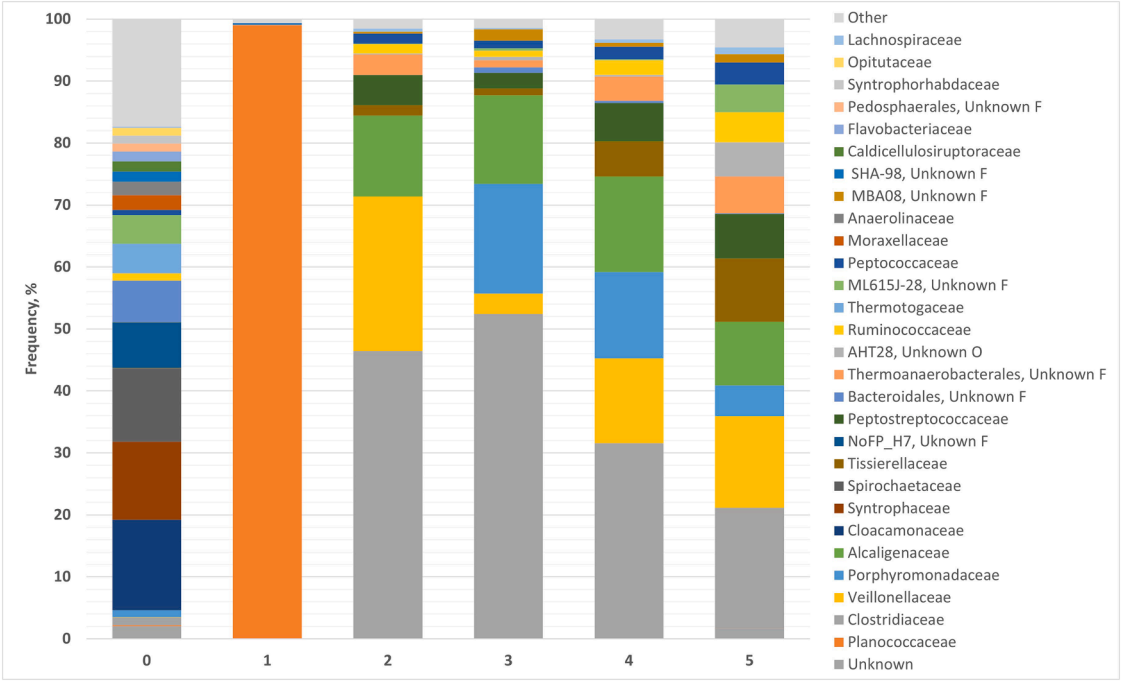

Fig. 6. Changes in the microbial assemblage upon the fermentation based on the family level.

Funding

The Norwegian Ministry of Education and Research funded this research through the PhD program in Process, Energy, and Automation Engineering at the University of South-Eastern Norway, grant number 2700095.

CRediT authorship contribution statement

Vasan Sivalingam: Conceptualization, Methodology, Experiments, Formal analysis, Investigation, Validation, Original draft preparation, Writing – review & editing. **Pouria Parhizkarabyaneh:** Experiments, Formal analysis, Investigation. **Dietmar Winkler:** Software, Methodology. **Pai Lu:** Formal analysis, Methodology, Visualization. **Tone Haugen:** Formal analysis, Methodology, Visualization. **Alexander Wentzel:** Formal analysis, Methodology, Visualization, Investigation, Writing – review & editing. **Carlos Dinamarca:** Conceptualization, Methodology, Investigation, Validation, Writing – review & editing, Supervision, Project administration, Funding acquisition.

Declaration of Competing Interest

The authors declare that they have no known competing financial interests or personal relationships that could have appeared to influence the work reported in this paper.

Acknowledgements

The authors want to acknowledge the Norwegian Ministry of Education and Research for this project's financial support. Also, thank Dr. Tonje Marita Bjerkan Heggeset and Dr. Pawel Piatek for contributing on micriobiome data analysis.

Appendix A. Supplementary data

Supplementary data to this article can be found online at https://doi.org/10.1016/j.biortech.2021.126512.

References

American Public Health Association (APHA), American Water Works Association, Water Pollution Control Federation, Water Environment Federation., 1995. Standard methods for the examination of water and wastewater. American Public Health Association.

Annie Modestra, J., Katakojwala, R., Venkata Mohan, S., 2020. CO2 fermentation to short chain fatty acids using selectively enriched chemolithoautotrophic acetogenic bacteria. Chem. Eng. J. 394, 124759. https://doi.org/10.1016/j.cej.2020.124759.

Annie Modestra, J., Venkata Mohan, S., 2019. Capacitive biocathodes driving electrotrophy towards enhanced CO2 reduction for microbial electrosynthesis of fatty acids. Bioresour. Technol. 294, 122181. https://doi.org/10.1016/j.biortech.2019.122181.

Arends, J.B.A., Patil, S.A., Roume, H., Rabaey, K., 2017. Continuous long-term electricity-driven bioproduction of carboxylates and isopropanol from CO2 with a mixed microbial community. J. CO2 Util. 20, 141–149.

Avtar, R., Tripathi, S., Aggarwal, A.K., Kumar, P., 2019. Population–Urbanization–Energy Nexus: A Review. Resources 8 (3), 136. https://doi.org/10.3390/resources8030136.

Baek, G., Rossi, R., Logan, B.E., 2021. Changes in electrode resistances and limiting currents as a function of microbial electrolysis cell reactor configurations. Electrochim. Acta 388, 138590. https://doi.org/10.1016/j.electacta.2021.138590.

Bian, B., Bajracharya, S., Xu, J., Pant, D., Saikaly, P.E., 2020. Microbial electrosynthesis from CO2: Challenges, opportunities and perspectives in the context of circular bioeconomy. Bioresour. Technol. 302, 122863. https://doi.org/10.1016/j.biortech.2020.122863.

Chatterjee, S., Jeevanandham, S., Mukherjee, M., Vo, D.-V., Mishra, V., 2021. Significance of re-engineered zeolites in climate mitigation – A review for carbon capture and separation. J. Environ. Chem. Eng. 9 (5), 105957. https://doi.org/10.1016/j.jece:2021.105957.

Choi, O., Sang, B.-I., 2016. Extracellular electron transfer from cathode to microbes: application for biofuel production. Biotechnol, Biofuels, p. 9.

Das, S., Diels, L., Pant, D., Patil, S.A., Ghangrekar, M.M., 2020. Review—Microbial Electrosynthesis: A Way Towards The Production of Electro-Commodities Through Carbon Sequestration with Microbes as Biocatalysts. J. Electrochem. Soc. 167 (15), 155510. https://doi.org/10.1149/1945-7111/abb836.

Dinh, C.-T., García de Arquer, F.P., Sinton, D., Sargent, E.H., 2018. High Rate, Selective, and Stable Electroreduction of CO2 to CO in Basic and Neutral Media. ACS Energy Lett. 3 (11), 2835–2840.

Drake, H.L., 2012. Acetogenesis. Springer Science & Business Media.

ElMekawy, A., Hegab, H.M., Mohanakrishna, G., Elbaz, A.F., Bulut, M., Pant, D., 2016. Technological advances in CO2 conversion electro-biorefinery: A step toward commercialization. Bioresour. Technol. Waste Biorefinery - Advocating Circular Economy 215, 357–370.

Enzmann, F., Mayer, F., Rother, M., Holtmann, D., 2018. Methanogens: biochemical background and biotechnological applications. AMB Express 8, 1.

Espina, G., Atalah, J., Blamey, J.M., 2021. Extremophilic Oxidoreductases for the Industry: Five Successful Examples With Promising Projections. Front. Bioeng. Biotechnol. 9, 654.

Figueras, J., Benbelkacem, H., Dumas, C., Buffiere, P., 2021. Biomethanation of syngas by enriched mixed anaerobic consortium in pressurized agitated column. Bioresour. Technol. 338, 125548. https://doi.org/10.1016/j.biortech.2021.125548.

Gutiérrez-Sánchez, O., Daems, N., Offermans, W., Birdja, Y.Y., Bulut, M., Pant, D., Breugelmans, T., 2021. The inhibition of the proton donor ability of bicarbonate promotes the electrochemical conversion of CO2 in bicarbonate solutions. J. CO2 Util. 48, 101521. https://doi.org/10.1016/j.jcou.2021.101521.

Hartshorne, R.S., Jepson, B.N., Clarke, T.A., Field, S.J., Fredrickson, J., Zachara, J., Shi, L., Butt, J.N., Richardson, D.J., 2007. Characterization of Shewanella oneidensis MtrC: a cell-surface decaheme cytochrome involved in respiratory electron transport to extracellular electron acceptors. J. Biol. Inorg. Chem. JBIC Publ. Soc. Biol. Inorg. Chem. 12 (7), 1083–1094.

Hernandez-Aldave, S., Andreoli, E., 2020. Fundamentals of Gas Diffusion Electrodes and Electrolyzers for Carbon Dioxide Utilization: Challenges and Opportunities. Catalysts 10, 713.

Izadi, P., Fontmorin, J.-M., Godain, A., Yu, E.H., Head, I.M., 2020. Parameters influencing the development of highly conductive and efficient biofilm during microbial electrosynthesis: the importance of applied potential and inorganic carbon source. Npj Biofilms Microbiomes 6, 1–15.

Izadi, P., Fontmorin, J.-M., Virdis, B., Head, I.M., Yu, E.H., 2021. The effect of the polarised cathode, formate and ethanol on chain elongation of acetate in microbial electrosynthesis. Appl. Energy 283, 116310. https://doi.org/10.1016/j.apenergy.2020.116310.

Kwon, E.E., Kim, S., Lee, J., 2019. Pyrolysis of waste feedstocks in CO2 for effective energy recovery and waste treatment. J. CO2 Util. 31, 173–180.

Köpke, M., Simpson, S.D., 2020. Pollution to products: recycling of 'above ground' carbon by gas fermentation. Curr. Opin. Biotechnol. 65, 180–189.

Li, H., Opgenorth, P.H., Wernick, D.G., Rogers, S., Wu, T.-Y., Higashide, W., Malati, P., Huo, Y.-X., Cho, K.M., Liao, J.C., 2012. Integrated Electromicrobial Conversion of CO2 to Higher Alcohols. Science 335, 1596–1596.

Liang, Q., Gao, Y., Li, Z., Cai, J., Chu, N., Hao, W., Jiang, Y., Zeng, R.J., 2021. Electricity-driven ammonia oxidation and acetate production in microbial electrosynthesis systems. Front. Environ. Sci. Eng. 16, 42.

Lim, S.S., Fontmorin, J.-M., Izadi, P., Wan Daud, W.R., Scott, K., Yu, E.H., 2020. Impact of applied cell voltage on the performance of a microbial electrolysis cell fully catalyzed by microorganisms. Int. J. Hydrog. Energy 45, 2557–2568.

Lu, X.u., Leung, D.Y.C., Wang, H., Leung, M.K.H., Xuan, J., 2014. Electrochemical Reduction of Carbon Dioxide to Formic Acid. ChemElectroChem 1 (5), 836–849.

Malico, I., Nepomuceno Pereira, R., Gonçalves, A.C., Sousa, A.M.O., 2019. Current status and future perspectives for energy production from solid biomass in the European industry. Renew. Sustain. Energy Rev. 112, 960–977.

Martin, A.L., Satjaritanun, P., Shimpalee, S., Devivo, B.A., Weidner, J., Greenway, S., Henson, J.M., Turick, C.E., 2018. In-situ electrochemical analysis of microbial activity. AMB Express 8, 162.

Nelabhotla, A.B.T., Dinamarca, C., 2018. Electrochemically mediated CO 2 reduction for bio-methane production: a review. Rev. Environ. Sci. Biotechnol. 17 (3), 531–551.

Nelabhotla, A., Dinamarca, C., 2019. Bioelectrochemical CO2 Reduction to Methane: MES Integration in Biogas Production Processes. Appl. Sci. 9 (6), 1056. https://doi.org/10.3390/app9061056.

Nelabhotla, A.B.T., Pant, D., Dinamarca, C., 2021. Chapter 8 - Power-to-gas for methanation. In: Aryal, N., Mørck Ottosen, L.D., Wegener Kofoed, M.V., Pant, D. (Eds.), Emerging Technologies and Biological Systems for Biogas Upgrading. Academic Press, pp. 187–221.

Olabi, A.G., Obaideen, K., Elsaid, K., Wilberforce, T., Sayed, E.T., Maghrabie, H.M., Abdelkareem, M.A., 2022. Assessment of the pre-combustion carbon capture contribution into sustainable development goals SDGs using novel indicators. Renew. Sustain. Energy Rev. 153, 111710. https://doi.org/10.1016/j.rser.2021.111710.

Pant, D., Bajracharya, S., Mohanakrishna, G., Vanbroekhoven, K., 2016. Bioelectrochemical CO2 Reduction to Acetic Acid and Ethanol: Improved Microbial Electrosynthesis Using Gas Diffusion Electrodes. Presented at the Qatar Foundation Annual Research Conference Proceedings Volume 2016 Issue 1, Hamad bin Khalifa University Press (HBKU Press), p. EEPP1739.

Ray, S., G., Ghangrekar, M., M., 2017. Mechanisms of Charge Transfer during Bio-Cathodic Electro-Synthesis of CO2-Neutral Methane. Adv. Biotechnol. Microbiol. 3, 555625.

Schievano, A., Pant, D., Puig, S., 2019. Editorial: Microbial Synthesis, Gas-Fermentation and Bioelectroconversion of CO2 and Other Gaseous Streams. Front, Energy Res, p. 7.

Shen, Yafei, Ma, Dachao, Ge, Xinlei, 2017. CO 2 -looping in biomass pyrolysis or gasification. Sustain. Energy Fuels 1 (8), 1700–1729.

Shi, Xiao-Chen, Tremblay, Pier-Luc, Wan, Lulu, Zhang, Tian, 2021. Improved robustness of microbial electrosynthesis by adaptation of a strict anaerobic microbial catalyst to

molecular oxygen. Sci. Total Environ. 754, 142440. https://doi.org/10.1016/j.scitotenv.2020.142440.
Sivalingam, Vasan, Dinamarca, Carlos, Samarakoon, Gamunu, Winkler, Dietmar, Bakke, Rune, 2020. Ammonium as a Carbon-Free Electron and Proton Source in Microbial Electrosynthesis Processes. Sustainability 12 (8), 3081. https://doi.org/10.3390/su12083081.
Sivalingam, Vasan, Ahmadi, Vafa, Babafemi, Omodara, Dinamarca, Carlos, 2021a. Integrating Syngas Fermentation into a Single-Cell Microbial Electrosynthesis (MES) Reactor. Catalysts 11 (1), 40. https://doi.org/10.3390/catal11010040.
Sivalingam, V., Haugen, T., Wentzel, A., Dinamarca, C., 2021b. Effect of Elevated Hydrogen Partial Pressure on Mixed Culture Homoacetogenesis. Chem, Eng. Sci. X, p. 100118.
Sivalingam, V., Dinamarca, C., 2021. High Pressure Moving Bed Biofilm Reactor for Syngas Fermentation. Chem. Eng. Trans. 86, 1483–1488.
Stąsiek, Jan, Szkodo, Marek, 2020. Thermochemical Conversion of Biomass and Municipal Waste into Useful Energy Using Advanced HiTAG/HiTSG Technology. Energies 13 (16), 4218. https://doi.org/10.3390/en13164218.
Tchobanoglous, G., Burton, F.L., Stensel, H.D., Metcalf & Eddy (Boston), 2014. Wastewater engineering: treatment and resource recovery. McGraw-Hill Higher Education, New York.
Tharak, Athmakuri, Venkata Mohan, S., 2021. Electrotrophy of biocathodes regulates microbial-electro-catalyzation of CO2 to fatty acids in single chambered system. Bioresour. Technol. 320, 124272. https://doi.org/10.1016/j.biortech.2020.124272.
Wang, Wei, Zhang, Baogang, He, Zhen, 2019. Bioelectrochemical deposition of palladium nanoparticles as catalysts by Shewanella oneidensis MR-1 towards enhanced hydrogen production in microbial electrolysis cells. Electrochim. Acta 318, 794–800.
Weekes, David M., Salvatore, Danielle A., Reyes, Angelica, Huang, Aoxue, Berlinguette, Curtis P., 2018. Electrolytic CO2 Reduction in a Flow Cell. Acc. Chem. Res. 51 (4), 910–918.
Xiao, Shuai, Fu, Qian, Xiong, Kerui, Li, Zhuo, Li, Jun, Zhang, Liang, Liao, Qiang, Zhu, Xun, 2020. Parametric study of biocathodes in microbial electrosynthesis for CO2 reduction to CH4 with a direct electron transfer pathway. Renew. Energy 162, 438–446.
Yenigün, Orhan, Demirel, Burak, 2013. Ammonia inhibition in anaerobic digestion: A review. Process Biochem. 48 (5-6), 901–911.
Yerga, Rufino M. Navarro, 2021. Catalysts for Production and Conversion of Syngas. Catalysts 11 (6), 752. https://doi.org/10.3390/catal11060752.

Article 4: E - Supplementary Material

Impact of Electrochemical Reducing Power on Homoacetogenesis

Vasan Sivalingam[1], Pouria Parhizkarabyaneh[1], Dietmar Winkler[2], Pai Lu[3], Tone Haugen[4], Alexander Wentzel[4], Carlos Dinamarca[1]

[1] Department of Process, Energy and Environmental Technology, University of South-Eastern Norway, Norway
[2] Department of Electrical Engineering, Information Technology and Cybernetics, University of South-Eastern Norway, Norway
[3] Department of Microsystems, University of South-Eastern Norway, Norway
[4] Department of Biotechnology and Nanomedicine, SINTEF Industry, Trondheim, Norway

Supplementary A

Linear Sweep Voltammetry (LSV) performed at the cathode (0.0 to -1.0 V), the top panel explains the cathodic voltage change and the current response. The bottom panel shows the corresponded anodic voltage while the LSV was performed.

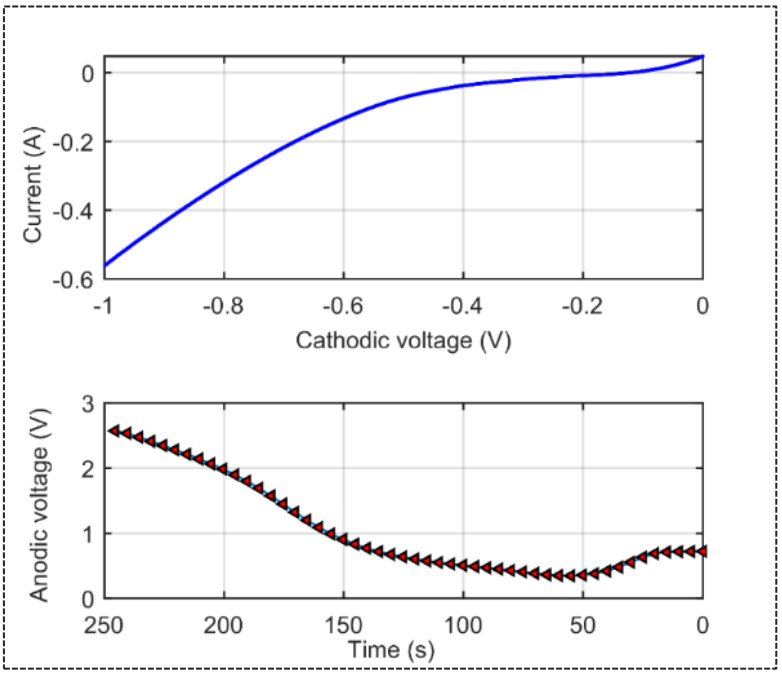

Supplementary B

Cyclic voltammograms for the plain electrode, Open Circuit Mode (OCM) and Close Circuit Mode (CCM) experiments.

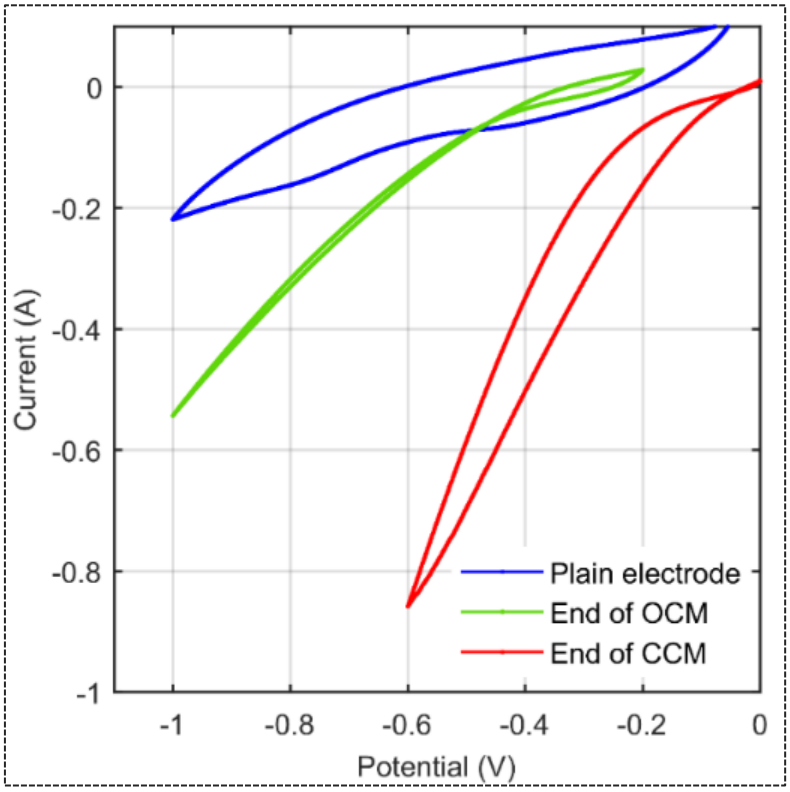

Supplementary C – Performance analysis

The homoacetogenic yield of acetic acid in the CCM is estimated based on the optimum acetic acid production rate achieved from the OCM, which is 0.178 mmol L^{-1} h^{-1}.

Voltage range in CCM	Estimated homoacetogenic acetic acid yield (mmol)	Total measured acetic acid yield (mmol)	Acetic acid production Efficiency %
-25 mV	93.52	58.99	63
-75 mV	40.60	31.77	78
-125 mV	26.54	11.64	44
-175 mV	90.34	95.25	105

Supplementary D – SEM images

SEM images of the cathode, top: plain electrode at the beginning of the experiment, middle: at the end of OCM, bottom: at the end of CCM. The scale of the images moves from 500 µm, 50 µm and 10 µm rightward.

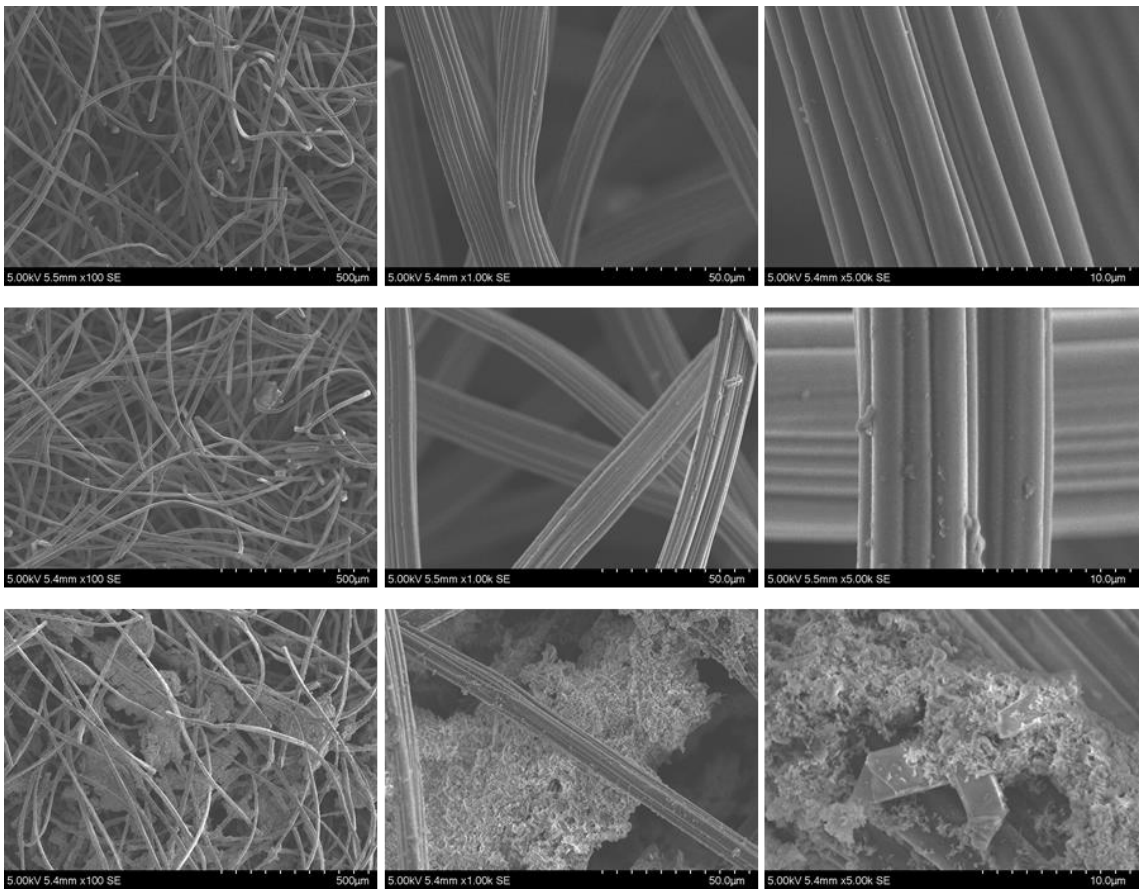

Article 5

Syngas Fermentation and Microbial Electrosynthesis Integration as a Single Process Unit

Vasan Sivalingam[1], Dietmar Winkler[2], Tone Haugen[3], Alexander Wentzel[3], Carlos Dinamarca[1]

[1] Department of Process, Energy and Environmental Technology, University of South-Eastern Norway, Norway
[2] Department of Electrical Engineering, Information Technology and Cybernetics, University of South-Eastern Norway, Norway
[3] Department of Biotechnology and Nanomedicine, SINTEF Industry, Trondheim, Norway

Submitted to Bioresource Technology, 2022 (Level 1) Journal.

Original Article

Syngas Fermentation and Microbial Electrosynthesis Integration as a Single Process Unit

Vasan Sivalingam[1], Dietmar Winkler[2], Tone Haugen[3], Alexander Wentzel[3] and Carlos Dinamarca[*1]

[1] Department of Process, Energy and Environmental Technology, University of South-Eastern Norway, Norway

[2] Department of Electrical Engineering, Information Technology and Cybernetics, University of South-Eastern Norway

[3] Department of Biotechnology and Nanomedicine, SINTEF Industry, Trondheim, Norway

*Correspondence: carlos.dinamarca@usn.no

Postal address: University of South-Eastern Norway, Kjølnes ring 56, 3918 Porsgrunn, Norway; Telephone: 0047 35 57 52 45

Highlights

- Syngas fermentation and microbial electrosynthesis are integrated as a single unit.
- Fermentation was performed on mixed culture homoacetogenic medium.
- CO rich syngas did not show any adverse impact on fermentation.
- Predominant acetic acid synthesis occurred at – 150 mV reducing power.

Abstract

Industrially relevant syngas gas (15 % CO, 15 % H_2, 20 % N_2 in 50 % CO_2) fermentation and microbial electrosynthesis were integrated as a single process unit in open and closed-circuit modes. This study examined the impact of electrochemical reducing power from – 50 to – 400 mV on the acetic acid synthesis and CO inhibition on fermentation. – 150 mV vs. Ag/AgCl (3.0 NaCl) was identified as the lowest benchmark potential for an optimum acetic acid synthesis rate (0.263 mmol L^{-1} h^{-1}), which is 15-fold

higher than the open circuit mode's rate. No significant inhibition by CO in the fermentation was observed, while 60 % of the gas was consumed. Anodic potential above 2.0 V substantially lowered the product formation. Superseding the fermentation medium with fresh inoculum through a fed-batch operation helped lower the anodic potential.

Keywords: *Syngas fermentation; CO_2 reduction; Wood-Ljungdahl; Microbial electrosynthesis; Carbon monoxide*

1 Introduction

Syngas fermentation is a bioprocess that converts syngas (CO_2, CO, H_2) to low-carbon biofuel and valuable chemicals (Schievano et al., 2019). This attractive eco-friendly carbon capture and utilisation (CCU) technique can combat the climate crisis, complying with United Nations Sustainable development goals. However, several bottlenecks must be overcome to reach the optimum technology readiness. The inefficient gas-liquid (GL) mass transfer of H_2 and CO due to low solubility, the slow growth rate of the microorganisms accounting for the fermentation, and CO toxicity are commonly encountered challenges (Phillips et al., 2017).

Extensive research is ongoing about elevating the headspace pressure of the gases to enhance the GL mass transfer (Stoll et al., 2019; Van Hecke et al., 2019), and biofilm carriers are incorporated into the syngas fermentation process to overcome the kinetic limitations (Gunes, 2021; Sivalingam and Dinamarca, 2021). Moreover, a bioelectrochemical technique called microbial electrosynthesis (MES) has also been investigated to provide ancillary redox power to convert CO_2 into low-carbon chemicals by yielding electrons through cathodic biofilm (Marshall et al., 2013; Shen et al., 2014).

Elevating partial pressure of H_2 and CO_2 depicts a clear improvement in the fermentation process (Sivalingam et al., 2021b). However, a rise in CO partial pressure inhibits the metabolic pathway, thus adversely impacting fermentation (Hurst and Lewis, 2010). The metabolic process that accounts for syngas fermentation is called Wood Ljungdahl Pathway (WLP). The WLP mainly addresses how CO_2 can be reduced to acetate

by utilising H_2 as the sole energy source. Firstly, CO_2 transforms into CO and formic acid or formyl group. Then the formyl group becomes methyl through several subsequent steps. Eventually, the methyl group is combined with CO and co-enzyme CoA to synthesise acetyl-CoA, which is further converted to acetate. That can be used as the chemical or precursor to biogas production through acetoclastic methanogenesis. The WLP has been well explained in literature; therefore, only a brief description is given here. However, (Drake, 2012; Phillips et al., 2017) are recommended for interested readers.

Carboxidotrophic microbial species from the fermentation medium can oxidise CO for cell growth and energy conservation, resulting in acetate production (Eq. 1) (Esquivel-Elizondo et al., 2017). In addition, butyrate, ethanol, and butanol can also be synthesised depending on the available microbial diversity. Those product syntheses can occur due to direct CO utilisation or through the water gas shift reaction (Eq. 2) (Esquivel-Elizondo et al., 2017). However, tolerance to CO concentration is limited, rendering elevating partial pressure unsuccessful for increasing CO utilisation.

$$4CO + 2H_2O \longrightarrow CH_3COOH + 2CO_2 \quad (\Delta G^0 = -43.6\ \text{kJ mol}\ CO^{-1}) \tag{1}$$

$$CO + H_2O \longrightarrow H_2 + CO_2 \quad (\Delta G^0 = -20\ \text{kJ mol}\ CO^{-1}) \tag{2}$$

The enzymes involved in the WLP, contain low valent metal sites. CO (C≡O) containing a triple bond act as a weak Lewis base. Therefore, it functions as a sigma donor and pi acceptor to form low valent complexes with the enzymes' metal sites, thus inhibiting the metabolic process (Ragsdale, 2004). The nature of accepting metal d(pi) is referred to as back bonding.

The metabolic conversion of one mole of CO into acetate releases two moles of CO_2 (Eq. 1). This additional CO_2 requires extra reducing equivalents, usually H_2, in the syngas fermentation. The H_2 concentration is usually limited in the syngas mixture; therefore, an additional source of energy/electrons is needed. MES integration is one sustainable solution that can provide additional reducing equivalents through renewable electricity (Katuri et al., 2018).

The benchmark cathodic potential needs to be determined to examine the possibility of using MES as a source of reducing equivalents for syngas fermentation. Firstly, the optimum cathodic potential for syngas fermentation, excluding CO, has previously been investigated (Sivalingam et al., 2022). The study revealed that -175 mV vs. Ag/AgCl cathodic voltage as the lowest benchmark potential for the acetic acid synthesis at 75% Columbic Efficiency (CE). Moreover, the applied potential did not improve the H_2 gas-liquid mass transfer.

The present study is a continuation of this previous work (Sivalingam et al., 2022). The distinct advancement is that an industrially relevant syngas gas mixture includes CO (15 % CO, 15 % H_2,20 % N_2 in CO_2) was utilised as the gaseous substrate. The fermentation was initially performed in open circuit mode (OCM); after that, the MES cathodic potential escalated from -50 mV to -400 mV to determine the lowest benchmark potential.

Related studies have already been published on CO fermentation of monocultures and electrochemically mediated syngas fermentation (excluding CO) (Igarashi and Kato, 2017; Sivalingam et al., 2022, 2021a). However, electrochemically assisted CO rich syngas fermentation by mixed cultures has rarely been studied (Barbosa et al., 2021; Bhagchandanii et al., 2020; Kumar et al., 2017). To fill this gap, this study examines the feasibility of integrating MES into CO rich syngas fermentation, investigating the lowest benchmark potential and the impact on acetic acid synthesis.

2 Material and methods

1.1.1 2.1 Culture enrichment

Digestate from Knardalstrand (Porsgrunn, Norway) wastewater treatment plant anaerobic digester was used as the inoculum. It underwent several treatment steps for microbial culture enrichment. The coarse impurities were removed by sieving through 300 microns. Since this mixed culture medium is rich in methanogens, the digestate was heat-treated (105 °C for 48 hours), and 5 mM 2-bromoethanesulfonic acid was added as an inhibitor (1 g L^{-1} Inoculum) to obliterate methanogens, as well as to concentrate

spore-forming acetogens. The pH of the medium was adjusted to neutral by 1.0 M HCl. The inoculum's total solids (TS) and volatile solids (VS) were 22.2 and 3.8 g L^{-1}, respectively. The inoculum's soluble chemical oxygen demand (sCOD) was 3.9 g L^{-1}; however, no volatile fatty acids were detected. Vitamins, minerals, and salt solutions were incorporated into the treated inoculum to favour microbial growth; compositions were adapted from (Dinamarca and Bakke, 2009).

1.1.2 2.2 Electrodes and reactor configurations

The experiments were performed in the same reactor used in the previous study (Sivalingam et al., 2022), setting with fresh medium and new electrode materials. In brief, a borosilicate (4.125 L) glass reactor was modified as the fermenter. The liquid working volume was 3.25 L, while the remaining headspace (0.875 L) was connected to a 1.8 L pressure cylinder (BR-1500, Berghof, Eningen, Germany), resulting in a total headspace volume of 2,675 L. A digital manometer (LEO-3, Keller, Winterthur, Switzerland) was attached to the pressure cylinder to log the gauge pressure.

The liquid part of the reactor was equipped with three electrodes. Carbon felt was used as cathode (Alfa Aesar, Germany) graphite rods as anode (ThermoFisher GmbH, Germany). An Ag/AgCl electrode was used as reference (3 M NaCl, Prosense, Netherland). The carbon felt (25 cm length, 12 cm width and 24 holes with 0.4 cm radius) was modified as a hollow cylinder with holes, and ten graphite rods (15.2 cm length and 0.61 cm diameter) were mounted on a frame with 1 cm equidistance from the carbon felt. The reference electrode was placed as close as possible to the cathode. Two potentiostats from Gamry (1010E Interface, Pennsylvania, USA) were used to perform the electrochemical tests. The complete reactor setup and the electrode assembly is presented in Fig. 1.

Fig. 1.

1.1.3 2.3 Operation

The reactor was fed with treated inoculum and agitated continuously by a magnetic stirrer at 1000 rpm. The liquid medium and the headspace were flushed with N_2 gas for five minutes to create an anaerobic environment before the experiment started. The medium was then saturated with syngas mixture (15 % CO, 15 % H_2, 20 % N_2 in 50 % CO_2), and the headspace pressure was set at 1 bar. The pressure change was logged every ten minutes. When the headspace pressure change became minimal, headspace gas and liquid samples were collected for analysis. Following, the headspace pressure was released and repressurised to ~1 bar. This cyclic operation was performed for 27 days. During this period, none of the electrodes was connected or poised with any voltages, referred to as open circuit mode (OCM) operation.

After achieving a stable gas consumption in OCM, redox potential was applied at the cathode. This operation is referred to as a closed-circuit mode (CCM) operation. The cathode potential was increased from – 50 mV to - 100, - 150, - 200, - 250, - 300, - 350, and - 400 mV orderly in two-week intervals. All potentials referred here are with respect to the Ag/AgCl (3.0 NaCl) standard electrode. Simultaneously, while voltages were applied to the electrodes, the cyclic gas feeding operation was continued similarly to during OCM operation, while the anodic potential was also recorded.

At – 400 mV CCM operation, the anodic potential exceeded 2.0 V, oxidising the fermentation products, ammonium, and water: thus, rendering electrochemically mediated syngas fermentation ineffectual. Therefore, the operation mode was shifted to fed-batch mode (30 days of hydraulic retention time) by refreshing the liquid medium for additional 30 days. In addition, various liquid chemical and gas composition analyses were performed.

Though the fed-batch mode experiment was not the primary aim of this work, the authors took advantage of checking the feasibility to lower the anodic voltage by replacing the fermentation medium with fresh inoculum/medium.

1.1.4 2.4 Analytical methodology

The sCOD and ammonium concentrations were measured by Spectroquant® Pharo 300 UV/VIS photometer (Merck KGaA, Darmstadt, Germany). The methods are equivalent to APHA 5220 and 4500 standards (American Public Health Association et al., 1995). Volatile fatty acids (VFA) were quantified on a Clarius 500 PE gas chromatograph (Perkin Elmer, MA, USA). The instrument consists of a scion-wax capillary column (25 m length, 0.25 mm diameter, and 0.2 µm film) and a flame ionisation detector (250 °C). The initial oven temperature was set to be at 80 °C for 0.7 minutes, then increased to 200 °C to 240 °C at 25 °C min^{-1} rate. H_2 was used as carrier gas at a 45 mL min^{-1} flow rate.

The headspace gas composition was determined by a 8610C gas chromatograph (SRI Instruments, CA, USA), featuring 6' Haysep-D (MXT-1) and 6' Molecular Sieve (MS13X) columns and a thermal conductivity detector. Helium 5.0 was used as the carrier gas at the flow rate of 20 mL min^{-1} and 2.1 bar pressure. The oven temperature was maintained at 80°C for four minutes and ramped up to 120°C at 10 °C/min.

1.1.5 2.5 Electrochemical experiments

The cathode potential was imposed by a potentiostat (Gamry 1010 E interface) via potentiostatic mode. The voltage was increased stepwise from -50 to -400 mV at a rate of 50 mV every two weeks. Simultaneously, another potentiostat recorded the anodic potential (Gamry 1010 E interface). Furthermore, cyclic voltammetry (CV) and electrochemical impedance spectroscopy (EIS) were performed on the plain electrode at the ends of open and closed circuits mode. The CV was performed at a potential range of 0 to -1 V at 10 mV s^{-1} scan rate. The EIS was performed in a frequency range of 2.0 MHz to 0.1 Hz through a 10 mV alternating current perturbation at a 10 decay/points measurement rate. The EIS data were fitted to an equivalent circuit model through Gamry model editor, version 7.8.4, and the circuit elements responsible for the impedance were estimated. Mainly ohmic and charge transfer resistance were quantified.

1.1.6 2.6 16S rRNA gene sequencing analysis

Samples of the inoculum and the planktonic cultures after OCM and CCM and anode and cathode biofilm samples at the end of the experiment were analysed by 16S rRNA gene metabarcoding. Metabarcode sequencing libraries targeting the V3V4 region of the 16S ribosomal RNA gene were generated by PCR using the primers 5'-TCGTCGGCAGCGTCAGATGTGTATAAGAGACAGCCTACGGGNGGCWGCAG-3' and 5'-GTCTCGTGGGCTCGGAGATGTGTATAAGAGACAGGACTACHVGGGTATCTAATCC-3' according to the protocol "16S Metagenomic Sequencing Library Preparation, preparing 16S Ribosomal RNA Gene Amplicons for the Illumina MiSeq System" (Illumina part # 15044223 rev. B). The Nextera XT Index Kit was used for multiplexing. DNA was quantified using the Qubit dsDNA BR Assay Kit (Thermo Fisher Scientific). DNA libraries were pooled and sequenced on a MiSeq sequencer (Illumina) using the MiSeq Reagent Kit v3 in the 2·300 bp paired-end mode. Sequencing reads were demultiplexed in Local Run Manager (Illumina), and further data processing was performed in CLC Genomics Workbench v.21.0.2 (Qiagen). Sequence reads were adapter trimmed, filtered and Operational Taxonomic Unit (OTU)- classified using the Data QC and OTU clustering workflow of the Microbial Genomics Module.

1.1.7 2.8 Performance analysis

During OCM, acetic acid is synthesised only via the homoacetogenic pathway, while it is produced homoacetogenically and electrochemically in CCM. The acetic acid production rate was calculated for each cycle in the OCM operation. Based on the highest rate, the possible homoacetogenically mediated synthesis is estimated in the CCM and compared with the measured acetic acid. The surplus acetic acid is considered as the result of applied reducing power (Sivalingam et al., 2022). The efficiency of such electrochemically mediated acetic acid production (Columbic Efficiency, CE) is calculated via Eq. 3; therein, the electrochemically mediated acetic acid concentration is denoted as n_{AA}; F is the Faraday constant (96 485 C mol-e^{-1}), and $\int_{t_i}^{t_f} I(t)dt$ denotes the sum of the charges transferred through the system. The constant eight is added to the equation to specify

that eight moles of electrons are required to produce one mole of acetic acid from CO_2 (Eq. 4). A small amount of propionic acid was measured in CCM, also considered synthesised electrochemically assisted. Fourteen electrons are required to synthesise one mole of propionic acid (Eq. 5), equivalent to 1.75 mol of acetic acid production. That way, propionic acid is also considered for the CE calculation.

$$\mathrm{CE}\ (\%) = \frac{8 \times F \times n_{AA}}{\int_{t_i}^{t_f} I(t)dt} * 100 \quad (3)$$

$$2CO_2 + 8e^- + 8H^+ \rightarrow CH_3COOH + 2H_2O \quad (4)$$

$$3CO_2 + 14e^- + 14H^+ \rightarrow C_2H_5 - COOH + 4H_2O \quad (5)$$

1.2 3 Results and Discussion

1.2.1 3.1. Acetic acid synthesis

Acetic acid accounted for approximately 96 % of the fermentation products; the balance was propionic acid. At the end of OCM, the acetic acid synthesis stabilised at 36 mmol at an average rate of 0.017 mmol L^{-1} h^{-1}, subsequently fluctuating around 75±25 mmol during - 50 and - 100 mV CCM operation. Once the cathode was run with -150 mV, the acetic acid production drastically increased to 262 mmol at a maximum rate of 0.263 mmol L^{-1} h^{-1}, which is ~15 times higher than the rate during OCM. At this point, the cathodic current was 10 mA, and the anodic voltage reached almost 2.0 V (Fig. 2).

During -200 mV CCM, the anodic voltage exceeded 2.0 V, which resulted in 30 mV current and a remarkable fall in acetic acid production. The acetic acid dropped to 100 mmol. The anodic voltage and cathodic current dropped to < 0.5 V and < 1 mA, respectively, during -250 and -300 mV CCM operation. This is because an anodic potential above 2.0 V causes the shift of the electrodes' biotic nature to abiotic reactions start dominating. However, it recovered during the – 350 to – 400 mV CCM operation, but no significant rise in acetic acid production could be observed. At the end of -400

mV operation, the anodic voltage reached 2.0 V. Therefore, operation mode was changed from batch to fed-batch by hypothesising that refreshing the electrolyte (fermentation medium) could help lower the anodic voltage less than 2.0 V to prevent anodic oxidation reactions. This is the most common problem in single-chamber MES reactors (Sivalingam et al., 2022, 2021a; Wang et al., 2021). During fed-batch mode, cathodic current varied between 10 and 80 mA, while the anodic voltage remained between 1.5 to 2.0 V. Consequently, a clear upward trend in acetic acid synthesis was observed, reaching 450 mmol at the end of the experiment. Though anodic voltage exceeded 2.0 V during the – 400 mV cycle, neither current nor anodic voltage declined as it dropped as much as occurred at – 250 mV CCM. This may point to the biofilm adapting to the electrochemical potential.

Fig. 2.

1.2.2 3.2. Gas consumption and composition analysis

Fig.3 depicts the headspace gas pressure profiles and respective gas consumption. At the beginning of the experiment, the headspace (2.675 L) was occupied with raw syngas consisting of 16.46 mmol CO, 54.88 mmol CO_2, 16.46 mmol H_2, and 21.95 mmol N_2 at 1 bar pressure. Based on the hydrogen consumption rate achieved from our previous studies (Sivalingam et al., 2022; Sivalingam and Dinamarca, 2021), the available H_2 from the headspace is assumed to be rapidly consumed. The N_2 remains inert. Approximately 37 % of the CO_2 from the headspace is consumed throughout the experiments. CO_2 consumption does not correlate with acetic acid production due to the bicarbonate present in the fermentation medium. In addition, oxidation of organic compounds at the anode also releases CO_2, which could also cause stochastic variation in the apparent CO_2 consumption. At – 200 and – 400 mV CCM operation, a clear CO_2 production was observed, which corresponds to the anodic potential exceeding 2.0 V (Fig. 2), leading to oxidation of an ample amount of organics to CO_2 (Eq. 6) (Sivalingam et al., 2022). Furthermore, N_2 and O_2 production were also noted, simultaneously to CO_2

production. This is due to the oxidation of ammonium (Eq. 7) and water (Eq. 8) at the anode (Samarakoon et al., 2021; Sivalingam et al., 2020).

$$C_nH_{2n+1} - COOH + 2nH_2O \rightarrow (n+1)CO_2 + (6n+2)H^+ + (6n+2)e^- \quad (6)$$

$$2NH_4^+ \rightarrow N_2 + 8H^+ + 6e^- \quad (7)$$

$$4H_2O \rightarrow 2O_2 + 8H^+ + 8e^- \quad (8)$$

Fig. 3.

Approximately 50 % CO (8.3 mmol) from the headspace was consumed in the OCM, while 62 % (10.2 mmol) in the – 250 mV CCM cycle. The acetic acid synthesis profile and CO consumption did not significantly correlate. However, remarkably less CO consumption was observed during the -200 mV and -400 mV CCM cycles. At this point, the evolution of N_2, O_2, and CO_2 at the anode were noticed, which may diminish CO utilisation. Moreover, a trace amount of CO production was observed (< 4 mmol) at the beginning of the fed-batch operation (- 400 mV). This could be due to the reduction of CO_2 to CO (Eq.9) (Sun et al., 2017; Zhang et al., 2018). The CO synthesis from CO_2 is a bi-electron transfer process. Firstly, one set of electrons and protons (e&p) from the electrolyte reduces one CO_2 molecule to a carboxyl intermediate, then another set of e&p reacts with oxygen atoms in the carboxyl intermediate to generate CO and H_2O (Hansen et al., 2013; Sun et al., 2017). Eventually, produced CO desorbs from the electrode and reaches the headspace.

The conversion steps of CO_2 to carboxyl intermediate and CO desorption from the electrode surface are the primary rate-limiting steps due to the weak binding behaviour of the carboxyl group, as well as the strong binding nature of CO (Hansen et al., 2013). All these reactions are metal catalyst mediated, and the required redox potentials are much higher than the applied voltages in this experiment. However, the biofilm on the cathode could work as the biocatalyst, thus potentially lowering the

required potential. A detailed study is recommended for future research to investigate these observations further.

$$CO_2 + 2H^+ + 2e \rightarrow CO + H_2O \quad (E^0 = -0.53\ V) \qquad (9)$$

Eventually, the results indicate that the industrially relevant syngas mixture can be bio electrochemically fermented to synthesise acetic acid at a lower benchmark potential of – 150 mV and at – 400 mV potential when applying fed-batch operation. Those potentials lies under the range of direct and indirect electron transfer potential windows from cathode to microbes (Choi and Sang, 2016; Hartshorne et al., 2007). Though the fed-batch operation at – 400 mV shows an improved acetic acid production, it is not comparable with other CCM cycles because of the lack of OCM fed-batch experiments. However, using fed-batch as a strategy to lower the anodic potential is the primary new focus triggered by these results.

1.2.3 3.4 Chemical analysis

The pH of the fermentation medium in OCM stayed around 6.7. It dropped to 6.4 at the beginning of CCM and remained relatively stable (±0.09) towards the end of the experiment. Previous studies performed similarly (Sivalingam et al., 2022, 2021a) exhibited increasing pH above 9.0 during both the open and closed circuits operation due to the basification of the electrolyte. The reason is that therein bicarbonate was deployed as the dissolved form of CO_2. In addition, protons consumption at the cathode while OH^- are being released during the CCM, thus causing pH increment. However, this study confirmed that using CO_2 gas instead of bicarbonate is better for maintaining the pH, thus substantially improving the fermentation processes. The alkalinity was also decreased by 50 % due to acetic acid synthesis. The ammonium concentration shows a downward trend due to the anodic oxidation, which complies with N_2 gas evolution. The pH, alkalinity, and ammonium variation profiles are available in the E-supplementary data for this work can be found in the e-version of this paper online.

1.2.4 3.5 Electrochemical studies

The redox catalytic current generation from applied potential scans is presented as a cyclic voltammogram (Annie Modestra and Venkata Mohan, 2019) can be found in the E-supplementary data for this work can be found in the e-version of this paper online. The plain electrode generated a – 0.18 A current. Due to the biofilm assimilation on the cathode over time, the reduction processes and electron transfer mediated chemical reactions were facilitated, causing a substantial redox current enhancement at the end of OCM and CCM, respectively – 0.81 A and – 0.97 A. However, the current decreased to – 0.45 A at the end of the fed-batch operation. The fed-batch operation mode could deprive biomass/biofilm from the cathode, which usually accounts for the cathodic current generation.

The EIS spectrum revealed the electron transferability of a system (Anwer et al., 2021). The spectra from this study are presented in Fig. 4 as Nyquist plots and a representative equivalent circuit model. Ru and Rp indicate the ohmic and charge transfer resistances. The capacitance is represented as constant phase elements, therein Y_0_film is biofilm capacitance, and Y_0_dl is double-layer capacitance. The Y_0_film occurs due to the biofilm growth and adhesion while Y_0_dl represents the electrical double layer between the electrode and the adjacent fermentation medium (Kim et al., 2011). Initially, the charge transfer resistance was 1.067 ohm and decreased to 0.569 ohm at the end of – 400 mV CCM due to the biofilm accumulation. The microbiome results affirmed the presence of several microbial communities in the cathode. In addition, the accumulation of fermentation products in the medium enhanced the ionic conductivity (Samarakoon et al., 2021; Sivalingam et al., 2021), thus decreasing the charge transfer resistance. However, the ohmic resistance remains stable around 0.533 ohm (± 0.017) throughout the experiment. Since the carbon felt cathode usually has a large capacitance, distinguishing the biofilm and double layer capacitance is challenging.

Fig. 4.

1.2.5 3.6 Microbiome analysis

16S rRNA gene metabarcoding was performed on the heat-treated inoculum, planktonic samples at the end of OCM and CCM operations, and biofilm samples from anode and cathode at the end of the CCM phase. The results are presented in microbial community changes at the Family level (Fig. 5) and phylogenetic diversity and Shannon entropy graphs, available in the E-supplementary data for this work, which can be found in the e-version of this paper online.

Fig. 5.

Throughout the experiment, the microbial community structure changed in response to the change of fermentation conditions. The inoculum, containing only heat-resistant microbial species, e.g. through the formation of spores, was found to be dominated by taxa grouped under *Rhodobacteraceae*, accounting for almost two-thirds of the biodiversity. This family of Gram-negative bacteria features a large number of genera that occur in aquatic environments and form endospores. Other notable taxa represented in the inoculum are methanotrophs of the *Methylocystaceae*, gut bacteria of the *Dehalobacteriaceae*, heterotrophic denitrificants of the *Comamonadaceae*, as well as *Dietziaceae*, *Xanthomonadaceae*, and *Tissierellaceae*. Most of these families contain a large share of aerobic taxa. It is therefore expected that during OCM and CCM, a significant shift occurs, and most of the taxa dominating the inoculum are largely reduced based on the anaerobic gas fermentative conditions applied.

After OCM, the dominance of *Rhodobacteraceae* has been largely reduced, and while some *Xanthomonadaceae*, *Tissierellaceae*, and *Dehalobacteriaceae* taxa remain, the share of *Methylocystaceae* has expanded, and together with *Burkholderiaceae* and families belonging to *Shingomonadales* and *Thermoanaerobacterales* have taken over as the dominating taxa in the planktonic phase of the fermentation (approx. 60%). After switching to CCM operations, the culture shifted to almost 50% of taxa belonging to an unknown family of *Actinomycetales* 2, with the share of *Methylocystaceae* and *Burkholderiaceae* reduced compared to after OCM.

Largely unknown genera of *Actinomycetales* were also found to be dominating the cathodic biofilm, while the anodic biofilm was dominated by 30% of the *Campylobacteraceae*. Overall phylogenetic diversity approximately doubled from the inoculum to the OCM sample. Further, it increased to the CCM and associated electrode biofilm samples, while Shannon entropy increased from 3.2 for the inoculum to between 4.1 and 4.4 for the OCM, CCM and electrode samples. In general, a large share of the taxa in the analysed microbial assemblages belonged to unknown genera and species, limiting the significance of potential more detailed analysis below the family level that was chosen in this study.

1.2.6 3.8 Performance analysis

The highest OCM acetic acid production rate was 0.037 mmol L^{-1} h^{-1}. Based on this value, the electrochemically mediated acetic acid was quantified as explained in section 2.8. Only the -150 mV CCM operation produced electrochemically assisted 123 mmol acetic acid, resulting in 49 % CE. In addition, the fed-batch regime at -400 mV CCM produced a notable amount of acetic acid, but the CE was less considerable. Fed-batch fermentation effectively lowered and controlled the anodic voltage at the end of the CCM operations. Detailed OCM fed-batch experiments are suggested for future studies, also to be able to compare fed-batch performance in OCM vs. CCM.

1.3 4 Conclusions

This study shows that industrially relevant syngas can be bioelectrochemical fermented into acetic acid using substrate and a mixed microbial community from AD effluents adapted to anaerobic conditions and MES. 60 % of the offered CO is consumed throughout the experiment without any apparent inhibitory effects. – 150 mV was the lowest benchmark potential for acetic acid synthesis from the applied syngas mixture. An increase over 2.0 V at the anode had a negative impact on MES performance through the oxidation of fermentation products. Fed-batch operation mode was successfully tested to lower the anodic potential and restore acetogenesis.

1.4 Declarations

- Competing interests: The authors declare that they have no competing interests.
- CRediT authorship contribution statement:

  Vasan Sivalingam: Conceptualisation, Methodology, Experiments, Formal analysis, Investigation, Validation, Original draft preparation, Writing – review & editing. **Dietmar Winkler:** Software, Methodology. **Tone Haugen:** Formal analysis, Methodology, Visualization. **Alexander Wentzel:** Formal analysis, Methodology, Visualisation, Writing – review & editing. **Carlos Dinamarca:** Conceptualisation, Methodology, Investigation, Validation, Writing – review & editing, Supervision, Project administration, Funding acquisition.

- Funding: The Norwegian Ministry of Education and Research funded this research through the PhD program in Process, Energy, and Automation Engineering at the University of South-Eastern Norway, grant number 2700095.
- Acknowledgements: The authors want to thank the Norwegian Ministry of Education and Research for this project's financial support.

1.5 References

[1] American Public Health Association, American Water Works Association, Water Pollution Control Federation, Water Environment Federation, 1995. Standard methods for the examination of water and wastewater. American Public Health Association.

[2] Annie Modestra, J., Venkata Mohan, S., 2019. Capacitive biocathodes driving electrotrophy towards enhanced CO2 reduction for microbial electrosynthesis of fatty acids. Bioresour. Technol. 294, 122181.

[3] Anwer, A.H., Khan, N., Umar, M.F., Rafatullah, M., Khan, M.Z., 2021. Electrodeposited Hybrid Biocathode-Based CO2 Reduction via Microbial Electro-Catalysis to Biofuels. Membranes 11, 223.

[4] Barbosa, S.G., Peixoto, L., Alves, J.I., Alves, M.M., 2021. Bioelectrochemical systems (BESs) towards conversion of carbon monoxide/syngas: A mini-review. Renew. Sustain. Energy Rev. 135, 110358.

[5] Bhagchandanii, D.D., Babu, R.P., Sonawane, J.M., Khanna, N., Pandit, S., Jadhav, D.A., Khilari, S., Prasad, R., 2020. A Comprehensive Understanding of Electro. Fermentation 6, 92.

[6] Choi, O., Sang, B.-I., 2016. Extracellular electron transfer from cathode to microbes: application for biofuel production. Biotechnol. Biofuels 9, 11.

[7] Dinamarca, C., Bakke, R., 2009. Apparent hydrogen consumption in acid reactors: observations and implications. Water Sci. Technol. J. Int. Assoc. Water Pollut. Res. 59, 1441–1447.

[8] Drake, H.L., 2012. Acetogenesis. Springer Science & Business Media.

[9] Esquivel-Elizondo, S., Delgado, A.G., Krajmalnik-Brown, R., 2017. Evolution of microbial communities growing with carbon monoxide, hydrogen, and carbon dioxide. FEMS Microbiol. Ecol. 93.

[10] Gunes, B., 2021. A critical review on biofilm-based reactor systems for enhanced syngas fermentation processes. Renew. Sustain. Energy Rev. 143, 110950.

[11] Hansen, H.A., Varley, J.B., Peterson, A.A., Nørskov, J.K., 2013. Understanding Trends in the Electrocatalytic Activity of Metals and Enzymes for CO2 Reduction to CO. J. Phys. Chem. Lett. 4, 388–392.

[12] Hartshorne, R.S., Jepson, B.N., Clarke, T.A., Field, S.J., Fredrickson, J., Zachara, J., Shi, L., Butt, J.N., Richardson, D.J., 2007. Characterisation of Shewanella oneidensis MtrC: a cell-surface decaheme cytochrome involved in respiratory electron transport to extracellular electron acceptors. J. Biol. Inorg. Chem. JBIC Publ. Soc. Biol. Inorg. Chem. 12, 1083–1094.

[13] Hurst, K.M., Lewis, R.S., 2010. Carbon monoxide partial pressure effects on the metabolic process of syngas fermentation. Biochem. Eng. J. 48, 159–165.

[14] Igarashi, K., Kato, S., 2017. Extracellular electron transfer in acetogenic bacteria and its application for conversion of carbon dioxide into organic compounds. Appl. Microbiol. Biotechnol. 101, 6301–6307.

[15] Katuri, K.P., Kalathil, S., Ragab, A., Bian, B., Alqahtani, M.F., Pant, D., Saikaly, P.E., 2018. Dual-function electrocatalytic and macroporous hollow-fiber cathode for converting waste streams to valuable resources using microbial electrochemical systems. Adv. Mater. 30, 1707072.

[16] Kim, T., Kang, J., Lee, J.-H., Yoon, J., 2011. Influence of attached bacteria and biofilm on double-layer capacitance during biofilm monitoring by electrochemical impedance spectroscopy. Water Res. 45, 4615–4622.

[17] Kumar, G., Saratale, R.G., Kadier, A., Sivagurunathan, P., Zhen, G., Kim, S.-H., Saratale, G.D., 2017. A review on bio-electrochemical systems (BESs) for the

syngas and value added biochemicals production. Chemosphere 177, 84–92. https://doi.org/10.1016/j.chemosphere.2017.02.135

[18] Marshall, C.W., LaBelle, E.V., May, H.D., 2013. Production of fuels and chemicals from waste by microbiomes. Curr. Opin. Biotechnol., Energy biotechnology • Environmental biotechnology 24, 391–397.

[19] Phillips, J.R., Huhnke, R.L., Atiyeh, H.K., 2017. Syngas Fermentation: A Microbial Conversion Process of Gaseous Substrates to Various Products. Fermentation 3, 28.

[20] Ragsdale, S.W., 2004. Life with carbon monoxide. Crit. Rev. Biochem. Mol. Biol. 39, 165–195.

[21] Samarakoon, G., Winkler, D., Sivalingam, V., Dinamarca, C., Bakke, R., 2021. Simple modelling approach using Modelica for microbial electrosynthesis.

[22] Schievano, A., Pant, D., Puig, S., 2019. Editorial: Microbial Synthesis, Gas-Fermentation and Bioelectroconversion of CO2 and Other Gaseous Streams. Front. Energy Res. 7, 110.

[23] Shen, Y., Brown, R., Wen, Z., 2014. Enhancing mass transfer and ethanol production in syngas fermentation of Clostridium carboxidivorans P7 through a monolithic biofilm reactor. Appl. Energy 136, 68–76.

[24] Sivalingam, V., Ahmadi, V., Babafemi, O., Dinamarca, C., 2021a. Integrating Syngas Fermentation into a Single-Cell Microbial Electrosynthesis (MES) Reactor. Catalysts 11, 40.

[25] Sivalingam, V., Dinamarca, C., 2021. High Pressure Moving Bed Biofilm Reactor for Syngas Fermentation. Chem. Eng. Trans. 86, 1483–1488.

[26] Sivalingam, V., Dinamarca, C., Samarakoon, G., Winkler, D., Bakke, R., 2020. Ammonium as a Carbon-Free Electron and Proton Source in Microbial Electrosynthesis Processes. Sustainability 12, 3081.

[27] Sivalingam, V., Haugen, T., Wentzel, A., Dinamarca, C., 2021b. Effect of Elevated Eydrogen Partial Pressure on Mixed Culture Homoacetogenesis. Chem. Eng. Sci. X 12, 100118.

[28] Sivalingam, V., Parhizkarabyaneh, P., Winkler, D., Lu, P., Haugen, T., Wentzel, A., Dinamarca, C., 2022. Impact of electrochemical reducing power on homoacetogenesis. Bioresour. Technol. 345, 126512.

[29] Stoll, I.K., Boukis, N., Sauer, J., 2019. Syngas Fermentation at Elevated Pressure - Experimental Results. Eur. Biomass Conf. Exhib. Proc. 27th EUBCE-Lisbon 2019, 1255–1261.

[30] Sun, Z., Ma, T., Tao, H., Fan, Q., Han, B., 2017. Fundamentals and Challenges of Electrochemical CO2 Reduction Using Two-Dimensional Materials. Chem 3, 560–587.

[31] Van Hecke, W., Bockrath, R., De Wever, H., 2019. Effects of moderately elevated pressure on gas fermentation processes. Bioresour. Technol. 293, 122129.

[32] Wang, H., Du, H., Zeng, S., Pan, X., Cheng, H., Liu, L., Luo, F., 2021. Explore the difference between the single-chamber and dual-chamber microbial

electrosynthesis for biogas production performance. Bioelectrochemistry 138, 107726.

[33] Zhang, W., Hu, Y., Ma, L., Zhu, G., Wang, Y., Xue, X., Chen, R., Yang, S., Jin, Z., 2018. Progress and Perspective of Electrocatalytic CO2 Reduction for Renewable Carbonaceous Fuels and Chemicals. Adv. Sci. 5, 1700275.

1.6 Figure Legends

Figure 1: Electrode assembly and experimental setup.

Figure 2: Profiles of; Top: accumulated acetic acid, Middle: current, Bottom: anodic voltage.

Figure 3: Syngas headspace pressure profile and gas composition variation during open and closed-circuit modes.

Figure 4: Nyquist plots and equivalent circuit model.

Figure 5: Microbial assemblages, changes in the microbial community at the Family level. A: heat-treated inoculum, B: planktonic culture after OCM, C: planktonic culture after CCM, D: cathodic biofilm after OCM, E: anodic biofilm after OCM.

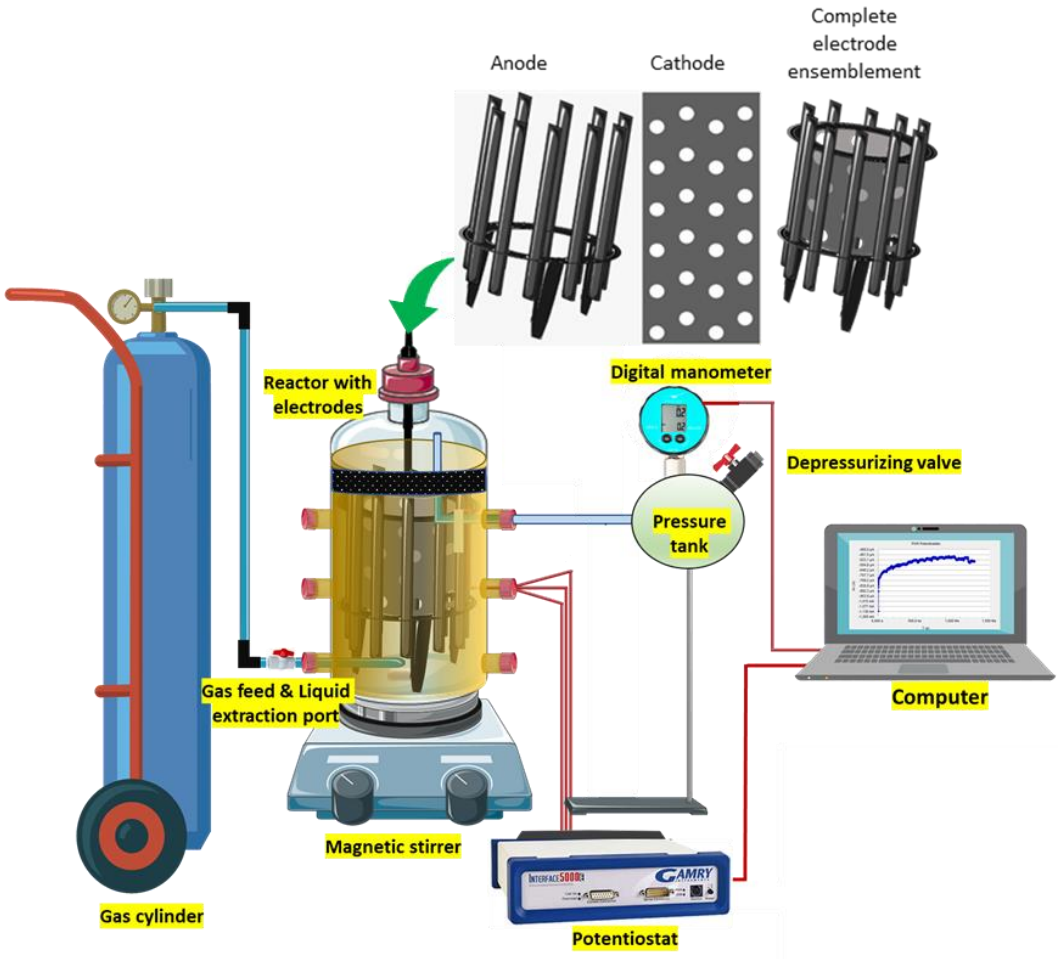
Anode
Cathode
Complete electrode ensemblement
Reactor with electrodes
Digital manometer
Depressurizing valve
Pressure tank
Gas feed & Liquid extraction port
Computer
Magnetic stirrer
Gas cylinder
Potentiostat

Fig. 1.

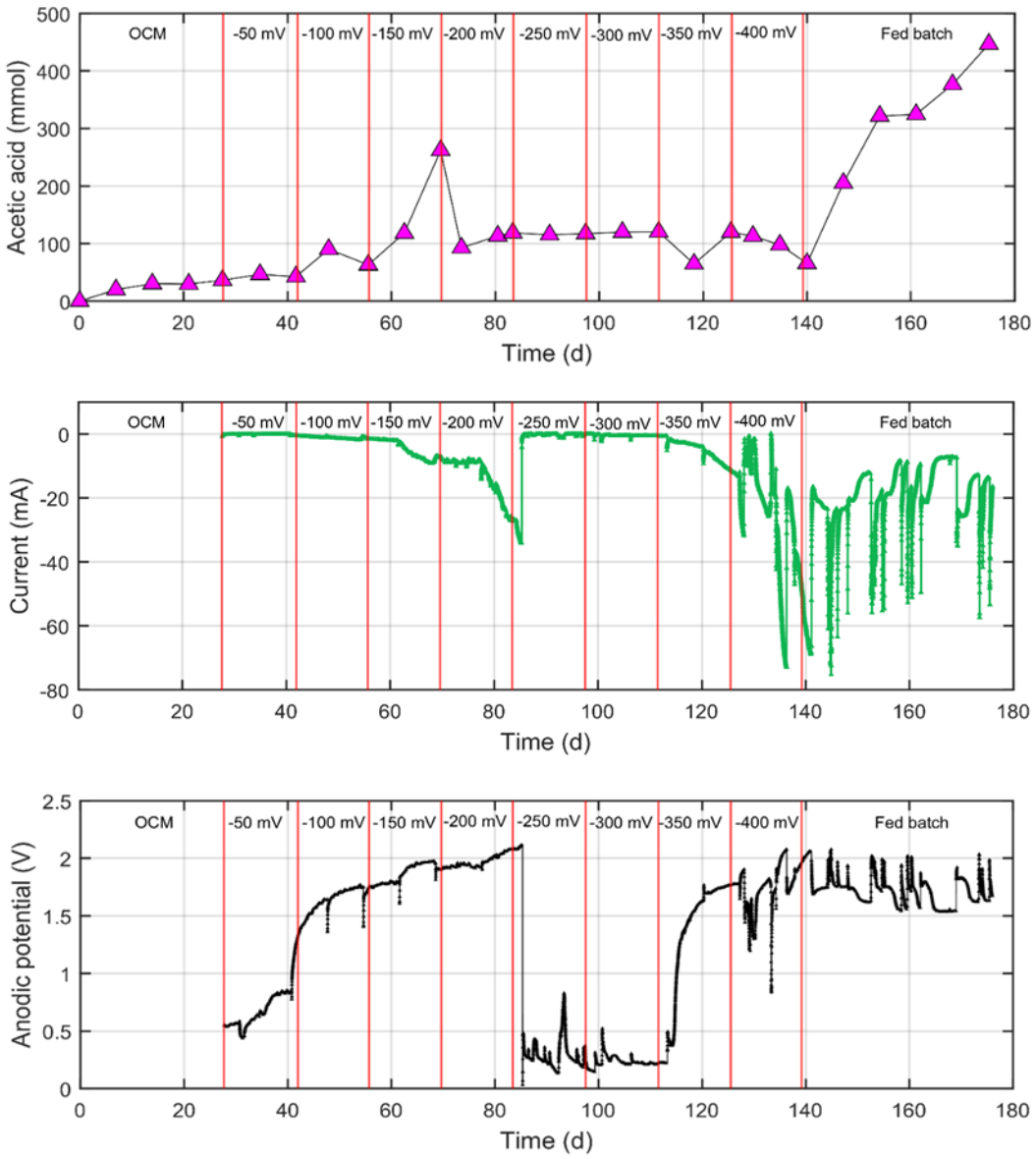
OCM
-50 mV
-100 mV
-150 mV
-200 mV
-250 mV
-300 mV
-350 mV
-400 mV
Fed batch
Acetic acid (mmol)
Current (mA)
Anodic potential (V)
Time (d)

Fig. 2.

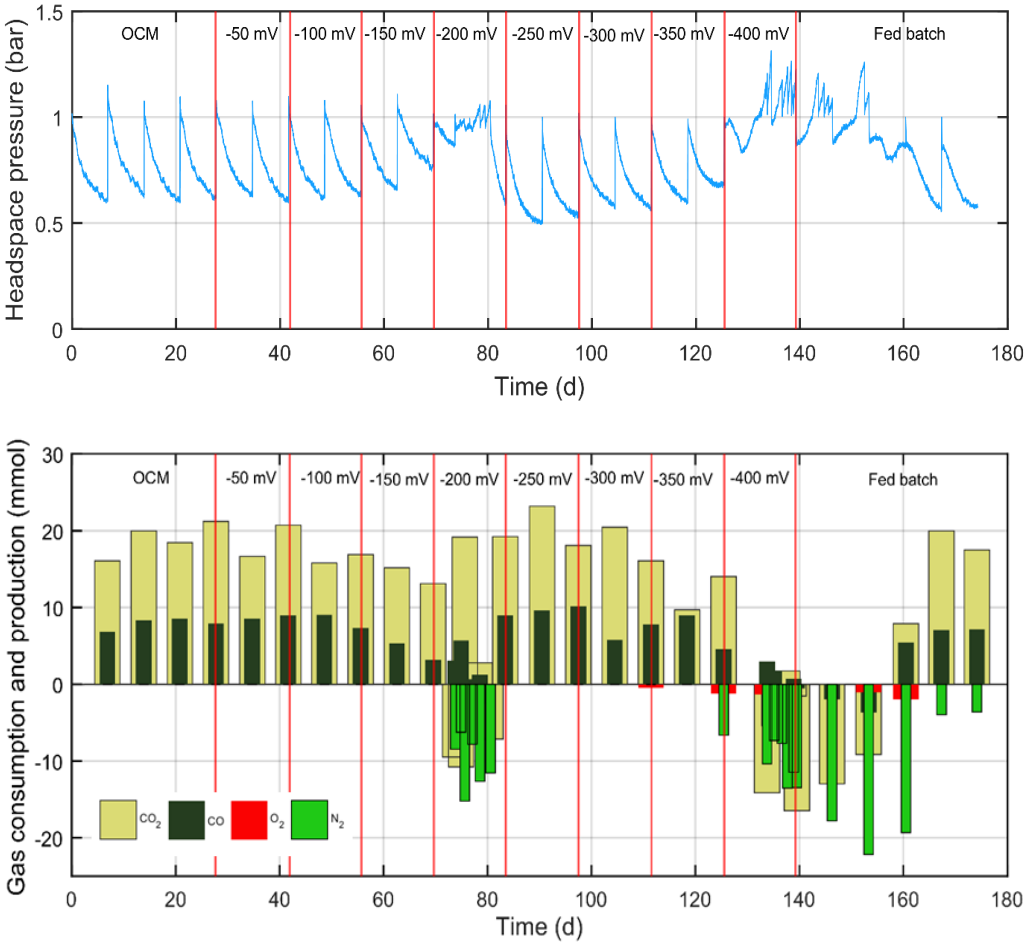
Headspace pressure (bar)
OCM
-50 mV
-100 mV
-150 mV
-200 mV
-250 mV
-300 mV
-350 mV
-400 mV
Fed batch
Time (d)
Gas consumption and production (mmol)
CO2
CO
O2
N2
Time (d)

Fig. 3.

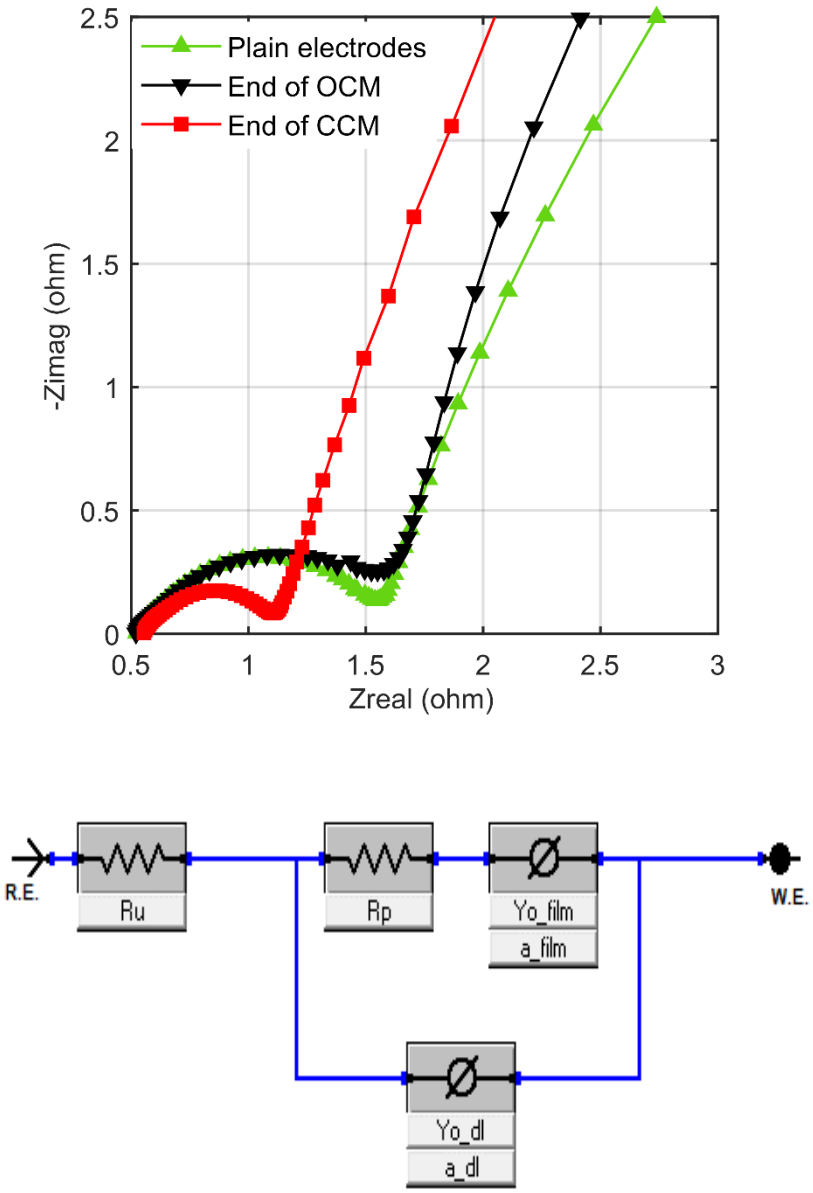
Plain electrodes
End of OCM
End of CCM
-Zimag (ohm)
Zreal (ohm)
2.5
2
1.5
1
0.5
0
0.5
1
1.5
2
2.5
3
R.E.
Ru
Rp
Yo_film
a_film
W.E.
Yo_dl
a_dl

Fig. 4.

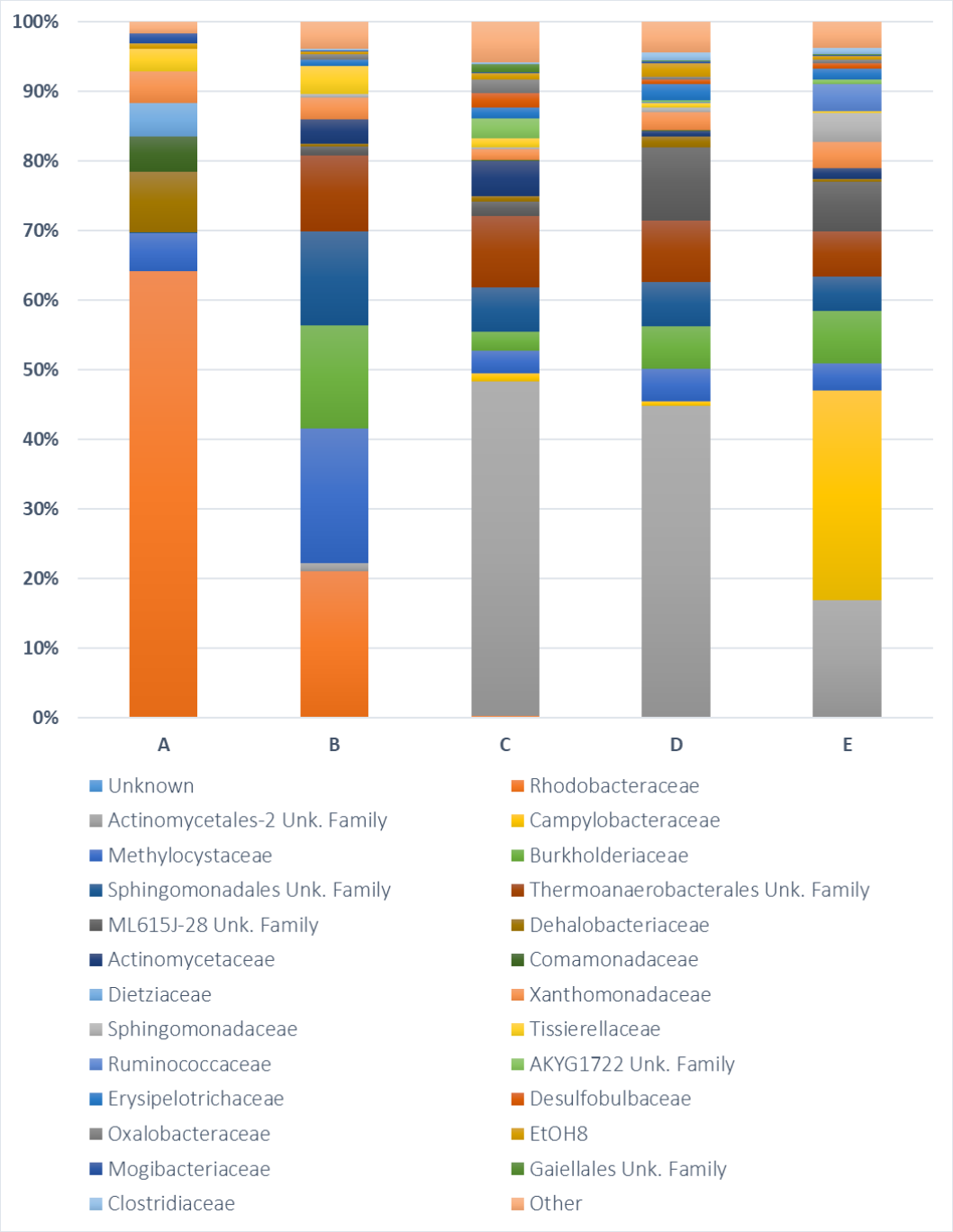
100%
90%
80%
70%
60%
50%
40%
30%
20%
10%
0%
A
B
C
D
E
Unknown
Rhodobacteraceae
Actinomycetales-2 Unk. Family
Campylobacteraceae
Methylocystaceae
Burkholderiaceae
Sphingomonadales Unk. Family
Thermoanaerobacterales Unk. Family
ML615J-28 Unk. Family
Dehalobacteriaceae
Actinomycetaceae
Comamonadaceae
Dietziaceae
Xanthomonadaceae
Sphingomonadaceae
Tissierellaceae
Ruminococcaceae
AKYG1722 Unk. Family
Erysipelotrichaceae
Desulfobulbaceae
Oxalobacteraceae
EtOH8
Mogibacteriaceae
Gaiellales Unk. Family
Clostridiaceae
Other

Fig. 5.

Article 5: E - Supplementary Material

Syngas Fermentation and Microbial Electrosynthesis Integration as a Single Process Unit

Vasan Sivalingam[1], Dietmar Winkler[2], Tone Haugen[3], Alexander Wentzel[3] and Carlos Dinamarca[*1]

[1] Department of Process, Energy and Environmental Technology, University of South-Eastern Norway, Norway

[2] Department of Electrical Engineering, Information Technology and Cybernetics, University of South-Eastern Norway

[3] Department of Biotechnology and Nanomedicine, SINTEF Industry, Trondheim, Norway

*Correspondence: carlos.dinamarca@usn.no

Postal address: University of South-Eastern Norway, Kjølnes ring 56, 3918 Porsgrunn, Norway; Telephone: 0047 35 57 52 45

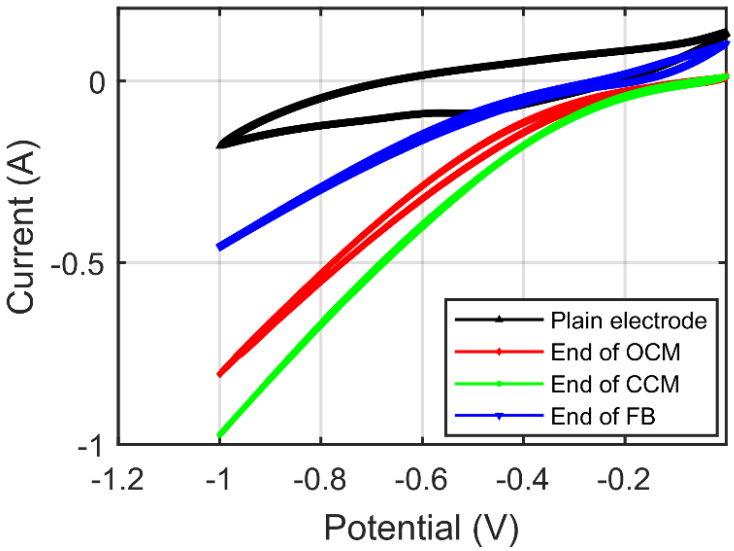

Figure S1: Cyclic voltammograms.

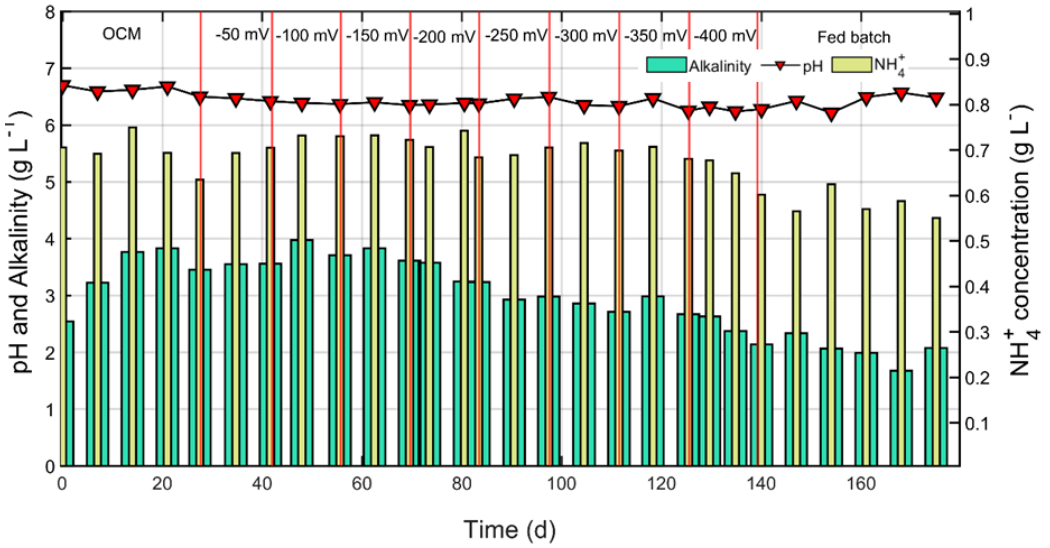

Figure S2: pH, alkalinity and ammonium profiles during open and closed circuits modes.

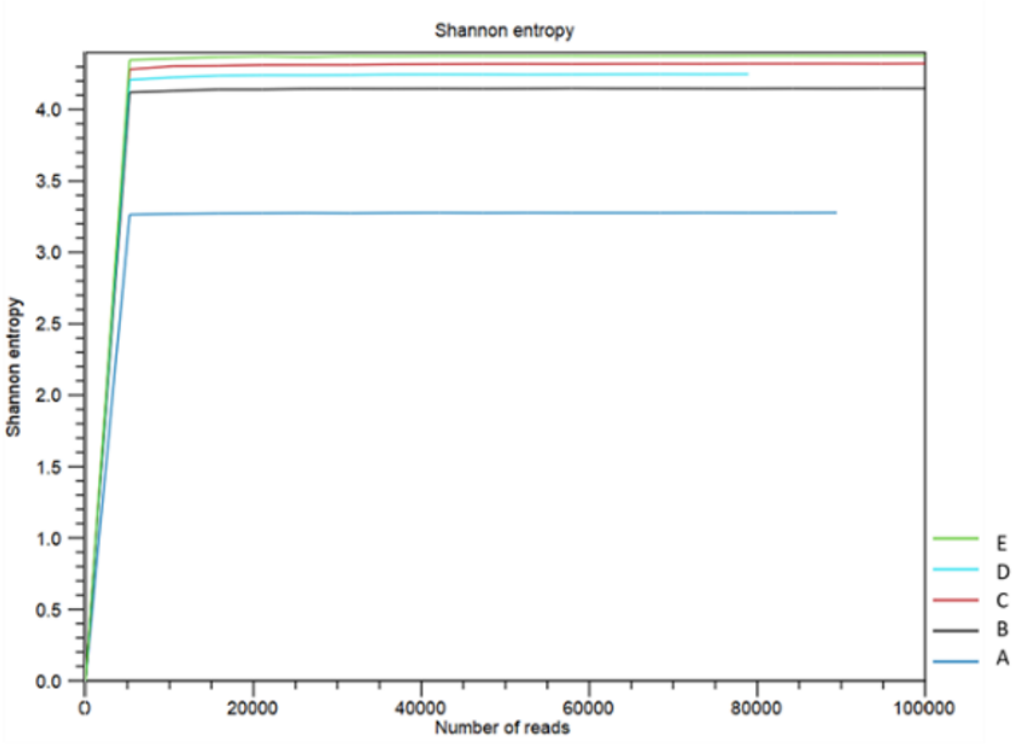

Figure S3: Shannon entropy

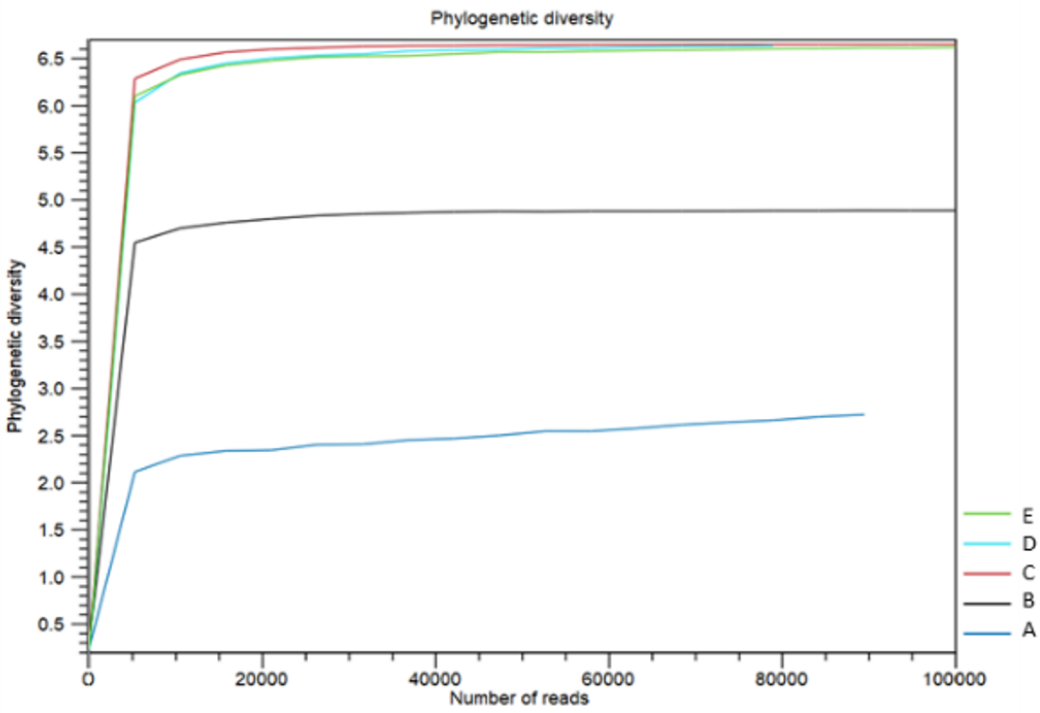

Figure S4: Phylogenetic diversity

Article 6

Simple Modelling Approach Using Modelica for Microbial Electrosynthesis (MES)

Gamunu Samarakoon, Dietmar Winkler, Vasan Sivalingam, Carlos Dinamarca, Rune Bakke

Department of Process, Energy and Environmental Technology, University of South-Eastern Norway, Norway

Published in Proceedings of SIMS, 2020 (Level 1).
DOI: 10.3384/ecp20176306

Simple modelling approach using Modelica for microbial electrosynthesis

Gamunu Samarakoon[1] Dietmar Winkler[2] Vasan Sivalingam[1] Carlos Dinamarca[1] Rune Bakke[1]

[1]Department of Process, Energy and Environmental Technology, [2]Department of Electrical Engineering, Information Technology and Cybernetics, University of South-Eastern Norway, Porsgrunn 3918, Norway,
{gamunu.arachchige, dietmar.winkler, vasan.sivalingam, carlos.dinamarca, rune.bakke@usn.no}

Abstract

This study intends to develop a simple mathematical model that contributes to the integration of Microbial Electrosynthesis (MES) in AD to reduce CO_2 to CH_4. Open-source modelling language Modelica was used to build the model. The MES internal resistances are important parameters for the model and an Electrochemical Impedance Spectroscopy (EIS) experiment was employed to estimate the resistances and distinguish the contribution from each resistance element. The model preliminary simulations show that it is possible to determine the voltage required to keep the potential difference across the cathode biofilm within optimal conditions. The system is sensitive to effects of biofilm development on electron transfer at both electrodes, which implies effects on the electrons from anode to cathode (i.e. electric current). The model will be a useful tool for extrapolating experimental results and to enhance our understanding of MES.

Keywords: microbial electrosynthesis, bio-methane, CO_2 reduction, Modelica

1 Introduction

Microbial electrosynthesis is a novel technology for chemical synthesis of desired product through chemical reaction catalysed by microorganisms and powered by electric energy (Rabaey and Rozendal, 2010). MES occurs in microbial electrolysis cell. The working electrode (WE) of the microbial electrolysis cell is in general the cathode at which the reduction half reaction is controlled by the potential to achieve the desired product.

Recently, MES for biogas upgrading (Nelabhotla and Dinamarca, 2018) by CO_2 (carbon dioxide) reduction to CH_4 (methane) has received attention. A typical biogas reactor (anaerobic digester; AD) produces biogas containing 50-70 % CH_4 and 30-50 % CO_2, implying low calorific value (Angelidaki et al., 2018). Biogas upgrading by MES should preferably use electricity from renewable sources and may thereby also serve as a way of storing renewable surplus electricity as CH_4 (Geppert et al., 2016). Other valuable chemical products from CO_2 may also be obtained by adjusting the MES cathode potential (Schievano et al., 2019).

The conversion of CO_2 to CH_4 occurs at the cathode through direct electron transfer (Table 1, eq. (1)) or indirectly via production of intermediates. The conversion of CO_2 to CH_4 with intermediate production of hydrogen (H_2) follows two steps: protons reduction to H_2 (Table 1, eq. (2.1)) and then the produced H_2 is used as electron donor for biological CO_2 reduction to CH_4 (Table 1, eq. (2.2)). CH_4 production is also possible from acetate (CH_3COO^-) produced bio-electrochemically via CO_2 reduction.

Table 1. Chemical reactions at cathode with standard potential (S.P.) [4] vs. Normal Hydrogen Electrode (NHE)

Reactions at cathode	*S.P.[V]*	
$CO_2 + 8H^+ + 8e^- \rightarrow CH_4 + 2H_2O$	-0.24	(1)
$8H^+ + 8e^- \rightarrow 4H_2$	-0.41	(2.1)
$CO_2 + 4H_2 \rightarrow CH_4 + 2H_2O$		(2.2)

The standard potential of CH_4 production via direct electron transfer (- 0.24V vs. NHE) is lower than that of an indirect electron transfer (- 0.41V vs. NHE) (Table 1), implying that direct electron transfer is the more energy efficient path. The cathode potential also influences current (electron flow) and hence the CH_4 production rate (Geppert et al., 2016) and is the key parameter that determines mechanism of electron transfer.

The protons (H^+) and electrons (e) needed for the reduction reaction at the cathode are generated at the anode, such as by oxidizing water eq. (3) or easily degradable short-chain volatile fatty acid (VFA) such as acetate eq. (4). Oxidation of these components may have some downsides. Thus, other possible oxidation reactions, e.g., ammonium oxidation (Sivalingam et al., 2020), may be relevant.

$2H_2O \rightarrow 4H^+ + O_2 + 4e^-$ 0.82 V vs. NHE (3)

$$CH_3COO^-H^+ + 2H_2O \rightarrow 2CO_2 + 8H^+ + 8e^-$$

-0.28 V vs. NHE (4)

The minimum voltage required to bring about electrolysis can be estimated from the standard reduction potentials of desired reaction and is called thermodynamic cell voltage eq. (5).

$$E^0_{cell} = E^0_{cath} - E^0_{anod} \quad (5)$$

However, the applied cell voltage consists of not only the thermodynamically calculated cell voltage, but also internal energy losses or over-potentials. These internal losses originate from three sources; activation over-potential (η_{act}, related to the rates of electrode reaction), concentration over-potential (η_{conc}, related to mass transfer limitations of chemical species transported to or from the electrode), ohmic over-potential (η_{ohm} ,related to the resistance to the flow of ions in the electrolyte and to the flow of electrons through the electrode material) (Picioreanu et al., 2007). The activation and concentration over-potentials incur separately both at cathode and anode, see eq. (6).

$$V_{cell} = \left(E^0_{cath} - \eta_{C,act} - \eta_{C,con}\right) - \left(E^0_{anod} - \eta_{A,act} - \eta_{A,conc}\right) - \eta_{ohm} \quad (6)$$

1.1 Electrochemical Impedance Spectroscopy and Equivalent Electrical Circuit

The electrochemical balance eq. (6) expressed as the potential drops at each electrode are influenced by the resistances to the bioelectrochemical reactions and electrochemical processes in MES. These resistances can be converted into an Equivalent Electrical Circuit (EEC) (Jiya et al., 2018). Figure 1 shows a typical EEC of an electrode, where C is the capacitance of the electrical double layer (between the electrode and the electrolyte solution), R_p represents charge transfer resistance originating from MES reactions (related to the activation energy of the electrodes) and R represents resistance by the electrolyte solution. The electrochemical impedance spectroscopy (EIS) has been used to characterize electrochemical system by means of EECs (Wagner, 2002).

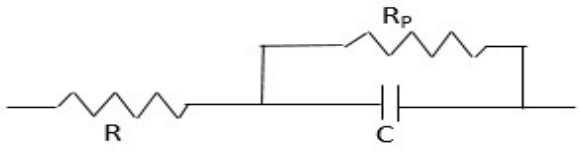

Figure 1: Classical equivalent circuit of a double layer capacitor showing its three basic characteristics: The internal resistance (R), its Capacitance (C), and self-discharge resistance (Rp) (Jiya et al., 2018).

EIS characterizes the response of an electrical circuit to alternative current (AC) or voltage. For a certain amplitude and frequency of applied AC signal, the circuit responds with a particular amplitude of alternating current at the same frequency. This response is quantified as impedance based on Ohm's law (E = I Z, where E and I are AC voltage and current respectively and Z is the impedance). The impedance depends on the frequency of the applied signal (voltage) and the time shift (or phase shift) between the input and output signals.

This technique can be applied to electrochemical cells (in this case MES). An AC signal is applied to the cell and the corresponding response (the impedance) depicts the resistance to charge flow. The charge flow depends on the bio electrochemical reactions and processes in the cell. The different frequencies of the applied AC voltage can distinguish the different processes that have different time scales. The lower frequencies are corresponding to the slow processes such as diffusion and slow electrochemical reactions. The higher frequencies are corresponding to the faster processes. At higher frequencies we can approximate the impedance due to the flow of ions in the electrolyte (i.e., the resistance of the electrolyte solution). Then the impedance response is mainly due to the charge and discharge of the double layer (capacitance).

The impedance data is generated in the form of a spectrum typically on a plot called Nyquist plot. The response impedance Z is composed of a real and imaginary part. The “Nyquist Plot” represents the real part on X-axis and the imaginary part on Y-axis. Bode plot is also another important graph used in EIS analysis where the absolute values of the frequency response (i.e., impedance) and the phase-shift are plotted vs the applied frequency.

The EEC associated with the corresponding spectrum can be constructed with the amplitude of the circuit elements using computer aided tools.

1.2 Aims

This study intends to develop a simple mathematical model that contributes to the integration of MES in AD to reduce CO_2 to CH_4. The experimental work on this is so far limited and will require large efforts to test wide variety of operational conditions, while mathematical modelling can extrapolate on such results and enhance our understanding of MES. In this case, our aim is to develop a simple model to understand the variation in resistances in a MES system as the biofilm grow and in its fully-grown operation. An EIS experiment is employed to estimate the resistances of the electrolyte solution and the charge transfer and distinguish the contribution from each to the MES internal resistance. The Open-source Modelling language Modelica (Modelica Association, 2017) is used to build the simple model. Typical applications of the models as such also include design of power management systems from lab.- to full-scale reactor setups, and the biofilm

resistance values are important to understand the kinetic behaviours of bio-electrochemical reactions.

2 Materials and methods

2.1 MES reactor and operation

The present MES experiments were performed in a 100 mL Borosilicate glass bottle with a 3-ports Teflon screw cap. The reactor was operated in a semi-continuous mode. A carbon nanotube composite (made in-house, area ~1 cm^2) was used as the cathode. A Graphite rod (L: 152 mm × D: 6.15 mm; Alfa Aesar, Thermo Fisher GmbH, Karlsruhe, Germany) was used as the anode. An Ag/AgCl electrode (+0.209 V vs. SHE; 3 M NaCl, QVMF2052, ProSense, BB Oosterhout, The Netherlands) was used as the reference electrode. The electrodes were connected with titanium wire. The voltage between cathode and reference was kept constant at -0.42 V vs SHE by Potentiostat (Interface 1000B, Gamry instruments, Pennsylvania, USA) with the intention of synthesising CH_4.

The reactor was operated at 35°C and 10 days HRT with a fully growth biofilm condition. A synthetic feed prepared according to Kenarsari et al. (2020) at a flow rate of 10 mL/day was used. Anaerobic digester sludge from the local municipal wastewater treatment plant (Knarrdalstrand, Porsgrunn, Norway) was used as the inoculum.

2.2 EIS experiment

The current EIS experiment results were generated by running EIS in a cell with a fully-grown biofilm cathode. This experiment work was type of "lesson-learned" and our first attempt was to estimate the impedance associated with the cathode (i.e., WE). We relied on the EIS instrument capacity available in our lab at the time of the study (We intent to improve the capacity and expand our knowledge targeting a pilot scale MES). The EIS experiment was performed by using a potentiostat (Interface 1000B, Gamry instruments, Pennsylvania, USA). The initial frequency was set to 20 kHz, which is the maximum limit of interface 1000B and stepped down to 0.2 Hz through 10 points/decade ratio. The impedance data is generated in the form of a spectrum on Nyquist plot and the Bode plot. The two plots were used to estimate the electrolyte solution resistance. On the Nyquist plot, the intercept of the spectrum with the X-axis (real part of the impedance) in the high-frequency range gives the electrolyte resistance. The impedance in the high frequency range and zero phase-shift was confirmed using Bode plot.

2.3 Model development

The equivalent electrical circuit as given in Figure 1 can be further simplified depending on the application. Though the biofilm can be represented as an impedance consisting mainly of both resistance and capacitance, in a MES application we will be purely dealing with direct current flows. This means that the capacitance does not have any significant influence on the electrical behaviour of the reactor. Furthermore, we assumed that the resistance of the anode (connected to the counter-electrode, (CE) of the potentiostat) side is negligible compared to the resistance of the solution and biofilm (for this stage of model development). The electrolyte solution itself can be represented by a resistance that also does not change over time since the ionic strength of the solution will stay almost the same.

Figure 2 shows the developed model consisting of an ideal regulated potentiostat voltage source, including sub-models for the development of electrode biofilms and solution properties. The model was build using the open-source Modelling language Modelica (Modelica Association, 2017).

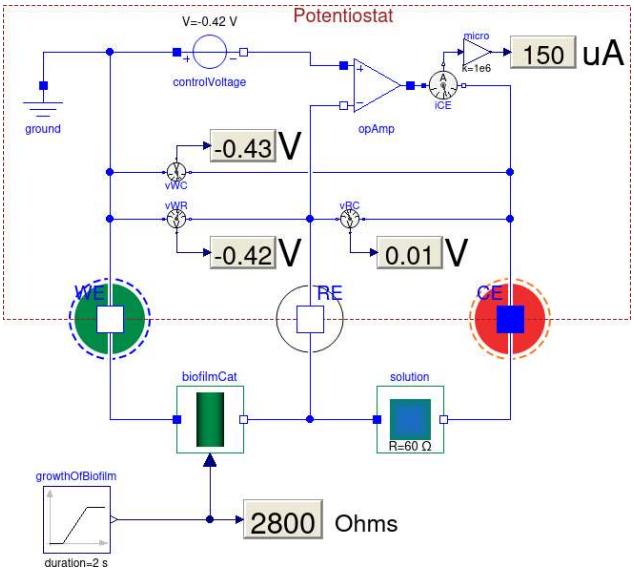

Figure 2: Graphical presentation of potentiostat controlled MES for CO_2 reduction to CH_4 model implemented in Modelica.

3 Result and discussion

Based on our EIS experiment, we could estimate the electrolyte solution resistance at the cathode side as 60 Ω by observing the Nyquist plot and the Bode plot. Our estimation is based on the frequency response of the highest frequency we could reach with our EIS instrument capacity and the frequency response at zero phase shift. The highest frequency was 20 kHz.

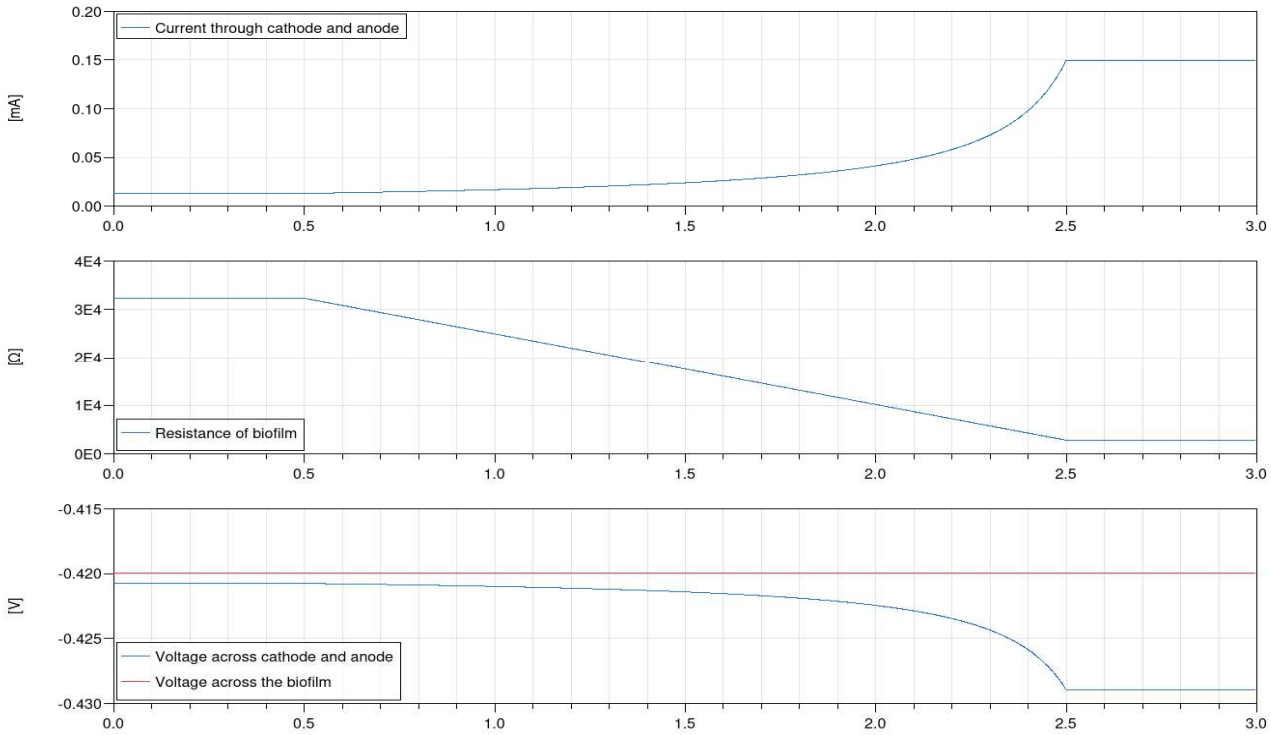

Figure 3: Simulation results for biofilm growth over time in seconds (in reality the growth happened over 21 days).

3.1 Simulation result

The model presented in Figure 2 is used to verify if the voltage level between anode and cathode does not exceed a certain set value (above which undesirable oxidation reactions can occur at the anode or CE) whilst still keeping the voltage across the biofilm at the optimal value of V_biofilm = -0.42 V at the cathode (WE) for CH_4 production.

The resistance between anode and solution is neglected for this stage of model development. The resistance of the solution (R_solution) itself has been experimentally determined to be = 60 Ω. Also, from measurements obtained from MES experiments, we could find that at the beginning of the biofilm growth (i.e., abiotic condition), the current flow was 13 µA and after the growth period of 21 days the current went up to 150 µA. Those measurement were taken whilst the potential across the biofilm was always kept at a constant, (i.e. V_biofilm= -0.42 V).

According to Ohm's law this translates to a biofilm resistance of about R_biofilm = 32 kΩ at the beginning of the growth period and 3 kΩ once the biofilm was fully established.

These values were then used in the simulation model in order to determine how high the voltage potential between anode and cathode will get when the voltage drop across the biofilm is kept constant whilst the resistance of the biofilm itself is getting smaller as it is growing.

Figure 3 is showing the simulation results for a change of resistance of the biofilm over time. The maximum voltage drop in this case does not exceed V_biofilm ≤ 0.43 V. So, the model simulations show that it is possible to determine the voltage required to keep the potential difference across the cathode biofilm within optimal conditions. The system is sensitive to effects of biofilm development on electron transfer at both electrodes, which implies effects on the electric current flow in the cell. This is useful for experimental design.

4 Conclusions and future development

- A functional mathematical model for the integration of MES in AD to reduce CO_2 to CH_4 is developed in Modelica. It is useful in extrapolating experimental results and to enhance our understanding of MES.
- The cathode resistance was reduced by a factor ten when biofilm was established, compared to the clean electrode. This implies an efficient electron transfer and utilization in the cathode where biofilm develops to reduce CO_2 to CH_4
- The simulations show that it is possible to determine the voltage required to keep the potential difference across the cathode biofilm within optimal conditions (e.g. V_biofilm ≤ 0.43 V for CO_2 to CH_4 reduction).

4.1 Further development

We expect to modify this model to better understand impedance variation in the MES system from the abiotic

condition (without biofilm), to the fully-grown biofilm operation (i.e., steady state). Hence, the model can predict the cell voltage (across the WE and CE), whilst keeping the optimum potential at the biocathode (or a WE) at different stage of MES operation. EIS experiments will also be carried out accordingly.

References

Irini Angelidaki, Laura Treu, Panagiotis Tsapekos, Gang Luo, Stefano Campanaro, Henrik Wenzel, and Panagiotis G. Kougias. Biogas upgrading and utilization: Current status and perspectives. *Biotechnology Advances, 36*(2): 452-466, 2018. doi:https://doi.org/10.1016/j.biotechadv.2018.01.011.

Florian Geppert, Dandan Liu, Mieke van Eerten-Jansen, Eckhard Weidner, Cees Buisman, and Annemiek ter Heijne. Bioelectrochemical Power-to-Gas: State of the Art and Future Perspectives. *Trends in Biotechnology, 34*(11): 879-894, 2016. doi:https://doi.org/10.1016/j.tibtech.2016.08.010.

Immanuel N. Jiya, Nicoloy Gurusinghe, and Rupert Gouws. Electrical Circuit Modelling of Double Layer Capacitors for Power Electronics and Energy Storage Applications: A Review. *Electronics, 7*(11): 268, 2018.

Zahra Nikbakht Kenarsari, Nirmal Ghimire, Rune Bakke, and Wenche Hennie Bergland. (2020). *Thermophilic Anaerobic Digestion Modeling of Lignocellulosic Hot Water Extract using ADM1*. Paper presented at the Proceedings of The 60th SIMS Conference on Simulation and Modelling SIMS 2019, August 12-16, Västerås, Sweden.

Modelica_Association. Modelica®–A Unified Object-Oriented Language for Systems Modeling, Language Specification, Version 3.4, April 2017. *Online: https://www.modelica.org/documents*, 2017.

A. B. T. Nelabhotla and C. Dinamarca. Electrochemically mediated CO_2 reduction for bio-methane production: a review. *Reviews in Environmental Science and Bio/Technology, 17*(3): 531-551, 2018. doi:10.1007/s11157-018-9470-5.

Anirudh Bhanu Teja Nelabhotla and Carlos Dinamarca. Bioelectrochemical CO_2 Reduction to Methane: MES Integration in Biogas Production Processes. *Applied Sciences, 9*(6): 1056, 2019.

Cristian Picioreanu, Ian M. Head, Krishna P. Katuri, Mark C. M. van Loosdrecht, and Keith Scott. A computational model for biofilm-based microbial fuel cells. *Water Research, 41*(13): 2921-2940, 2007. doi:https://doi.org/10.1016/j.watres.2007.04.009.

Korneel Rabaey and René A. Rozendal. Microbial electrosynthesis — revisiting the electrical route for microbial production. *Nature Reviews Microbiology, 8*: 706, 2010. doi:10.1038/nrmicro2422.

Andrea Schievano, Deepak Pant, and Sebastia Puig. Editorial: Microbial Synthesis, Gas-Fermentation and Bioelectroconversion of CO_2 and Other Gaseous Streams. *Frontiers in Energy Research, 7*(110), 2019. doi:10.3389/fenrg.2019.00110.

Vasan Sivalingam, Carlos Dinamarca, Gamunu Samarakoon, Dietmar Winkler, and Rune Bakke. Ammonium as a Carbon-Free Electron and Proton Source in Microbial Electrosynthesis Processes. *Sustainability, 12*(8): 3081, 2020.

N. Wagner. Characterization of membrane electrode assemblies in polymer electrolyte fuel cells using a.c. impedance spectroscopy. *Journal of Applied Electrochemistry, 32*(8): 859-863, 2002. doi:https://doi.org/10.1023/A:1020551609230.

Doctoral dissertation no. 131
2022

—

Syngas Fermentation and Microbial Electrosynthesis Process Integration to Advance Biogas Production

Dissertation for the degree of Ph.D

—

Vasan Sivalingam

—

ISBN: 978-82-7206-679-5 (print)
ISBN: 978-82-7206-680-1 (online)

usn.no